

University of Alberta

Nanoparticle Pt-Ru adatom catalysts for direct methanol fuel cells.

The study of a direct 2-propanol polymer electrolyte fuel cell.

by

Dianxue Cao



A thesis submitted to the Faculty of Graduate Studies and Research in partial fulfillment  
of the requirements for the degree of Doctor of Philosophy

Department of Chemistry

Edmonton, Alberta

Spring 2004



Library and  
Archives Canada

Bibliothèque et  
Archives Canada

Published Heritage  
Branch

Direction du  
Patrimoine de l'édition

395 Wellington Street  
Ottawa ON K1A 0N4  
Canada

395, rue Wellington  
Ottawa ON K1A 0N4  
Canada

*Your file* *Votre référence*

*ISBN: 0-612-96248-2*

*Our file* *Notre référence*

*ISBN: 0-612-96248-2*

The author has granted a non-exclusive license allowing the Library and Archives Canada to reproduce, loan, distribute or sell copies of this thesis in microform, paper or electronic formats.

L'auteur a accordé une licence non exclusive permettant à la Bibliothèque et Archives Canada de reproduire, prêter, distribuer ou vendre des copies de cette thèse sous la forme de microfiche/film, de reproduction sur papier ou sur format électronique.

The author retains ownership of the copyright in this thesis. Neither the thesis nor substantial extracts from it may be printed or otherwise reproduced without the author's permission.

L'auteur conserve la propriété du droit d'auteur qui protège cette thèse. Ni la thèse ni des extraits substantiels de celle-ci ne doivent être imprimés ou autrement reproduits sans son autorisation.

---

In compliance with the Canadian Privacy Act some supporting forms may have been removed from this thesis.

Conformément à la loi canadienne sur la protection de la vie privée, quelques formulaires secondaires ont été enlevés de cette thèse.

While these forms may be included in the document page count, their removal does not represent any loss of content from the thesis.

Bien que ces formulaires aient inclus dans la pagination, il n'y aura aucun contenu manquant.

# Canada

## Abstract

Pt-Ru systems are the most active, stable anode catalysts tested in direct methanol fuel cells. Investigations into the real activity and optimum surface composition of nanoparticle Pt-Ru catalysts toward methanol electrooxidation are difficult because there is a lack of proven, accurate methods to measure the number of active sites and the surface Pt/Ru ratio. In this study, Pt-Ru<sub>ad</sub> systems (Ru<sub>ad</sub> is a ruthenium adatom) were employed to address these problems because controlled amounts of Ru<sub>ad</sub> can be deposited onto Pt nanoparticles of known surface area to produce Pt-Ru<sub>ad</sub> nanoparticles of known surface areas and controlled surface compositions. Two non-electrochemical, self-limiting methods to deposit Ru adatoms onto nanoparticle Pt were devised and investigated. The organometallic precursor, Ru<sub>4</sub>(μ-H)<sub>4</sub>(CO)<sub>12</sub>, reacts with hydrogen over either blacked Pt gauze or Pt nanoparticles to deposit Ru adatoms and CO onto the Pt surface. The deposition is self-poisoned by the adsorbed CO, and it stops after ca. 0.05 surface equivalents (moles Ru<sub>ad</sub> vs. moles surface Pt) of Ru<sub>ad</sub> are deposited onto blacked Pt gauzes, and after ca. 0.10 surface equivalents of Ru<sub>ad</sub> are deposited onto nanoparticle Pt black.

Aqueous RuCl<sub>3</sub> reacts with hydrogen pre-adsorbed onto nanoparticle Pt black surfaces to deposit 0.18 surface equivalents of Ru<sub>ad</sub>. The deposition was repeated several times, with each reaction depositing ca. 0.18 surface equivalents of more Ru<sub>ad</sub> onto the Pt-Ru<sub>ad</sub> nanoparticles. The resulting nanoparticle Pt-Ru<sub>ad</sub> electrocatalysts with Ru<sub>ad</sub> surface coverages ranging from 0.18 to 0.75 were studied as catalysts for methanol electrooxidation in 1.0 M H<sub>2</sub>SO<sub>4</sub> (3-electrode experiments), as well as in prototype direct methanol fuel cells. The optimum Ru<sub>ad</sub> surface coverage is ca. 0.33 between 22 °C and 60

°C. It shifts to higher values as the temperature is increased. A Nafion<sup>®</sup>-117 membrane fuel cell consisting of a Pt-Ru anode and a Pt black cathode was operated at 90 °C using aqueous 2-propanol as fuel. The performance of the cell operating on 2-propanol was substantially higher than operating on methanol at current densities lower than ~ 200 mA/cm<sup>2</sup>. This result shows that direct 2-propanol fuel cells are promising alternatives to direct methanol fuel cells.



## Acknowledgement

I would like to thank my supervisor Professor Steve H. Bergens for his advice and teaching throughout my Ph. D program.

I wish to thank Youbin Shao and Professor Gary Horlick. Their help on inductively coupled plasma spectrophotometry is very important for my work.

I also thank all of the group members, both past and present, in particular, Christopher Lee, Yue Xing, and Okwado Akotsi, and Rongbing Du. Chris gave me many helpful suggestions. Yue has been a great friend and coworker.

## Table of Contents

### Chapter 1

#### Introduction

1. Fuel Cells .....	1
1.1 Principles and Structures of Fuel Cells .....	1
1.2 Types of Fuel Cells .....	2
1.3 Why Fuel Cells?.....	7
1.4 Factors Influencing the Practical Efficiencies of Fuel Cells (What are the Fuel Cell People Working on?) .....	9
2. Direct Methanol Fuel Cells.....	13
3. The Mechanism of Methanol Electrooxidation over Pt-Ru Systems.....	19
4. Deposition of Ru <sub>ad</sub> on Pt Surfaces .....	22
4.1 Spontaneous Deposition .....	23
4.2 Surface Organometallic Chemistry.....	24
4.3 Surface Reductive Deposition.....	25
5. Research Proposal.....	27
References.....	28

### Chapter 2

**An Organometallic Deposition of Ruthenium Adatoms on Platinum that Self  
Poisons at a Specific Surface Composition. A Direct Methanol Fuel Cell Using a  
Platinum-Ruthenium Adatom Anode Catalyst.**

1. Introduction.....	37
2. Experimental .....	42
2.1. General.....	42
2.2 Self-Poisoning Deposition Using $\text{Ru}_4(\mu\text{-H})_4(\text{CO})_{12}$ over Blacked Pt Gauzes.....	44
2.3. Electrooxidation of Methanol .....	45
2.4 Self-Poisoning Deposition Using $\text{Ru}_4(\mu\text{-H})_4(\text{CO})_{12}$ over Pt Black .....	46
2.5 Preparation and Operation of Prototype DMFCs.....	47
3. Results and Discussion .....	48
3.1 Blacked Pt-Ru <sub>ad</sub> Gauze .....	50
3.2 Nanoparticle Pt-Ru <sub>ad</sub> Black.....	56
4. Conclusions.....	60
References.....	61

### Chapter 3

#### Nanoparticle Pt-Ru<sub>ad</sub> Catalysts for Direct Methanol Fuel Cells.

##### Part I: Preparation, Methanol and CO Electrooxidation

1. Introduction.....	68
2. Experimental .....	75
2.1 General.....	75
2.2 Preparation of Pt-Ru <sub>ad</sub> Catalysts .....	76
2.3 Methanol Electrooxidation.....	77
2.4 Adsorbed CO Electrooxidation.....	78
3. Results and Discussion .....	78
3.1 Ruthenium Deposition .....	78

3.2 Methanol Electrooxidation.....	92
3.3 Adsorbed CO Electrooxidation.....	102
4. Conclusions.....	109
References.....	110

## Chapter 4

### Nanoparticle Pt-Ru<sub>ad</sub> Catalysts for Direct Methanol Fuel Cells.

#### Part II: Performance as Anode Catalysts for Direct Methanol Fuel Cells

1. Introduction.....	118
2. Experimental .....	121
2.1 Materials .....	121
2.2 Preparation of Pt-Ru <sub>ad</sub> Catalysts .....	121
2.3 Fabrication of Membrane Electrode Assemblies.....	121
2.4 Operation of Direct Methanol Fuel Cells.....	123
2.5 Cyclic Voltammetry.....	124
3. Results and Discussion .....	125
3.1 Unsupported Pt-Ru <sub>ad</sub> Anode Catalysts.....	125
3.2 Supported Pt-Ru <sub>ad</sub> Anode Catalysts.....	134
3.3 Stability of Pt-Ru <sub>ad</sub> and Catalyst Utilization.....	138
4. Conclusions.....	145
References.....	145

## Chapter 5

### A Direct 2-Propanol Polymer Electrolyte Fuel Cell

1. Introduction.....	149
----------------------	-----

2. Experimental.....	151
3. Results.....	154
4. Discussion.....	162
5. Conclusions.....	164
References.....	165

## **Chapter 6**

### **Conclusions**

References.....	171
-----------------	-----

## List of Tables

### Chapter 1

<b>Table 1-1.</b> Summary of major differences between fuel cell types.....	3
<b>Table 1-2.</b> Electrode reactions in fuel cells.....	4

### Chapter 3

<b>Table 3-1.</b> Nanoparticle Pt-Ru <sub>ad</sub> catalysts prepared by surface reductive deposition of Ru on nanoparticle Pt black.....	81
<b>Table 3-2.</b> The optimum surface composition of Pt-Ru catalysts toward methanol electrooxidation.....	96
<b>Table 3-3.</b> The real activity of Pt-Ru system toward methanol electrooxidation .....	98

### Chapter 4

<b>Table 4-1.</b> Pt-Ru <sub>ad</sub> catalysts prepared by surface reductive deposition of Ru on nanoparticle Pt black and Pt/C.....	122
---	-----

## List of Figures

### Chapter 1

<b>Figure 1-1.</b> Schematic of a hydrogen-oxygen fuel cell.....	1
<b>Figure 1-2.</b> Comparison of the energy conversion processes in an ICE and a fuel cell .....	8
<b>Figure 1-3.</b> Ideal and actual fuel cell voltage-current characteristic.....	13
<b>Figure 1-4.</b> Schematic of a DMFC.....	14
<b>Figure 1-5.</b> Structure of Nafion <sup>®</sup> .....	15
<b>Figure 1-6.</b> A schematic representation of ion transport channels in hydrated Nafion <sup>®</sup> ..	16
<b>Figure 1-7.</b> Methanol adsorption and dehydrogenation on Pt surfaces .....	22

### Chapter 2

<b>Figure 2-1.</b> Cyclic voltammograms of blacked Pt gauze (a) before hydrogenation, (b) after hydrogenation .....	52
<b>Figure 2-2.</b> Potentiodynamic electrooxidations of methanol over a blacked Pt gauze substrate and over a blacked Pt-Ru <sub>ad</sub> gauze surface resulting from hydrogenation of Ru <sub>4</sub> (μ-H) <sub>4</sub> (CO) <sub>12</sub> .....	55
<b>Figure 2-3.</b> Potentiostatic electrooxidation of methanol over a blacked Pt-Ru <sub>ad</sub> gauze resulting from hydrogenation of Ru <sub>4</sub> (μ-H) <sub>4</sub> (CO) <sub>12</sub> , and over a blacked Pt gauze.....	57
<b>Figure 2-4.</b> Polarization curves for 90 °C DMFCs with Nafion <sup>®</sup> -117 membranes .....	59
<b>Figure 2-5.</b> Cyclic voltammograms of a Pt-Ru <sub>ad</sub> anode and a Pt-black cathode obtained in a DMFC .....	60

### Chapter 3

<b>Figure 3-1.</b> Two extreme ways $Ru_{ad}$ may deposit on the surface of Pt.....	82
<b>Figure 3-2.</b> Schematic of a model for Ru reductive deposition on Pt.....	84
<b>Figure 3-3.</b> The deposition of $Ru_{ad}$ on the surface of Pt based on an electrochemical mechanism .....	86
<b>Figure 3-4.</b> Cyclic voltammograms of (a) Pt, (b-f) Pt- $Ru_{ad}$ with different $Ru_{ad}$ coverages, and (g) 50:50 Pt-Ru from Johnson Matthey .....	89
<b>Figure 3-5.</b> Potentiostatic electrooxidation of methanol over Pt- $Ru_{ad}$ with $Ru_{ad}$ coverages of (a) 0, (b) 0.18, (c) 0.33, (d) 0.45, (e) 0.63, and (f) 0.75.....	93
<b>Figure 3-6.</b> Methanol adsorption and dehydrogenation on the surface of Pt.....	94
<b>Figure 3-7.</b> Comparison of the real activity of Pt- $Ru_{ad}$ to that of 50-50 Pt-Ru from Johnson Matthey .....	100
<b>Figure 3-8.</b> Comparison of the mass activity of Pt- $Ru_{ad}$ -0.33 to that of 50-50 Pt-Ru from Johnson Matthey and 50-50 (Pt-Ru)Ox from E-TEK.....	103
<b>Figure 3-9.</b> CO stripping cyclic voltammograms for (a-d) Pt- $Ru_{ad}$ with different Ru coverages, (e) Pt, (f) 50-50 (Pt-Ru)Ox from E-TEK, and (g) 50-50 Pt-Ru from Johnson Matthey .....	104
<b>Figure 3-10.</b> Dependence of CO stripping peak potential and charge on $Ru_{ad}$ coverages for Pt- $Ru_{ad}$ .....	107

### Chapter 4

<b>Figure 4-1.</b> Polarization curves for a series of DMFCs operating with Pt- $Ru_{ad}$ anode catalysts of differing surface composition.....	126
---	-----



<b>Figure 4-2.</b> DMFC polarization curves with currents normalized by the total surface area of the anode catalysts.....	129
<b>Figure 4-3.</b> DMFC polarization curves with currents normalized by the mass of the anode catalyst. The insert is the potentiostatic methanol oxidation current densities normalized by the mass of the catalysts.....	132
<b>Figure 4-4.</b> Power-current and voltage-current curves for DMFCs employing Pt-Ru <sub>ad</sub> , Pt-Ru from Johnson Matthey and (Pt-Ru)Ox from E-TEK anode catalysts .....	133
<b>Figure 4-5.</b> Polarization curves for DMFCs with carbon supported Pt-Ru <sub>ad</sub> anode catalysts.....	137
<b>Figure 4-6.</b> Comparison of carbon supported and unsupported Pt-Ru <sub>ad</sub> as anode catalyst in a PEM-DMFC.....	139
<b>Figure 4-7.</b> Cyclic voltammograms of anode catalysts recorded in PEM-DMFCs .....	141
<b>Figure 4-8.</b> Durability test for the PEM-DMFC with PtRu <sub>ad</sub> /C anode catalyst .....	143

## Chapter 5

<b>Figure 5-1.</b> Performance of a direct 2-propanol fuel cell versus a direct methanol fuel .....	155
<b>Figure 5-2.</b> Plots of electrical efficiency versus power density for a direct 2-propanol fuel cell and a direct methanol fuel cell .....	156
<b>Figure 5-3.</b> Effect of cathode catalyst loading on performance of a direct 2-propanol fuel cell.....	157
<b>Figure 5-4.</b> Effect of anode catalyst Loading on performance of a direct 2-propanol fuel cell.....	158

**Figure 5-5.** Effect of 2-propanol concentration on performance of a direct 2-propanol fuel cell.....159

**Figure 5-6.** Effect of oxygen pressure on performance of a direct 2-propanol fuel cell .....161

## List of Schemes

### Chapter 2

**Scheme 2-1.** Schematic of self-poisoning deposition of Ru<sub>ad</sub> on Pt.....49

**Scheme 2-2.** Self-poisoning deposition of Ru<sub>ad</sub> on Pt using Ru<sub>4</sub>(μ-H)<sub>4</sub>(CO)<sub>12</sub>.....50

### Chapter 5

**Scheme 5-1.** Reaction scheme of 2-propanol oxidation over a platinum electrode in acidic solution .....150

## List of Symbols and Abbreviations

$\beta$	transfer coefficient	
$d$	diameter	m
$D$	dispersion	%
$\Delta G$	Gibbs free energy change	kJ/mol
$\Delta H$	enthalpy change	kJ/mol
$\Delta S$	entropy change	kJ/(mol K)
$\varepsilon$	efficiency	%
$\varepsilon_{\text{faradaic}}$	faradaic efficiency	%
$\varepsilon_{\text{fuelcell}}$	overall efficiency of a fuel cell	%
$\varepsilon_{\text{voltage}}$	voltage efficiency	%
$\eta$	overpotential, overvoltage	mV, V
$\eta_{\text{act}}$	activation overpotential	mV, V
$\eta_{\text{ohm}}$	ohmic overpotential	mV, V
$\eta_{\text{conc}}$	concentration overpotential	mV, V
$E$	potential	mV, V
$E_{\text{anode}}$	anode potential	mV, V
$E_{\text{cathode}}$	cathode potential	mV, V
$E_{\text{fuelcell}}$	fuel cell potential	mV, V
$F$	Charge per mole of electrons (Faraday)	96485 C/mol e-
$i$	current	mA, A
$i_L$	limiting current	mA, A
$j$	current density	mA/cm <sup>2</sup>
$j_o$	exchange current density	mA/cm <sup>2</sup>
$n$	number of moles of electrons transferred	mol
$P$	power	mW, W
$Q$	charge	mC, C
$R$	resistance	$\Omega$
$\rho$	density	g/cm <sup>3</sup>

$S$	specific surface area	$\text{m}^2/\text{g}$
$\theta_{\text{Ru}}$	surface coverage by $\text{Ru}_{\text{ad}}$	
$T$	temperature	$^{\circ}\text{C}, \text{K}$
$t$	time	s
$W_{el}$	Electrical Work	$\text{kJ}/\text{mol}$
ad	Adatom	
ads	Adsorbed Species	
AES	Auger Electron Spectroscopy	
AFC	Alkaline Fuel Cell	
CV	Cyclic Voltammetry	
CVD	Chemical Vapor Deposition	
DEMS	Differential Electrochemical Mass Spectrometry	
DMFC	Direct Methanol Fuel Cell	
EDX	Energy Dispersive X-Ray Analysis	
EQCM	Electrochemical Quartz Crystal Microbalance	
EXAFS	Extended X-Ray Adsorption Fine Structure	
FC	Fuel Cell	
GC	Gas Chromatography	
GDE	Gas Diffusion Electrode	
HRSEM	High Resolution Scanning Electron Microscopy	
HRTEM	High Resolution Transmission Electron Microscopy	
ICE	Internal Combustion Engine	
ICP	Inductively Coupled Plasma	
JM	Johnson & Matthey	
LEED	Low Energy Electron Diffraction	
LEISS	Low Energy Ion Scattering Spectroscopy	
LHV	Low Heat Value	
MCFC	Molten Carbonate Fuel Cell	
MEA	Membrane Electrode Assembly	
MVD	Metal Vapor Deposition	
PAFC	Phosphoric Acid Fuel Cell	

PEFC	Polymer Electrolyte Fuel Cell
PEM	Polymer Electrolyte Membrane
PEMFC	Polymer Electrolyte Membrane Fuel Cell
PTFE	Polytetrafluoroethylene
r.d.s.	rate determining step
RHE	Reversible Hydrogen Electrode
RHEED	Reflection High Energy Electron Diffraction
sccm	standard cubic centimeter per minute
SEM	Scanning Electron Microscopy
SHE	Standard Hydrogen Electrode
SOFC	Solid Oxide Fuel Cell
SOMC	Surface Organometallic Chemistry
SPEFC	Solid Polymer Electrolyte Fuel Cell
STM	Scanning Tunneling Microscopy
TEM	Transmission Electron Microscopy
UHV	Ultra High Vacuum
upd	Underpotential Deposition
XANES	X-ray absorption near edge spectroscopy
XPS	X-Ray Photoelectron Spectroscopy
XRD	X-Ray Diffraction

## Chapter 1

### Introduction

#### 1. Fuel Cells

##### 1.1 Principles and Structures of Fuel Cells

Fuel cells are electrochemical devices that convert the chemical free energy of a reaction directly into electrical energy.<sup>1-5</sup> A fuel cell consists of a positive electrode (cathode), a negative electrode (anode), and an electrolyte layer that is sandwiched between the two electrodes, and that conducts ions between the two electrodes. The principle of a fuel cell is demonstrated with a  $H_2/O_2$  fuel cell in Figure 1-1. Hydrogen

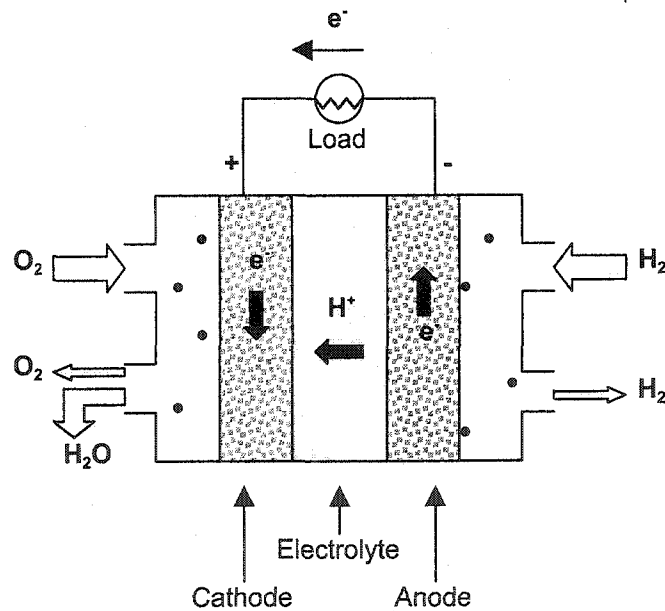


**Figure 1-1.** Schematic of a hydrogen/oxygen fuel cell.

fuel is fed continuously to the anode compartment, where it is oxidized to form protons and electrons (Eq. 1-1). The protons are transported to the cathode by the electrolyte. The electrons flow through the external circuit to the cathode. Air is fed continuously to the cathode compartment, where oxygen is reduced by the electrons while combining with the protons to form water (Eq. 1-2). The overall process is that the hydrogen is oxidized by oxygen to form water and to release the free energy of oxidation ( $\Delta G$ ) in the form of electrical work (Eq. 1-3).



### 1.2 Types of Fuel Cells<sup>1-5</sup>

There are many types of classification systems for fuel cells. The most common classification is by the type of electrolyte used in the fuel cells and includes (1) polymer electrolyte membrane fuel cells (PEMFCs, also called polymer electrolyte fuel cells (PEFCs), or solid polymer electrolyte fuel cells (SPEFCs)); (2) alkaline fuel cells (AFCs); (3) phosphoric acid fuel cells (PAFCs); (4) molten carbonate fuel cells (MCFCs); and (5) solid oxide fuel cells (SOFCs). An exception to this classification is the direct methanol fuel cells (DMFCs), which will be discussed in detail in section 2 of this chapter. Another way to classify fuel cells is by the temperature range in which fuel cells operate. Accordingly there are low-temperature fuel cells (PEMFCs, AFCs), medium-temperature fuel cells (AFCs, PAFCs), and high-temperature fuel cells (MCFCs and SOFCs). Besides the electrolyte, the fuel, oxidant, electrode materials used in a fuel



cell vary among the different types of fuel cells. The major differences between the different types of fuel cells are shown in Table 1-1. Electrode reactions for these fuel cells are given in Table 1-2. Not included in these tables are DMFCs.

**Table 1-1.** Summary of major differences between fuel cell types.<sup>1,5</sup>

	PEMFC	AFC	PAFC	MCFC	SOFC
Electrolyte	Ion Exchange Membranes	Potassium Hydroxide	Phosphoric Acid	Molten Carbonate	Ceramic $Y_2O_3-ZrO_2$
Operating Temperature (°C)	70-90	65-220	180-220	600-700	650-1000
Anode Catalyst	Pt/C, PtRu/C	Pt/C	Pt/C	Ni-Cr/Ni-Al	Ni/ZrO <sub>2</sub> cermet
Cathode Catalyst	Pt/C	Pt/C	Pt/C	Lithiated NiO	Sr-doped LaMnO <sub>3</sub>
Fuel	H <sub>2</sub>	H <sub>2</sub>	H <sub>2</sub>	H <sub>2</sub> , CO, etc.	H <sub>2</sub> , CO, CH <sub>4</sub> , CH <sub>3</sub> OH, etc.
Charge Carrier	H <sup>+</sup>	OH <sup>-</sup>	H <sup>+</sup>	CO <sub>3</sub> <sup>2-</sup>	O <sup>2-</sup>
Currently Achieved Electric Efficiency (LHV*)	40-45%	40-50%	40-45%	50-60%	50-65%
Prime Cell Components	Carbon-based	Carbon-based	Graphite-based	Stainless steel-based	Ceramic

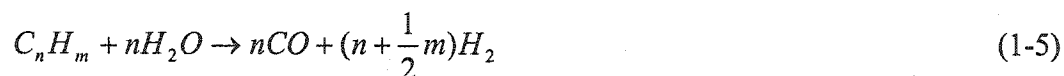
\* LHV: low heating value--The net energy released during oxidation of a unit of fuel when the water vapor created in the combustion reaction is not condensed.

**Table 1-2.** Electrode reactions in fuel cells.<sup>1</sup>

Fuel Cell	Anode Reaction(s)	Cathode Reaction(s)
PEMFC PAFC	$H_2 \rightarrow 2H^+ + 2e^-$	$\frac{1}{2} O_2 + 2H^+ + 2e^- \rightarrow H_2O$
AFC	$H_2 + 2(OH)^- \rightarrow 2H_2O + 2e^-$	$\frac{1}{2} O_2 + H_2O + 2e^- \rightarrow 2(OH)^-$
MCFC	$H_2 + CO_3^{2-} \rightarrow H_2O + CO_2 + 2e^-$ $CO + CO_3^{2-} \rightarrow 2CO_2 + 2e^-$	$\frac{1}{2} O_2 + CO_2 + 2e^- \rightarrow CO_3^{2-}$
SOFC	$H_2 + O^{2-} \rightarrow H_2O + 2e^-$ $CO + O^{2-} \rightarrow CO_2 + 2e^-$ $CH_4 + 4O^{2-} \rightarrow 2H_2O + CO_2 + 8e^-$	$\frac{1}{2} O_2 + 2e^- \rightarrow O^{2-}$

**Polymer Electrolyte Membrane Fuel Cells (PEMFCs):**<sup>1-5</sup> The electrolytes used in these fuel cells are ion exchange membranes (e.g., fluorinated sulfonic acid polymer (commercial name Nafion<sup>®</sup>)). PEMFCs operate at relatively low temperatures, have high power density, can vary their output quickly to meet shifts in power demand, and therefore are suited for applications in automobiles. PEMFCs operate on hydrogen gas, which can be generated on-board (on-site) from common fuels (such as alcohols or gasoline) using a reformer. The conversion process occurring in the reformer involves steam reforming (Eq. 1-4, -5, -6), partial oxidation (Eq. 1-7, -8, -9) or autothermal reforming.<sup>5-8</sup> The reforming product is a mixture of H<sub>2</sub>, CO<sub>2</sub>, and small portion of CO (this mixture is referred to as reformat). The CO content in the reformat must be reduced to less than 10 ppm because CO poisons the Pt anode catalyst.





**Alkaline Fuel Cells (AFCs):**<sup>1-5</sup> In this type of fuel cell, aqueous KOH (85 wt% for higher temperature operation, 35-50 wt% for lower temperature operation) soaked in a matrix (usually asbestos) is used as the electrolyte. AFCs operate on pure hydrogen and pure oxygen because the CO<sub>2</sub> in reformat and in the air will react with KOH to form K<sub>2</sub>CO<sub>3</sub>, which reduces the electrolyte's ion mobility and fouls the electrodes. The H<sub>2</sub>O produced in AFCs must be removed in order to prevent dilution of the electrolyte. Due to these limits, AFCs are too costly for commercial applications, and they are only used for special applications such as space missions (e.g., Apollo spacecraft). An advantage of AFCs is that they can achieve power generating efficiencies of up to 70%; that is the highest among other types of H<sub>2</sub>/O<sub>2</sub> fuel cells. This is because oxygen reduction at the cathode in alkaline electrolyte is easier than in acidic electrolyte.<sup>9</sup> The other advantage is that non-precious metal electrocatalysts (e.g., Ni (anode) and Ag (cathode)) can be used in AFCs.<sup>1</sup>

**Phosphoric Acid Fuel Cells (PAFCs):**<sup>1-5</sup> Phosphoric acid concentrated to 100% is used for the electrolyte in these fuel cells. Concentrated phosphoric acid is a relatively stable acid, which allows PAFCs to operate at temperatures between 150 and 220 °C. At these

operating temperatures, CO poisoning of the anode electrocatalyst (Pt/C) becomes less severe; therefore impure hydrogen can be used as fuel (PAFCs can tolerate a CO concentration of about 1.5% in reformat).<sup>2</sup> The use of impure hydrogen simplifies the fuel conversion processes. The rejected heat from PAFCs is high enough in temperature to produce hot water or steam, and thereby can be utilized. The major problem for PAFCs is the sintering (particle agglomeration) of Pt electrocatalysts during operation at a temperature of ca. 200 °C. This sintering results in a decrease in the specific surface area of the Pt electrocatalysts. PAFCs are the most mature fuel cell technology. They are commercially available today. More than 200 PAFCs have been installed all over the world in hospitals, hotels, large office buildings, manufacturing sites, and wastewater treatment plants.<sup>1</sup>

***Molten Carbonate Fuel Cells (MCFCs):***<sup>1-5</sup> The electrolytes used in these fuel cells are liquid solutions of lithium, sodium and/or potassium carbonates, soaked in  $\text{LiAlO}_2$ . MCFCs operate at 600 to 700 °C, where the alkali carbonates form a highly conductive molten salt with carbonate ions ( $\text{CO}_3^{2-}$ ) providing ionic conduction through the electrolyte matrix. At the high operating temperatures in MCFCs, relatively inexpensive nickel (Ni) and nickel oxide (NiO) are adequate to promote reactions on the anode and cathode, respectively. Noble metals are not required. MCFCs offer greater fuel flexibility (hydrogen, carbon monoxide, natural gas, propane etc.) and higher fuel-to-electricity efficiencies than lower temperature fuel cells, approaching 60%. The higher operating temperatures of MCFCs also make them candidates for combined-cycle applications, in which the exhaust heat is used to drive gas turbines and/or produce high-pressure steam for use in steam turbines to generate additional electricity. When the waste heat is used

for co-generation, total thermal efficiencies can approach 85%. They are best suited to large stationary applications (power plants). A disadvantage to MCFCs is that high temperatures enhance corrosion and the breakdown of cell components.

**Solid Oxide Fuel Cells (SOFCs):**<sup>1-5</sup> These fuel cells use solid metal oxide, usually  $Y_2O_3$ -stabilized  $ZrO_2$ , as electrolyte. They operate between 650 and 1000 °C, where ionic conduction is accomplished by oxygen ions ( $O^{2-}$ ). Typically, the anode is Co- $ZrO_2$  or Ni- $ZrO_2$  cermet, and the cathode is Sr-doped  $LaMnO_3$ .<sup>1</sup> Like MCFCs, SOFCs allow more flexibility in the choice of fuels and can produce very good performance in combined-cycle. SOFCs approach 60% electrical efficiency in the simple cycle system, and 85% total thermal efficiency in co-generation applications. The primary disadvantages of SOFCs are their excessive manufacturing costs, and the lack of thermal compatibility or long-term stability of the materials used for their construction.

### 1.3 Why Fuel Cells?

The most widely used energy converters are internal combustion engines and boiler + steam turbines. These engines convert the chemical energy stored in fossil fuels into heat by combustion. The heat is then converted into mechanical energy, or further into electrical energy by a generator (Figure 1-2). Such energy conversion systems have two major shortcomings: *low efficiencies and severe pollutant emissions*. The maximum efficiency of an ICE is limited by the Carnot efficiency, as given in Eq. 1-10, where  $T_1$  and  $T_2$  are the temperatures of the heat source and the heat sink (in degree Kelvin), respectively. Typical efficiencies of ICEs are usually less than 40%.<sup>5</sup> Toady's ICE converts only 19% of the useful energy in gasoline to turning a car's wheel.<sup>10</sup>

$$\varepsilon_{ICE} = \frac{T_1 - T_2}{T_2} \quad (1-10)$$

The direct combustion of fossil fuels in ICEs also releases harmful emissions ( $\text{NO}_x$ ,  $\text{SO}_x$ ,  $\text{CO}_2$ , and dust particles etc.) into the environment. Whereas, the presence of  $\text{NO}_x$  increases the level of ozone in the lower atmosphere, the presence of  $\text{SO}_x$  causes acid rain, and  $\text{CO}_2$  is a greenhouse gas, which is believed to be responsible for the global warming.<sup>5,6</sup>

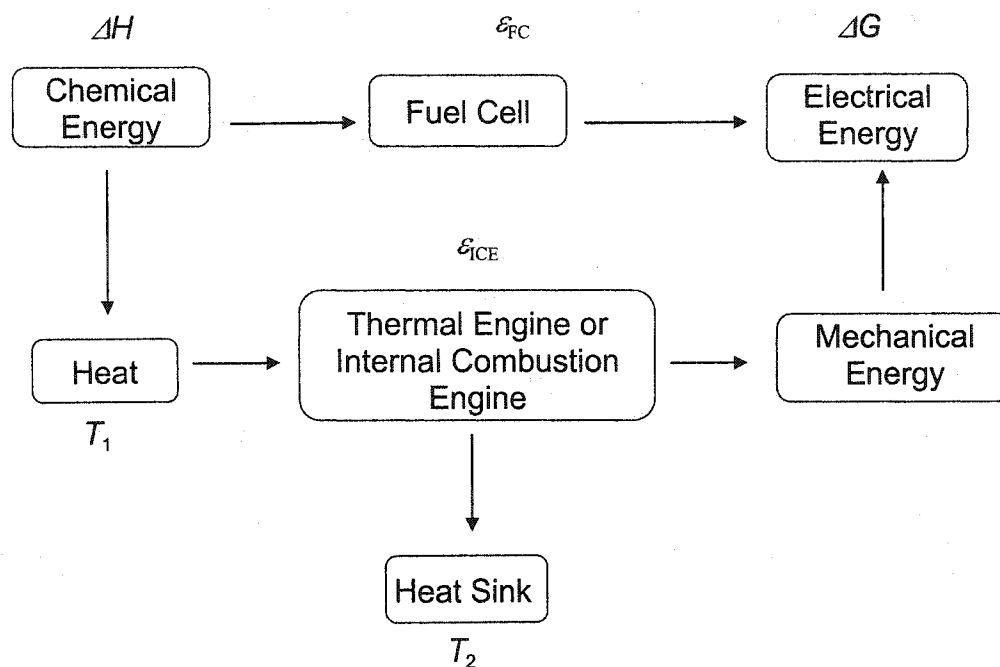


**Figure 1-2.** Comparison of the energy conversion processes in an ICE and a fuel cell.

Fuel cells, on the other hand, are more efficient and cleaner than ICEs. The theoretical, reversible efficiency of a fuel cell is given by Equation 1-11, where  $W_{el}$  is the

$$\varepsilon_{fuelcell,r} = \frac{W_{el}}{\Delta H_r} = \frac{\Delta G_r}{\Delta H_r} = 1 - T \frac{\Delta S_r}{\Delta H_r} \quad (1-11)$$

maximum electrical work,  $\Delta H_r$ ,  $\Delta G_r$ , and  $\Delta S_r$  are the changes in enthalpy, Gibbs free energy, and entropy of the cell reaction, respectively, and  $T$  is the operating temperature

of the cell. As the maximum efficiency of a fuel cell is not limited by the Carnot cycle, it is generally close to 100% at room temperature. For example, the maximum efficiency of a  $\text{H}_2/\text{O}_2$  fuel cell operating at 25 °C and 1 atmosphere is 83%.<sup>1</sup> The electric efficiencies currently achieved in pilot fuel cell plants (PAFCs, PEMFCs) are ca. 45% based on the low heating value of the fuels.<sup>1</sup> The overall efficiencies of plants operating on MCFCs or SOFCs can be as high as ca. 85%, if the heat rejected by the fuel cells is utilized.

Pollutant emissions by fuel cells are very low (virtually no acid gas and solid particles), and can meet the strictest emission requirement in the world. If hydrogen is used as fuel, there are no local pollutant emissions at all. The high efficiencies of fuel cells also effectively reduce the emission of  $\text{CO}_2$ .

Fuel cells are quiet, have no moving parts, and need only minimum maintenance. They are modular, and can thereby be easily stacked together to meet diverse power demands ranging from a few watts to megawatts. Fuel cells can be installed on-site, thereby eliminating the long distance electricity distribution network from central power plants to remote users. The advantages that fuel cells offer as energy converters, and the urgency for clean and high efficiency energy conversion technologies (for sustainable and environmentally friendly development), have resulted in a boom in research and development in fuel cells.<sup>11-13</sup>

#### *1.4 Factors Influencing the Practical Efficiencies of Fuel Cells (What are the Fuel Cell People Working on?)<sup>1,2,3,14</sup>*

The maximum electrical work ( $W_{el} = \Delta G_r$ ) is related to the reversible cell voltage ( $E_{\text{fuelcell}, r}$ ) via Equation 1-12, where  $n$  is the number of electrons involved in the cell reaction, and  $F$  is the Faraday constant ( $96\,485 \text{ C mol}^{-1}$ ).

$$\Delta G_r = -nFE_{fuelcell,r} \quad (1-12)$$

The reversible cell voltage  $E_{fuelcell,r}$  is the cell voltage at no net current, when the system is at equilibrium.  $E_{fuelcell,r}$  is the maximum voltage a cell can produce because there are no voltage losses to resistance or activation overpotential. It is equal to the difference between the reversible cathode reduction potential ( $E_{cathode,r}$ ) and the reversible anode reduction potential ( $E_{anode,r}$ ) (Eq. 1-13).

$$E_{fuelcell,r} = E_{cathode,r} - E_{anode,r} \quad (1-13)$$

Electrical energy is obtained from fuel cells only under load, when current is drawn through the cell. When current is drawn through a fuel cell, the electrode processes become irreversible, and the electrode potentials shift away from their equilibrium values. This behavior is called polarization. There are primarily three types of polarization: (1) activation polarization, (2) ohmic polarization, and (3) concentration polarization. Each polarization causes an overpotential, or overvoltage ( $\eta$ ) that reduces the overall cell potential.<sup>1,15</sup>

*Activation polarization* -- Activation overpotential ( $\eta_{act}$ ) arises from sluggish electrode kinetics (i.e., the activation barriers to the reactions occurring at the electrode). If  $\eta_{act} \geq 50$  mV,  $\eta_{act}$  is described by the Tafel equation (Eq. 1-14), where  $\beta$  is the electron transfer coefficient of the electrode reaction, and  $j_o$  is the exchange current density.<sup>15</sup>

$$\eta_{act} = \frac{RT}{(1-\beta)F} \ln \frac{j}{j_o} \quad (1-14)$$

The exchange current density is a measure of the intrinsic activity of an electrocatalyst under reversible conditions (i.e., when rates of the forward and reverse



reactions at the electrode are equal, so the net current is zero). The Tafel equation can be written as Eq. 1-15, where  $a = (-2.3RT/(1-\beta)F)\log j_0$ , and  $b = 2.3RT/(1-\beta)F$ .

$$\eta_{act} = a + b \log j \quad (1-15)$$

Accordingly, a plot of  $\eta_{act}$  vs.  $\log j$  is a straight line with the slope “ $b$ ”, which is called the Tafel slope. It is a measure of the amount of activation overpotential required to increase current density by tenfold. An effective electrocatalyst yields a high exchange current density  $j_0$ ; thereby a low  $\eta_{act}$  at a given current density.<sup>15</sup>

*Ohmic polarization* -- Ohmic overpotential ( $\eta_{ohm}$ ) results from resistance to the transport of ions in the electrolyte, and the resistance to the conduction of electrons through the electrode and other cell components.  $\eta_{ohm}$  is expressed as Eq. 1-16, where  $R$  is the total cell resistance, including electronic, ionic, and contact resistance.<sup>1,3</sup>

$$\eta_{ohm} = iR \quad (1-16)$$

*Concentration polarization* -- Concentration overpotential ( $\eta_{conc}$ ) is caused by the concentration gradient of reactants between the catalyst surface and the bulk fluid. This concentration gradient occurs whenever the supply rate of the reactants to the catalyst surfaces cannot match the consumption rate of the reactants on the catalysts surfaces.  $\eta_{conc}$  is given by Equation 1-17, where  $i_L$  is the limiting current, which is a measure of the maximum rate at which a reactant can be supplied to an electrode.<sup>3,15</sup>

$$\eta_{conc} = \frac{RT}{nF} \ln \left( 1 - \frac{i}{i_L} \right) \quad (1-17)$$

Activation and concentration polarization result in a decrease in the cathode potential and an increase in the anode potential from their equilibrium values as shown

by Eq. 1-18, 1-19. The ohmic polarization results in a cell potential loss that is equal to  $iR$ . Taking into account all these polarizations, the actual cell voltage can be written as

$$E_{cathode} = E_{cathode,r} - |(\eta_{act,c} + \eta_{conc,c})| = E_{cathode,r} - |\eta_{cathode}| \quad (1-18)$$

$$E_{anode} = E_{anode,r} + |(\eta_{act,a} + \eta_{conc,a})| = E_{anode,r} + |\eta_{anode}| \quad (1-19)$$

$$\begin{aligned} E_{fuelcell} &= E_{cathode} - E_{anode} - iR \\ &= E_{cathode,r} - E_{anode,r} - (|\eta_{cathode}| + |\eta_{anode}|) - iR \\ &= E_{fuelcell,r} - (|\eta_{anode}| + |\eta_{cathode}| + iR) \end{aligned} \quad (1-20)$$

Eq. 1-20. As shown by this equation, current flow in a fuel cell results in a decrease in the cell voltage because of losses caused by electrode and ohmic polarizations. The goal of fuel cell developers is to minimize polarizations so that the cell voltage under operating conditions ( $E_{fuelcell}$ ) approaches the reversible cell voltage ( $E_{fuelcell,r}$ ). This goal is achieved by increasing the activity of the electrocatalysts (thereby reducing  $\eta_{act}$ ), by increasing the ionic conductivity of the electrolyte (thereby reducing  $iR$ ), and by optimizing the electrode structures for mass transport and electrical conduction (thereby decreasing  $\eta_{conc}$  and  $iR$ ). For a given cell design, the cell performance can be improved by optimizing the operation parameters, such as temperature, pressure, fuel or oxidant composition, etc.

Figure 1-3 shows ideal and actual fuel cell voltage-current characteristics. The activation polarization loss is dominant at low current density. Ohmic polarization loss increases with the increase of current over the whole range of current because resistance remains essentially constant. Mass transport loss becomes prominent at high current density.

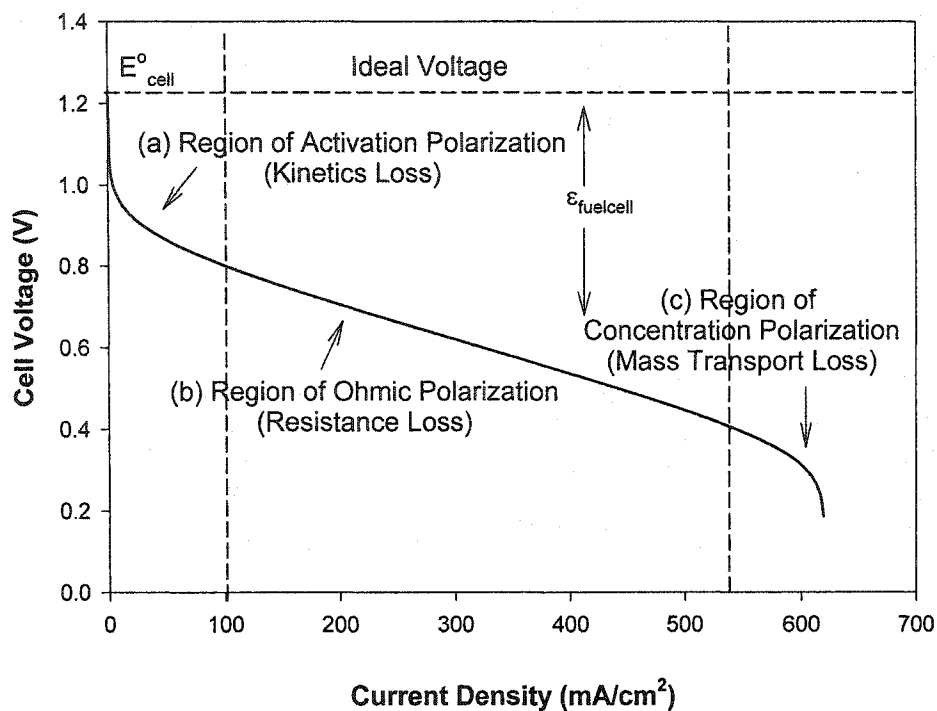


Figure 1-3. Ideal and actual fuel cell voltage-current characteristics.<sup>1,5</sup>

## 2. Direct Methanol Fuel Cells (DMFCs)<sup>16-24</sup>

A DMFC consists of a polymer electrolyte membrane, such as Nafion<sup>®</sup>-117, sandwiched between two porous electrodes containing electrocatalysts (Figure 1-4). Methanol is delivered to the anode, where it is oxidized directly to carbon dioxide over the anode catalyst (Eq. 1-21). Oxygen (from air) is supplied to the cathode, where it is reduced by electrons, and it combines with protons to form water (Eq. 1-22). Accordingly, carbon dioxide and water are the only products (Eq. 1-23).

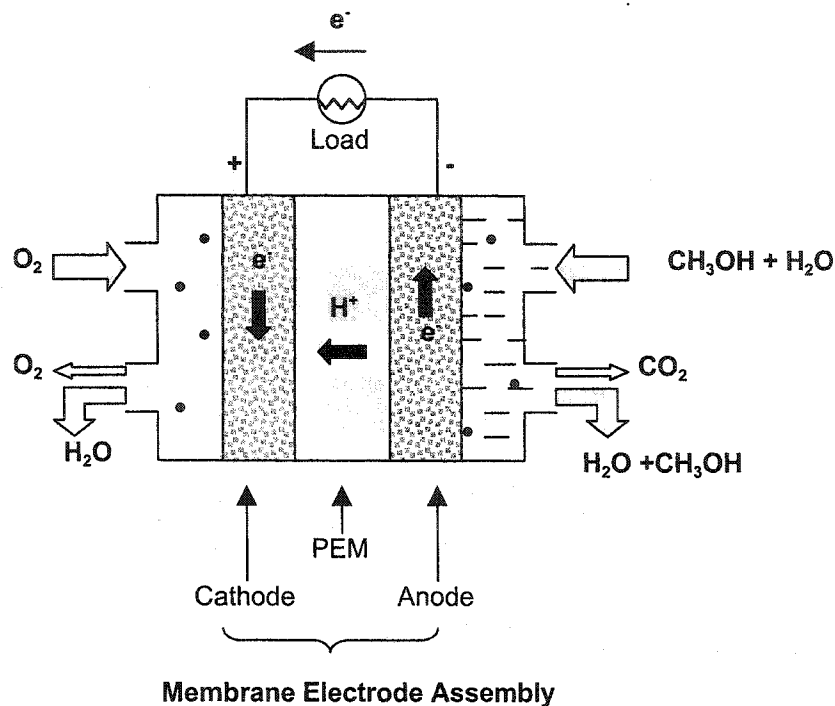


Figure 1-4. Schematic of a DMFC.



The theoretical efficiency of a DMFC operating under standard conditions (25 °C, 1 atmosphere) is 0.97, higher than that of a H<sub>2</sub>/O<sub>2</sub>-PEMFC (0.83).<sup>1,5,6</sup> The equilibrium cell voltage for a DMFC is 1.213 V, which is comparable to that of a H<sub>2</sub>/O<sub>2</sub>-PEMFC (1.229 V).<sup>2,14,25-27</sup>

The anode|membrane|cathode composite is called the membrane electrode assembly (MEA), which is the core of a DMFC. The polymer electrolyte membranes most-used in present DMFCs are DuPont's Nafion<sup>®</sup> membranes. Nafion<sup>®</sup> is composed of

a fluorocarbon backbone (hydrophobic) with perfluoro side chains containing sulfonic acid groups (hydrophilic) (Figure 1-5).<sup>28, 29</sup> When the membrane is hydrated, ion transport channels are formed within the membrane (Figure 1-6), allowing protons to migrate from the anode to the cathode.<sup>19</sup> Nafion<sup>®</sup> membranes have high proton conductivity (when fully hydrated), and good chemical, mechanical, and thermal stability. This combination of properties is well-suited for use in H<sub>2</sub>/O<sub>2</sub> fuel cells. But Nafion membranes are also permeable to methanol. Methanol crossover from the anode to the cathode of Nafion<sup>®</sup>-based DMFCs severely limits their performance (*vide infra*).

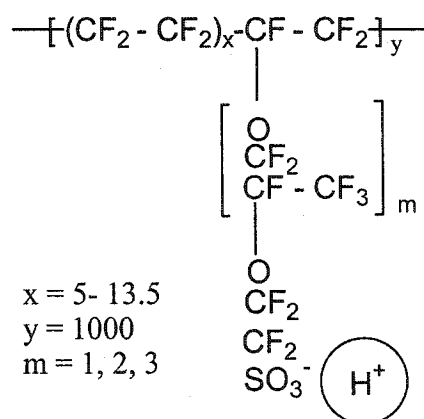


**Figure 1-5.** Structure of Nafion<sup>®</sup>.

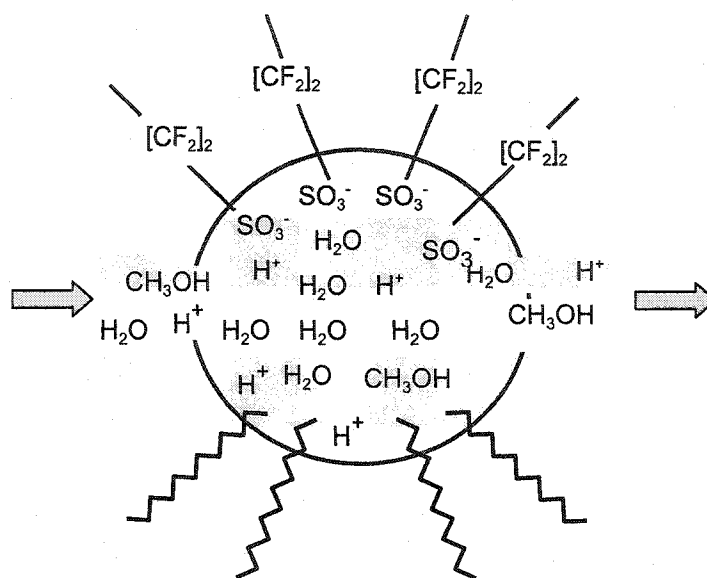


**Figure 1-6.** A schematic representation of ion transport channels in a hydrated Nafion<sup>®</sup> polymer.<sup>19</sup>

The electrode layers are generally composed of electrocatalyst and Nafion<sup>®</sup> ionomer. The electrodes have to be porous to allow methanol or oxygen to diffuse to the catalyst and to allow CO<sub>2</sub> or water to diffuse from the catalyst. The electrochemical reactions occur only in the *active zones* within the catalyst layers, where the nanoparticle metal catalyst is in contact with the electrolyte, and the electronic conductor, and it is in a region with good product and reactant mass transport. The structure of the electrode is crucial for catalyst utilization, and thereby for cell performance. It must be optimized so most of the catalyst particles are in active zones. The electrode structure depends strongly on the fabrication technique and the composition of the catalyst layer. Usually, MEAs for DMFCs are fabricated as follows: the catalyst is made into an ink with water and Nafion<sup>®</sup> ionomer solution. The ink is painted onto a Teflon<sup>®</sup> decal, and the resulting catalyst layer

on the decal is then transferred to a Nafion<sup>®</sup> membrane by hot-pressing.<sup>30, 31</sup> The catalyst ink can also be applied directly onto the Nafion<sup>®</sup> membrane by pour deposition or by spray deposition followed by evaporation.<sup>32</sup> Alternatively, the catalyst layer can be first applied onto wet-proofed carbon paper (or carbon cloth), and then hot-pressed into the Nafion<sup>®</sup> membrane.<sup>33-35</sup> The carbon paper acts as a gas diffusion layer in the fuel cell. Other methods for the fabrication of MEAs can be found in a recent review.<sup>36</sup>

The most likely applications for DMFCs are transportation (i.e. for fuel cell vehicles)<sup>2, 3, 37, 38</sup> and portable power (i.e. for cell phones, notebook computers, military communications).<sup>20, 39, 40</sup> The closest alternatives to DMFCs for such applications are H<sub>2</sub>/air PEMFC systems. H<sub>2</sub>/air PEMFC systems would likely operate on reformat (H<sub>2</sub> + CO<sub>2</sub>) generated on-board using a separate fuel processor (comprised of a reformer, a catalytic burner, and a CO removal unit). DMFC systems have advantages over such systems including simple system design (no fuel processing equipment is required), ease of operation, reduced weight, volume, and cost, and low emission (no NO<sub>x</sub>). As compared to H<sub>2</sub>/air PEMFC systems operating on compressed pure H<sub>2</sub> gas stored on-board, DMFC systems use liquid methanol as fuel, which is easier to handle, store, and distribute than high pressure H<sub>2</sub> gas. In addition, methanol has a higher volumetric energy density than H<sub>2</sub> and it is available in large quantities from natural gas or renewable biomass.<sup>19</sup>

The major problems in the development of direct methanol fuel cells are: (1) methanol electrooxidation is slow, resulting in high anode activation overpotentials ( $\eta_{act}$ ).<sup>41</sup> The poor anode kinetics results from the complex electrochemical oxidation of methanol to CO<sub>2</sub>, which involves transfer of six electrons in several steps (*vide infra*). (2)

currently available solid electrolyte membranes (e.g. Nafion<sup>®</sup>) are permeable to methanol. As a result, methanol migrates from the anode to the cathode (methanol crossover). Methanol crossover leads to degradation of cathode performance by establishing a mixed potential, and it leads to oxidation of methanol at the cathode, degrading the fuel efficiency of the cell.<sup>42</sup> In addition, methanol vapor appears in the cathode exhaust, from which it would have to be removed. As a result of sluggish anode kinetics and methanol crossover, the performance and power densities of DMFCs are lower than H<sub>2</sub>/O<sub>2</sub>-PEMFCs. The ideal solution to methanol crossover would be the development of methanol impermeable solid electrolytes. An alternative would be the development of cathode catalysts that do not react with methanol. The use of such methanol insensitive cathode catalysts would still require that methanol vapor be removed from the cathode exhaust.

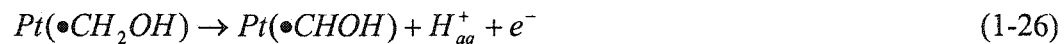
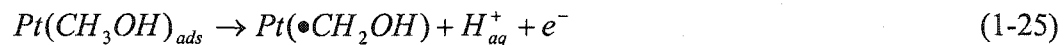
Better anode electrocatalysts are required to overcome the sluggish kinetics for electrooxidation of methanol.<sup>19</sup> These anode electrocatalysts must be (1) highly active, (2) cost-effective, (3) stable toward strong acid electrolytes, and (4) good electronic conductors. Numerous studies have been devoted to the development of catalysts for methanol electrooxidation in acid medium. Only Pt-based noble metal catalysts have fulfilled the requirements to a certain degree, i.e., relatively high activity, high stability, and good electronic conductivity, but at high cost. These Pt-based electrocatalysts include binary (e.g. Pt-Ru,<sup>43, 44</sup> Pt-Sn,<sup>45-59</sup> Pt-Mo,<sup>58, 60-62</sup> Pt-Re,<sup>63, 64</sup> Pt-WO<sub>x</sub>,<sup>65-67</sup> Pt-Ti,<sup>58</sup> Pt-Os,<sup>68-71</sup> and Pt-Ni<sup>72</sup>), ternary (e.g. Pt-Ru-Sn,<sup>73</sup> Pt-Ru-Os,<sup>74</sup> Pt-Ru-W,<sup>75</sup> Pt-Ru-Mo,<sup>76</sup> and Pt-Ru-Ni<sup>77</sup>), and quaternary systems (e.g. Pt-Ru-Os-Ir,<sup>78, 79</sup> Pt-Ru-Sn-W,<sup>80</sup> and Pt-Ru-Mo-W<sup>81</sup>). Among these Pt-based electrocatalysts, the Pt-Ru system is the most



studied, and it is demonstrably the most promising anode catalyst in actual prototype PEM-DMFCs.

### 3. The Mechanism of Methanol Electrooxidation over Pt-Ru Systems

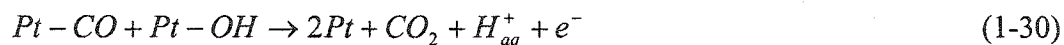
The mechanism of methanol electrooxidation over Pt and Pt-Ru surfaces has been extensively studied over the last four decades. A typical mechanism is given below.<sup>82-85</sup> The dots in the following equations denote the atoms possibly bound to the Pt or Ru surface sites.



The first step in the reaction is the physical adsorption of methanol onto the Pt surface (Eq. 1-24). This adsorption is followed by a sequence of dehydrogenation steps that eventually lead to the formation of adsorbed CO (Eq. 1-25 to 1-28). The removal of the adsorbed CO requires the presence of labile, adsorbed oxygen containing species (denoted as OH), which are generated from the dissociation of water according to the reaction (Eq. 1-29):

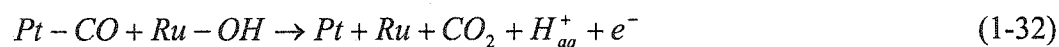


The final step is the oxidation of adsorbed CO by the adsorbed oxygen containing species OH to give carbon dioxide (Eq. 1-30).



Steps 1-24 to 1-28 proceed fast even at low temperature and at low electrode potentials (i.e. < 0.2 V vs. RHE).<sup>86, 87</sup> The adsorbed OH is not formed at a significant rate on Pt surfaces at low potentials (i.e., < 0.7 V vs. RHE)<sup>88, 89</sup> and low temperatures. Therefore, step (1-29) is the rate-determining step (r.d.s.).<sup>82</sup> The rapidly accumulated strongly adsorbed CO species poison the Pt catalysts by blocking the surface active sites from the adsorption of methanol molecules.<sup>82, 83, 84</sup> As a result, pure Pt surfaces are not effective electrocatalysts for methanol electrooxidation.

Incorporation of ruthenium, either as an adatom or a bimetal enhances the rate of electrooxidation of methanol over Pt.<sup>43, 87, 90</sup> This improvement mainly arises from the dissociation of water over Ru surfaces to form labile oxygen-containing species OH occurring at potentials as low as 0.2 V (Eq. 1-31).<sup>91-94</sup> The presence of Ru increases the amount of OH on the catalyst surface at low potentials, thereby accelerating the oxidative removal of adsorbed CO (Eq. 1-32).



This mechanism is called the *bifunctional mechanism*, in which Pt activates methanol to form CO, and Ru activates H<sub>2</sub>O to form OH.<sup>43</sup> Studies also show that the presence of Ru alters the electronic structure of Pt in a way that weakens the Pt-CO bond (e.g., by decreasing the back donation to CO), thereby increasing the CO oxidation rate.<sup>95</sup>  
<sup>96</sup> This electronic effect is referred to as the *ligand effect*, and its contribution relative to the bifunctional effect is believed to be small.<sup>97 98</sup>

Gasteiger and co-workers<sup>99, 100</sup> studied methanol electrooxidation over well-defined shiny Pt-Ru alloy surfaces. They found that Pt-Ru surfaces with 10% Ru were the most active at 25 °C, and pure Ru is inactive at this temperature. Based on this result and the fact that the maximum concentration of three-fold Pt ensembles on Pt-Ru alloy surfaces occurs near 10% Ru, they proposed that, at room temperature, methanol dehydrogenation to CO is the rate-limiting step. This dehydrogenation of methanol occurs only at threefold Pt ensembles because three neighbor Pt atoms are needed for a complete dehydrogenation of one methanol molecule (Figure 1-7). When the reaction temperature was increased to 60 °C, the Pt-Ru alloy surface with 33% Ru was the most active, and pure Ru became active at this temperature. They suggest that at temperatures > 60 °C, methanol dehydrogenation to CO, as well as water dissociation to OH are in pre-equilibrium; the bi-molecular surface reaction between CO and OH is the rate-limiting step, so the rate of methanol electrooxidation is determined by the product of the surface coverage of CO and OH ( $r = k\theta_{\text{CO}}\theta_{\text{OH}}$ ). The formation of OH primarily occurs at Ru sites, and methanol dehydrogenation occurs on both Pt and Ru sites at temperatures > 60 °C (any three surface sites can serve to dehydrogenate methanol). A 1:1 Pt-Ru surface atomic ratio will maximize the product of the surface coverage of CO and OH, so Pt<sub>50</sub>-Ru<sub>50</sub> is the most active at temperatures > 60 °C. These conclusions were made using shiny bulk Pt-Ru alloys assuming a uniform distribution of Ru in Pt. Studies on the optimum surface ratio of Pt to Ru using other Pt-Ru systems (Ru decorated Pt single crystal, nanoparticle Pt-Ru) will be discussed in Chapter 3.

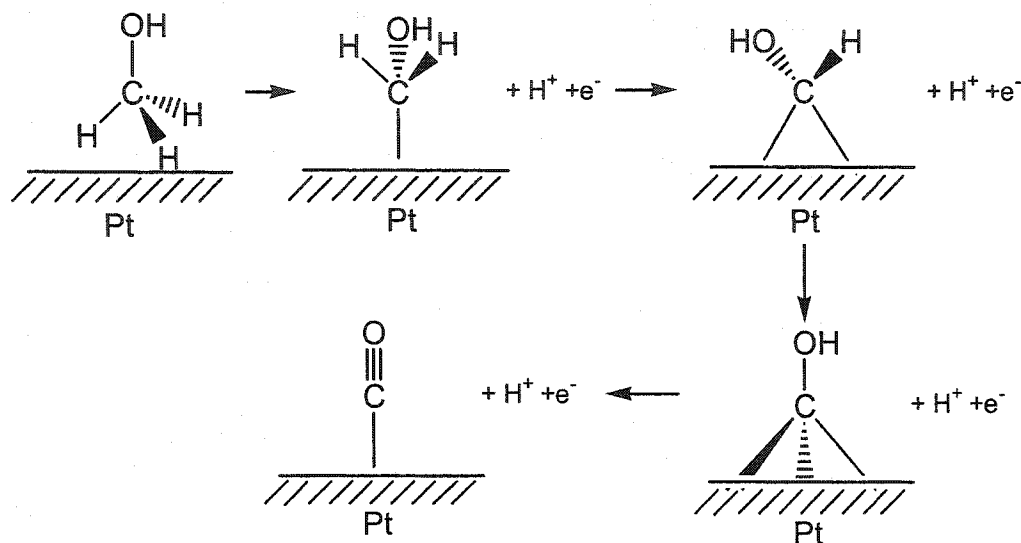


Figure 1-7. Methanol adsorption and dehydrogenation on Pt surfaces.<sup>22</sup>

#### 4. Deposition of $\text{Ru}_{\text{ad}}$ (adatom) on Pt Surfaces

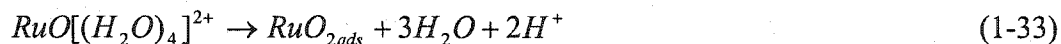
Deposition of  $\text{Ru}_{\text{ad}}$  onto Pt surfaces is the most convenient method to prepare Pt-Ru catalysts for studies. For example, Pt- $\text{Ru}_{\text{ad}}$  catalysts with various surface properties (structure, composition, chemical state) can be obtained by employing different Pt substrates (single crystals, polycrystallines, nanoparticles), different deposition techniques, or different deposition conditions. One of the major challenges for the study of Pt-Ru nanoparticles is the measurement of the number of surface active sites (see introduction sections in Chapters 2 and 3). If Pt-Ru nanoparticles are prepared by depositing submonolayer  $\text{Ru}_{\text{ad}}$  onto Pt nanoparticles, and if no major changes in surface area of Pt nanoparticles occur during the  $\text{Ru}_{\text{ad}}$  deposition reaction, then the surface area of the resulting Pt- $\text{Ru}_{\text{ad}}$  nanoparticles is equal to the surface area of Pt nanoparticles. The surface area of Pt nanoparticles can be determined using electrochemical methods, such as cyclic voltammetry in aqueous acid (see experimental section in Chapter 2). The real

activity of the Pt-Ru<sub>ad</sub> nanoparticles (turnover number) can, thereby, be obtained by normalizing the currents to the initial surface area of the Pt nanoparticles. Several methods to deposit Ru<sub>ad</sub> onto surfaces of Pt have been studied. These methods include electrodeposition (electrochemical reduction of Ru),<sup>43, 44, 76, 101-112</sup> Ru metal vapor deposition (MVD)<sup>97, 113-116</sup> chemical vapor deposition (CVD),<sup>117-119</sup> spontaneous deposition,<sup>70, 71, 96, 103, 120-128</sup> organometallic surface chemistry deposition,<sup>129-132</sup> and surface reductive deposition.<sup>58, 133-136</sup> Of these methods, spontaneous deposition, surface organometallic chemistry, and surface reductive deposition can be used to prepare Pt-Ru<sub>ad</sub> nanoparticles. These methods will be discussed below.

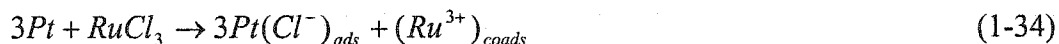
#### 4.1 Spontaneous Deposition

Spontaneous deposition of Ru<sub>ad</sub> onto Pt surfaces was developed by Wieckowski and co-workers.<sup>121-127</sup> This method has been adopted in other research groups recently.<sup>103, 128</sup> Spontaneous deposition can be virtually carried out on any Pt substrate (Pt single crystal surfaces, smooth polycrystalline Pt surfaces, nanoparticle Pt surfaces) to prepare both model and technical grade Pt-Ru<sub>ad</sub> catalysts. The spontaneous deposition is generally carried out as follows: a solution of RuCl<sub>3</sub> in 0.1 M HClO<sub>4</sub> is prepared and aged for 2-3 weeks to obtain a stable yellow/orange solution containing the complex [RuO(H<sub>2</sub>O)<sub>4</sub>]<sup>2+</sup>. Pt substrates (cleaned by several potential sweeps) are immersed into the RuO[(H<sub>2</sub>O)<sub>4</sub>]<sup>2+</sup>-containing solution at open circuit. Irreversible chemisorption of the RuO[(H<sub>2</sub>O)<sub>4</sub>]<sup>2+</sup> on surfaces of Pt occurs during the immersion period, resulting in the formation of adsorbed Ru oxides on Pt surfaces (Eq. 1-33). The Pt-Ru oxide system is removed from the ruthenium solution and is rinsed with pure water. The adsorbed Ru oxides are then reduced electrochemically (by applying several potential sweeps between 0.06 V to 0.8 V

vs. RHE) to form strongly adsorbed ruthenium or  $RuO_{ads}$  islands. The deposition stops after a fixed quantity of Ru oxides was deposited. The amount of Ru deposited depends on the crystallography of the Pt substrates, and can be increased by repeating the whole deposition process. This spontaneous deposition is a self-limiting, two-step process.



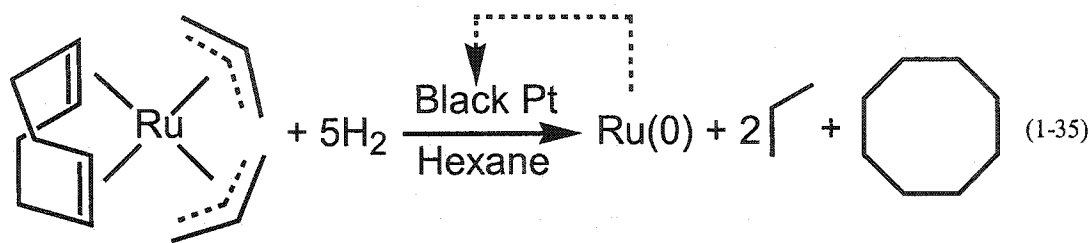
Vielstich and co-workers also investigated spontaneous deposition of Ru on single crystal Pt.<sup>128</sup> They carried out the deposition using freshly prepared, instead of aged,  $RuCl_3$  solution (with or without  $HClO_4$ ). Aging effects were observed in a few minutes to hours, which affected the reproducibility of the Ru depositions. They suggest that the deposition proceeds via prior adsorption of  $Cl^-$  on the clean Pt, with  $Ru^{3+}(aq)$  acting as counterions and thereby being coadsorbed on Pt (Eq. 1-34). The co-adsorbed  $Ru^{3+}$  is then electrochemically reduced to  $Ru^0$ , and the  $Cl^-$  is desorbed during the electrochemical reduction. Vielstich and co-workers also carried out direct reduction deposition of Ru on Pt(111) by bubbling hydrogen gas through aqueous  $RuCl_3$  in the presence of Pt(111).<sup>128</sup>



#### 4.2 Surface Organometallic Chemistry(SOMC)

In Bergens' group, the deposition of Ru on Pt (either polycrystalline Pt gauzes or nanoparticle Pt black) was carried out using the surface-directed hydrogenation of  $Ru(1,5\text{-cyclooctadiene})(\eta^3\text{-}C_3H_5)_2$  over Pt surfaces.(Eq. 1-35).<sup>129-137</sup> The amount of Ru deposited was monitored in real time by measuring the amount of cyclooctane produced, so this organometallic surface chemistry approach realized real time control over the Ru

surface concentration of the resulting Pt-Ru<sub>ad</sub> systems. The Ru metal was deposited on Pt in one step, without post electrochemical treatment.

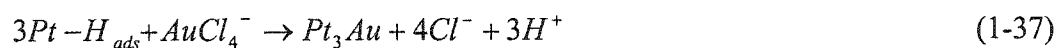


#### 4.3 Surface Reductive Deposition

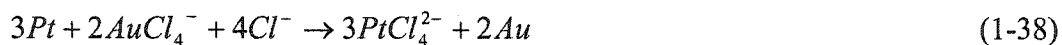
Surface reductive deposition of Ru on Pt surfaces was carried out in aqueous solution using RuCl<sub>3</sub> as the Ru<sub>ad</sub> source and using pre-adsorbed hydrogen on Pt surfaces as reducing agent. This method was first described in a patent three decades ago by Pott,<sup>134</sup> and it was used later on by Janssen et al.<sup>58, 133</sup> and Szabo et al.<sup>135, 136</sup> to prepare Pt-Ru<sub>ad</sub> for methanol electrooxidation (Eq. 1-36).



In the studies performed by Janssen and Szabo et al., pre-adsorbed hydrogen on Pt surfaces was formed electrochemically by holding the Pt electrode potential at 0.05 V vs RHE in an acid electrolyte, the Pt surface with saturated hydrogen was then transferred to an aqueous RuCl<sub>3</sub> solution. The hydrogen adsorbed by the Pt surface reduced a certain amount of RuCl<sub>3</sub> to deposit Ru<sub>ad</sub> onto Pt surfaces. In the last decade, Barbier, Szabo and their co-workers prepared a series of M-M'<sub>ad</sub> catalysts for non-electrochemical reactions using a similar methodology (Eq. 1-37). These catalysts include Pt-Au<sub>ad</sub>,<sup>138-144</sup> Pt-Cu<sub>ad</sub>,<sup>145</sup> Pd-Pt<sub>ad</sub>,<sup>146-150</sup> Pt-Re<sub>ad</sub>,<sup>151-156</sup> Rh-Cu<sub>ad</sub>,<sup>157</sup> Pt-Rh<sub>ad</sub>,<sup>158</sup> Pd-Sn<sub>ad</sub>,<sup>159</sup> and Pt-Pd<sub>ad</sub>.<sup>160</sup> They also found that the substrate metal itself can act as the



reducing agent for the ions of the second metal. For example, in Equation 1-38, Pt acts as the substrate metal as well the reducing agent.  $AuCl_4^-$  was reduced by the surface Pt atoms, resulting in the formation of Pt-Au<sub>ad</sub>.



Recently, Adzic and co-workers<sup>161-165</sup> applied this technique to the deposition of Pt on Ru to prepare Ru-Pt<sub>ad</sub> catalysts for fuel cell applications. In this deposition, Ru acts as reducing agent. The driving force for the deposition is in part the difference between the potential for  $[PtCl_6]^{2-}$  reduction, and that for Ru<sup>0</sup> oxidation. This deposition is not a self-limiting process, i.e., it will, in principle, proceed until all the accessible Ru is oxidized. Adzic and co-workers showed that the amount and distribution of Pt deposited on the surface of Ru(0001) depend on the concentration of  $[PtCl_6]^{2-}$  and the deposition time. For example, if a freshly prepared Ru(0001) single crystal is immersed in a  $10^{-4}$  M  $[PtCl_6]^{2-} + 0.1$  M  $H_2SO_4$  solution for 2 min, about 35% of the Ru surface is covered with a great number of Pt nanoparticles. The Pt nanoparticles have a columnar shape and relatively uniform size, with heights in the range of 3-5 nm (10-15 monolayer), and with diameters between 6 and 10 nm. If the Ru(0001) single crystal is immersed in a  $10^{-2}$  M  $[PtCl_6]^{2-} + 0.1$  M  $H_2SO_4$  solution for 1 min, the entire Ru surface is covered with 2-6 nm-sized Pt clusters. This deposition of Pt also occurs on carbon-supported Ru nanoparticles (10 wt% Ru/Vulcan XC-72, E-TEK) reduced in  $H_2$  at elevated temperatures (e.g., 300 °C). The resulting Ru-Pt<sub>ad</sub>/C (nominal atomic ratio of Pt:Ru is 1:20) catalyst has high activity and CO tolerance surpassing those of a commercial 1:1 Pt-Ru alloy catalyst (E-TEK) as tested in an electrochemical cell (not in real fuel cells).



## 5. Research Proposal

It is known that the catalytic activity of Pt-Ru surfaces toward methanol electrooxidation depends on Pt-Ru surface properties, including surface composition (the ratio of surface Pt to surface Ru), surface structure (Ru distribution on surfaces, Pt crystal faces), and surface chemical states, as well as particle size. A large number of studies have been carried out to identify how these surface properties of Pt-Ru systems affect their catalytic activities toward methanol electrooxidation in order to optimize Pt-Ru surfaces for application as the anode catalyst in DMFCs. The majority of these studies were performed on flat, well-defined model catalysts, because these flat model systems are easier to experimentally investigate than rough, nanoparticle systems in terms of obtaining information about surface properties, and information about the number of active sites, thereby allowing for better normalized and controlled comparison of absolute catalyst activity. However, the relatively poorly surface characterized, less-studied rough Pt-Ru nanoparticles more represent real world catalysts in prototype fuel cells. The highest level of accurate catalyst optimization would be the use of Pt-Ru nanoparticles of known, controlled surface properties in actual prototype fuel cells over long periods of operation.

My research mission is, first, to prepare technical-scale nanoparticle Pt-Ru catalysts of known surface area (number of active sites) and controlled surface composition, and then to investigate methanol electrooxidation over these practical nanoparticle Pt-Ru catalysts in both liquid acid electrolyte environments (3-electrode cells) and in real prototype DMFCs. Such studies are expected to help to clarify the controversial results regarding the optimum Pt-Ru composition obtained using model and

technical systems. These studies may also help to determine if there is a difference between methanol electrooxidation on model and on technical Pt-Ru catalysts. Further, these studies will show if Pt-Ru catalysts perform differently in a 3-electrode electrochemical cell and a prototype DMFC.

The strategy that will be used for the preparation of nanoparticle Pt-Ru catalysts of known surface area is the use of the Pt-Ru<sub>ad</sub> system. Pt-Ru<sub>ad</sub> will be prepared by the deposition of Ru on nanoparticle Pt of known surface area. The resulting Pt-Ru<sub>ad</sub> catalysts will have the same surface area as Pt substrates, if no significant changes in Pt surfaces occur during the depositions. To realize control over the surface composition of Pt-Ru<sub>ad</sub>, self-limiting deposition of Ru on surfaces of Pt will be developed. The stability of Pt-Ru<sub>ad</sub> systems will be investigated to address the concern that such systems are impractical catalysts for fuel cells because desorption of Ru adatoms from Pt surfaces may occur during cell operation.

Some exploratory investigations on direct liquid feed 2-propanol fuel cells based on Nafion® membrane technology will be carried out.

## References

- (1) EG&G Services Parsons, Inc. Science Applications International Corporation, *Fuel Cell Handbook (Fifth Edition)*, 2000.
- (2) Kordesch, K.; Simander, G. *Fuel Cells and Their Applications*, VCH, New York, 1996.
- (3) Larminie, J.; Dicks, A. *Fuel cell systems explained*; Wiley: New York, 2000.
- (4) Hoogers, G. *Fuel cell technology handbook*; CRC Press: Boca Raton, Fla., 2003.
- (5) Carrette, L.; Friedrich, K. A.; Stimming, U. *Fuel Cells* **2001**, *1*, 5-39.

- (6) Carrette, L.; Friedrich, K. A.; Stimming, U. *Phys. Chem. Chem. Phys.* **2000**, *1*, 162-193.
- (7) Rostrup-Nielsen, J.R. *Phys. Chem. Chem. Phys.* **2001**, *3*, 283-288.
- (8) Geissler, K.; Newson, E.; Vogel, F.; Troung, T-B.; Hottinger, P.; Wokaun, A. *Phys. Chem. Chem. Phys.* **2001**, *3*, 289-293.
- (9) Cairns, E.J.; Liebhaf, H. A. *Energy Conversion* **1969**, *9*, 63-69.
- (10) Nowell, G.P. *The Promise of Methanol Fuel Cell Vehicles*, American Methanol Institute, **2000**.
- (11) Cacciola, G.; Antonucci, V.; Freni, S. *J. Power Sources* **2001**, *100*, 67-79.
- (12) <http://www.fuelcelltoday.com>.
- (13) <http://www.fuelcells.org>.
- (14) Oniciu, L. *Fuel cells*; Abacus Press: Tunbridge Wells, 1976.
- (15) Bard, A. J.; Faulkner, L. R. *Electrochemical methods: fundamentals and applications*; 2nd ed.; Wiley: New York, 2001.
- (16) Aricò, A. S.; Srinivasan, S.; Antonucci, V. *Fuel Cells* **2001**, *1*, 133-161.
- (17) Narayanan, S. R.; Valdez, T.; Kindler, A.; Witham, C.; Surampudi, S.; Frank, H. In *Annual battery conference on applications and advances Manufacturers Association.*; Das, R. S. L., Frank, H., Eds.; Ieee; 1999: Long Beach, CA, 2000; pp 33-36.
- (18) Baldauf, M.; Preidel, W. *J. Power Sources* **2000**, *84*, 161-166.
- (19) Schultz, T.; Zhou, S.; Sundmacher, K. *Chem. Eng. Tech.* **2001**, *24*, 1223-1233.
- (20) Ren, X.; Zelenay, P.; Thomas, S.; Davey, J.; Gottesfeld, S. *J. Power Sources* **2000**, *86*, 111-116.
- (21) Wasmus, S.; Kuver, A. *J. Electroanal. Chem.* **1999**, *461*, 14-31.
- (22) Hogarth, M. P.; Hards, G. A. *Plat. Met. Rev.* **1996**, *40*, 150-159.
- (23) Cameron, D. S.; Hards, G. A.; Harrison, B.; Potter, R. J. *Plat. Met. Rev.* **1987**, *31*, 173-181.
- (24) Williams, K. R. *Advan. Sci.* **1966**, *22*, 617-622.
- (25) Lamy, C.; Lima, A.; LeRhun, V.; Delime, F.; Coutanceau, C.; Leger, J. M. *J. Power Sources* **2002**, *105*, 283-296.
- (26) Adams, D. R. *Fuel cells: power for the future*, Fuel Cell Research Associations, **1960**.

- (27) Lamy, C.; Belgsir, E. M.; Leger, J. M. *J. Appl. Electrochem.* **2001**, *31*, 799-809.
- (28) Gottesfeld, S. (with Zawodzinski, T.), Polymer electrolyte fuel cells, in: Tobias, C.; Gerischer, H.; Kolb, D.; Alkire, R. (Eds.), *Advances in Electrochemistry and Electrochemical Engineering*, Wiley, VCH, New York, **1997**, *5*, 195.
- (29) Appleby, A.J.; Foulkes, F.R. *Fuel Cell Handbook*, Van Nostrand Reinhold, New York, **1989**.
- (30) Ren, X.; Wilson, M. S.; Gottesfeld, S. *J. Electrochem. Soc.* **1996**, *143*, L12-L15.
- (31) Wilson, M. S.; Gottesfeld, S. *J. Appl. Electrochem.* **1992**, *22*, 1-7.
- (32) Chun, W.; Narayanan, S. R.; Jeferies-Nakamura, B.; Valdnz, T.L.; Link, J. WO99/39841, **1999**.
- (33) Shukla, A. K.; Christensen, P. A.; Dickinson, A. J.; Hamnett, A. *J. Power Sources* **1998**, *76*, 54-59.
- (34) Shukla, A. K.; Ravikumar, M. K.; Neergat, M.; Gandhi, K. S. *J. Appl. Electrochem.* **1999**, *29*, 129-132.
- (35) Scott, K.; Taama, W.; Cruickshank, J. *J. Appl. Electrochem.* **1998**, *28*, 289-297.
- (36) Metha, V.; Cooper, J. S. *J. Power Source* **2003**, *114*, 32-53
- (37) Shukla, A. K.; Ravikumar, M. K.; Gandhi, K. S. *J. Solid-State Electrochem.* **1998**, *2*, 117-122.
- (38) Moore, R. M. In *Fuel cell power for transportation*; Sae; 2000: Detroit, MI, **2000**; pp 71-76.
- (39) Valdez, T. I.; Narayanan, S. R.; Frank, H.; Chun, W. In *Annual battery conference on applications and advances*; Frank, H. A., Seo, E. T. p., platform. All Rights, R., Eds.; Ieee; 1997: Long Beach; CA, **1997**; pp 239-244.
- (40) Gottesfeld, S.; Ren, X.; Thomas, S.; Zelenay, P. In *Fuel cell: clean energy for today's world*; Washington DC; Courtesy Associates; 1998: Palm Springs; CA, **1998**; pp 745-748.
- (41) Burstein, G. T.; Barnett, C. J.; Kucernak, A. R.; Williams, K. R. *Catal. Today* **1997**, *38*, 425-438.
- (42) Heinzl, A.; Barragán, V. M. *J. Power Sources* **1999**, *84*, 70-74.
- (43) Watanabe, M.; Motoo, S. *J. Electroanal. Chem.* **1975**, *60*, 267-273.
- (44) Watanabe, M.; Motoo, S. *J. Electroanal. Chem.* **1975**, *60*, 275-283.

- (45) Jones, F. E.; Milne, S. B.; Gurau, B.; Smotkin, E. S.; Stock, S. R.; Lukehart, C. M. *J. Nanosci. Nanotech.* **2002**, *2*, 81-87.
- (46) Rahim, M. A. A.; Khalil, M. W.; Hassan, H. B. *J. Appl. Electrochem.* **2000**, *30*, 1151-1155.
- (47) Morimoto, Y.; Yeager, E. B. *J. Electroanal. Chem.* **1998**, *444*, 98-100.
- (48) Wang, K.; Gasteiger, H. A.; Markovic, N. M.; Ross, P. N. *Electrochim. Acta* **1996**, *41*, 2587-2593.
- (49) Wei, Z.; Guo, H.; Tang, Z. *J. Power Sources* **1996**, *58*, 239-242.
- (50) Arico, A. S.; Antonucci, V.; Giordano, N.; Shukla, A. K.; Ravikumar, M. K.; Roy, A.; Barman, S. R.; Sarma, D. D. *J. Power Sources* **1994**, *50*, 295-309.
- (51) Frelink, T.; Visscher, W.; Van Veen, J. A. R. *Electrochim. Acta* **1994**, *39*, 1871.
- (52) Frelink, T.; Visscher, W.; Veen, J. A. R. v. *Surf. Sci.* **1995**, *335*, 353-360.
- (53) Sobkowski, J.; Franaszuk, K.; piasecki, A. *J. Electroanal. Chem.* **1985**, *169*, 145-156.
- (54) Bittins-Cattaneo, B.; Iwasita, T. *J. Electroanal. Chem.* **1987**, *238*, 151-161.
- (55) Watanabe, M.; Furuuchi, Y.; Motoo, S. *J. Electroanal. Chem.* **1985**, *191*, 367-375.
- (56) Motoo, S.; Shibata, M.; Watanabe, M. *J. Electroanal. Chem.* **1980**, *110*, 103-109.
- (57) McNicol, B. D.; Short, R. T.; Chapman, A. G. *J. Chem. Soc., Faraday Trans. 1* **1976**, *72*, 2735-2743.
- (58) Janssen, M. M. P.; Moolhuysen, J. *Electrochim. Acta* **1976**, *21*, 869-878.
- (59) Ishikawa, Y.; Liao, M.-S.; Cabrera, C. R. *Surf. Sci.* **2000**, *463*, 66-80.
- (60) Wang, Y.; Fachini, E. R.; Cruz, G.; Zhu, Y.; Ishikawa, Y.; Colucci, J. A.; Cabrera, C. R. *J. Electrochem. Soc.* **2001**, *148*, C222-C226.
- (61) Lukehart, C. M.; Boxall, D. L.; Corn, J. D.; Hariharasarma, M.; King, W. D.; Kwiatkowski, K. C.; Steigerwalt, E. S.; Kenik, E. A. *Prepr. Symp. Am. Chem. Soc., Div. Fuel Chem.* **1999**, *44*, 982-986.
- (62) Shropshire J.A. *J. Electrochem. Soc.* **1965**, *112*, 465-471.
- (63) Cathro, K.J. *J. Electrochem. Soc.* **1969**, *116*, 1608-1611.
- (64) Grgur, B.N.; Markovic, N.M.; Ross, P.N. *Electrochim. Acta* **1998**, *43*, 3631-3635.
- (65) Rajesh, B.; Karthik, V.; Karthikeyan, S.; Ravindranathan Thampi, K.; Bonard, J.-M.; Viswanathan, B. *Fuel* **2002**, *81*, 2177-2190.

- (66) Shukla, A. K.; Ravikumar, M. K.; Arico, A. S.; Candiano, G. *J. Appl. Electrochem.* **1995**, *25*, 528-532.
- (67) Shen, P. K.; Tseung, A. C. C. *J. Electrochem. Soc.* **1994**, *141*, 3082-3090.
- (68) Zhu, Y. M.; Cabrera, C. R. *Electrochem. Solid-State Lett.* **2001**, *4*, A45-A48.
- (69) Moore, J. T.; Lukehart, C. M.; Deluga, G.; Chu, D. *Abstr. Papers Am. Chem. Soc.* **2001**, *222*, 561-INOR.
- (70) Crown, A.; Wieckowski, A. *Phys. Chem. Chem. Phys.* **2001**, *3*, 3290-3296.
- (71) Crown, A.; Moraes, I. R.; Wieckowski, A. *J. Electroanal. Chem.* **2001**, *500*, 333-343.
- (72) Park, K. W.; Choi, J. H.; Kwon, B. K.; Lee, S. A.; Sung, Y. E.; Ha, H. Y.; Hong, S. A.; Kim, H.; Wieckowski, A. *J. Phys. Chem. B* **2002**, *106*, 1869-1877.
- (73) Troughton, G.L.; Hamnett, A. *Bull. Electrochem.* **1991**, *7*, 488-492.
- (74) Ley, K. L.; Liu, R.; Pu, C.; Fan, Q.; Leyarovska, N.; Segre, C.; Smotkin, E. S. *J. Electrochem. Soc.* **1997**, *144*, 1543-1548.
- (75) Götz, M.; Wendt, H. *Electrochim. Acta* **1998**, *43*, 3637-3644.
- (76) Lima, A.; Coutanceau, C.; Leger, J. M.; Lamy, C. *J. Appl. Electrochem.* **2001**, *31*, 379-386.
- (77) Gorer, A. *WO 055928*, 2000.
- (78) Reddington, E.; Sapienza, A.; Gurau, B.; Viswanathan, R.; Sarangapini, S.; Smotkin, E. S.; Mallouk, T. E. *Science* **1998**, *280*, 1735-1737.
- (79) Gurau, B.; Viswanathan, R.; Liu, R. X.; Lafrenz, T. J.; Ley, K. L.; Smotkin, E. S.; Reddington, E.; Sapienza, A.; Chan, B. C.; Mallouk, T. E.; Sarangapani, S. *J. Phys. Chem. B* **1998**, *102*, 9997-10003.
- (80) Arico, A. S.; Creti, P.; Giordano, N.; Antonucci, V.; Antonucci, P. L.; Chuvilin, A. *J. Appl. Electrochem.* **1996**, *26*, 959-967.
- (81) Choi, W. C.; Kim, J. D.; Woo, S. I. *Catal. Today* **2002**, *74*, 235-240.
- (82) Leger, J. M. *J. Appl. Electrochem.* **2001**, *31*, 767-771.
- (83) Beden, B.; Lamy, C.; Leger, J-M. in *Modern Aspects of Electrochemistry* Bockris, J. O'M.; Conway, B.E.; Whites. R.E. (eds.) Plenum Press, New York **1992**, *22*, 97.
- (84) Jarvi, T.J.; Stuve, E.M. in *Electrocatalysis*, Lipkowski, J.; Ross, P.N. (eds.) Wiley-VCH, New York, 1998, Chapter 3.

- (85) Hamnett, A. *Catal. Today* **1997**, *38*, 445-457.
- (86) Bagotzky, V.S.; Vasilyev, Yu. B. *Electrochim. Acta* **1964**, *9*, 869-877.
- (87) Petry, O.A.; Podlovchenko, B.I.; Frumpkin, A.N.; Lal, H. *J. Electroanal. Chem.* **1965**, *10*, 253-269.
- (88) Tilak, T.V.; Conway, B.E.; Angerstein-Kozłowska H. *J. Electroanal. Chem.* **1973**, *48*, 1-23.
- (89) Li, N.H.; Sun, S.G.; Chen, S.P. *J. Electroanal. Chem.* **1997**, *430*, 57-67.
- (90) Bockris, J. O' M.; Wroblowa, H. *J. Electroanal. Chem.* **1964**, *7*, 428-451.
- (91) Ticanelli, E.; Beery, J. G.; Paffett, M. T.; Gottesfeld, S. *J. Electroanal. Chem.* **1989**, *258*, 61-77.
- (92) Breiter, M. W. *J. Electroanal Chem* **1986**, *214*, 547-554.
- (93) Wasmus, S.; Vielstich, W. *J. Appl. Electrochem.* **1993**, *23*, 120-124.
- (94) Wasmus, S.; Wang, J. T.; Savinell, R. F. *J. Electrochem. Soc.* **1995**, *142*, 3825-3833.
- (95) Lin, W. F.; Iwasita, T.; Vielstich, W. *J Phys. Chem. B* **1999**, *103*, 3250-3257.
- (96) Tong, Y. Y.; Kim, H. S.; Babu, P. K.; Waszczuk, P.; Wieckowski, A.; Oldfield, E. *J. Am. Chem. Soc.* **2002**, *124*, 468-473.
- (97) Lu, C.; Masel, R. I. *J Phys. Chem. B* **2001**, *105*, 9793-9797.
- (98) Lu, C.; Rice, C.; Masel, R. I.; Babu, P. K.; Waszczuk, P.; Kim, H. S.; Oldfield, E.; Wieckowski, A. *J. Phys. Chem. B* **2002**, *106*, 9581 -9589.
- (99) Gasteiger, H. A.; Markovic, N.; Ross, P. N., Jr.; Cairns, E. J. *J. Phys. Chem.* **1993**, *97*, 12020-12029.
- (100) Gasteiger, H. A.; Markovic, N.; Ross, P. N.; Cairns, E. J. *J. Electrochem. Soc.* **1994**, *141*, 1795-1803.
- (101) Watanabe, M.; Genjima, Y.; Turumi, K. *J. Electrochem. Soc.* **1997**, *144*, 423-427.
- (102) Friedrich, K. A.; Geyzers, K. P.; Linke, U.; Stimming, U.; Stumper, J. *J. Electroanal. Chem.* **1996**, *402*, 123-128.
- (103) Vigier, F.; Gloaguen, F.; Leger, J. M.; Lamy, C. *Electrochim. Acta* **2001**, *46*, 4331-4337.
- (104) Laborde, H.; Leger, J.-M.; Lamy, C. *J. Appl. Electrochem.* **1994**, *24*, 1019-1027.

- (105) Meli, G.; Leger, J.-M.; Lamy, C.; Durand, R. *J. Appl. Electrochem.* **1993**, *23*, 197-202.
- (106) Frelink, T.; Visscher, W.; van Veen, J. A. R. *Langmuir* **1996**, *12*, 3702-3708.
- (107) Frelink, T.; Visscher, W.; Cox, A. P.; Veen, J. A. R. v. *Ber. Bunsen-Ges. Phys. Chem.* **1996**, *100*, 599-606.
- (108) Frelink, T.; Visscher, W.; Cox, A. P.; Van Veen, J. A. R. *Electrochim. Acta* **1995**, *40*, 1537-1543.
- (109) Kim, H.; de Moraes, I. R.; Tremiliosi, G.; Haasch, R.; Wieckowski, A. *Surf. Sci.* **2001**, *474*, L203-L212.
- (110) Massong, H.; Wang, H. S.; Samjeske, G.; Baltruschat, H. *Electrochim. Acta* **2000**, *46*, 701-707.
- (111) Chrzanowski, W.; Wieckowski, A. *Langmuir* **1998**, *14*, 1967-1970.
- (112) Lin, W. F.; Zei, M. S.; Eiswirth, M.; Ertl, G.; Iwasita, T.; Vielstich, W. *J Phys. Chem. B* **1999**, *103*, 6968-6977.
- (113) Hoster, H.; Iwasita, T.; Baumgartner, H.; Vielstich, W. *Phys. Chem. Chem. Phys.* **2001**, *3*, 337-346.
- (114) Davies, J. C.; Hayden, B. E.; Pegg, D. J.; Rendall, M. E. *Surf. Sci.* **2002**, *496*, 110-120.
- (115) Davies, J. C.; Hayden, B. E.; Pegg, D. J. *Surf. Sci.* **2000**, *467*, 118-130.
- (116) Davies, J. C.; Hayden, B. E.; Pegg, D. J. *Electrochim. Acta* **1998**, *44*, 1181-1190.
- (117) Lamouri, A.; Gofer, Y.; Luo, Y.; Chottiner, G.S.; Scherson, D.A. *J. Phys. Chem. B* **2001**, *105*, 6172-6177.
- (118) Lu, C.; Rice, C.; Masel, R. I.; Babu, P. K.; Waszczuk, P.; Kim, H. S.; Oldfield, E.; Wieckowski, A. *J Phys. Chem. B* **2002**, *106*, 9581-9589.
- (119) Waszczuk, P.; Lu, G. Q.; Wieckowski, A.; Lu, C.; Rice, C.; Masel, R. I. *Electrochim. Acta* **2002**, *47*, 3637-3652.
- (120) Franaszczuk, K.; Sobkowski, J. *J. Electroanal. Chem.* **1992**, *327*, 235-246.
- (121) Chrzanowski, W.; Wieckowski, A. *Langmuir* **1997**, *13*, 5974-5978.
- (122) Chrzanowski, W.; Kim, H.; Wieckowski, A. *Catal. Lett.* **1998**, *50*, 69-75.
- (123) Waszczuk, P.; Solla-Gullon, J.; Kim, H. S.; Tong, Y. Y.; Montiel, V.; Aldaz, A.; Wieckowski, A. *J. Catal.* **2001**, *203*, 1-6.



- (124) Crown, A.; Kim, H.; Lu, G. Q.; de Moraes, I. R.; Rice, C.; Wieckowski, A. *J. New Mat. Electrochem. Sys.* **2000**, *3*, 275-284.
- (125) Tremiliosi-Filho, G.; Kim, H.; Chrzanowski, W.; Wieckowski, A.; Grzybowska, B.; Kulesza, P. *J. Electroanal. Chem.* **1999**, *467*, 143-156.
- (126) Herrero, E.; Feliu, J. M.; Wieckowski, A. *Langmuir* **1999**, *15*, 4944-4948.
- (127) Crown, A.; Johnston, C.; Wieckowski, A. *Surf. Sci.* **2002**, *506*, L268-L274.
- (128) Iwasita, T.; Hoster, H.; John-Anacker, A.; Lin, W. F.; Vielstich, W. *Langmuir* **2000**, *16*, 522-529.
- (129) Lee, C. E.; Tiege, P. B.; Xing, Y.; Nagendran, J.; Bergens, S. H. *J. Am. Chem. Soc.* **1997**, *119*, 3543-3549.
- (130) Lee, C. E.; Bergens, S. H. *J. Phys. Chem. B* **1998**, *102*, 193-199.
- (131) Lee, C. E.; Bergens, S. H. *J. Electrochem. Soc.* **1998**, *145*, 4182-4185.
- (132) Fachini, E. R.; Cabrera, C. R. *Langmuir* **1999**, *15*, 717-721.
- (133) Janssen, M. M. P.; Moolhuysen, J. *Electrochim. Acta* **1976**, *21*, 861-868.
- (134) Pott, G. T. British Patent Application 7429/74 (see also British Patent 1,106,708).
- (135) Szabo, S.; Bakos, I. *J. Electroanal. Chem.* **1987**, *230*, 233-240.
- (136) Szabo, S.; Bakos, I.; Nagy, F. *J. Electroanal. Chem.* **1989**, *271*, 269-277.
- (137) Lee, C. E. Doctorate Thesis, Spring **2003**.
- (138) Del Angel, P.; Dominguez, J. M.; Del Angel, G.; Montoya, J. A.; Capilla, J.; Lamy-Pitara, E.; Barbier, J. *Topics in Catalysis* **2002**, *18*, 183-191.
- (139) Del Angel, P.; Dominguez, J. M.; Del Angel, G.; Montoya, J. A.; Lamy-Pitara, E.; Labruquere, S.; Barbier, J. *Langmuir* **2000**, *16*, 7210-7217.
- (140) Espinosa, G.; Del Angel, G.; Barbier, J.; Bosch, P.; Lara, V.; Acosta, D. *J. Mol. Catal. A-Chem.* **2000**, *164*, 253-262.
- (141) Barbier, J.; Marecot, P.; Del Angel, G.; Bosch, P.; Boitiaux, J. P.; Didillon, B.; Dominguez, J. M.; Schifter, I.; Espinosa, G. *Appl. Catal. A-Gen.* **1994**, *116*, 179-186.
- (142) Bertin, V.; Bosch, P.; Delangel, G.; Gomez, R.; Barbier, J.; Marecot, P. *J. Chim. Phys.-Chim. Biol.* **1995**, *92*, 120-133.
- (143) Bakos, I.; Szabo, S. *J. Electroanal. Chem.* **1994**, *369*, 223-226
- (144) Bakos, I.; Szabo, S. *J. Electroanal. Chem.* **1993**, *344*, 303-311.

- (145) Dumas, J. M.; Rmili, S.; Barbier, J. *J. Chim. Phys.-Chim. Biol.* **1998**, *95*, 1650-1665.
- (146) Micheaud-Especel, C.; Bazin, D.; Guerin, M.; Marecot, P.; Barbier, J. *React. Kinet. Catal. Lett.* **2000**, *69*, 209-216.
- (147) Szabo, S.; Bakos, I. *React. Kinet. Catal. Lett.* **2000**, *71*, 245-251.
- (148) Micheaud, C.; Marecot, P.; Guerin, M.; Barbier, J. *Appl. Catal. A-Gen.* **1998**, *171*, 229-239.
- (149) Micheaud, C.; Marecot, P.; Guerin, M.; Barbier, J. *J. Chim. Phys.-Chim. Biol.* **1997**, *94*, 1897-1905.
- (150) Micheaud, C.; Guerin, M.; Marecot, P.; Geron, C.; Barbier, J. *J. Chim. Phys.-Chim. Biol.* **1996**, *93*, 1394-1411.
- (151) Pieck, C. L.; Marecot, P.; Barbier, J. *Appl. Catal. A-Gen.* **1996**, *134*, 319-329.
- (152) Pieck, C. L.; Marecot, P.; Barbier, J. *Appl. Catal. A-Gen.* **1996**, *141*, 229-244.
- (153) Pieck, C. L.; Marecot, P.; Barbier, J. *Appl. Catal. A-Gen.* **1996**, *143*, 283-298.
- (154) Szabo, S.; Bakos, I. *React. Kinet. Catal. Lett.* **1997**, *62*, 267-271.
- (155) Szabo, S.; Bakos, I. *Preparation of Catalysts Vii* **1998**, *118*, 269-276.
- (156) Szabo, S.; Bakos, I. *React. Kinet. Catal. Lett.* **1998**, *65*, 259-263.
- (157) Dumas, J. M.; Geron, C.; Hadrane, H.; Marecot, P.; Barbier, J. *J. Mol. Catal. A-Chem.* **1992**, *77*, 87-98.
- (158) Bakos, I.; Szabo, S. *J. Electroanal. Chem.* **2003**, *547*, 103-107.
- (159) Bakos, I.; Szabo, S. *Electrochim. Acta* **2001**, *46*, 2507-2513.
- (160) Szabo, S.; Bakos, I. *React. Kinet. Catal. Lett.* **2000**, *71*, 245-251.
- (161) Brankovic, S. R.; Wang, J. X.; Adzic, R. R. *Electrochem. Solid-State Lett.* **2001**, *4*, A217-A220.
- (162) Brankovic, S. R.; Mcbreen, J.; Adzic, R. R. *J. Electroanal. Chem.* **2001**, *503*, 99-104.
- (163) Brankovic, S. R.; Mcbreen, J.; Adzic, R. R. *Surf. Sci.* **2001**, *479*, L363-L368.
- (164) Brankovic, S. R.; Wang, J. X.; Adzic, R. R. *J. Serbian Chem. Soc.* **2001**, *66*, 887-898.
- (165) Brankovic, S. R.; Wang, J. X.; Zhu, Y.; Sabatini, R.; Mcbreen, J.; Adzic, R. R. *J. Electroanal. Chem.* **2002**, *524*, 231-241.

## Chapter 2

### **An Organometallic Deposition of Ruthenium Adatoms on Platinum that Self Poisons at a Specific Surface Composition. A Direct Methanol Fuel Cell Using a Platinum-Ruthenium Adatom Anode Catalyst.<sup>†</sup>**

#### **1. Introduction**

A self-poisoning method to deposit Ru<sub>ad</sub> (adatom) onto Pt surfaces using an organometallic Ru precursor [Ru<sub>4</sub>(μ-H)<sub>4</sub>(CO)<sub>12</sub> (**1**)] was developed. This deposition uses a fairly air-stable, easily prepared Ru precursor, and it self-poisons by adsorbed CO at a specific surface Ru concentration (surface ratio of Ru<sub>ad</sub> to Pt).

It was first reported during the mid 1960's that Ru significantly enhances the activity of Pt towards the electrooxidation of methanol.<sup>1-6</sup> Much research has been carried out on Pt-Ru systems, and high specific surface area Pt-Ru nanoparticles (unsupported or supported on carbon) are now the most active anode electrocatalysts used in direct methanol fuel cells (DMFCs).<sup>7-15</sup> An issue indigenous to the study of Pt-Ru nanoparticles and rough (not atomically smooth) Pt-Ru surfaces is that their surface compositions and their real surface areas (number of active sites) are difficult to determine with accuracy. A further complication is that the most active commercial catalyst precursors exist as a mixture of mainly metallic Pt, with a small amount of hydrous and anhydrous Pt oxides (PtO<sub>v</sub>H<sub>x</sub>), some metallic Ru, and large amounts of hydrous and anhydrous Ru oxides

---

<sup>†</sup> A version of this chapter has been published. Cao, D. X.; Bergens, S. H. *J. Electroanal. Chem.* **2002**, *533*, 91-100.

( $\text{RuO}_y\text{H}_z$ ).<sup>16-20</sup> These oxides are to some degree either chemically or electrochemically reduced during conditioning and operation of the direct methanol fuel cell.<sup>16-20</sup> The nature and activity of Pt-PtO<sub>w</sub>H<sub>x</sub>-Ru-RuO<sub>y</sub>H<sub>z</sub> catalyst precursors change upon incorporation into, conditioning of, and operation of a DMFC.

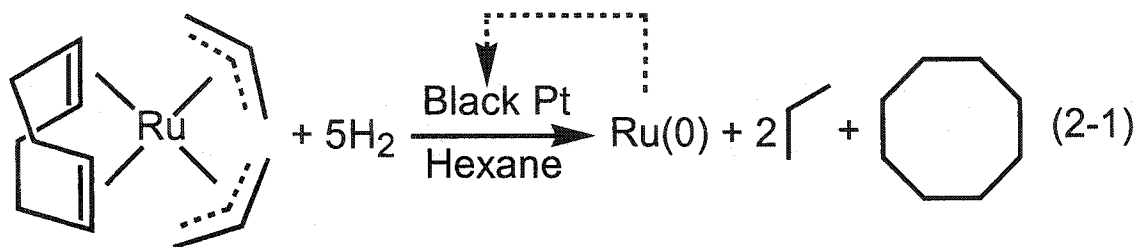
The most readily available method to probe the surface composition and real surface area of the metallic component in Pt-Ru nanoparticles is the potentiodynamic electrooxidation of a saturated monolayer of adsorbed CO.<sup>18, 21-35</sup> The real surface area of the metallic components (but not of the nonmetallic oxides) within these catalysts is estimated (or normalized) from the Faradaic charge for electrooxidation of the CO monolayer. This measurement can be complicated by uncertainties in the ratio of adsorbed CO to surface metal atoms at saturation, as well as by overlap of the Faradaic CO electrooxidation charge with charges associated with oxide formation.<sup>36, 37</sup> This overlap of the Faradaic CO electrooxidation and pseudocapacitive charges has been addressed using differential electrochemical mass spectroscopy (DEMS).<sup>38, 39</sup> The surface composition of the metallic component of these catalysts is estimated by comparing the peak potentials for the potentiodynamic electrooxidation of CO over the Pt-Ru nanoparticles to peak potentials obtained over bulk, atomically smooth Pt-Ru alloys of known surface composition (measured by low energy ion scattering).<sup>18</sup> Application of this method to nanoparticles remains to be confirmed by independent measurement. The potentiodynamic response in aqueous acid has also been used to estimate the surface composition and the real surface area of Pt-Ru nanoparticles.<sup>36, 37, 40-44</sup> This technique is complicated, however, by overlap of the hydride, double layer, and oxide regions of the voltammograms. Other methods used to measure the surface composition and real

surface area of supported Pt-Ru particles are selective gas titration<sup>45</sup> and underpotential deposition of Cu.<sup>46</sup>

An approach that addresses some of these issues in the study of Pt-Ru nanoparticle and bulk alloy surfaces is the use of Pt-Ru<sub>ad</sub> systems prepared by deposition of Ru<sub>ad</sub> on Pt. By using Pt substrates of known real surface area, the electrocatalytic activities of Pt-Ru<sub>ad</sub> electrodes can be normalized to the initial real surface area of Pt (if no major changes in the number of active sites occur during the Ru<sub>ad</sub> deposition reaction). Depending on the distribution of Ru<sub>ad</sub> on the Pt surface, the ratio of moles Ru<sub>ad</sub> deposited on Pt to the moles surface atoms initially on Pt indicates the Pt-Ru<sub>ad</sub> initial surface composition. Further, the use of single crystal Pt as the substrate allows studies of face-specific activities as well as quantitative characterization of the Pt-Ru<sub>ad</sub> faces using ultra high vacuum surface techniques.

Pt-Ru<sub>ad</sub> systems have been prepared by electrochemical,<sup>28-30, 33, 34, 40, 47-57</sup> by evaporative,<sup>58-63</sup> and by spontaneous deposition of Ru<sub>ad</sub> on Pt substrates.<sup>19, 22, 60, 64-71</sup> The most convenient of these approaches is the spontaneous deposition of Ru<sub>ad</sub> precursors on Pt. For example, Ru<sub>ad</sub> precursors (largely oxides) spontaneously deposit from perchloric acid solutions of [RuO(H<sub>2</sub>O)<sub>4</sub>]<sup>2+</sup> onto electrochemically cleaned Pt single crystal surfaces.<sup>19, 22, 60, 65-71</sup> These Ru<sub>ad</sub> precursors are then electrochemically conditioned to form Ru<sub>ad</sub> adsorbed on the Pt single crystal surfaces. Such spontaneous deposition reactions offer the advantage over other deposition techniques that it is not necessary to monitor the deposition while it proceeds. These depositions are self limiting, halting at a specific surface coverage by the Ru precursor. Further, these depositions can be repeated to obtain higher coverages.<sup>71</sup>

As part of investigations into electrooxidation of methanol over polycrystalline Pt-Ru<sub>ad</sub> surfaces carried out in Bergens' group, Lee and co-workers found that Pt surfaces affect the hydrogenation of Ru(COD)( $\eta^3$ -C<sub>3</sub>H<sub>5</sub>)<sub>2</sub> (**2**, COD is 1,5-cyclooctadiene) under very mild conditions (e.g. -20 °C, 1 atm H<sub>2</sub>, in hexanes) to deposit Ru<sub>ad</sub> on Pt with the concomitant formation of cyclooctane (COA) and propane (Eq. 2-1).<sup>72</sup>



This reaction is conceptually similar to the surface organometallic chemistry work largely carried out by Coq and co-workers,<sup>73-78</sup> Candy and coworkers,<sup>79-86</sup> and recently applied to other electrocatalysts by Crabb and co-workers,<sup>87-90</sup> except that the hydrogenation of **2** over Pt is designed to provide a real time control over the number of surface equivalents of Ru<sub>ad</sub> deposited. Lee and co-workers used this reaction to prepare a series of blacked, polycrystalline Pt-Ru<sub>ad</sub> gauze electrodes of reasonably well-defined real surface areas and surface compositions. They also measured the real activities (current per active site) of these Pt-Ru<sub>ad</sub> gauzes towards the electrooxidation of methanol (MeOH) ( $E = 0.4$  V, [MeOH] = [H<sub>2</sub>SO<sub>4</sub>] = 0.50 M, 25 °C) as a function of surface equivalents Ru<sub>ad</sub> deposited by hydrogenation of **2**.<sup>91</sup> It was found that such Pt-Ru<sub>ad</sub> surfaces with low surface equivalents Ru<sub>ad</sub> (0.05 to 0.10) were the most active, producing 28 - 50 times more current per active site than blacked Pt gauzes without Ru<sub>ad</sub>. These results are similar to those reported by Gasteiger and co-workers using shiny bulk Pt-Ru alloys with well-defined surface compositions and real surface areas under these conditions.<sup>23-25</sup> The

results are also similar to those of van Veen and co-workers, who report the optimum percentage of Ru at the surface ( $\theta_{\text{Ru}}$ ) of co-electrodeposited Pt-Ru electrodes for the potentiostatic electrooxidation of methanol at  $E = 0.48$  V ( $T = 25$  °C, 0.1 M MeOH, 0.5 M  $\text{H}_2\text{SO}_4$ ) was ca. 15 %.<sup>30, 31</sup> Further, Lamy and co-workers recently reported that the optimum surface composition of shiny, flat bulk Pt-Ru alloys (prepared by melting in a high frequency furnace with magnetic levitation and characterized by electron microprobe and electrochemically) for the electrooxidation of methanol was 10 to 15 % Ru.<sup>26</sup> Lee and co-workers also found that even at low coverages (with only small amounts of  $\text{Ru}_{\text{ad}}$  on the surface), the blacked Pt- $\text{Ru}_{\text{ad}}$  gauzes were surprisingly stable as electrocatalysts for the oxidation of methanol and other organic fuels. A blacked Pt gauze with 0.10 surface equivalents  $\text{Ru}_{\text{ad}}$  deposited by hydrogenation of **2** was used for a variety of electrooxidations and experiments over a period of one month without change in activity towards electrooxidation of methanol.<sup>91, 92</sup> It is important to note, however, that as Pt- $\text{Ru}_{\text{ad}}$  nanoparticles may not be as stable as Pt- $\text{Ru}_{\text{ad}}$  gauzes, it remained unproven by the gauze experiments whether nanoparticle Pt- $\text{Ru}_{\text{ad}}$  catalysts made from Pt black nanoparticles could survive hot pressing into a membrane electrode assembly and operation as the anode catalyst in a DMFC. Further, despite several attractive features, the hydrogenation of **2** over Pt is not a self-limiting process as are the spontaneous depositions. The hydrogenation of **2** must be monitored *in situ*, and halted when the desired surface stoichiometry is reached.

In this study, a method to deposit  $\text{Ru}_{\text{ad}}$  onto Pt (blacked Pt gauzes and Pt nanoparticles) using an organometallic precursor that self-poisons at a pre-determined

surface composition was developed. A nanoparticle Pt-Ru<sub>ad</sub> catalyst prepared by this deposition method was tested as an anode electrocatalyst in a prototype DMFC.

## 2. Experimental

### 2.1. General

The argon (Linde, prepurified) and dihydrogen (Linde, prepurified) gas were used as received. The water was deionized, distilled, and finally distilled from alkaline permanganate, and purged with argon gas for 30 min prior to use. Hexanes (BDH, HPLC grade) were passed through aluminum oxide (Aldrich, standard grade), hydrogenated (1 atm) over Pt black for 24 h, and distilled through a Vigreux column from potassium metal under an atmosphere of argon. The methanol (BDH, HPLC grade) was distilled from Mg(OCH<sub>3</sub>)<sub>2</sub> under an atmosphere of argon. H<sub>2</sub>SO<sub>4</sub> (Alfa Aesar 99.9999%) was used as received. Ru<sub>4</sub>(μ-H)<sub>4</sub>(CO)<sub>12</sub> was prepared by a literature method.<sup>93</sup> The nanoparticle Pt black was Johnson Matthey fuel cell grade with a specific surface area of 27 m<sup>2</sup>/g (both quoted by Johnson Matthey and measured independently by us). A shiny Pt gauze (52 mesh, 99.9%, 25 × 25 mm, Aldrich) was threaded with Pt wire (200 mm in length, 0.127 mm in diameter, 99.9%, Aldrich) and supported by flame sealing the wire leads through 3 mm uranium glass tubing. The gauze was blacked<sup>94</sup> and its surface area was determined from the coulometric charge of the hydrogen adsorption region in cyclic voltammograms recorded in 1.0 M H<sub>2</sub>SO<sub>4</sub>.<sup>95-97</sup> The lower limits to the surface roughness factors of the blacked platinum gauzes ranged from 250 to 500. These lower limits were determined by comparing the real surface areas of the shiny Pt gauze before and after blacking. It is necessary to use high surface area Pt substrates in order to generate a sufficient amount



of Ru to allow reliable quantitative analysis by Inductively Coupled Plasma spectroscopy (ICP) (*vide infra*).

All glassware was rinsed in the following sequence: a 1:5 mixture of 30% aqueous hydrogen peroxide and concentrated  $\text{H}_2\text{SO}_4$ , water, a 5% mixture of ammonium hydroxide in absolute ethanol, absolute ethanol, water again and then dried in an oven. Rubber septa were extracted for 20 h with toluene (Caledon, reagent) in a Soxhlet extractor, boiled in deionized water, and dried under vacuum prior to use to remove the plasticiser. The deposition reactor was a  $2.3 \times 10.8$  cm Pyrex tube containing a  $4 \times 14$  mm Teflon-coated magnetic stir bar and fitted with a rubber septum and a side-arm with a Teflon stopcock.

Electrochemical experiments were performed in a typical three-electrode electrochemical cell using a Pine Bipotentiostat Model AFCBP1 controlled with Pinechem 2.00 software. Electrolytes were purged with argon for at least 10 min prior to use and protected under an atmosphere of argon at bubbler pressure during experiments. The reference electrode was a reversible hydrogen electrode (RHE). The counter electrode was a blacked Pt gauze behind a D-porosity glass frit.

To determine the amount of Ru deposited on Pt gauzes, Ru was first stripped off Pt gauze surfaces electrochemically (exhaustive anodic stripping) using the following procedure. The Pt-Ru<sub>ad</sub> gauze was transferred in air to an electrochemical cell that contained a Teflon-coated stir bar and a 1.0 M solution of NaOH (80 mL). The black Pt gauze counter electrode was fitted behind a D-porosity glass frit. The cathode (“+” terminal) of a 9 V battery was connected to the Pt-Ru<sub>ad</sub> gauze electrode, and the anode (“-” terminal) was connected to the counter electrode. The solution was stirred

under argon for 25 min as the color of the solution turned orange. The solution was quantitatively transferred to a 100 mL volumetric flask and diluted to volume with 1.0 M NaOH. UV-vis spectra of the solutions indicated that the product of the anodic stripping was sodium ruthenate.<sup>98</sup> Further anodic stripping in fresh electrolyte showed that all the ruthenium was stripped from the electrode by this treatment. The amount of Ru in solution was determined by ICP. The ICP was carried out using a Perkin-Elmer Optima equipped with an atomic emission detector.<sup>72, 91</sup>

## 2.2. Self-Poisoning Deposition Using $Ru_4(\mu-H)_4(CO)_{12}$ (I) over Blacked Pt Gauzes

The blacked Pt gauze was cleaned by continuous potential sweeps between 0.0 - 1.4 V (all potentials are reported relative to the RHE) until a stabilized cyclic voltammogram was obtained. The following procedure was used to transfer the gauze from the electrochemical cell to the reactor in which the hydrogenation was carried out. First, the surface of the gauze was protected as oxides by holding the potential at 1.4 V for 2 min. Second, the gauze was raised above the electrolyte and rinsed with purified water under argon. Third, while protected by drops of purified water, the gauze was quickly transferred through air to the hydrogenation reactor. Fourth, the gauze was dried with a stream of argon for 3h and then exposed to a stream of hydrogen gas for a further 1 h to reduce the surface oxides and to remove the resulting water. A saturated solution of  $Ru_4(\mu-H)_4(CO)_{12}$  (20 mL) in hydrogen-purged hexanes was then transferred via a cannula to the deposition reactor containing the cleaned, characterized, and reduced blacked Pt gauze under an atmosphere of hydrogen. The reactor was placed in an autoclave, the stopcock was slightly opened, and the autoclave was quickly sealed and flushed with hydrogen gas. The autoclave was pressurized to 60 atm and kept at room

temperature for 3 h with magnetic stirring. The autoclave was then slowly vented, opened, and the reactor stopcock was closed as quickly as possible to avoid exposing the reaction mixture to air. The solvent was cannulated from the reactor under hydrogen gas, the Pt-Ru<sub>ad</sub> gauze was rinsed with five 5 mL portions of hydrogen-purged hexanes, and then dried under a stream of hydrogen gas for 30 min.

To obtain a voltammogram showing the state of the Pt-Ru<sub>ad</sub> surface after the deposition self-poisoned, the dried gauze was transferred under argon to an electrochemical cell. The procedure was carried out in a glovebox flushed and filled with argon to eliminate risk of exposure to air that would oxidize the surface carbonyls. The potential of the Pt-Ru<sub>ad</sub> gauze was set to 75 mV concomitant with immersion into the argon-saturated, aqueous sulfuric acid electrolyte to protect the adsorbed carbonyls from oxidation by adventitious oxygen.

### *2.3. Electrooxidation of Methanol*

The Pt-Ru<sub>ad</sub> gauze was transferred under argon (in a glovebox) from the deposition reactor to an electrochemical cell containing the argon-purged electrolyte ( $[\text{H}_2\text{SO}_4] = 1.0 \text{ M}$ ), and equipped with reference and counter electrodes. The potential of Pt-Ru<sub>ad</sub> gauze was set to 75 mV concomitant with immersion into the electrolyte. Continuous potential sweeps were carried out between 0 and 700 mV at 5 mV/s until a steady potentiodynamic response was obtained to remove CO and any contaminants that adsorbed to the Pt-Ru<sub>ad</sub> during the reaction or the transfer. The potential was then held at 75 mV while an equal volume of an argon-purged 1.0 M aqueous solution of methanol was added to the cell while stirring to bring the final  $[\text{MeOH}] = [\text{H}_2\text{SO}_4] = 0.5 \text{ M}$ . The stirring was stopped, and potentiodynamic cycling was started (sweep rate = 5 mV/s,

sweep range 0 to 600 mV) with the first sweep in the negative direction. The potential was then held at 75 mV for 5 min and then the potentiostatic oxidation was begun by stepping the potential to 400 mV.

#### *2.4 Self-Poisoning Deposition Using $Ru_4(\mu-H)_4(CO)_{12}$ (I) over Pt Black*

The reactor was charged with Pt black (50 mg) and then evacuated and back-filled with argon three times to remove all oxygen from inside the vessel. Hydrogen gas was slowly bled into the reactor, and the system was then flushed with hydrogen gas for 1 hour to remove the water generated by reduction of the surface Pt oxides by hydrogen. A saturated solution of  $Ru_4(\mu-H)_4(CO)_{12}$  (20 mL) in hydrogen-purged hexanes was transferred via a cannula to the deposition reactor, the reactor was placed in an autoclave, the stopcock was slightly opened, and the autoclave was quickly sealed and flushed with hydrogen gas. The autoclave was pressurized to 60 atm, and then kept at room temperature for 3 h with magnetic stirring. The autoclave was slowly vented, opened, and the reactor stopcock was closed as quickly as possible to avoid exposing the reaction mixture to air. The solvent was cannulated from the reactor under argon. The Pt-Ru<sub>ad</sub> black was rinsed with five 5 ml portions of argon-purged hexanes, and then dried under a stream of argon gas over night.

To obtain the amount of Ru<sub>ad</sub> deposited on the Pt black after the deposition self-poisoned, Ru was chemically oxidized and dissolved in alkaline solution as follows: 15 mg resulting Pt-Ru<sub>ad</sub> black was suspended in a 25.0 mL saturated solution of potassium persulfate ( $K_2S_2O_8$ , Certified Regent, Fisher Scientific Company) in 4.0 M KOH, the solution was stirred for 1 hour at room temperature, and then it was left overnight without stirring.<sup>99</sup> ICP analysis was carried out on the resulting solution to measure the

amount of Ru. Further oxidizing on the leftover Pt black in fresh  $K_2S_2O_8$  solution showed that all the adsorbed  $Ru_{ad}$  and some of the surface Pt are oxidized from such surfaces to form soluble oxides under these conditions

### *2.5 Preparation and Operation of prototype DMFCs*

The membrane electrode assemblies were fabricated using the decal transfer method developed in Los Alamos National Laboratory.<sup>10</sup> The Pt- $Ru_{ad}$  black obtained from the hydrogenation of 1 was used as the anode catalyst, and Pt black was used as the cathode catalyst. To make the catalyst/ionomer ink, the catalyst was suspended in water and agitated in an ultrasonic bath for 30 min to thoroughly wet and disperse the catalyst. Enough 5% Nafion<sup>®</sup> solution (ElectroChem. Inc.) was added to the mixture to give a dry ink composition of 80 wt% catalyst with 20 wt% Nafion<sup>®</sup> ionomer. The mixtures were ultrasonicated for another 2 h to obtain uniformly dispersed inks. A Nafion<sup>®</sup>-117 membrane was cleaned and converted into the acid form by boiling in 3%  $H_2O_2$  for 1 h, followed by boiling in 0.5 M  $H_2SO_4$  for 2 h, and finally boiling in ultra-pure water for 2 h with the water being changed every 30 min. The cleaned membrane was stored in ultra-pure water, and dried on a heated vacuum table before use. The catalyst inks were painted onto 5 cm<sup>2</sup> Teflon decals to give a metal loading of approximately 2 mg/cm<sup>2</sup>. The catalyst inks were transferred from the Teflon decals to the Nafion<sup>®</sup> membrane by hot-pressing (125 to 127 °C, 1450 to 1550 psig for ca. 2 min). The membrane electrode assembly was then mounted into commercial fuel cell hardware (ElectroChem. Inc.) using Teflon-treated carbon papers (ElectroChem. Inc.) as backings/current collectors.

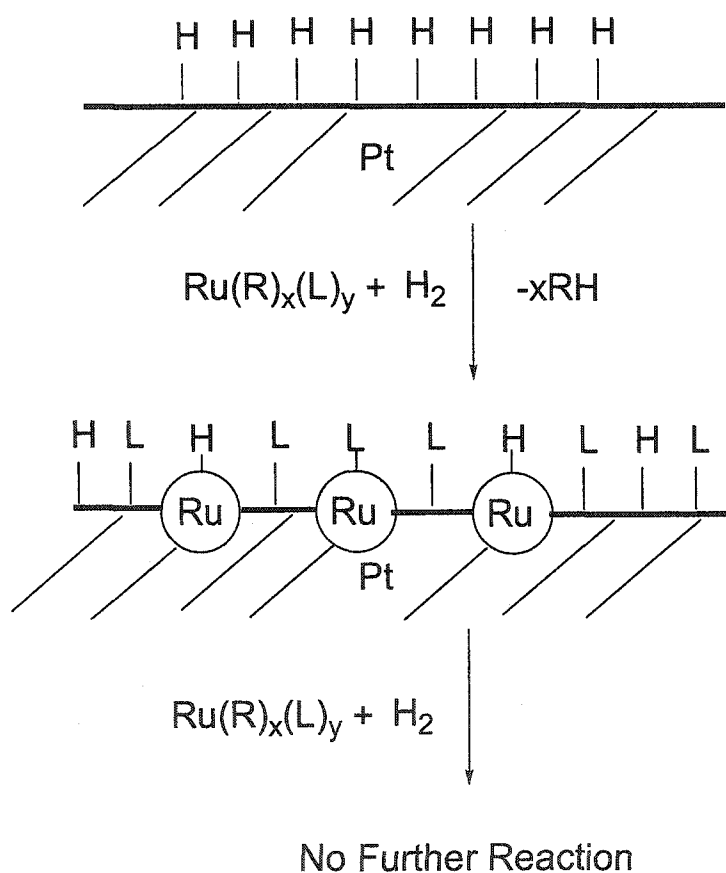
The fuel cell was operated at 90 °C with a 1.0 M aqueous methanol solution pumped through the anode compartment at 1 mL/min and zero back pressure, and with

oxygen passed through the cathode compartment at 400 standard cubic centimeter per minute (sccm) and 20 psig back pressure. Pure oxygen was used to maximize the activity of the cathode so that the differences in cell performance would reflect as much as possible the differences in anode catalyst activity. The cell potential-current curves were obtained using 890 Series computer controlled fuel cell test load (Scribner Associate Inc.). The reported cell potentials are not IR compensated.

### 3. Results and Discussion

One strategy for a self-poisoning version of the hydrogenation of **2** is to use a Ru precursor that contains ligands (**L**) that do not hydrogenate, but rather remain adsorbed on the surface after the  $\text{Ru}_{\text{ad}}$  is deposited. The adsorbed ligands **L** would then block one or more sites of the evolving Pt- $\text{Ru}_{\text{ad}}$  surface from further reaction with the remaining Ru precursor in solution. Eventually, enough ligands **L** would adsorb on the evolving Pt- $\text{Ru}_{\text{ad}}$  surface to stop further deposition of  $\text{Ru}_{\text{ad}}$  (Scheme 2-1). The amount of  $\text{Ru}_{\text{ad}}$  deposited on the surface when the deposition self-poisons would depend on the nature of **L**, the mechanism of the deposition, and on the ratio of **L** to Ru in the precursor. Further, unlike the hydrogenation of **2**, which needed to be carried out under reaction-rate limiting conditions (to avoid variations in mass transport to the active sites) to ensure a uniform coverage of Pt by  $\text{Ru}_{\text{ad}}$ ,<sup>72, 91</sup> self-poisoning depositions can be carried out over longer periods of time under mass-transport limiting conditions. Given enough time, all the particles or sites will react and be poisoned, regardless of variations in mass transport to the sites. The Ru precursor should be easily prepared and maintained in pure form, and the poisoning ligands **L** should be easily removed. We now disclose that the cluster

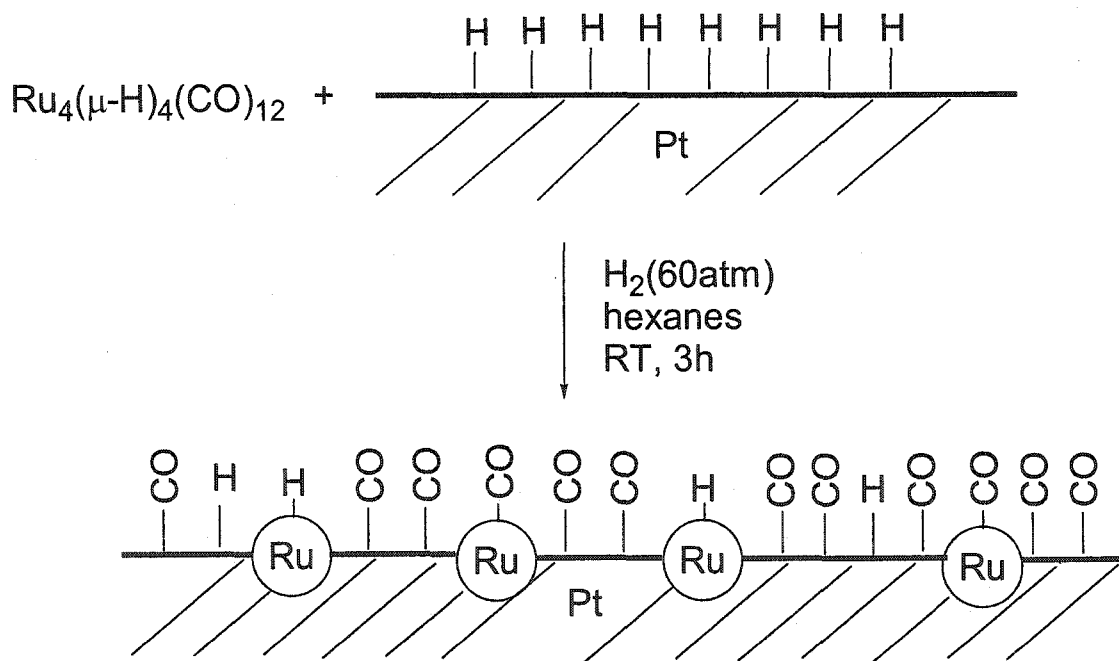
compound  $\text{Ru}_4(\mu\text{-H})_4(\text{CO})_{12}$  (1, L = CO, R = H) fulfills these requirements. This compound is a moderately air stable, crystalline compound prepared by reaction of  $\text{Ru}_3(\text{CO})_{12}$  with hydrogen gas.<sup>93</sup> The poisoning ligand L in this system is CO, which is easily removed after the deposition by either electrooxidation or by exposure to atmospheric oxygen. Another Ru carbonyl cluster,  $\text{Ru}_3(\text{CO})_9(\text{CH}_3\text{CN})_3$ , has been used to deposit Ru-carbonyl species on Pt oxide (Pt/Pt-O, or Pt-O/PtO<sub>2</sub>) surfaces in dichloromethane as reported in a recent study.<sup>100</sup>



**Scheme 2-1.** Schematic of self-poisoning deposition of  $\text{Ru}_{\text{ad}}$  on Pt

### 3.1 Blacked Pt-Ru<sub>ad</sub> Gauze

A blacked Pt gauze, prepared and characterized as described previously<sup>72, 91</sup> (the surface was cleaned and its real surface area was measured by potential sweeping in H<sub>2</sub>SO<sub>4</sub>(aq)) was used as the substrate/promoter for the deposition. The deposition reactions were carried out in hexanes solutions. The hexane solvent was rigorously purified and all olefin impurities removed by hydrogenation as described previously.<sup>72, 91</sup> It was found that the deposition did not occur under 1 atm of hydrogen at room temperature. The deposition did occur, however, under 60 atm of H<sub>2</sub> (Scheme 2-2).



Scheme 2-2. Self-poisoning deposition of Ru<sub>ad</sub> on Pt using Ru<sub>4</sub>(μ-H)<sub>4</sub>(CO)<sub>12</sub>

Scheme 2-2 shows a cartoon of one of the possible structures of the resulting surface (*vide infra*). Since Pt surfaces are saturated with hydrogen (reduced with no or few surface oxides) even under 1 atm of H<sub>2</sub>, the high pressures of H<sub>2</sub> required for this



deposition probably serve to activate the cluster **1** towards reaction with the Pt-H surface. The deposition of **1** self-poisoned after 3 h under 60 atm H<sub>2</sub> at room temperature - use of longer reaction times (9 and 18 h) did not result in further deposition of Ru<sub>ad</sub>. The resulting black Pt-Ru<sub>ad</sub> gauze was characterized and studied using techniques effective for Pt-Ru<sub>ad</sub> gauzes prepared by hydrogenation of Ru(COD)( $\eta^3$ -C<sub>3</sub>H<sub>5</sub>)<sub>2</sub> (**2**): base cyclic voltammetry, anodic stripping of Ru<sub>ad</sub>, and the potentiodynamic and potentiostatic electrooxidation of methanol.<sup>72, 91</sup>

Figure 2-1 shows the voltammograms of a blacked Pt gauze before and immediately after the deposition using **1**. There are two anodic peaks at ca. 0.46 and 0.58 V in the first positive-going sweep recorded after the deposition self-poisons (Figure 2-1b, short-dashed line). The upper potential of these sweeps was limited to 0.7 V to avoid dissolution of Ru. These peaks are similar to those observed using Pt-Ru<sub>ad</sub> gauzes prepared by hydrogenation of **2**.<sup>72, 91</sup> Wieckowski and co-workers recently observed two peaks for the electrooxidation of CO adsorbed on Pt-Ru<sub>ad</sub> surfaces obtained by spontaneous deposition of Ru on Pt black.<sup>22, 71</sup> To confirm that these peaks arose from electrooxidation of adsorbed CO, the surface of the Pt-Ru<sub>ad</sub> gauze was subsequently saturated with CO (using a procedure described previously<sup>68, 80</sup>), and then a CV was recorded under identical conditions. It was found that the first positive going sweep contained two anodic peaks of similar size and shape at ca. 0.53 and 0.58 V. These experiments show that CO is adsorbed on the Pt-Ru<sub>ad</sub> surface after the hydrogenation of **1** self-poisons. It should be noted that more information is required, however, to determine how the COs are distributed on the surface, or whether the Pt-Ru<sub>ad</sub> surface retains components or fragments of the structure of **1** before the CO is removed.

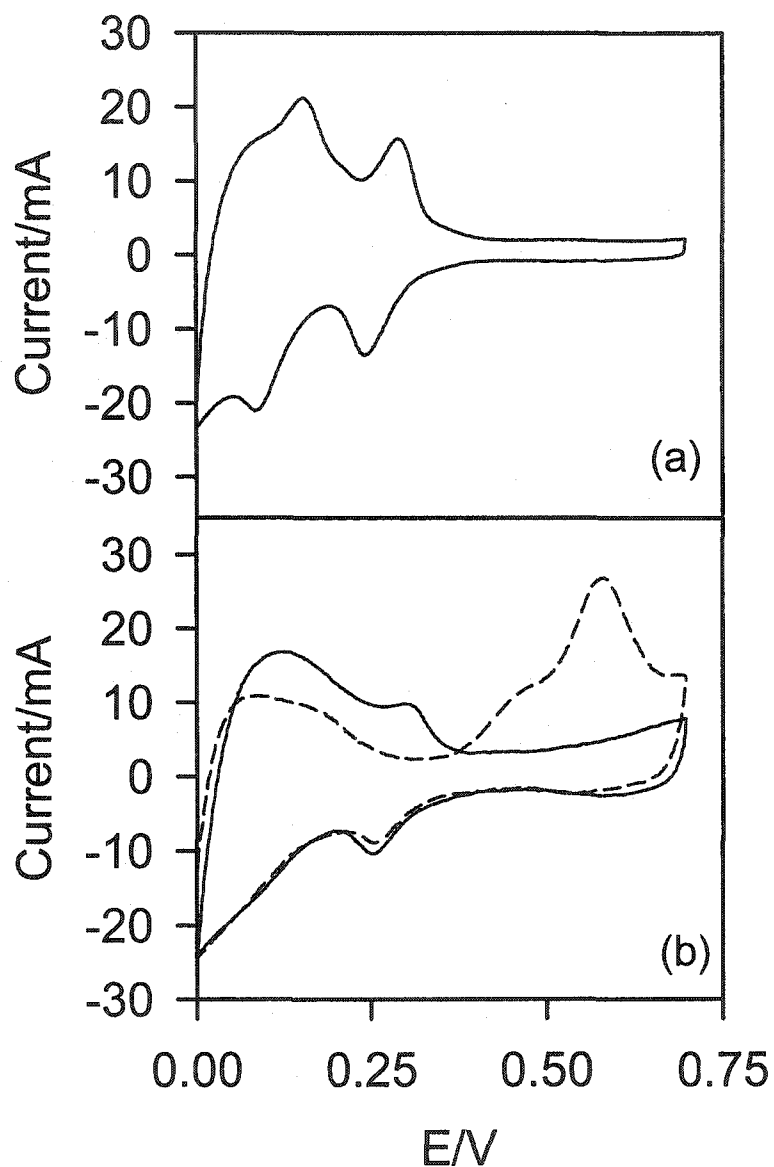


**Figure 2-1.** Cyclic voltammograms of blacked Pt gauze (a) before hydrogenation, (b) after hydrogenation: first potential sweep(---), stabilized(—).  $[\text{H}_2\text{SO}_4] = 1.0 \text{ M}$ ,  $T = 25 \text{ }^\circ\text{C}$ , sweep rate =  $5 \text{ mV/s}$ , sweep range =  $0.00$  to  $0.70 \text{ V}$ .

The stabilized base voltammogram of the  $\text{Pt-Ru}_{\text{ad}}$  surface after CO stripping (Figure 2-1b, solid line) contains features typical of Pt-Ru surfaces: less resolution in the hydrogen region, and an enlarged double layer region when compared to polycrystalline

Pt.<sup>36, 37, 40-44</sup> The stabilized voltammogram closely resembles those reported by us previously for 0.05 and 0.10 equivalent Pt-Ru<sub>ad</sub> surfaces generated by hydrogenation of 2 over black Pt gauzes.<sup>91</sup> It also resembles that reported by Ross and co-workers for a bulk, shiny Pt-Ru alloy with 7% Ru at the surface.<sup>43, 44</sup> This resemblance in potentiodynamic response suggests that the hydrogenation using 1 self-poisons after depositing small amounts (0.05 - 0.10 surface equivalents) of Ru<sub>ad</sub> on the blacked Pt gauzes. Notably, Wieckowski and co-workers recently reported that voltammograms of Pt-Ru<sub>ad</sub> systems prepared by spontaneous deposition of appreciable amounts of Ru<sub>ad</sub> on Pt black contained features largely resembling Pt as well as features resembling Ru. This intriguing result shows that the nature and therefore the activities of surfaces obtained by Ru<sub>ad</sub> deposition is preparation specific.<sup>22, 71</sup> To determine, as the voltammetry suggests, whether the hydrogenation of 1 over the blacked gauze self-poisoned at low coverages, the exhaustive anodic stripping-inductively coupled plasma spectrophotometry (ICP) analysis was carried out. This analysis shows that 0.05 surface equivalents Ru<sub>ad</sub> (relative to the number of surface atoms initially on the black Pt gauze) were deposited on the surface when the hydrogenation self-poisoned by adsorbed CO - consistent with the amounts indicated by the base voltammograms.

Assuming that all the CO from Ru<sub>4</sub>(μ-H)<sub>4</sub>(CO)<sub>12</sub> was adsorbed on the Pt-Ru<sub>ad</sub> surface, the CO stripping charge will reflect the amount of Ru<sub>ad</sub> deposited on the Pt surface. The CO stripping charge was estimated by integrating the current-time curve for the second positive going sweep over the voltage range 0.34 to 0.7 V, and subtracting this value from the charge measured from the first positive going sweep over the same range. As shown by the voltammograms (Figure 2-1b), all or most of the adsorbed CO is

oxidized by the end of the first positive going sweep. Further, the negative going sweep after the first positive sweep is quite similar to all subsequent negative going sweeps, showing that the amount of oxides on the surface at the end of the first positive going sweep is equal, or nearly equal, to the amount of oxides at the end of all subsequent positive going sweeps. Thus the first positive going sweep over this range contains the current for oxidation of adsorbed CO and for formation of surface oxides, the second positive going sweep contains only the current for formation of surface oxides, which was subtracted to estimate the CO stripping charge. Assuming from the stoichiometry of 1 that three CO molecules are adsorbed by the surface for every  $\text{Ru}_{\text{ad}}$ , the measured CO stripping charge predicts that ca. 0.10 surface equivalents  $\text{Ru}_{\text{ad}}$  were deposited on Pt when the deposition self-poisoned. Considering the uncertainties involved in measuring CO electrooxidation charges (*vide supra*), this number is in reasonable agreement with the amount (ca. 0.05 equiv) obtained from the exhaustive anodic stripping of  $\text{Ru}_{\text{ad}}$ . This value also correlates with the low coverage of Pt by  $\text{Ru}_{\text{ad}}$  indicated by the voltammetry experiments.

Figure 2-2 shows the first, second, and third positive-going sweeps for the potentiodynamic oxidation of methanol over the black Pt- $\text{Ru}_{\text{ad}}$  gauze made by the self-poisoning deposition. Also shown is the stabilized, positive-going sweep measured over a blacked Pt gauze. The currents are normalized to the initial real surface areas of the blacked Pt gauzes. The first sweep over the blacked Pt- $\text{Ru}_{\text{ad}}$  gauze surface contains the well-known anodic peak at ca. 0.2 V observed using polycrystalline Pt-Ru.<sup>43, 91, 101, 102</sup> Also well-known for Pt-Ru surfaces is the subsequent decrease in currents between the first, second, and third positive going sweeps.<sup>43, 91</sup> The third, stabilized sweep over Pt-

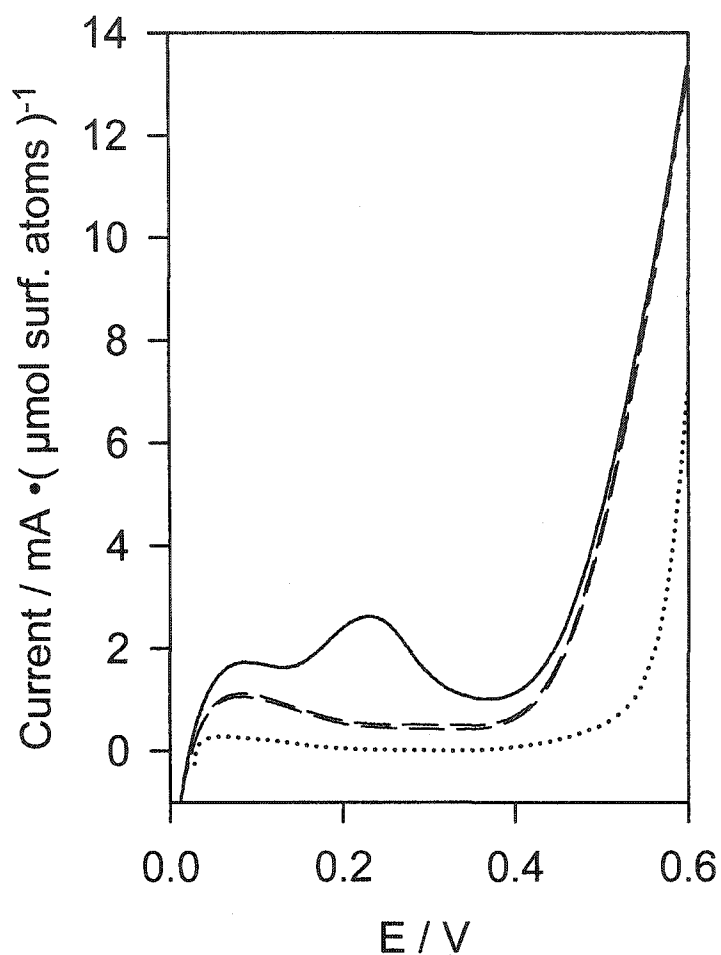


**Figure 2-2.** Potentiodynamic electrooxidations of methanol over a blacked Pt gauze substrate (.....) and over a blacked Pt-Ru<sub>ad</sub> gauze surface resulting from hydrogenation of 1: first potential sweep(—), subsequent(— — —). Currents are normalized to real surface area. [MeOH] = [H<sub>2</sub>SO<sub>4</sub>] = 0.5 M,  $T = 25\text{ }^{\circ}\text{C}$ , sweep rate = 5 mV/s, sweep range = 0.00 to 0.60 V.

Ru<sub>ad</sub> made with the self-poisoning deposition is similar to that over 0.05 equivalent Pt-Ru<sub>ad</sub> made with the hydrogenation of 2 over a blacked Pt gauze.<sup>91</sup> These potentiodynamic methanol electrooxidations, therefore, also indicate that the deposition using 1 self-poisoned at low (0.05 - 0.10 surface equiv.) Ru concentrations.

Figure 2-3 shows a plot of current versus time for the potentiostatic electrooxidation of methanol over the blacked Pt-Ru<sub>ad</sub> gauze made by the self-poisoning deposition. Also shown is the curve obtained using a blacked Pt gauze.<sup>91</sup> The currents are normalized to the initial real surface area of the Pt gauzes. The electrooxidations exhibit the well-known, initial rapid decrease in current followed by a region of more stable activity, in which the current slowly decreases.<sup>41, 103</sup> As expected, the normalized activity of the surface made by the self-poisoning deposition is between those previously reported for 0.05 and 0.10 equivalent Pt-Ru<sub>ad</sub> surfaces prepared by hydrogenation of **2**.<sup>91</sup> As it is reasonable to expect uncertainties in the stoichiometries of 0.05 and 0.10 equivalent Pt-Ru<sub>ad</sub> surfaces made by hydrogenations of **2** over Pt gauzes, the results from the potentiostatic oxidations also show that the deposition **1** self-poisons after small amounts (< 10 %) of Ru<sub>ad</sub> are deposited on Pt.

### 3.2 Nanoparticle Pt-Ru<sub>ad</sub> Black

The self-poisoning deposition was carried out over Johnson Matthey fuel cell grade nanoparticle Pt black (27 m<sup>2</sup>/g). Wieckowski and co-workers have recently reported the spontaneous deposition of Ru<sub>ad</sub> precursors on fuel cell grade Pt black and use of the Pt-Ru<sub>ad</sub> blacks as electrocatalysts for the electrooxidation of methanol.<sup>22, 71</sup> The amount of Ru<sub>ad</sub> deposited on Pt black when the deposition self-poisoned was determined by exhaustive oxidative dissolution of Ru by S<sub>2</sub>O<sub>8</sub><sup>2-</sup> in alkaline solution<sup>99</sup> followed by ICP analysis for Ru ions. The amount of Ru ions in the resulting electrolyte showed the deposition self-poisoned after ca. 0.10 surface equivalents Ru<sub>ad</sub> were deposited on the Pt black. This result appears to differ from the anodic stripping experiments run after the deposition over black Pt gauzes, which showed that ca. 0.05 surface equivalents Ru<sub>ad</sub> are

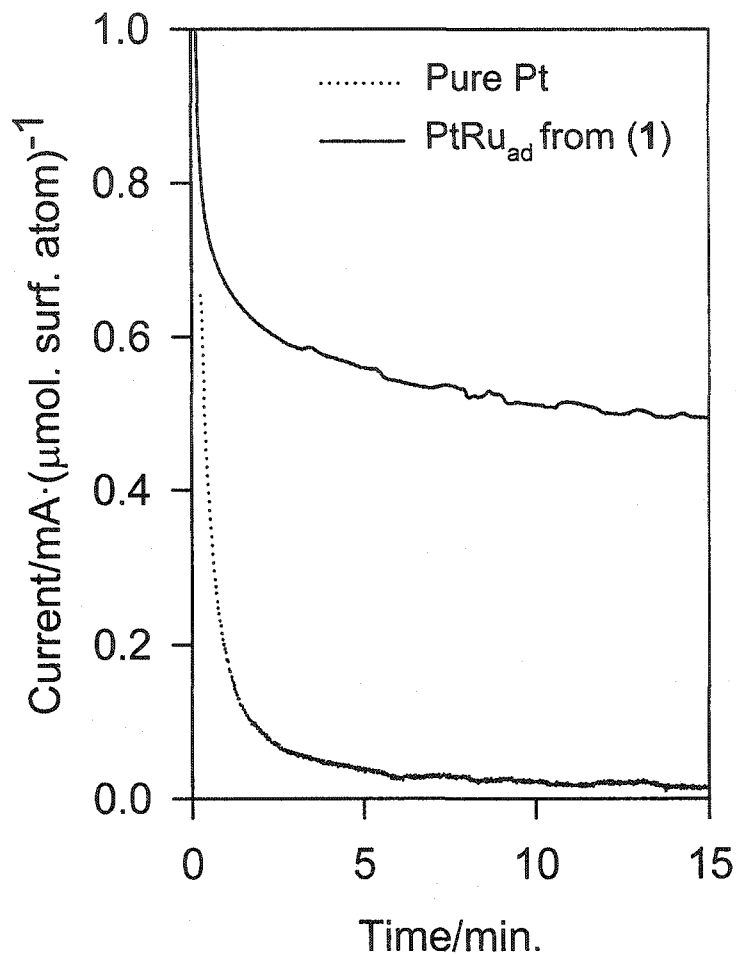


**Figure 2-3.** Potentiostatic electrooxidation of methanol over a blacked Pt-Ru<sub>ad</sub> gauze resulting from hydrogenation of **1**, and over a blacked Pt gauze. Currents are normalized to real surface area.  $T = 25\text{ }^{\circ}\text{C}$ ,  $E = 0.4\text{ V}$ ,  $[\text{MeOH}] = [\text{H}_2\text{SO}_4] = 0.5\text{ M}$ .

adsorbed (*vide supra*). Further investigations are required to determine the origins or significance of this difference. Considering factors include surface structure and particle size effects. The blacked Pt gauzes and nanoparticle Pt black powder may not behave in precisely the same manner.

A DMFC was constructed by hot pressing the nanoparticle Pt-Ru<sub>ad</sub> black into a Nafion<sup>®</sup> membrane using the decal transfer method developed by Gottesfeld and co-

workers.<sup>10</sup> The cathode catalyst was made from the same batch of Pt black that was used to make the Pt-Ru<sub>ad</sub> anode catalyst. The catalyst loadings on both sides of the cell were 2 mg/cm<sup>2</sup>. The utilization of the cathode catalyst (and presumably also of the anode catalyst) was 85 %, obtained by comparing the initial real surface area of the Pt black to the real surface area of the cathode Pt black measured in the cell (*vide infra*) by cyclic voltammetry. The fabrication parameters were not optimized to maximize the performance of this cell.

Figure 2-4 shows the normalized polarization curves for this cell and for a control cell using bare Pt black as anode catalyst. The currents are mass normalized per gram anode catalyst (the loadings at the cathode and anode were the same). The normalized currents using the Pt-Ru<sub>ad</sub> anode electrocatalyst were substantially higher than those using the Pt anode catalyst. The Pt-Ru<sub>ad</sub> cell was operated intermittently for 5 days at 8 h per day. Various polarization curves and electrode voltammograms were recorded before the cell was disconnected. No decrease in performance was observed during this time.

Figure 2-5 shows the cyclic voltammograms of the anode and the cathode of the Pt-Ru<sub>ad</sub> cell after several days of operation at 90 °C. The voltammograms were recorded at 25 °C in the fuel cell test block as described by Gottesfeld and co-workers.<sup>18</sup> The working electrode was placed under purified water, and the opposite electrode was used as both counter and reference by placing it under 1 atm of hydrogen gas. The potentiodynamic response of the Pt-Ru<sub>ad</sub> anode had less resolution in the hydrogen region and a thicker double layer region than that of the Pt cathode. As only ca. 0.10 equivalents Ru<sub>ad</sub> were initially present on its surface, it is expected that the performance of this Pt-Ru<sub>ad</sub> anode catalyst would be a sensitive probe to loss of surface Ru<sub>ad</sub> - a small loss would



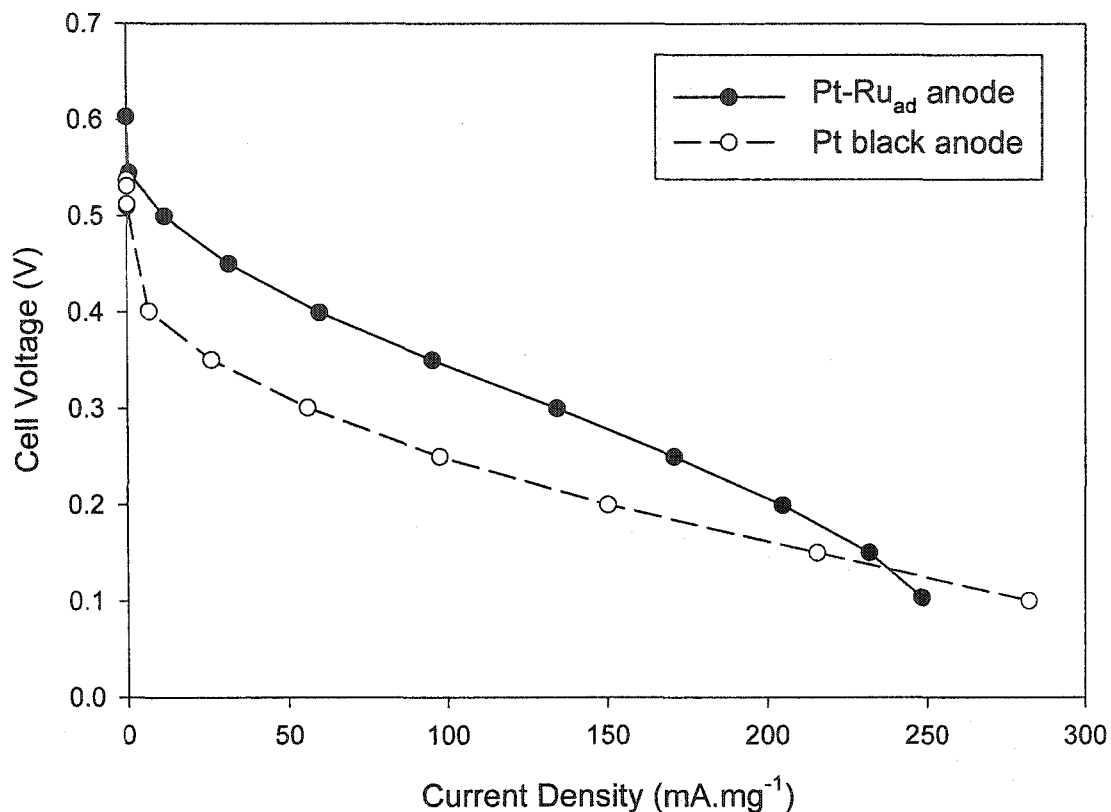


**Figure 2-4.** Polarization curves for 90 °C DMFCs with Nafion<sup>®</sup>-117 membranes. Anode: 2 mg/cm<sup>2</sup> catalyst, 1.0 M methanol at 1.0 ml/min. Cathode: 2 mg/cm<sup>2</sup> Pt-black catalyst, 20 psig oxygen at 400 sccm.

bring the activity down to that of pure Pt. This expectation, combined with both the voltammograms recorded in the cell and with the higher performance of Pt-Ru<sub>ad</sub> than Pt as anode electrocatalyst, lead us to conclude that significant surface segregation or dissolution resulting in loss of Ru<sub>ad</sub> did not occur during construction and initial (days long) operation of this DMFC.

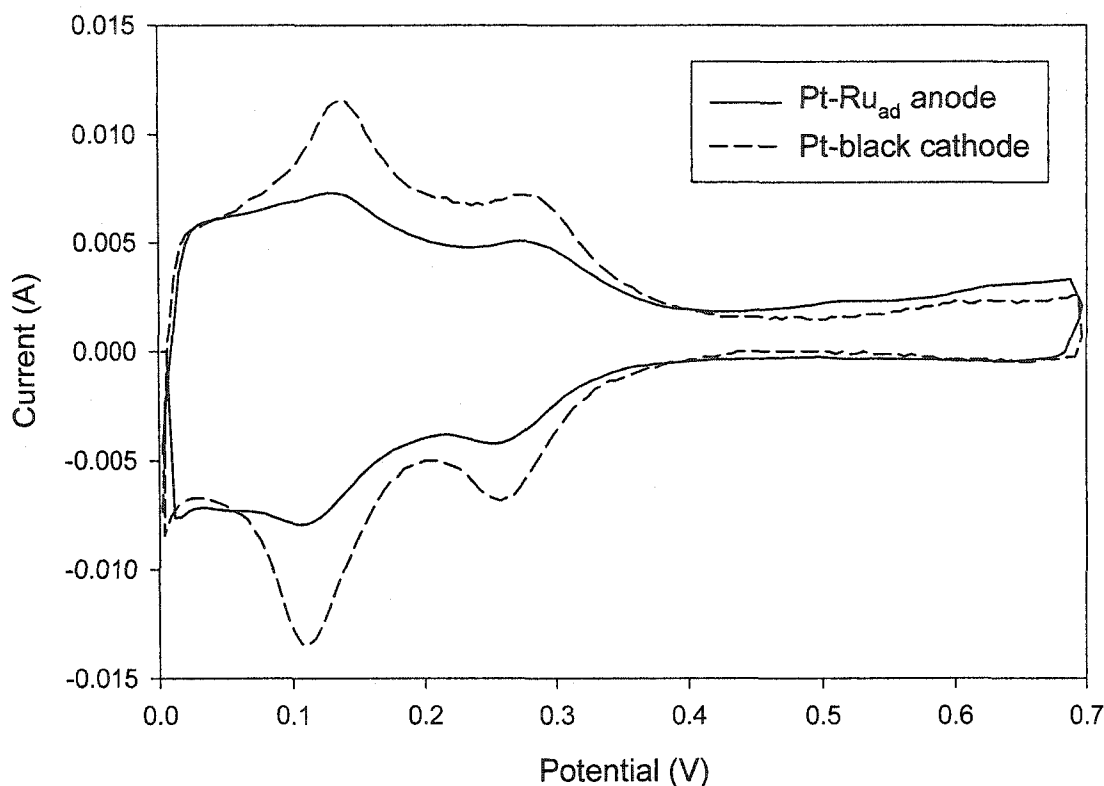


**Figure 2-5.** Cyclic Voltammograms of a Pt-Ru<sub>ad</sub> anode and a Pt-black cathode obtained in a DMFC at 25 °C, 5 mV/s sweep rate. 2 mg/cm<sup>2</sup> catalyst on both sides.

#### 4. Conclusions

Combined, the results from the adsorbed CO stripping charge, from base voltammograms, from anodic stripping, and from potentiodynamic and potentiostatic electrooxidations of methanol show that the deposition using 1 self-poisoned after ca. 0.05 surface equivalents of Ru<sub>ad</sub> are deposited on black Pt gauzes. This is the optimum surface composition for electrooxidation of methanol over blacked Pt-Ru<sub>ad</sub> gauzes prepared by hydrogenation of 2.<sup>72, 91</sup> The deposition self-poisons when ca. 0.10 surface equivalents is deposited on nanoparticle Pt black. This Pt-Ru<sub>ad</sub> black can be used to

prepare and operate a direct methanol fuel cell. Further investigations are underway in our laboratories to study other Ru precursors, as well as to determine the longevity and to optimize prototype Pt-Ru<sub>ad</sub> DMFCs.

Although ca. 0.05 surface equivalents Ru<sub>ad</sub> is the optimum composition for electrooxidation of methanol over blacked Pt-Ru<sub>ad</sub> gauzes, it may not be the optimum composition over nanoparticle Pt-Ru<sub>ad</sub> black powder. Wieckowski and co-workers recently reported that the optimum surface composition for the electrooxidation of methanol over Pt-Ru<sub>ad</sub> blacks prepared by spontaneous deposition is ca. 0.50 equivalents Ru<sub>ad</sub>.<sup>22, 71</sup> As it is reasonable to assume that the activities and optimum surface compositions of Pt-Ru<sub>ad</sub> catalysts will be preparation specific, the optimized surface prepared under one set of conditions and reagents may not be of the same composition or activity of the optimized surface prepared under another set of conditions and reagents. Factors including the distribution of Ru<sub>ad</sub> on the Pt surface (towering, islands, etc) will vary between preparation techniques and they will affect the activities of such catalysts. The optimum surface composition and activity of nanoparticle Pt-Ru<sub>ad</sub> blacks were studied and are reported in chapter 3 and chapter 4.

## References

- (1) Frumkin, A. N.; Podlovchenko, B. I. *Bok. Akad. Naak SSSR* **1963**, *150*, 345-352.
- (2) Bockris, J. O' M.; Wroblowa, H. *J. Electroanal. Chem.* **1964**, *7*, 428-451.
- (3) Petry, D. A.; Podlovchenko, B. I.; Frumkin, A. N.; Lal, H. *J. Electroanal. Chem.* **1965**, *10*, 253-269.
- (4) Binder, H.; Kohling, A.; Sandstede, G. In *Symposium on Hydrocarbon Fuel Cell Technology, American Chemical Society, 150th National Meeting*; Baker, B. S., Ed.;

- New York, N.Y. : Academic Press: Atlantic City, N.J., 1965; p 91.
- (5) Petrii, O. A. *Dokl. Akad. Nauk SSSR (RUSS)* **1965**, *160*, 871-874.
- (6) Williams, K. R. *Advan. Sci.* **1966**, *22*, 617-622.
- (7) Watanabe, M.; Uchida, M.; Motoo, S. *J. Electroanal. Chem.* **1987**, *229*, 395-406.
- (8) Surampudi, S.; Narayanan, S. R.; Vamos, E.; Frank, H.; Halpert, G.; Laconti, A.; Kosek, J.; Prakash, G. K. S.; Olah, G. A. *J. Power Sources* **1994**, *47*, 377-385.
- (9) Garche, J.; Vielstich, W.; Waidhas, M. *Proc. Erste Ulmer Tage Universitatesverlag Ulm: Ulm, Germany*, **1994** 178-190.
- (10) Ren, X.; Wilson, M. S.; Gottesfeld, S. *J. Electrochem. Soc.* **1996**, *143*, L12-L15.
- (11) Hogarth, M. P.; Hards, G. A. *Plat. Met. Rev.* **1996**, *40*, 150-159.
- (12) Gottesfeld, S. (with Zawodzinski, T.), Polymer electrolyte fuel cells, in: Tobias, C.; Gerischer, H.; Kolb, D.; Alkire, R. (Eds.), *Advances in Electrochemistry and Electrochemical Engineering*, Wiley/VCH, New York, **1997**, *5*, 195.
- (13) Arico, A. S.; Shukla, A. K.; El-Khatib, K. M.; Creti, P. *J. Appl. Electrochem.* **1999**, *29*, 671-676.
- (14) Ren, X.; Zelenay, P.; Thomas, S.; Davey, J.; Gottesfeld, S. *J. Power Sources* **2000**, *86*, 111-116.
- (15) Boxall, D. L.; Deluga, G. A.; Kenik, E. A.; King, W. D.; Lukehart, C. M. *Chem. Mater.* **2001**, *13*, 891-900.
- (16) Rolison, D. R.; Hagans, P. L.; Swider, K. E.; Long, J. W. *Langmuir* **1999**, *15*, 774-779.
- (17) Long, J. W.; Stroud, R. M.; Swider-Lyons, K. E.; Rolison, D. R. *J Phys. Chem. B* **2000**, *104*, 9772-9776.
- (18) Dinh, H. N.; Ren, X.; Garzon, F. H.; Zelenay, P.; Gottesfeld, S. *J. Electroanal. Chem.* **2000**, *491*, 222 - 233.
- (19) Crown, A.; Kim, H.; Lu, G. Q.; de Moraes, I. R.; Rice, C.; Wieckowski, A. *J. New Mat. Electrochem. Sys.* **2000**, *3*, 275-284.
- (20) O'Grady, W. E.; Hagans, P. L.; Pandya, K. I.; Maricle, D. L. *Langmuir* **2001**, *17*, 3047-3050.
- (21) Schmidt, T. J.; Noeske, M.; Gasteiger, H. A.; Behm, R. J.; Britz, P.; Brijous, W.;

- Bonnemann, H. *Langmuir* **1997**, *13*, 2591-2595.
- (22) Tong, Y. Y.; Kim, H. S.; Babu, P. K.; Waszczuk, P.; Wieckowski, A.; Oldfield, E. *J. Am. Chem. Soc.* **2002**, *124*, 468-473.
- (23) Gasteiger, H. A.; Markovic, N.; Ross, P. N., Jr.; Cairns, E. J. *J Phys. Chem.* **1994**, *98*, 617-625.
- (24) Gasteiger, H. A.; Markovic, N.; Ross, P. N.; Cairns, E. J. *Electrochim. Acta* **1994**, *39*, 1825-1832.
- (25) Markovic, N. M.; Gasteiger, H. A.; Ross, P. N.; Jiang, X. *Electrochim. Acta* **1995**, *40*, 91-98.
- (26) Kabbabi, A.; Faure, R.; Durand, R.; Beden, B.; Hahn, F.; Leger, J.-M.; Lamy, C. J. *Electroanal. Chem.* **1998**, *444*, 41-53.
- (27) Lin, W. F.; Iwasita, T.; Vielstich, W. *J Phys. Chem. B* **1999**, *103*, 3250-3257.
- (28) Friedrich, K. A.; Geysers, K. P.; Linke, U.; Stimming, U.; Stumper, J. J. *Electroanal. Chem.* **1996**, *402*, 123-128.
- (29) Lin, W. F.; Zei, M. S.; Eiswirth, M.; Ertl, G.; Iwasita, T.; Vielstich, W. *J Phys. Chem. B* **1999**, *103*, 6968-6977.
- (30) Massong, H.; Wang, H. S.; Samjeske, G.; Baltruschat, H. *Electrochim. Acta* **2000**, *46*, 701-707.
- (31) Iúdice De Souza, J. P.; Iwasita, T.; Nart, F. C.; Vielstich, W. *J. Appl. Electrochem.* **2000**, *30*, 43-48.
- (32) Krausa, M.; Vielstich, W. *J. Electroanal. Chem.* **1994**, *379*, 307-314.
- (33) Frelink, T.; Visscher, W.; van Veen, J. A. R. *Langmuir* **1996**, *12*, 3702-3708.
- (34) Frelink, T.; Visscher, W.; Cox, A. P.; Veen, J. A. R. *Ber. Bunsen-Ges. Phys. Chem.* **1996**, *100*, 599-606.
- (35) Napporn, W. T.; Leger, J. M.; Lamy, C. J. *Electroanal. Chem.* **1996**, *408*, 141-147.
- (36) Weaver, M. J.; Chang, S.-C.; Leung, L.-W. H.; Jiang, X.; Rubel, M.; Szklarczyk, M.; Zurawski, D.; Wieckowski, A. *J. Electroanal. Chem.* **1992**, *327*, 247-260.
- (37) Gómez, R.; Feliu, J. M.; Aldaz, A.; Weaver, M. J. *Surf. Sci.* **1998**, *410*, 48-61.
- (38) Jusys, Z.; Massong, H.; Baltruschat, H. *J. Electrochem. Soc.* **1999**, *146*, 1093-1099.
- (39) Jusys, Z.; Kaiser, J.; Behm, R. J. *Electrochim. Acta* **2002**, *47*, 3693-3706.

- (40) Watanabe, M.; Motoo, S. *J. Electroanal. Chem.* **1975**, *60*, 267-273.
- (41) McNicol, B. D.; Short, R. T. *J. Electroanal. Chem.* **1978**, *92*, 115-120.
- (42) Mahmood, T.; Williams, J. O.; Miles, R.; McNicol, B. D. *J. Catal.* **1981**, *72*, 218-235.
- (43) Gasteiger, H. A.; Markovic, N.; Ross, P. N., Jr.; Cairns, E. J. *J. Phys. Chem.* **1993**, *97*, 12020-12029.
- (44) Gasteiger, H. A.; Markovic, N.; Ross, P. N.; Cairns, E. J. *J. Electrochem. Soc.* **1994**, *141*, 1795-1803.
- (45) Miura, H.; Gonzalez, R. D. *J. Catal.* **1982**, *74*, 216-224.
- (46) Green, C. L.; Kucernak, A. *J. Phys. Chem. B* **2002**, *106*, 1036-1047.
- (47) Watanabe, M.; Motoo, S. *J. Electroanal. Chem.* **1975**, *60*, 275-283.
- (48) Meli, G.; Leger, J.-M.; Lamy, C.; Durand, R. *J. Appl. Electrochem.* **1993**, *23*, 197-202.
- (49) Laborde, H.; Leger, J.-M.; Lamy, C. *J. Appl. Electrochem.* **1994**, *24*, 1019-1027.
- (50) Frelink, T.; Visscher, W.; Cox, A. P.; Van Veen, J. A. R. *Electrochim. Acta* **1995**, *40*, 1537-1543.
- (51) Cramm, S.; Friedrich, K. A.; Geyzers, K. P.; Stimming, U.; Vogel, R. *Fresenius J. Anal. Chem.* **1997**, *358*, 189-192.
- (52) Watanabe, M.; Genjima, Y.; Turumi, K. *J. Electrochem. Soc.* **1997**, *144*, 423-427.
- (53) Chrzanowski, W.; Wieckowski, A. *Langmuir* **1998**, *14*, 1967-1970.
- (54) Friedrich, K. A.; Geyzers, K. P.; Marmann, A.; Stimming, U.; Vogel, R. *Z. Phys. Chemie-Int. J. Res. Phys. Chem. Chem. Phys.* **1999**, *208*, 137-150.
- (55) Vigier, F.; Gloaguen, F.; Leger, J. M.; Lamy, C. *Electrochim. Acta* **2001**, *46*, 4331-4337.
- (56) Lima, A.; Coutanceau, C.; Leger, J. M.; Lamy, C. *J. Appl. Electrochem.* **2001**, *31*, 379-386.
- (57) Kim, H.; de Moraes, I. R.; Tremiliosi, G.; Haasch, R.; Wieckowski, A. *Surf. Sci.* **2001**, *474*, L203-L212.
- (58) Davies, J. C.; Hayden, B. E.; Pegg, D. *J. Electrochim. Acta* **1998**, *44*, 1181-1190.
- (59) Davies, J. C.; Hayden, B. E.; Pegg, D. *J. Surf. Sci.* **2000**, *467*, 118-130.

- (60) Iwasita, T.; Hoster, H.; John-Anacker, A.; Lin, W. F.; Vielstich, W. *Langmuir* **2000**, *16*, 522-529.
- (61) Hoster, H.; Iwasita, T.; Baumgartner, H.; Vielstich, W. *Phys. Chem. Chem. Phys.* **2001**, *3*, 337-346.
- (62) Lu, C.; Masel, R. I. *J Phys. Chem. B* **2001**, *105*, 9793-9797.
- (63) Davies, J. C.; Hayden, B. E.; Pegg, D. J.; Rendall, M. E. *Surf. Sci.* **2002**, *496*, 110-120.
- (64) Franaszczuk, K.; Sobkowski, J. *J. Electroanal. Chem.* **1992**, *327*, 235-246.
- (65) Chrzanowski, W.; Wieckowski, A. *Langmuir* **1997**, *13*, 5974-5978.
- (66) Chrzanowski, W.; Kim, H.; Wieckowski, A. *Catal. Lett.* **1998**, *50*, 69-75.
- (67) Herrero, E.; Feliu, J. M.; Wieckowski, A. *Langmuir* **1999**, *15*, 4944-4948.
- (68) Tremiliosi-Filho, G.; Kim, H.; Chrzanowski, W.; Wieckowski, A.; Grzybowska, B.; Kulesza, P. *J. Electroanal. Chem.* **1999**, *467*, 143-156.
- (69) Crown, A.; Moraes, I. R.; Wieckowski, A. *J. Electroanal. Chem.* **2001**, *500*, 333-343.
- (70) Crown, A.; Wieckowski, A. *Phys. Chem. Chem. Phys.* **2001**, *3*, 3290-3296.
- (71) Waszczuk, P.; Solla-Gullon, J.; Kim, H. S.; Tong, Y. Y.; Montiel, V.; Aldaz, A.; Wieckowski, A. *J. Catal.* **2001**, *203*, 1-6.
- (72) Lee, C. E.; Tiege, P. B.; Xing, Y.; Nagendran, J.; Bergens, S. H. *J. Am. Chem. Soc.* **1997**, *119*, 3543-3549.
- (73) Coq, B.; Figueras, F. *J. Mol. Catal. A-Chem.* **2001**, *173*, 117-134.
- (74) Coq, B.; Crabb, E.; Figueras, F. *J. Mol. Catal. A-Chem.* **1995**, *96*, 35-48.
- (75) Coq, B.; Crabb, E.; Warawdekar, M.; Bond, G. C.; Slaa, J. C.; Galvagno, S.; Mercadante, L.; Ruiz, J. G.; Sierra, M. C. S. *J. Mol. Catal.* **1994**, *92*, 107-121.
- (76) Coq, B.; Chaqroune, A.; Figueras, F.; Nciri, B. *Appl. Catal. A-Gen.* **1992**, *82*, 231-245.
- (77) Coq, B.; Goursot, A.; Tazi, T.; Figueras, F.; Salahub, D. R. *J. Am. Chem. Soc.* **1991**, *113*, 1485-1492.
- (78) Coq, B.; Bittar, A.; Dutartre, R.; Figueras, F. *J. Catal.* **1991**, *128*, 275-286.
- (79) Didillon, B.; Houtman, C.; Shay, T.; Candy, J. P.; Basset, J. M. *J. Am. Chem. Soc.*

1993, 115, 9380-9388.

(80) Candy, J. P.; Didillon, B.; Smith, E. L.; Shay, T. B.; Basset, J. M. *J. Mol. Catal.*

1994, 86, 179-204.

(81) Candy, J. P.; Didillon, B.; Smith, E. L.; Shay, T. B.; Basset, J. M. *J. Catal.* 1998, 179, 459-468.

(82) Humblot, F.; Didillon, D.; Lepeltier, F.; Candy, J. P.; Corker, J.; Clause, O.; Bayard, F.; Basset, J. M. *J. Am. Chem. Soc.* 1998, 120, 137-146.

(83) Humblot, F.; Candy, J. P.; Le Peltier, F.; Didillon, B.; Basset, J. M. *J. Catal.* 1998, 179, 459-468.

(84) Candy, J. P.; Humblot, F.; Didillon, B.; Lepeltier, F.; Basset, J. M. *Stud. Surf. Sci. Catal.* 1999, 126, 237-242.

(85) Bentahar, F. Z.; Candy, J. P.; Basset, J. M.; Le Peltier, F.; Didillon, B. *Catal. Today* 2001, 66, 303-308.

(86) Tena, E.; Candy, J. P.; Spagnol, M.; Basset, J. M. *J. Mol. Catal. A-Chem.* 2002, 182, 303-307.

(87) Crabb, E. M.; Marshall, R.; Thompsett, D. *J. Electrochem. Soc.* 2000, 147, 4440-4447.

(88) Crabb, E. M.; Ravikumar, M. K. *Electrochim. Acta* 2001, 46, 1033-1041.

(89) Crabb, E. M.; Marshall, R. *Appl. Catal. A-Gen.* 2001, 217, 41-53.

(90) Crabb, E. M.; Ravikumar, M. K.; Qian, Y.; Russell, A. E.; Maniguet, S.; Yao, J.; Thompsett, D.; Hurford, M.; Ball, S. C. *Electrochem. Sol. Stat. Lett.* 2002, 5, A5-A9.

(91) Lee, C. E.; Bergens, S. H. *J. Phys. Chem. B* 1998, 102, 193-199.

(92) Lee, C. E.; Bergens, S. H., 145(2), 4182 *J. Electrochem. Soc.* 1998, 145, 4182.

(93) Bruce, M. I.; Williams, M. L. *Inorg. Synth.* 1989, 26, 262-263.

(94) DiCosimo, R.; Whitesides, G. M. *J. Phys. Chem.* 1989, 93, 768-775.

(95) Gilman, S. *J. Electroanal. Chem.* 1964, 7, 385-391.

(96) Biegler, T.; Rand, A. J.; Woods, R. *J. Electroanal. Chem.* 1971, 29, 269-277.

(97) Woods, R. *J. Electroanal. Chem.* 1974, 49, 217-226.

(98) Connick, R. E.; Hurley, C. R. *J. Am. Chem. Soc.* 1952, 74, 5012-5015.

(99) Van Der Wiel, A. *Chem. Weekblad.* 1952, 48, 597.



- (100) Fachini, E. R.; Cabrera, C. R. *Langmuir* **1999**, *15*, 717-721.
- (101) Herrero, E.; Franaszczuk, K.; Wieckowski, A. *J Phys. Chem. B* **1994**, *98*, 5074-5083.
- (102) Vielstich, W.; Xia, X. H. *J Phys. Chem.* **1995**, *99*, 10421-10422.
- (103) Hoster, H.; Iwasita, T.; Baumgartner, H.; Vielstich, W. *J. Electrochem. Soc.* **2001**, *148*, A496-A450.

## Chapter 3

### Nanoparticle Pt-Ru<sub>ad</sub> Catalysts for Direct Methanol Fuel Cells.

#### Part I: Preparation, Methanol and Pre-adsorbed CO Electrooxidation.<sup>†</sup>

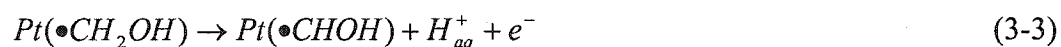
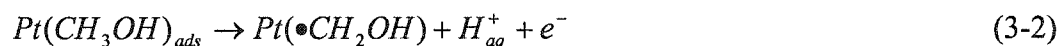
##### 1. Introduction

The interest in direct methanol fuel cell (DMFC) research has significantly increased over the last decade because DMFCs offer several attractive features as an alternative to internal combustion engines for transportation and as an alternative to batteries in portable electronic devices (see chapter 1). The closest alternatives to DMFCs for such applications are H<sub>2</sub>/air PEMFC systems operating on either reformat (H<sub>2</sub> + CO<sub>2</sub>) generated on-board using reformers, or on compressed H<sub>2</sub> gas stored on-board (generated off-board). Compared with H<sub>2</sub>/air PEMFC systems operating on reformat, DMFC systems have advantages including simple system design, ease of operation, reduced weight and volume, and lower cost. Compared with H<sub>2</sub>/air PEMFC systems operating on compressed H<sub>2</sub> gas stored on-board, DMFC systems use liquid methanol as the fuel. Liquid methanol is easier to handle, to store, and to distribute than H<sub>2</sub> gas. In addition, methanol has a higher energy density than hydrogen, and methanol is available in large quantities. The main challenges in DMFC research are the poor kinetics of anode methanol electrooxidation, and cathode polarization resulting from methanol crossover from the anode to the cathode (see Chapter 1). The lack of highly effective, low-cost anode catalysts is a key factor limiting the development of practical DMFC systems. This limitation has stimulated tremendous research effort towards development of active, cost-effective

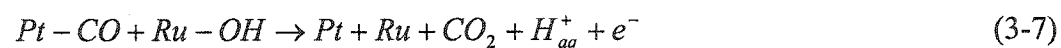
---

<sup>†</sup> A version of this chapter has been published. Cao, D. X.; Bergens, S. H. *Electrochim. Acta* 2003, 48, 4021-4031.

electrocatalysts for oxidation of methanol in fuel cells. Although many catalyst systems have been investigated,<sup>1</sup> only Pt-Ru nanoparticles demonstrably have the combination of high activity and stability in actual prototype DMFCs. The relatively high activity of Pt-Ru systems towards methanol electrooxidation is believed to primarily result from the catalyst acting through a so-called bi-functional mechanism.<sup>2</sup> The platinum's role in the bi-functional mechanism is to promote the adsorption/dehydrogenation of methanol to form adsorbed CO and surface hydrides that are quickly electrooxidized to protons and electrons (Eq. 3-1 to 3-5, the dots indicate the atoms bound to the catalyst surface).



Ruthenium's role in the bi-functional mechanism is to catalyze at low potentials the transfer of oxygen (likely as OH) from water to the adsorbed CO poison (Eq. 3-6, 3-7).



Some researchers have found evidence for electronic effects, that is, the presence of ruthenium changes the electronic structure of platinum in a way that weakens the Pt-CO bond, thereby promotes CO removal.<sup>3-6</sup>

In order to maximize the catalytic performance of Pt-Ru systems towards methanol electrooxidation, large numbers of studies on effects of surface properties on

activity have been carried out. These surface properties include surface composition, surface structure, and surface chemical state. The majority of these studies were performed on model Pt-Ru surfaces such as smooth shiny Pt-Ru alloy surfaces<sup>7-18</sup> and Ru decorated (by electrodeposition, spontaneous deposition, or chemical vapor deposition) Pt single crystal surfaces.<sup>19-41</sup> Surfaces of these flat model catalysts are relatively easily characterized to obtain information about Ru surface concentration, distribution, surface morphology, surface chemical state, and number of surface active sites, thus enabling a close look at the dependence of real activities on these surface properties. Some important results obtained using these model catalysts are summarized below, and will be further discussed in the “results and discussion” section in this chapter. The optimum surface composition of Pt-Ru catalysts for electrooxidation of methanol is between 10% and 50% Ru.<sup>7, 9, 19, 20</sup> The number of surface Pt-Ru neighbor sites appears essential for the activity. For example, Pt-Ru alloys, which have a homogeneous distribution of Pt-Ru sites, and thereby the largest number of Pt-Ru neighbor sites among all forms of model Pt-Ru surfaces, has higher specific activity than single crystal Pt surfaces decorated with Ru adatom islands. Among the Ru decorated Pt(*hkl*) surfaces, Ru/Pt(111) is the most active, showing that methanol electrooxidation over Pt-Ru surfaces is structure sensitive.<sup>24, 26</sup> It is also believed that metallic Pt and Ru are more active than metallic Pt mixed with Ru oxides.<sup>31</sup> Other types of model catalysts that have been studied are electro-codeposited Pt-Ru surfaces<sup>3, 42-45</sup> and rough, polycrystalline Pt surfaces modified by Ru adatoms.<sup>46-53</sup> These rough polycrystalline catalyst systems do not have near atomically smooth, well defined surfaces. As a result, the surfaces of such catalysts are difficult to fully

characterize. These rough surface model catalysts, however, are one-step closer to practical, in-cell Pt-Ru catalysts.

The effects of surface properties on activity for nanoparticle technical-scale Pt-Ru catalysts have not been well studied.<sup>4, 54-69</sup> This is mainly because surface properties of Pt-Ru nanoparticles (i.e., surface composition, number of active surface sites, surface structure) cannot be measured with accuracy (*vide infra*). For example, in the majority of the studies on effects of surface composition on activity for Pt-Ru nanoparticles, the *bulk* Pt-Ru compositions instead of *surface* compositions were used because of the difficulties in measurements of surface compositions of Pt-Ru nanoparticles.<sup>55, 56, 60, 61, 65, 66, 69</sup> However, the bulk compositions may not represent the surface compositions in case of surface segregation occurring.<sup>69</sup> Another critical surface parameter, active surface areas (number of active sites) of Pt-Ru nanoparticles are also difficult to measure accurately. The number of active sites is critical because it provides the inherent (intrinsic, absolute, real) activity (*current density normalized by the real active surface area of the catalysts*, i. e., turnover number) of nanoparticle Pt-Ru surfaces toward methanol electrooxidation. The following methods have been used to investigate the number of active sites and/or surface compositions of *nanoparticle* Pt-Ru systems.

BET surface areas have been used to represent the active surface areas of Pt-Ru catalysts.<sup>55</sup> BET surface areas give the total number of surface sites, including active sites (i.e. metallic Pt and Ru surface atoms) and inactive sites (i.e. surface Pt and/or Ru oxides). In case of the presence of significant amount of Pt and/or Ru oxides on the surfaces of Pt-Ru catalysts, the use of BET surface area will likely over-estimate the metallic active surface area. Further, the surface oxidation states of Pt-Ru catalysts may change after the

catalysts are put into the operating fuel cell. Surface oxides are known to be reduced during operation of DMFCs,<sup>68, 70</sup> and the *ex-situ* BET surface area might thereby not represent the *in-situ* surface area under real working conditions. Another method to investigate the surface area of Pt-Ru nanoparticles is to measure the stripping charge of an adsorbed monolayer of CO, and then calculate the number of active sites by assuming that the ratio of adsorbed CO to surface metal atoms is 1:1.<sup>60, 62, 64, 66</sup> This measurement gives, in principle, the metallic surface area instead of the total surface area (metal sites and oxide sites), and it has been used for either *ex-situ* measurements (for catalysts before being put into MEAs),<sup>60, 61</sup> or *in-situ* measurements (for catalysts after being embedded into MEAs and operated in prototype cells).<sup>68</sup> Some uncertainties are associated with this method. For example, it has not been shown that the ratio of adsorbed CO to surface metal atoms is always 1:1. Further, measured CO stripping charge generally includes not only the Faradaic CO electrooxidation charge but also double-layer charges and charges associated with oxide formation.<sup>71, 72</sup> The measured CO stripping charge may, thereby, not represent only the Faradaic charge. From the studies of well-defined, shiny, flat Pt-Ru alloy systems, it has been found that the adsorbed CO stripping peak potential is a function of Ru surface content.<sup>12</sup> This relationship between the peak potential and surface composition has been extrapolated by some researchers to evaluate the surface compositions of nanoparticle Pt-Ru catalysts.<sup>68, 73</sup> This extrapolation remains to be confirmed by independent measurement. Another method employed to investigate the specific surface area of Pt-Ru nanoparticles is to measure the mean size of the Pt-Ru nanoparticles using TEM or XRD, and then calculate the specific surface area by assuming the particle is a sphere and using Equation 3-8, where  $d$  is the diameter of the particle,  $\rho$  is the density of Pt-Ru alloy.<sup>56, 69</sup>

$$S = \frac{6}{d\rho} \quad (3-8)$$

Accuracy of this measurement much depends on the actual shape of the particles and the distribution of particle size, as well as the measurement of alloy density. Data obtained using this method have proven unreasonable in some cases. For example, a specific surface area of 184 m<sup>2</sup>/g was measured for an unsupported Pt<sub>40</sub>Ru<sub>60</sub> catalyst using XRD. This specific surface area corresponds to a dispersion of 54% (dispersion is the ratio of the number of atoms on the particle surface to the total number of atoms in the particle), which is too high.<sup>69</sup>

The stripping charge of underpotential deposited (udp) Cu on Pt-Ru surfaces has been used to measure the surface area of Pt-Ru nanoparticles by assuming that the complete copper monolayer is deposited in a 1:1 ratio of Cu to surface metal atoms regardless of the Pt/Ru ratio.<sup>74</sup> This measurement gives the metal surface area of Pt-Ru systems, because udp copper does not deposit on surface oxides. In addition to the surface area, the metallic surface composition of Pt-Ru catalysts can also be determined using this technique, because the adsorption energy of Cu on Pt is different from that on Ru. The peak associated with udp Cu on Pt and the peak associated with udp Cu on Ru can be resolved. This recently developed method has not been independently confirmed by others, and it may be difficult to apply to in-cell measurements.

Combinations of spectroscopic techniques such as XPS (X-ray photoelectron spectroscopy), AES (Auger electron spectroscopy), EXAFS (extended X-ray absorption fine structure spectroscopy) etc. have been used to study the surface properties of Pt-Ru systems, which include surface chemical state, structure, and surface composition.<sup>70, 75-77</sup>

The properties detected using these instruments are better referred to as "surface layer

properties” because the X-rays employed by these techniques penetrate a few atomic distances underneath the surface; they actually examine a thin surface layer, not only the outer surface.

Studies on model catalysts have yielded a wealth of data. The fundamental question to all model studies in catalysis also applies to Pt-Ru systems: can the results and conclusions from model surfaces be directly applied to technical Pt-Ru nanoparticle catalysts? It has been known for several systems that catalysis over nanoparticles is different from that over smooth surfaces.<sup>78-83</sup> Particle size effects have been shown to influence the activity of methanol electrooxidation catalysts.<sup>61, 84, 85</sup> Christensen et al.<sup>83</sup> pointed out that extrapolation from bulk to particle electrodes could be dangerous. So it is necessary to further investigate methanol electrooxidation behavior on technical scale Pt-Ru nanoparticle surfaces to address if any similarities and differences exist between model and technical Pt-Ru catalysts.

In this study, nanoparticle Pt-Ru<sub>ad</sub> catalysts of known surface area and of reasonably defined surface composition were prepared by a surface reductive deposition of Ru<sub>ad</sub> onto nanoparticle Pt black (fuel cell grade). In contrast to other studies on nanoparticle Pt-Ru catalysts, in which complicated or uncertain methods were used to measure the real active surface areas and surface composition, we use the experimental procedure to directly control the specific active surface area, and use a straight-forward chemical analysis method to obtain the surface composition of nanoparticle Pt-Ru<sub>ad</sub> catalysts. Methanol and adsorbed CO electrooxidation were carried out over these Pt-Ru<sub>ad</sub> catalysts. The results were compared with those obtained using model Pt-Ru catalysts.



## 2. Experimental

### 2.1 General

The argon (Praxair, pre-purified), and carbon monoxide (Matheson, ultrahigh purity) were used as received. The hydrogen gas was generated by a hydrogen generator (Peak<sup>TM</sup>, Scientific). The water was deionized, distilled, and then distilled again from alkaline permanganate. The methanol (CH<sub>3</sub>OH) (Sigma-Aldrich, ACS HPLC grade, 99.93%), H<sub>2</sub>SO<sub>4</sub> (Alfa Aesar, 99.9999%), H<sub>2</sub>O<sub>2</sub> (ACP Chemicals Inc, Reagent ACS, 30%), ruthenium (III) chloride hydrate (RuCl<sub>3</sub> · xH<sub>2</sub>O) (AITHACH Chemical Corp.), KOH (BDH Inc. ACS), and K<sub>2</sub>S<sub>2</sub>O<sub>8</sub> (Fisher Scientific Company, Certified Reagent) were used as received. The Pt black was Johnson Matthey fuel cell grade with a specific surface area of 27 m<sup>2</sup>/g (both as quoted by Johnson Matthey and measured independently by us).

All glassware was rinsed in the following sequence: a 1:5 mixture of 30% aqueous hydrogen peroxide and concentrated H<sub>2</sub>SO<sub>4</sub>, water, a 5% mixture of ammonium hydroxide in absolute ethanol, absolute ethanol, water again and then dried in an oven. The deposition reactor was a 3 dram 21×50 mm vial containing a 4 × 14 mm Teflon-coated magnetic stir bar and capped with a rubber septum.

Electrochemical experiments were performed in a typical three-electrode electrochemical cell using a Pine Bipotentiostat Model AFCBP1 controlled with PineChem 2.00 software. Electrolytes were purged with argon for at least 15 min prior to use and protected under an atmosphere of argon at bubbler pressure during experiments. The reference electrode was a reversible hydrogen electrode. The counter electrode was a blacked Pt gauze behind a D-porosity glass frit. A constant temperature bath (Brinkmann,

Lauda Model RK20,  $\pm 0.03$  °C) was used to maintain the temperature of the electrochemical cell. Inductively coupled plasma spectroscopy (ICP) was carried out using a Perkin-Elmer Optima equipped with an atomic emission detector.<sup>47</sup>

## 2.2 Preparation of Pt-Ru<sub>ad</sub> Catalysts

Nanoparticle Pt-Ru<sub>ad</sub> catalysts were prepared by surface reductive deposition of Ru<sub>ad</sub> onto Pt surfaces using pre-adsorbed H as the reducing agent. Platinum substrates were first cleaned with 3% H<sub>2</sub>O<sub>2</sub> and then maintained in the remaining water in the reactor. The reactor was flushed with argon for 30 min to remove any oxygen, then flushed with argon-diluted hydrogen for 15 minutes, and with pure hydrogen for another 15 minutes to reduce the platinum, forming pre-adsorbed H on the Pt surface. The system was then flushed with argon to eliminate the excess H<sub>2</sub>. An argon-purged, freshly-made 0.05 M RuCl<sub>3</sub> aqueous solution was introduced into the reactor via a cannula. The ratio of Pt to RuCl<sub>3</sub> aqueous solution is 10 mg:1 mL. The solution was stirred under argon for 1 hour to complete the deposition. The Pt-Ru<sub>ad</sub> nanoparticles were separated from the liquid by vacuum filtration in air, then thoroughly washed with pure water, and dried under vacuum in a desiccator for 24 hours. The deposition could be repeated as many times as needed to obtain Pt-Ru<sub>ad</sub> with high Ru surface coverage. Drying and cleaning with H<sub>2</sub>O<sub>2</sub> are not necessary between each deposition.

To obtain the amount of Ru<sub>ad</sub> deposited on Pt surfaces, the Pt-Ru<sub>ad</sub> was suspended in a saturated solution of potassium persulfate in 4.0 M KOH. The ratio of Pt-Ru<sub>ad</sub> (mg) to the alkaline solution (mL) is 3:5. The solution was stirred for 1 hour in a sealed container, and then it was left overnight without stirring at room temperature.<sup>86</sup> It was found that all the adsorbed Ru<sub>ad</sub> and some of the surface Pt are oxidized from such surfaces to form

soluble oxides under these conditions (chapter 2). UV-Vis spectra of the resulting solutions indicated that the ruthenium oxides are primarily ruthenate. ICP analysis was carried out on the resulting solution to measure the amount of ruthenium. The amount of ruthenium obtained in this way was crosschecked by exhaustive anodic stripping of Ru<sub>ad</sub> from the Pt-Ru<sub>ad</sub> surface in 1.0 M aqueous NaOH using a 9 V battery as the power source and followed by ICP analysis.<sup>46</sup>

### *2.3 Methanol Electrooxidation*

To perform methanol electrooxidation over nanoparticle catalysts [e. g. Pt, Pt-Ru<sub>ad</sub>, Pt-Ru alloy (Johnson & Matthey) and (Pt-Ru)O<sub>x</sub> (E-TEK)], the catalyst was immobilized on a surface of a platinum foil (20×10×0.18mm) electrode using the following procedure: first, the platinum foil was cleaned with aqua regia, piranha solution, and then pure water; second, a catalyst ink was prepared by ultrasonically dispersing a known amount of the catalyst in pure water (typically 5 mg/mL) for 30 min; third, an aliquot of the suspension (typically 200 μL) was placed upon the platinum foil to typically deposit 1mg catalyst on the electrode; fourth, the suspension was air-dried to yield a uniform thin catalyst layer electrode. The amount of catalyst immobilized on the Pt foil surface was obtained by the volume of the suspension transferred and was crosschecked by weighing. The immobilized nanoparticle catalyst electrodes prepared this way were physically stable enough to withstand the operations involved in cyclic voltammetry and electrooxidation reactions. The use of bare particle surfaces (without binder like Nafion<sup>®</sup>) resulted in good contact between the particles and the Pt foil conductor, thereby minimizing the diffusion and catalyst utilization problems. The surface area and methanol electrooxidation activity of the Pt foil were measured and subtracted as background. This background is very small.

The electrode potential was set to 0.075 V upon immersion into the argon-purged electrolyte ( $[\text{H}_2\text{SO}_4] = 1.0 \text{ M}$ ). Continuous potential sweeps were carried out between 0 and 700 mV at 10 mV/s. No obvious changes in the CVs were found between the first and subsequent scans. The potential was then held at 0.075 V while the deoxygenated methanol was added to the cell to bring the final  $[\text{CH}_3\text{OH}] = [\text{H}_2\text{SO}_4] = 1.0 \text{ M}$ . The solution was stirred for 5 min to ensure the equilibration of both concentration and temperature gradients prior to electrochemical data acquisition. The potentiodynamic cycling was started after the stirring (sweep rate = 10 mV/s, sweep range 0 to 600 mV) with the first sweep in the negative direction. The potential was then held at 75 mV for 5 min and then the potentiostatic oxidation was started by stepping the potential to 450 mV at room temp and 400 mV at 60 °C.

#### *2.4 Adsorbed CO Electrooxidation*

CO was adsorbed on catalyst surfaces by bubbling CO at 1 atm through the stirred electrolyte ( $\text{H}_2\text{SO}_4$ , 1.0 M) for 25 min while holding the potential at 0.075 V. The excess CO was then flushed from the electrolyte with argon gas for 25 min, the stirring was stopped, and the potential was cycled between 0 and 0.70 V at 10 mV/s. The first sweep was in the positive direction.

### **3. Results and Discussion**

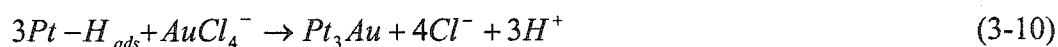
#### *3.1 Ruthenium Deposition*

Surface reductive deposition of a second metal on Pt surfaces using pre-adsorbed hydrogen as reducing agent was first described in a patent three decades ago by Pott,<sup>87</sup>

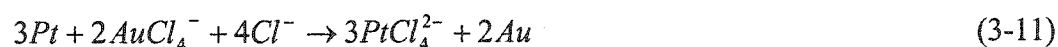
who claimed to use this technique to prepare Pt-M “alloy” (M=Sn, Ti, Ta, Re, Ru, Pb, As, Sb, Bi) catalysts for the electrooxidation of methanol in sulfuric acid (Eq. 3-9).



The description “alloy” is likely not correct here because it is unlikely that metal alloys will form by this method (the depositions were carried out in aqueous solutions at room temperature).<sup>88</sup> Instead, the bimetallic catalysts prepared using this method may better be described as M-M'<sub>ad</sub> systems. This methodology was used later by Janssen et al.<sup>1</sup>,<sup>89</sup> and Szabo et al.<sup>90,91</sup> to prepare Pt-Ru<sub>ad</sub> for methanol electrooxidation. In their studies, pre-adsorbed hydrogen on a Pt surface was formed electrochemically by holding the Pt electrode potential at 0.05 V vs. RHE in an acid electrolyte; the Pt surface with saturated hydrogen was then transferred to an aqueous RuCl<sub>3</sub> solution. In the last decade, Barbier, Szabo and their co-workers prepared a series of M-M'<sub>ad</sub> catalysts (e. g., Pt-Au<sub>ad</sub>,<sup>92-98</sup> Pt-Cu<sub>ad</sub>,<sup>99</sup> Pd-Pt<sub>ad</sub>,<sup>100-103</sup> Pt-Re<sub>ad</sub>,<sup>104-109</sup> Rh-Cu<sub>ad</sub>,<sup>110</sup> Pt-Rh<sub>ad</sub>,<sup>111</sup> Pd-Sn<sub>ad</sub>,<sup>112</sup> Pt-Pd<sub>ad</sub>,<sup>113</sup> ) using a similar methodology for non-electrochemical reactions (Eq. 3-10).



They also found that the substrate metal itself can act as the reducing agent for the ions of the second metal. For example, in Equation 3-11, Pt acts as the substrate metal as well the reducing agent; AuCl<sub>4</sub><sup>-</sup> was reduced by the surface Pt atoms, resulting in the formation of Pt-Au<sub>ad</sub>.



Recently, Adzic and co-workers<sup>114-118</sup> applied this technique to the deposition of Pt on Ru to prepare Ru-Pt<sub>ad</sub> catalysts for fuel cell applications. In this deposition, Ru acts as reducing agent. The driving force for the deposition is in part the difference between the

potential for  $[\text{PtCl}_6]^{2-}$  reduction, and the potential for  $\text{Ru}^0$  oxidation (chapter 1). This deposition is not a self-limiting process, i.e., it will, in principle, proceed until all the accessible Ru is oxidized. Adzic and co-workers show that the amount and distribution of Pt on the surface of Ru(0001) depend on the concentration of  $[\text{PtCl}_6]^{2-}$  and the deposition time. For example, if a freshly prepared Ru(0001) single crystal is immersed in a  $10^{-4}$  M  $[\text{PtCl}_6]^{2-}$  + 0.1 M  $\text{H}_2\text{SO}_4$  solution for 2 min, about 35% of the Ru surface is covered with a great number of Pt nanoparticles. The Pt nanoparticles have a columnar shape and relatively uniform size, with heights in the range of 3-5 nm (10-15 monolayer), and with diameters between 6 and 10 nm. If the Ru(0001) single crystal is immersed in a  $10^{-2}$  M  $[\text{PtCl}_6]^{2-}$  + 0.1 M  $\text{H}_2\text{SO}_4$  solution for 1 min, the entire Ru surface is covered with 2-6 nm-sized Pt clusters. This deposition of Pt also occurs on the carbon-supported Ru nanoparticles (10 wt% Ru on Vulcan XC-72, E-TEK) reduced in  $\text{H}_2$  at elevated temperatures (e. g. 300 °C). The resulting Ru-Pt<sub>ad</sub>/C (nominal atomic ratio of Pt:Ru is 1:20) catalyst has high activity and CO tolerance surpassing those of commercial 1:1 Pt-Ru alloy catalyst (E-TEK) as tested outside of a fuel cell.

In this work, we further explored this technique for the preparation of Pt-Ru<sub>ad</sub> nanoparticles. Unsupported Pt nanoparticles (fuel cell grade) of known specific surface area were used as the substrate. This Pt surface was first saturated with hydrogen, and the excess hydrogen was then flushed from the system. The deposition was carried out in aqueous  $\text{RuCl}_3$  solution at room temperature. If the reduction goes to completion, three surface adsorbed H atoms would be consumed for every Ru adatom deposition (Eq. 3-12).



In this system,  $\text{Ru}^{3+}$  can only be reduced by surface-adsorbed hydrogen, since the platinum cannot act as a reducing agent because the reduction potential of  $\text{PtCl}_4^{2-} | \text{Pt}, \text{Cl}^-$  (0.73 V) and  $\text{PtCl}_6^{2-} | \text{Pt}, \text{Cl}^-$  (0.74 V) are higher than that of  $\text{Ru}^{3+} | \text{Ru}$  (0.61 V) and  $\text{Ru}^{3+} | \text{Ru}^{2+}$  (0.24 V). Consequently, the deposition is expected to stop after the available pre-adsorbed hydrogen was consumed, with a maximum coverage by Ru of 0.33 for each deposition. The deposition can, in principle, be repeated as many times as needed to obtain high Ru coverage. A series of Pt-Ru<sub>ad</sub> catalysts with various Ru surface concentrations were prepared by repeating the deposition. Their Ru surface concentration (Ru%) (*defined as the ratio of the number of total Ru adatoms deposited to the number of surface atoms originally on the Pt substrate, also called surface equivalents Ru*) were measured, and the results are presented in Table 3-1.

**Table 3-1.** Nanoparticle Pt-Ru<sub>ad</sub> catalysts prepared by surface reductive deposition of Ru on nanoparticle Pt black.

Number of Deposition (n)	1	2	3	5	7
Ru Surface Concentration (Ru%)	18	38	57	85	131
$\frac{\text{Ru}\%}{n}$	18	19	19	17	19
Estimated Ru Coverage ( $\theta_{\text{Ru}}$ )	0.18	0.33	0.45	0.63	0.75

It should be pointed out that without knowing the distribution pattern of the Ru<sub>ad</sub> on the Pt surfaces, these Ru surface concentrations may not well reflect the true surface composition of Pt-Ru<sub>ad</sub> (the surface composition is defined as *the ratio of the number of exposed surface Ru atoms to the number of surface atoms originally on the Pt substrate,*

*this true surface composition will be referred to as 'Ru surface coverage', and denoted as  $\theta_{Ru}$  during this work*). The two extremes of how Ru can deposit on Pt is illustrated in a simplified way in Figure 3-1.

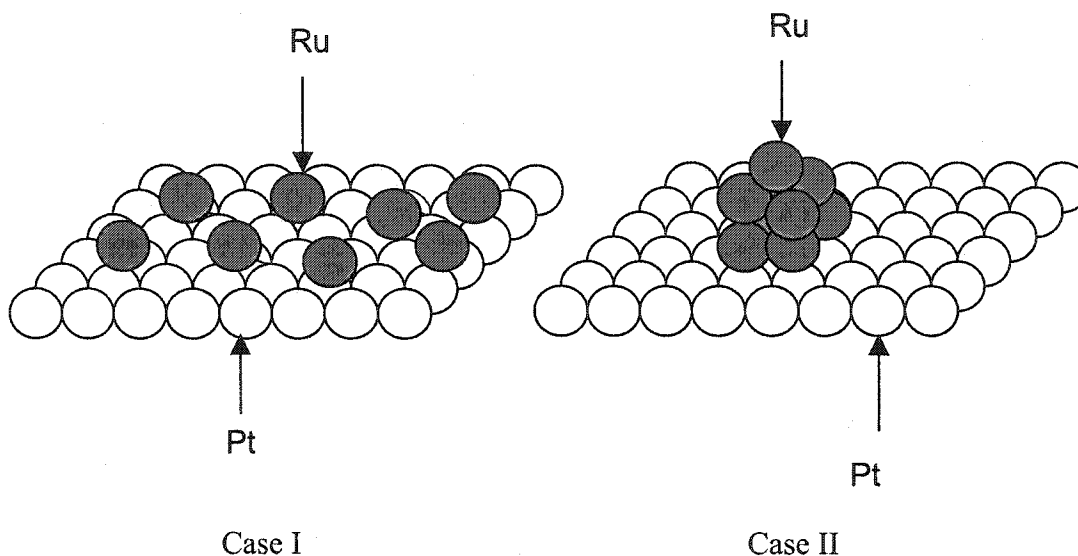


**Figure 3-1.** Two extreme ways  $Ru_{ad}$  may deposit on the surface of Pt.

In case I, all of the Ru atoms are in contact with surface Pt, and the Ru surface concentration is identical with the surface composition (Ru surface coverage). In case II, all Ru atoms form a three dimensional island on the Pt surface, and the Ru surface concentration is more than the real Ru surface coverage. The actual distribution of deposited Ru atoms on Pt surface is most likely somewhere between these two cases, depending on the Ru surface concentration and the properties of the deposition reactions. Now, there is a question to be asked for Pt- $Ru_{ad}$  nanoparticles prepared using the surface reductive deposition method in this study; that is, how are the Ru adatoms distributed on the surface of nanoparticle Pt black after each deposition? In another words, how close is



the Ru surface concentration (measured) to the real Ru surface coverage? As discussed early in this chapter, there isn't a confirmed technique that can be applied to look at the distribution of Ru on nanoparticle Pt surfaces. So the following model was proposed to try to address this issue.

The model is based on the following facts: (1) Ru surface concentration (measured by oxidation stripping of  $\text{Ru}_{\text{ad}}$ , see experimental) divided by the corresponding number of depositions gives a nearly constant number of 18% (see Table 3-1) regardless of the substrate surface identity (the substrate is Pt for the first deposition, and is Pt- $\text{Ru}_{\text{ad}}$  for the subsequent depositions). This means that the substrate surface mainly acts as an adsorbed-hydrogen carrier, and has no significant influence on where the Ru goes. Assuming that the Ru deposition reaction actually occurs between  $\text{Ru}^{3+}$  and adsorbed H, the deposition of Ru on Pt and Ru surfaces may occur at a nearly equal probability. (2) A Pt- $\text{Ru}_{\text{ad}}$  with more than 100% Ru surface concentration (131%, Table 3-1) was obtained after 7 depositions of Ru. This indicates that Ru atoms deposit not only on Pt surface sites but also on Ru surface sites formed in the previous depositions, because if Ru atoms only deposited on Pt sites, then the deposition would stop when all Pt sites are covered (near 100% Ru surface concentration), which is not the case. (3) 131% Pt- $\text{Ru}_{\text{ad}}$  is still much more active than either pure Pt or pure Ru (*vide infra*), especially at room temperature (pure Ru is inactive at room temperature). This means that the surface of 131% Pt- $\text{Ru}_{\text{ad}}$  is not completely covered by Ru; therefore, Ru must deposited on both the Pt and Ru surfaces. (4) Results obtained from baseline voltammetric studies in acid, from potentiostatic methanol electrooxidation, and from potentiodynamic electrooxidation of adsorbed CO (*vide infra*) all indicate that the coverage of Pt by Ru adatoms favours 2-dimensional growth over

3-dimensional growth. This assertion has to be investigated further, presumably by carrying out the deposition over surfaces of Pt single crystals. Pending the results of such single crystal studies, we propose the following crude model for the deposition (Figure 3-2).

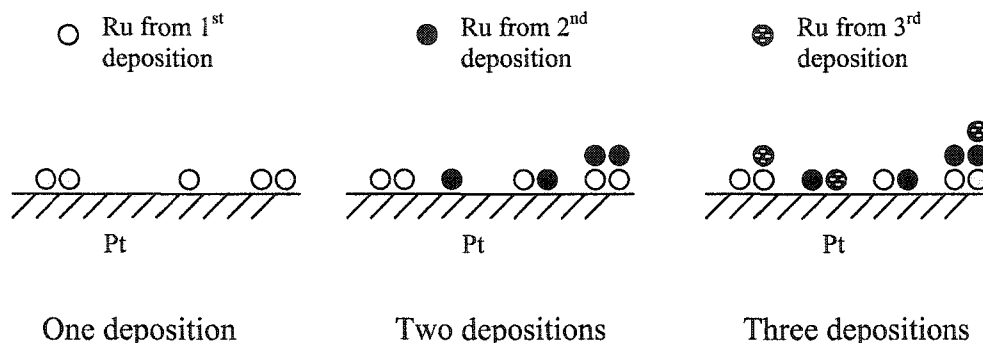


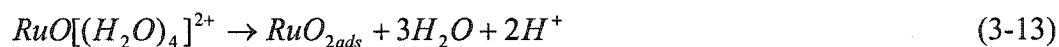
**Figure 3-2.** Schematic of the model for Ru reductive deposition on Pt.

The first deposition produces a near monatomic layer of Ru adatoms on the surface of Pt. In each subsequent deposition, Ru is deposited equally on exposed Pt surfaces and Ru surfaces, and forms a near monatomic Ru layer on the substrate surface (Pt-Ru<sub>ad</sub>). Using this model, the Ru surface coverage  $\theta_{Ru}$  can be estimated. Taking the two-times deposition as an example, the estimation is illustrated as follows: After the first deposition, 18% of the Pt surface was covered by Ru<sub>ad</sub>. 82% of the Pt surface was uncovered. After the second deposition, another 18% Ru was deposited on the Pt-Ru<sub>ad</sub> surface, of which,  $18\% \times 82\% = 15\%$  was deposited on uncovered Pt sites. Therefore,  $18\% + 15\% = 33\%$  of the Pt surface was covered after 2 depositions. The results obtained are given in Table 3-1.

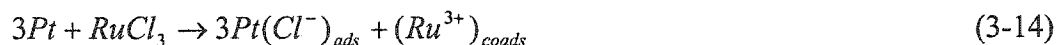
The theoretical maximum of 33% Ru is not obtained by these depositions in this study. Several factors may account for only 18% deposition versus 33%. These include

possible blockage of the surface by adsorbed chloride ions, loss of surface-adsorbed hydrogen through oxidation by trace oxygen in the system, and not all the surface-adsorbed hydrogen may be accessible (contribute, or participate in) to reaction with  $\text{Ru}^{3+}$ . A more likely explanation is that  $\text{RuCl}_3 \cdot x\text{H}_2\text{O}$  often contains significant amounts of Ru(IV) species,<sup>119</sup> which would decrease the stoichiometry of the deposition from that shown in Equation 3-12.

Wieckowski and co-workers<sup>22, 23</sup> reported that Ru can be deposited on Pt by immersing an electrochemically cleaned Pt surface into an aged solution of  $\text{RuCl}_3$  in 0.1 M  $\text{HClO}_4$ , following by several potential sweeps of the Pt electrode between 0.06 V and 0.8 V vs. RHE. This process is referred to as spontaneous deposition by the authors. These spontaneous depositions are believed to proceed first by the irreversible chemisorption of the aqua-complex  $\text{RuO}[(\text{H}_2\text{O})_4]^{2+}$  present in the aged  $\text{RuCl}_3$  solution onto the Pt surface to form adsorbed Ru oxides (Eq. 3-13). The adsorbed Ru oxides are reduced during the



potential sweeps to form strongly adsorbed ruthenium or RuO islands. Vielstich and co-workers<sup>20</sup> reported a deposition of Ru on Pt single crystals using freshly prepared  $\text{RuCl}_3$  solution (with or without  $\text{HClO}_4$ ). Aging effects were observed on the order ranging from a few minutes to hours, which affected the reproducibility of Ru deposits. They concluded that the deposition proceeds via prior adsorption of  $\text{Cl}^-$  on the clean Pt, with  $\text{Ru}^{3+}(\text{aq})$  acting as counterions and thereby in a sense being coadsorbed on Pt (Eq. 3-14). The co-adsorbed



$\text{Ru}^{3+}$  is then reduced to  $\text{Ru}^0$ , and the  $\text{Cl}^-$  is desorbed during subsequent electrochemical reduction. These depositions are two-step processes, adsorption followed by

electrochemical reduction. The electrochemical reduction has to be performed after the spontaneous adsorption in order to obtain strongly adsorbed ruthenium. Vielstich and co-workers<sup>20</sup> also carried out deposition of  $\text{Ru}_{\text{ad}}$  on Pt(111) by bubbling excess hydrogen gas through aqueous  $\text{RuCl}_3$  in the presence of Pt(111). In the surface reductive deposition studied here, the substrate (Pt or Pt- $\text{Ru}_{\text{ad}}$ ) surfaces were covered by adsorbed hydrogen prior to contact with aqueous  $\text{Ru}^{3+}$ . The  $\text{Ru}^{3+}$  was directly reduced on the substrate surface in a one-step procedure. Notably, it is possible that, if Eq. 3-14 holds for this system, the Ru adatoms reduced by pre-adsorbed hydrogen could serve as surface sites for the adsorption of  $\text{Cl}^-$ , and co-adsorption of  $\text{Ru}^{3+}$ ; thereby a spontaneous adsorption as described by Vielstich will follow the surface reductive deposition. However, we found that each deposition added 18% Ru to the surface, less than the 33% maximum predicted by Eq. 3-14. It, therefore, appears unlikely that a deposition process such as described by Vielstich occurs during these depositions.

The deposition of Ru may occur directly between adsorbed hydrogen and  $\text{Ru}^{3+}$ . It may also proceed by an electrochemical mechanism (electroless), as shown in Figure 3-3.

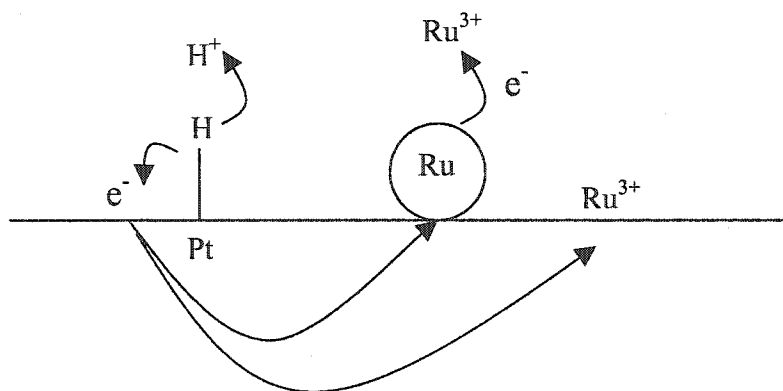


**Figure 3-3.** The deposition of  $\text{Ru}_{\text{ad}}$  on the surface of Pt based on an electrochemical mechanism.

In this case,  $\text{Ru}^{3+}$  could be reduced without direct reaction with adsorbed hydrogen. So it is possible that multilayer deposition occurs within each deposition. If this reaction mechanism dominates the deposition, then the assumption that a monatomic layer of Ru adatoms are formed at each deposition may not be valid.

The proposed model for the surface reductive deposition is based on assumptions that must be investigated further. However, the Ru surface coverage estimated using this model better represents the real surface composition than does the measured Ru surface concentration. Further, the experimental results obtained to date (cyclic voltammograms, methanol and adsorbed CO electrooxidation) support this model (*vide infra*). The activities of Pt-Ru<sub>ad</sub> catalysts prepared in this work are therefore reported using the estimated Ru surface coverage; the corresponding surface concentrations are given in Table 3-1. The Pt-Ru<sub>ad</sub> samples used in this study will be designated by Pt-Ru<sub>ad</sub>- $\theta$ , where  $\theta$  is the estimated Ru surface coverage.

The specific surface areas of Pt-Ru<sub>ad</sub> catalysts were obtained as follows. First, the specific surface area of nanoparticle Pt black was measured *before* deposition of Ru<sub>ad</sub>. This measurement gives 27 m<sup>2</sup>/g as the specific surface area, which is in excellent agreement with the manufacturer's quoted data. Then the specific surface area of nanoparticle Pt black *after* the Ru deposition was measured. To do so, the deposited Ru adatoms were first stripped off by electrooxidation of Ru in an alkaline solution (see experimental section in chapter 2). It was found that the specific surface area of Pt black did not change during the deposition of Ru. This is as expected, because under the deposition conditions used for this work (at room temperature in aqueous solution), the surface area of Pt black is in our hands stable. Further, the deposition of only submonolayers of Ru adatoms on Pt surfaces does

not change the surface area of Pt significantly. The mass of Pt-Ru<sub>ad</sub> is nearly the same as that of the Pt substrate because the amount of Ru<sub>ad</sub> is negligible relative to the mass of Pt. Therefore, it can be concluded that the specific surface area of nanoparticle Pt-Ru<sub>ad</sub> (m<sup>2</sup>/g) is the same as that of nanoparticle Pt black (27m<sup>2</sup>/g).

Figure 3-4 shows the cyclic voltammograms (CV) for Pt (a) and Pt-Ru<sub>ad</sub> (b-f) nanoparticles obtained in 1.0 M aqueous H<sub>2</sub>SO<sub>4</sub>. The CV for Johnson Matthey Pt-Ru black (HiSPEC-6000<sup>®</sup>, 50:50 Pt:Ru)(g) is also shown for comparison. The currents were normalized to the real surface area of the catalysts (obtained using specific surface areas of 27 m<sup>2</sup>/g for Pt-Ru<sub>ad</sub> and 70 m<sup>2</sup>/g, *vide infra*). As Figure 3-4 shows, the CV of the nanoparticle Pt black displays two well-resolved peaks in the “hydrogen region” (ca. 0.05~0.375 V) and small currents in the “double layer region” (ca. 0.4-0.6 V). As the coverage of the Pt surface by Ru<sub>ad</sub> increases, peaks in the “hydrogen region” become less resolved, and currents in the “double layer region” increase. These are typical features of Pt-Ru surfaces.<sup>7, 9, 48</sup> These features are attributed to formation and reduction of surface Ru oxides, which occur at potentials ranging from 0.2 to 1.2 V. Notably, the CV of the Pt-Ru<sub>ad</sub>-0.45 (Figure 3-4d) closely resembles that of Johnson Matthey 50:50 Pt-Ru black (Figure 3-4g). Cyclic voltammetric profiles for Pt-Ru<sub>ad</sub>-0.63 and Pt-Ru<sub>ad</sub>-0.75 are more characteristic of that for pure polycrystalline Ru.<sup>7, 54</sup> These observations suggest the estimated Ru coverage obtained using the deposition model fairly reflects the real surface composition.

In a recent study on nanoparticle Pt-Ru<sub>ad</sub> prepared by their spontaneous deposition of Ru<sub>ad</sub> on nanoparticle Pt black, Wieckowski and co-workers<sup>62</sup> observed, in contrast to our results, that the change in the voltammetric morphology in the hydrogen range upon Ru

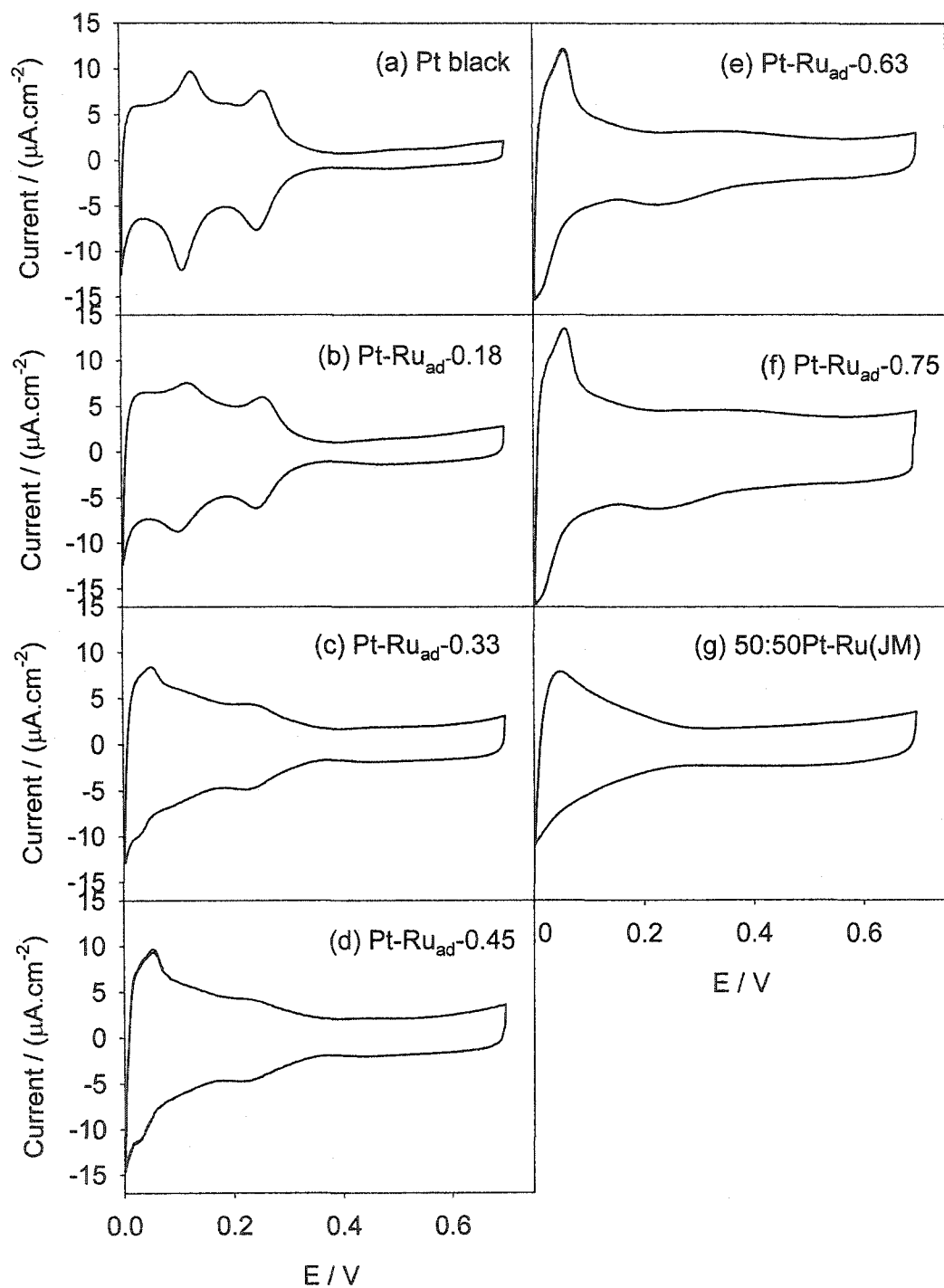


**Figure 3-4.** Cyclic voltammograms of (a) Pt, (b-f) Pt-Ru<sub>ad</sub> with different Ru coverage, and (g) 50:50 Pt-Ru from Johnson Matthey. The voltammograms were recorded in 1.0 M H<sub>2</sub>SO<sub>4</sub> at 10 mV/s and room temperature.

deposition from that of clean platinum is much less than the corresponding difference between the clean platinum and the Pt-Ru alloys (see Figure 1 in reference 62). Wieckowski and co-workers proposed two reasons that may be responsible for this unique feature they observed: (1) that hydrogen adsorbs on top of Ru deposited on Pt, and (2) that Ru islands are transparent to protons undergoing reduction to atomic hydrogen on the Pt surface, and hydrogen adsorption occurs underneath the Ru adlayer. Besides these two reasons, if Ru atoms deposited on Pt surfaces are highly packed at some locations of the Pt surface (e. g., the more active positions for the adsorption of Ru species) as large multilayer Ru islands, and not uniformly spread over the Pt surface (see Figure 3-4), then the actual Ru surface coverage will be much smaller than the measured Ru surface concentration. Therefore, even at high Ru surface concentrations (e. g., 40% Ru), the majority of the Pt-Ru<sub>ad</sub> surface is uncovered Pt (e. g., 80%), which will lead to the observation of less peak resolution change in the “hydrogen region” at high Ru surface concentration. Our surface reductive deposition seems to deposit Ru<sub>ad</sub> more evenly on Pt surfaces, so the CV of our Pt-Ru<sub>ad</sub>-0.45 closely resembles that of the Johnson Matthey 50:50 Pt-Ru alloy surface. These results show that the surface reductive deposition used in this work and the spontaneous deposition used by Wieckowski and co-workers produce Pt-Ru<sub>ad</sub> with different surface structures. The CVs of surfaces made by reductive deposition appear more like Pt-Ru alloys, with a more uniform distribution of Ru on nanoparticle Pt surfaces than spontaneous deposition. Studies using Pt single crystal substrates have shown that spontaneous deposition of Ru on Pt(111) is homogeneous, with no observed preferential deposition on step edges or surface defect sites,<sup>29</sup> and high Ru surface coverage (e.g., 30-35% STM after four depositions) can be obtained over Pt(111).<sup>32</sup> However, the



question still remains as to how well conclusions made using Pt(111) apply to nanoparticle surfaces. Another difference is evident between surface reductive deposition and spontaneous deposition. For surface reductive deposition, each deposition stops after about 18% Ru was deposited on the substrate surface, no matter if it is the first deposition (Pt substrate) or subsequent depositions (Pt-Ru<sub>ad</sub> substrate). For spontaneous deposition, the first deposition stops at about 20% Ru surface concentration, and each subsequent deposition adds only ca. 5% Ru surface concentration.<sup>32, 62</sup>

Except those features typical of Pt-Ru alloy systems, a sharp peak at ca. 0.07 V was observed in CVs of Pt-Ru<sub>ad</sub> catalysts prepared by more than one reductive deposition. The intensity of this sharp peak increases as more depositions were carried out. This peak has been observed on Ru decorated Pt(111) single crystal surfaces prepared by direct reduction of Ru on Pt by bubbling hydrogen through a perchloric acid solution of RuCl<sub>3</sub> in the presence of Pt(111).<sup>20</sup> The peak has also been observed on the surfaces of polycrystalline Ru<sup>120</sup> and Ru (0001).<sup>121-125</sup> In these studies, the authors related this peak to the surface adsorbed hydrogen on 3-D Ru. Very recently, Brankovic et al. challenged the above conclusion by pointing out that the peak is due to the oxidation of *several top atomic layers of Ru* to RuOH<sup>126</sup>. Even though there is no general agreement on the assignment of this sharp peak, one thing these authors agreed with is that the sharp peak is related to multiple atomic layers in the Ru structure. Accordingly, the sharp peak feature observed on our nanoparticle Pt-Ru<sub>ad</sub> catalysts suggests the presence of 3-D multilayer Ru islands on Pt-Ru<sub>ad</sub> surfaces. This result agrees with our deposition model, i. e., Ru not only deposited on Pt but also on Ru; thus, multilayer Ru islands were formed on Pt-Ru<sub>ad</sub> surfaces, when the deposition was performed for more than one cycle. Wieckowski's group reported recently

that the multiple spontaneous depositions of Ru on Pt single crystal surfaces result in the formation of pseudo 3-D multilayer Ru islands.<sup>32</sup>

### 3.2 Methanol Electrooxidation

Current-time curves for potentiostatic electrooxidation of methanol on Pt and Pt-Ru<sub>ad</sub> nanoparticles were measured in 1.0 M H<sub>2</sub>SO<sub>4</sub> + 1.0 M MeOH at 22 °C ( $E = 0.45$  V) and 60 °C ( $E = 0.40$  V). Figure 3-5 shows typical curves with the current normalized to the real surface area. It is seen that all nanoparticle Pt-Ru<sub>ad</sub> prepared in this work display much higher activities than nanoparticle Pt. Pt-Ru<sub>ad</sub>-0.33 is the most active at both 22 °C and 60 °C, and represents a factor of 6 and 45 enhancement versus the pure Pt at 22 °C and 60 °C, respectively. We noticed that Pt-Ru<sub>ad</sub>-0.18 is more active than Pt-Ru<sub>ad</sub>-0.64, followed by Pt-Ru<sub>ad</sub>-0.75, at 22 °C, but becomes the least active at 60 °C. This behavior agrees, to some extent, with the reaction mechanism suggested by Gasteiger and co-workers based on their temperature dependence studies on bulky *Pt-Ru alloy* model catalysts.<sup>9</sup> They proposed that the rate-determining step (rds) for methanol electrooxidation on Pt-Ru alloy surfaces at room temperature is methanol adsorption/dehydrogenation (Eq. 3-1 to 3-5). These reactions occur only at threefold Pt ensembles because three neighbor Pt atoms are needed for complete dehydrogenation of one methanol molecule (Figure 3-6). Therefore, Pt-Ru catalysts with lower Ru surface content (more threefold Pt ensembles) show higher activity at low temperature (e. g., 10% Ru is the best at 25 °C). As the temperature increases from 25 °C to 60 °C, the rate-determining step shifts to the bimolecular surface reaction between surfaced adsorbed CO and OH (Eq. 3-7). Since adsorbed OH primarily forms at Ru sites (Eq. 3-6), Pt-Ru catalysts with higher Ru surface content provide higher surface concentration of adsorbed OH, and thereby exhibit higher activity at high temperature.

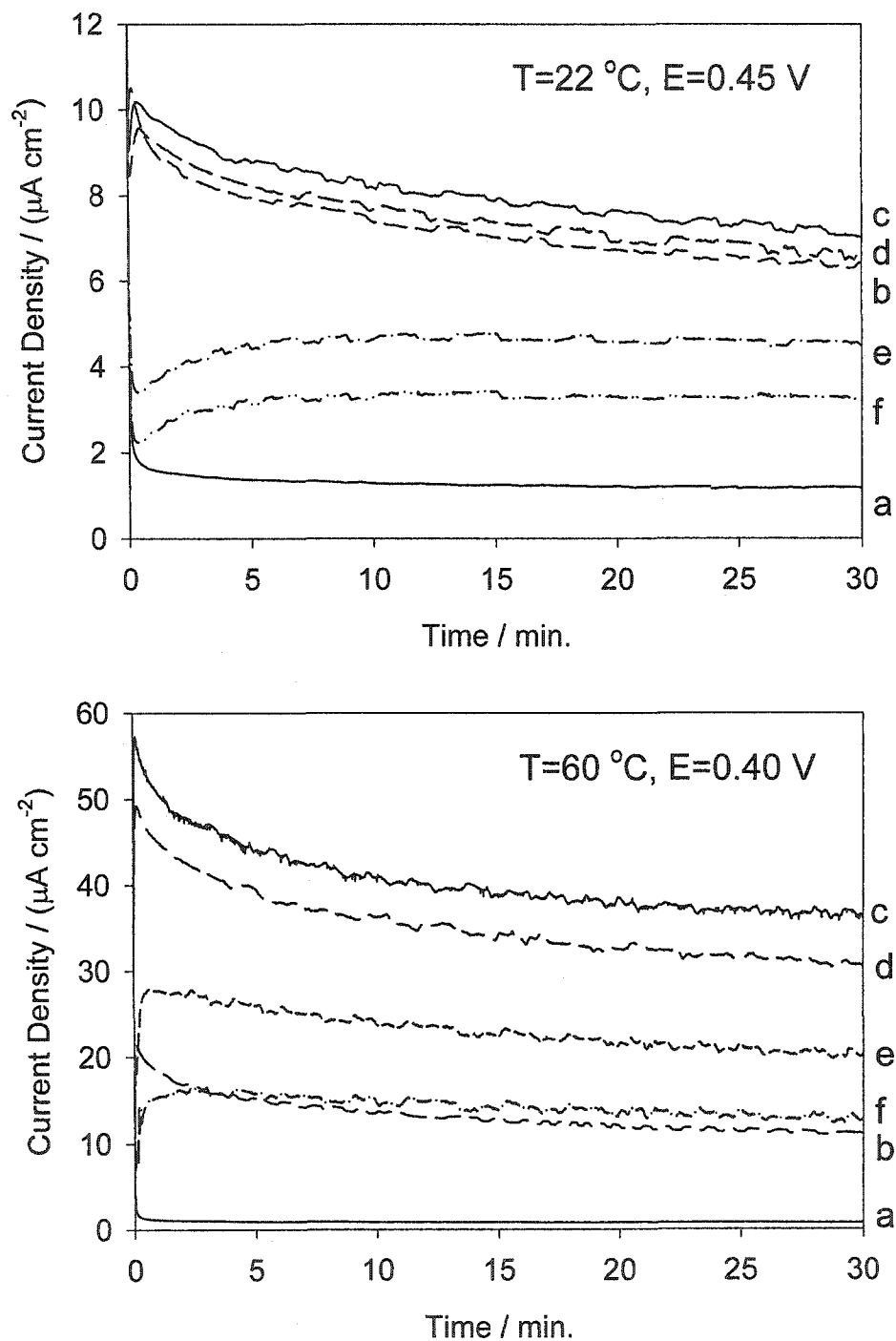


**Figure 3-5.** Potentiostatic electrooxidation of methanol ( $[\text{MeOH}] = 1.0\text{ M}$ ,  $[\text{H}_2\text{SO}_4] = 1.0\text{ M}$ ) over  $\text{Pt-Ru}_{\text{ad}}$  with Ru coverages of (a) 0, (b) 0.18, (c) 0.33, (d) 0.45, (e) 0.63, and (f) 0.75.

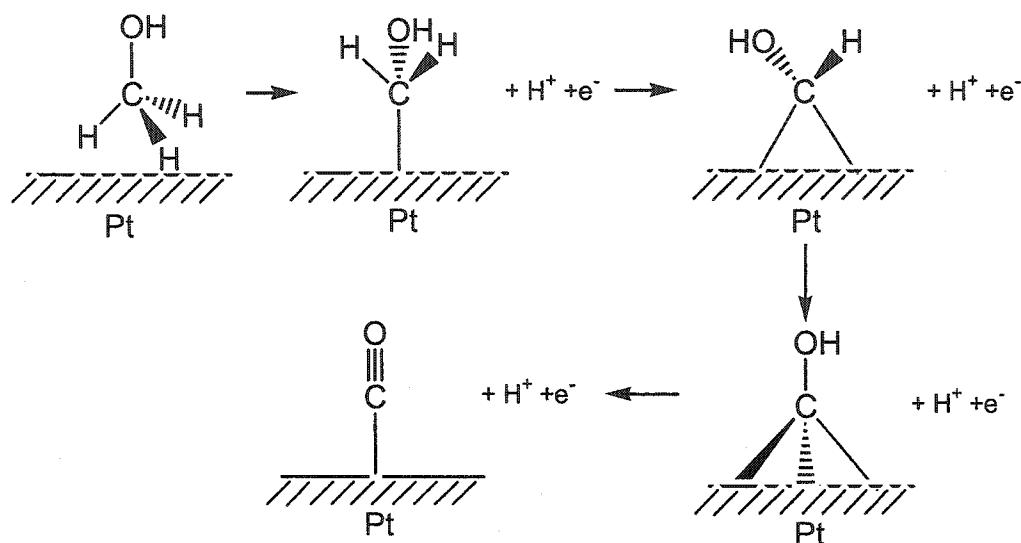


**Figure 3-6.** Methanol adsorption and dehydrogenation on the surface of Pt.

According to the above mechanism, Pt-Ru<sub>ad</sub>-0.18 has more threefold Pt ensembles than Pt-Ru<sub>ad</sub>-0.63 and Pt-Ru<sub>ad</sub>-0.75, so it exhibits higher activity than Pt-Ru<sub>ad</sub>-0.63 and Pt-Ru<sub>ad</sub>-0.75 at room temperature. On the other hand, Pt-Ru<sub>ad</sub>-0.63 and Pt-Ru<sub>ad</sub>-0.75 have more Ru sites than Pt-Ru<sub>ad</sub>-0.18, so Pt-Ru<sub>ad</sub>-0.63 and Pt-Ru<sub>ad</sub>-0.75 are more active than Pt-Ru<sub>ad</sub>-0.18 at 60 °C. Pt-Ru<sub>ad</sub>-0.33 has the optimal combination of the number of threefold Pt ensembles and Ru sites, thereby showing the highest activity at both room temperature and 60 °C. The relatively good agreement between the behavior of nanoparticle Pt-Ru<sub>ad</sub> and the smooth Pt-Ru alloy for methanol electrooxidation suggests that no significant fundamental difference in the methanol electrooxidation mechanism over technical scale and model Pt-Ru catalysts. Notably, Pt-Ru<sub>ad</sub>-0.75 (Ru surface concentration of 131%) displays a higher activity than pure Pt at 22 °C. This observation indicates that the surface of Pt-Ru<sub>ad</sub>-0.75 is not completely covered by Ru<sub>ad</sub> despite the Ru surface concentration

being more than 100%, because pure Ru is inactive for methanol electrooxidation at this temperature.<sup>7,9</sup> This conclusion strongly suggests that the proposed deposition model is reasonable.

The optimum surface composition of Pt-Ru systems toward methanol electrooxidation has been extensively investigated using model catalysts and technical-scale catalysts. The results are summarized in Table 3-2. It is clear that, even though numerous studies have been carried out, the subject remains controversial. The optimum surface compositions obtained using model catalysts are not quite consistent except that the optimum surface composition is never more than 50%. For practical Pt-Ru nanoparticle catalysts, it appears that 30~50% Ru surface contents tend to give the highest activity toward methanol electrooxidation over a wide range of temperature and potential. Possible origins of the discrepancy between the experimental data of different groups include: (1) the uncertainty in the measurement of surface composition; (2) the difference in the surface structure of these catalysts studied in different research groups. The surface structure includes surface Ru atom distribution, surface morphology, and surface oxidation state, which are catalyst preparation dependent.

In order to check if there is any difference in the intrinsic activity between practical and model Pt-Ru catalysts, the real activity of our nanoparticle Pt-Ru<sub>ad</sub> and some other practical Pt-Ru alloy catalysts are compared with that of some model Pt-Ru catalysts. Before this study, a few measurements on the real activity of technique-scale Pt-Ru catalysts have been made. However, most of these reported data are questionable because the surface area measured in these studies may not be accurate enough (see the following discussion and the discussion about the measurement of surface area of practical Pt-Ru

**Table 3-2.** The optimum surface composition of Pt-Ru catalysts toward methanol electrooxidation.

Pt-Ru system	Measuring condition	Optimum composition (Ru%)	Catalyst description	Reference
Pt-Ru alloy	25 °C, 0.4~0.5 V	ca. 10%	Polycrystalline smooth flat surface	7, 9
	60 °C, 0.4~0.5 V	ca. 30%		13
	25~60 °C, 0.5 V	10~15%		19
	R.T., 0.5 V	10~40%		
Pt(111)-Ru <sub>ad</sub>	R.T., 0.5 V	15~50%	Pt(111) decorated by Ru adatoms	19, 20, 21
Pt-Ru <sub>ad</sub>	R.T., 0.55 V	ca. 20%	Pt film decorated by electrodeposited Ru adatoms	53
Pt-Ru alloy	R.T., 0.48 V	ca. 15%	Co-electrodeposited Pt-Ru	42
Pt-Ru <sub>ad</sub>	40 °C, 0.5 V	ca. 50%	Pt wire decorated by electrodeposited Ru adatoms	51
	150 °C, 0.45 V	ca. 50%		50
Pt-Ru <sub>ad</sub>	25 °C, 0.4 V	5~10%	Polycrystalline Pt gauze decorated by Ru adatoms	48
Pt-Ru alloy	25 °C, 0.4 V	ca. 50%	Pt-Ru alloy nanoparticle (15-62 nm), 50% is the <b>bulk</b> composition	55
	60 °C, 0.5 V	ca. 50%		
Pt-Ru/C	60 °C, 0.4 V	ca. 50%	Carbon supported Pt-Ru alloy nanoparticle (3-4 nm), 50% is the <b>bulk</b> composition	56
Pt-Ru/C	60 °C, 0.4~0.5 V	ca. 50%	Carbon supported Pt-Ru alloy nanoparticle (3.1-3.4 nm), 50% is the <b>bulk</b> composition	60
Pt-Ru <sub>ad</sub>	R.T., 0.3 V	ca. 40%	Nanoparticle Pt black decorated by Ru adatoms, 20 m <sup>2</sup> /g	62, 63
	R.T., 0.4V	ca. 50%		
Pt-Ru alloy	130 °C, 0.2~0.3 V	ca. 40%	Pt-Ru alloy nanoparticles	69

Pt-Ru <sub>ad</sub>	R.T., 0.45 V 60 °C, 0.4V	ca. 35% ca. 35%	Nanoparticle Pt black decorated by Ru adatoms, 27 m <sup>2</sup> /g	This work
---------------------	-----------------------------	--------------------	---	-----------

catalysts in the introduction section of this chapter). In contrast, our results have no such problems because we have accurate specific surface area for our Pt-Ru<sub>ad</sub> catalysts. Of these studies on practical Pt-Ru catalysts, only two were performed under similar conditions as this study. Takasu and co-workers<sup>60,61</sup> observed a maximum activity of 23  $\mu\text{A}/\text{cm}^2$  at 0.4 V and 60 °C over a Pt-Ru/C catalyst (0.5 M H<sub>2</sub>SO<sub>4</sub>, 1 M CH<sub>3</sub>OH). The data were taken after 30 min reaction. The bulk composition of this Pt-Ru/C is 50% Ru 50% Pt. The surface composition is unknown. The catalyst has a specific surface area of 48 m<sup>2</sup>/g measured using the adsorbed CO stripping method (see the introduction of this chapter for the uncertainties of this method). Under the same conditions as Takasu's work (i. e., 0.4 V and 60 °C), we found a maximum activity of 38  $\mu\text{A}/\text{cm}^2$  on Pt-Ru<sub>ad</sub>-0.33 (1.0 M H<sub>2</sub>SO<sub>4</sub>, 1.0 M CH<sub>3</sub>OH). This current was recorded after 20 min reaction. Wieckowski and co-workers<sup>62</sup> recently reported a maximum activity of ca. 8  $\mu\text{A}/\text{cm}^2$  at 0.4 V and room temperature over a nanoparticle Pt-Ru<sub>ad</sub> catalyst prepared by spontaneous deposition (0.5 M H<sub>2</sub>SO<sub>4</sub>, 0.5 M CH<sub>3</sub>OH). The Pt-Ru<sub>ad</sub> of maximum activity had a Ru packing density of ca. 0.5 (the packing density is equivalent to the surface concentration), and a specific surface area of 20 m<sup>2</sup>/g. We found a maximum activity of ca. 8  $\mu\text{A}/\text{cm}^2$  on Pt-Ru<sub>ad</sub>-0.33 at 0.45 V and 22 °C. Our results are, therefore, in good agreement with those of Wieckowski and co-workers.

As to the real activity obtained using well-characterized model Pt-Ru catalysts, Gasteiger and co-workers observed that the smooth bulk Pt-Ru alloy with a surface composition of 33% Ru exhibits a real activity of 200  $\mu\text{A}/\text{cm}^2$  at 0.4 V and 60 °C (0.5 M H<sub>2</sub>SO<sub>4</sub>, 0.5 M CH<sub>3</sub>OH).<sup>9</sup> Vielstich and co-workers<sup>20</sup> found that, at 0.5 V and at room

temperature, the maximum real activity of smooth Pt-Ru alloy is ca.  $120 \mu\text{A}/\text{cm}^2$  (10-40% Ru), while the maximum real activity of Pt(111)/Ru prepared by spontaneous adsorption of Ru is ca.  $34 \mu\text{A}/\text{cm}^2$  (Ru coverage 0.15-0.5). The much higher real activity of Pt-Ru alloys than Ru-decorated Pt(111) surfaces was attributed to the difference in the surface structure between these two model catalysts. Pt and Ru atoms are homogeneously distributed on the Pt-Ru alloy surface, resulting in the highest number of Pt-Ru neighbor sites.  $\text{Ru}_{\text{ad}}$  is present as islands on the surface of Pt(111)/Ru. The above data are summarized in Table 3-3.

**Table 3-3.** The real activity of Pt-Ru system toward methanol electrooxidation.

Pt-Ru system	Catalysts character	Measuring condition	Real activity ( $\mu\text{A}/\text{cm}^2$ )	Reference
Pt-Ru/C	Carbon supported Pt-Ru alloy nanoparticle, 50% Ru, 48 $\text{m}^2/\text{g}$	0.5 M $\text{H}_2\text{SO}_4$ 1.0 M $\text{CH}_3\text{OH}$ T = 60 °C E = 0.4 V	23	60, 61
Pt-Ru <sub>ad</sub>	Nanoparticle Pt black decorated by Ru adatoms, 33% Ru, 27 $\text{m}^2/\text{g}$	1.0 M $\text{H}_2\text{SO}_4$ 1.0 M $\text{CH}_3\text{OH}$ T = 60 °C E = 0.4 V	38	This work
		1.0 M $\text{H}_2\text{SO}_4$ 1.0 M $\text{CH}_3\text{OH}$ R.T E = 0.45 V	8	This work
Pt-Ru <sub>ad</sub>	Nanoparticle Pt black decorated by Ru adatoms, ca. 50% Ru, 20 $\text{m}^2/\text{g}$	0.5 M $\text{H}_2\text{SO}_4$ 0.5 M $\text{CH}_3\text{OH}$ R.T. E = 0.4 V	8	62
Pt-Ru alloy	Polycrystalline smooth flat surface, 33% Ru	0.5 M $\text{H}_2\text{SO}_4$ 0.5 M $\text{CH}_3\text{OH}$ T = 60 °C E = 0.4 V	200	9
	Polycrystalline smooth flat surface, 10~40 % Ru	0.5 M $\text{H}_2\text{SO}_4$ 0.5 M $\text{CH}_3\text{OH}$ R.T E = 0.5 V	120	19, 20



Pt(111)-Ru <sub>ad</sub>	Pt(111) decorated by Ru adatom, 15~50%	0.5 M H <sub>2</sub> SO <sub>4</sub> 0.5 M CH <sub>3</sub> OH R.T E = 0.5 V	34	19, 20
--------------------------	---	--	----	--------

It appears that the maximum real activities of nanoparticle Pt-Ru<sub>ad</sub> and nanoparticle Pt-Ru alloy catalysts are smaller than those of smooth Pt-Ru alloy model catalysts at both room temperature and 60 °C. The Pt(111)/Ru<sub>ad</sub> model catalysts, having a comparable surface Ru distribution with our Pt-Ru<sub>ad</sub> catalyst also shows a higher maximum real activity than our nanoparticle Pt-Ru<sub>ad</sub> catalyst. This comparison is interesting because it illustrates that the activity of practical Pt-Ru catalysts can, in principle, be improved significantly by optimizing the surface structure.

The *real activities* of the homemade Pt-Ru<sub>ad</sub> nanoparticles toward methanol electrooxidation were compared with that of commercial nanoparticle Pt-Ru alloy catalyst (Johnson Matthey, HiSPEC-6000<sup>®</sup> 50:50 Pt:Ru) under identical reaction conditions (Figure. 3-7). This commercial Pt-Ru catalyst may be considered as the state-of-the-art industrial benchmark catalyst. The specific surface area of this Johnson Matthey Pt-Ru catalyst was taken from the literature. The BET surface area of this Pt-Ru black is 70 m<sup>2</sup>/g quoted by the manufacturer, and 67 m<sup>2</sup>/g measured by the Los Alamos National laboratory.<sup>68</sup> The electrochemically active surface area of this Pt-Ru alloy is 69 m<sup>2</sup>/g measured by CO stripping, and 74 m<sup>2</sup>/g by Cu stripping.<sup>74</sup> Notice that the as-received Pt-Ru black contains hydrous Ru oxides and/or Pt oxides as shown by XRD analysis.<sup>68</sup> These oxides are, however, reduced during conditioning and operation of fuel cells.<sup>68, 70, 74</sup> The good agreement between the BET surface areas and electrochemically active surface

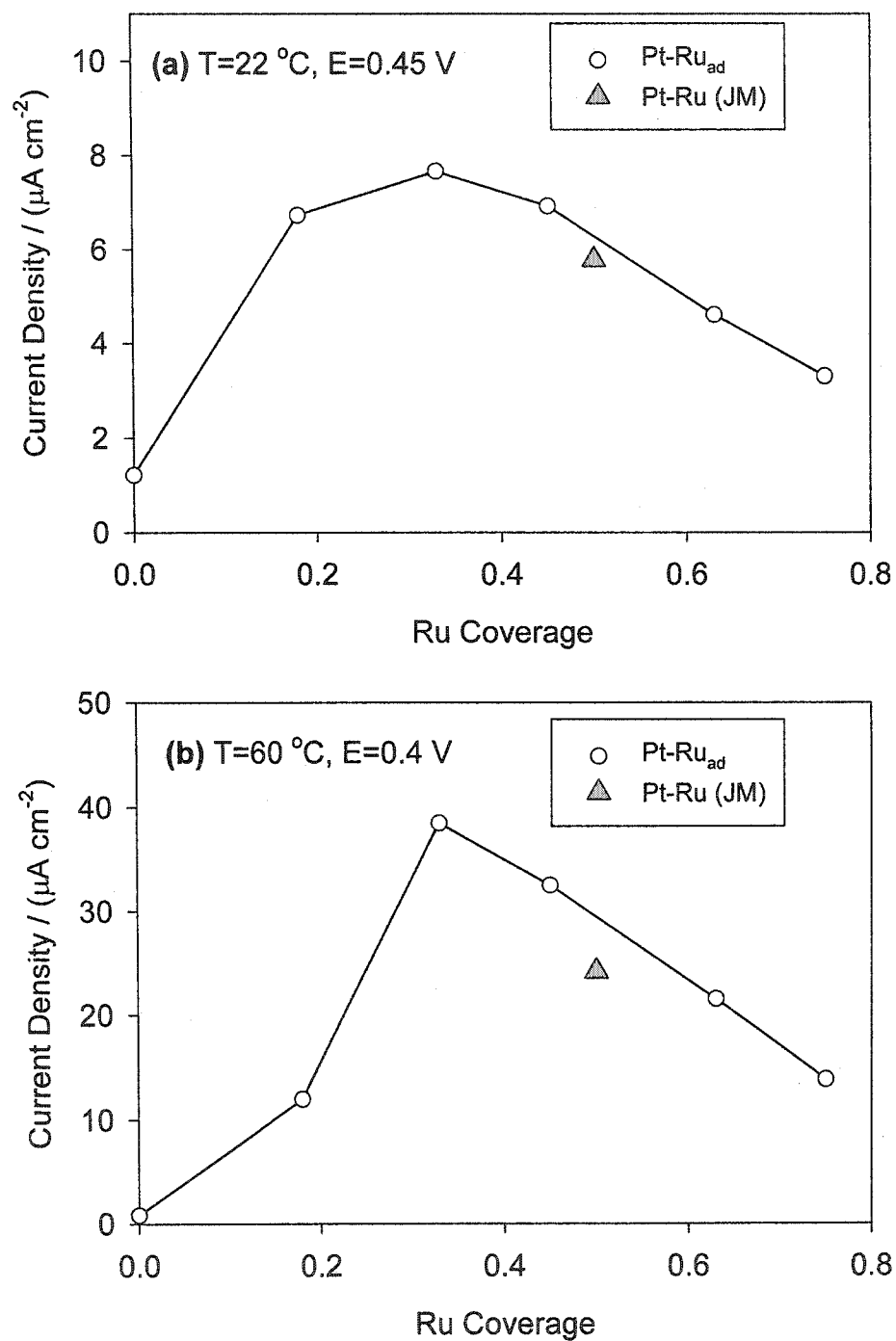


**Figure 3-7.** Comparison of the real activity of Pt-Ru<sub>ad</sub> with that of 50-50 Pt-Ru from Johnson Matthey. The data were obtained at 20 min.

areas indicates that nearly 100% of the surface of the Johnson Matthey Pt-Ru black is reduced to metallic Pt-Ru during operation of the fuel cell or during electrochemical measurement.  $70 \text{ m}^2/\text{g}$  was used as the specific surface area for the Johnson Matthey Pt-Ru black in this study. This value should fairly represent the specific active surface area under methanol electrooxidation conditions.

It can be seen from Figure 3-7 that the Pt-Ru<sub>ad</sub>-0.33 catalyst has a specific activity 1.3 times that of the Johnson Matthey catalyst at 22 °C (0.45 V), and 1.6 times as active as the Johnson Matthey catalyst at 60 °C (0.40 V). Similar results were reported recently by Wieckowski in their study of nanoparticle Pt-Ru<sub>ad</sub> prepared by spontaneous deposition<sup>62</sup> with the exception that their most active Pt-Ru<sub>ad</sub> has 50% Ru.

So far we don't have a convincing explanation for this observation. Surface composition could be a factor, but Pt-Ru<sub>ad</sub>-0.45, which has a surface composition similar to the Johnson Matthey Pt-Ru, also shows higher specific activity than the Johnson Matthey catalyst. Particle size may be a factor in this case due to the relative large particle size difference between Pt-Ru<sub>ad</sub> (ca. 10 nm) and Johnson Matthey Pt-Ru (ca. 5 nm). The particle size used here is calculated using the specific surface area by Equation 3-8. Indeed, size effects of Pt<sub>50</sub>-Ru<sub>50</sub> nanoparticles on the electrooxidation of methanol have been observed by Takasu and coworkers.<sup>61</sup> They found that the real activity for the electrooxidation of methanol on Pt<sub>50</sub>-Ru<sub>50</sub> decreases with decreasing particle size from 3.5 nm to 1.9 nm. Surface structure likely contributes more than the other factors in causing the activity difference. There is a better chance of finding more low-coordinated surface Ru atoms on Pt-Ru<sub>ad</sub> surfaces than on a Pt-Ru alloy. These low-coordinated Ru atoms may be

more active for water dissociation, and in part account for the enhanced activity.<sup>62</sup> In a recent study using Ru-decorated Pt(111) prepared by Ru vapor deposition in UHV as a model catalyst, Vielstich and co-workers<sup>19</sup> found that if the surface adsorbed Ru islands are alloyed into a smooth Pt(111) surface by annealing at 820 K, the activity significantly declined. This observation illustrates the importance of low-coordinated Ru sites to methanol electrooxidation.

It should be pointed out that the *per gram activity* of the commercial Johnson Matthey Pt-Ru black and of the E-TEK (Pt-Ru)O<sub>x</sub> catalyst are higher than those of Pt-Ru<sub>ad</sub> catalysts due to the high specific surface areas of these commercial catalysts (Figure 3-8). The BET surface area of the E-TEK (Pt-Ru)O<sub>x</sub> powder is 112 m<sup>2</sup>/g.<sup>127</sup> This catalyst contains Pt oxides and Ru oxides, as the formula indicates, and it is unclear if these surface oxides could be completely reduced to active metal Pt-Ru during methanol electrooxidation. Hence the real active surface area of this catalyst is unknown.

### 3.3 Adsorbed CO Electrooxidation

Carbon monoxide is the major poisoning intermediate in the electrooxidation of methanol. It strongly adsorbs to the electrocatalyst surfaces, blocking the surface active sites from the adsorption of methanol, and poisoning the catalysts.<sup>2</sup> The removal of surface-adsorbed CO is tremendously significant in methanol oxidation electrocatalysis. The electrooxidation of surface adsorbed CO on Pt-Ru<sub>ad</sub> nanoparticles with various Ru surface coverages was investigated. Figure 3-9 shows the CO stripping voltammograms recorded in 1.0 M H<sub>2</sub>SO<sub>4</sub> at 22 °C. The upper potential limit was set to 0.7 V in order to avoid the dissolution of Ru.<sup>128-130</sup> The first sweep was in the positive-going direction. A

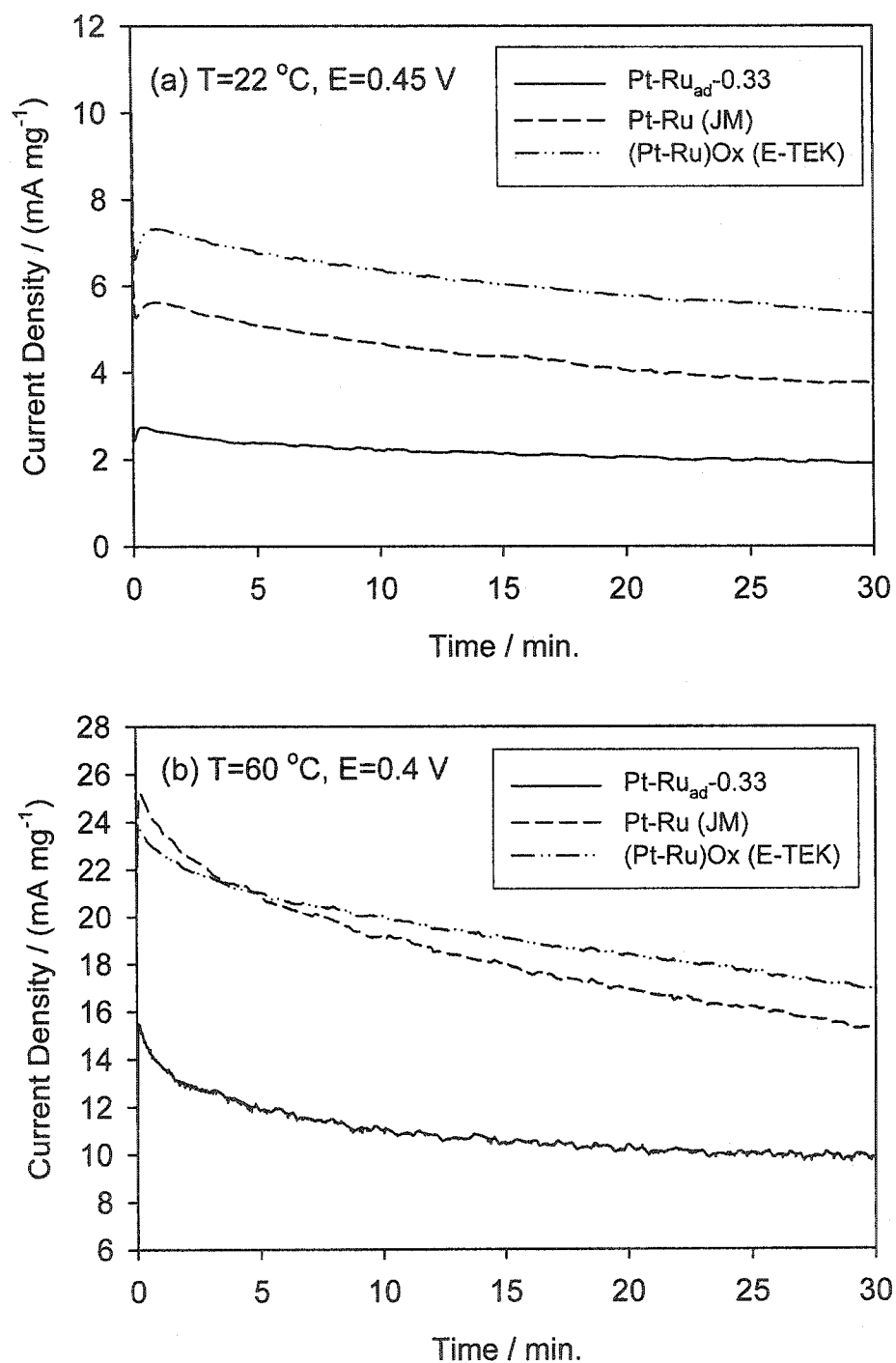


**Figure 3-8.** Comparison of the mass activity of Pt-Ru<sub>ad</sub>-0.33 with that of 50-50 Pt-Ru from Johnson Matthey and 50-50 (Pt-Ru)Ox from E-TEK.

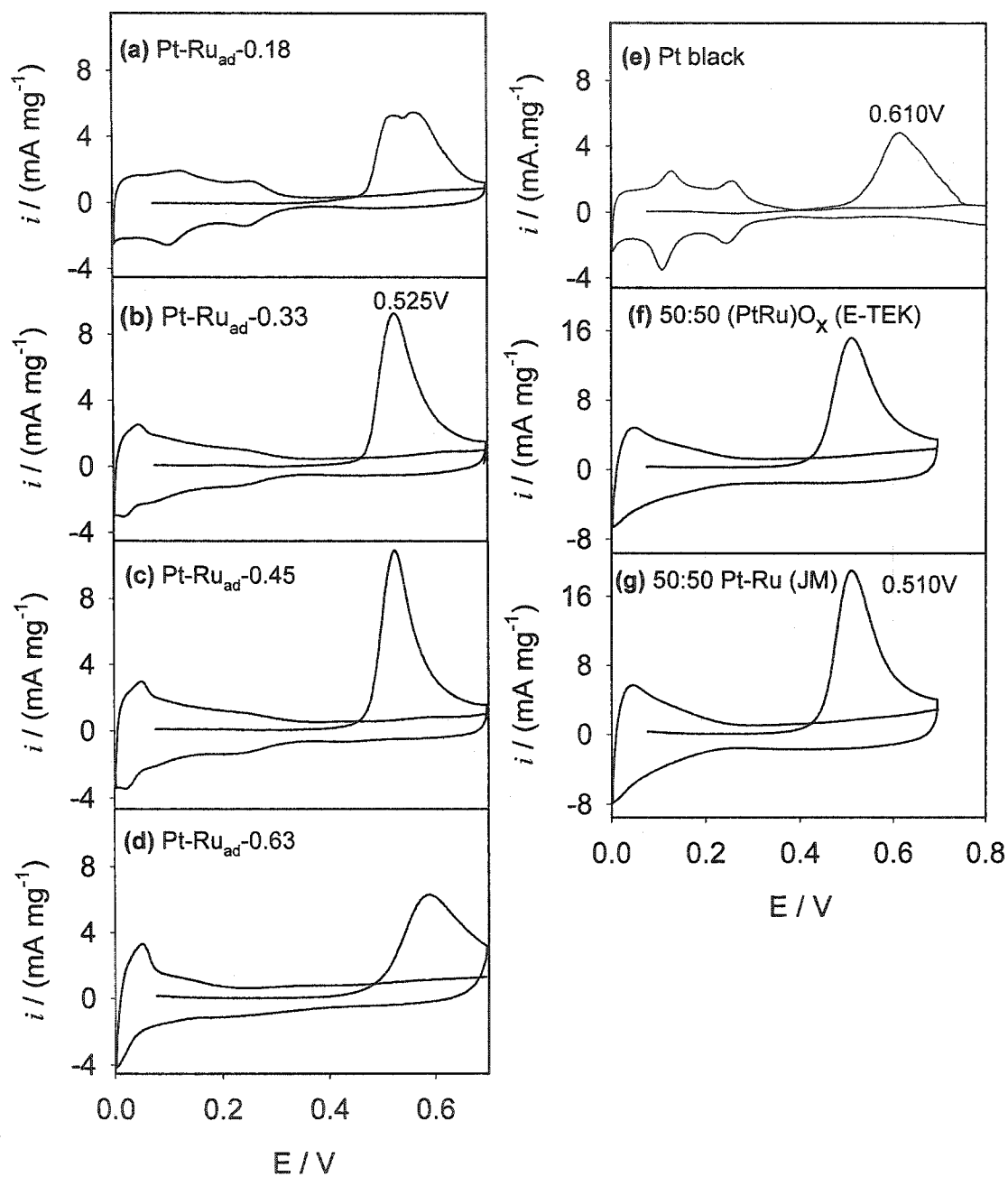


**Figure 3-9.** CO stripping cyclic voltammograms for (a-d) Pt-Ru<sub>ad</sub> with different Ru coverages, (e) Pt, (f) 50-50 (Pt-Ru)O<sub>x</sub> from E-TEK, and (g) 50-50 Pt-Ru from Johnson Matthey. The voltammograms were recorded in 1.0 M H<sub>2</sub>SO<sub>4</sub> at 10 mV/s and room temperature.

saturated monolayer of CO is formed on the catalyst surfaces, indicated by the complete blocking of the hydrogen adsorption peaks in the potential region below ca. 0.4 V.

As Figure 3-9 shows, two CO stripping peaks were observed on Pt-Ru<sub>ad</sub>-0.18 (a), but only a single peak was observed as the Ru surface coverage surpasses 0.33. The peak width decreases as Ru coverage increases up to 0.45, and then increases with further increase of the Ru coverage. This CO stripping result agrees very well with the CO stripping voltammetry from dynamic Monte Carlo simulation for Pt-Ru alloy surfaces.<sup>131</sup> The two-peak feature observed on the nanoparticle Pt-Ru<sub>ad</sub>-0.18 surface in this work was also found on the Pt-Ru<sub>ad</sub> gauze with 0.05 equiv of Ru<sub>ad</sub> in a previous study in this group,<sup>48</sup> and on Ru decorated Pt (111).<sup>33, 36, 132, 133</sup> Recently, Wieckowski and co-workers reported the observation of two CO stripping peaks on the nanoparticle Pt-Ru<sub>ad</sub> with a surface Ru packing density of 0.14 to 0.52 at a very slow potential scan rate (10 mV/min).<sup>63</sup> A two CO domain model was proposed to explain this observation in their studies, as summarized below. The low-potential CO stripping peak is assigned to CO electrooxidation on Pt sites next to the edge of Ru islands and on the Ru islands themselves (Pt/Ru pair domain). The peak at high potential is attributed to the electrooxidation of CO on Pt sites further away from Ru islands. Diffusion between the two domains is slow enough to enable the observation of the two CO stripping peaks. This model was supported by NMR,<sup>63</sup> IR studies,<sup>35,134</sup> and by theoretical calculations.<sup>135</sup> We have found that this model is successful for the interpretation of our observations; on the low Ru coverage Pt-Ru<sub>ad</sub> surfaces, there exists a certain number of Pt sites far away from Ru<sub>ad</sub>. CO bonded to these Pt sites needs to migrate over a long path to reach the Pt/Ru edge domain. Due to the long path and the relatively slow diffusion, two CO stripping peaks were observed on the Pt-Ru<sub>ad</sub>-0.18

surface. The one at low potential corresponds to CO oxidation on Pt/Ru domain; the other at high potential corresponds to the oxidation of CO on Pt sites remote from Ru adatoms. The number of Pt sites far away from Ru adatoms on Pt-Ru<sub>ad</sub> surfaces decreases with an increase in Ru surface coverage. Therefore, the high-potential peak disappeared as the Ru coverage increased above 0.33; only the low-potential peak corresponding to CO oxidation on the Pt/Ru domain was observed.

In order to compare the activity of adsorbed CO electrooxidation over various Pt-Ru<sub>ad</sub> catalysts, the CO stripping peak potential is plotted as a function of Ru surface coverage in Figure 3-10. It is clear from this figure that Pt-Ru<sub>ad</sub> nanoparticles with a Ru surface coverage of 0.33 and 0.45 yield the lowest oxidation peak potential of 0.525 V at 10 mV/s scan rate, which is around 90 mV lower than pure Pt black. This result is in good agreement with those obtained by Lamy, Gasteiger, and their coworkers.<sup>12, 13</sup> for the study of smooth Pt-Ru alloy surfaces, but differs with those obtained in a previous study in this group on Pt-Ru<sub>ad</sub> gauzes.<sup>48</sup> Lee and co-workers found the maximum shift in the CO stripping peak potential between Pt gauze and Pt-Ru<sub>ad</sub> gauze occurs at 0.05 Ru equivalents, and deposition of more Ru<sub>ad</sub> on Pt gauze did not cause significant further shift in the CO stripping peak potential. Similar results to those of Lee were reported by van Veen and co-workers<sup>42</sup> in their study on the CO oxidation over Pt-Ru<sub>ad</sub> surfaces prepared by electrodeposition of Ru<sub>ad</sub> on a Pt film electrode. We believe the divergence in activities toward adsorbed CO electrooxidation on various Pt-Ru samples is primarily caused by the difference in surface structures, more specifically, the distributions of Ru atoms on the surfaces of Pt-Ru. Nanoparticle Pt-Ru<sub>ad</sub> prepared in this work may more resemble a Pt-Ru alloy in terms of the distribution of surface Ru atoms, i. e., Ru adatoms are relatively



uniformly distributed on Pt black surfaces. In contrast, Ru atoms deposited on Pt surfaces by electrodeposition may form large islands.<sup>35</sup> Indirect evidence for the uniform distribution of Ru<sub>ad</sub> on nanoparticle Pt-Ru<sub>ad</sub> surfaces is that the two CO stripping peaks were only observed on low Ru coverage Pt-Ru<sub>ad</sub> surfaces.

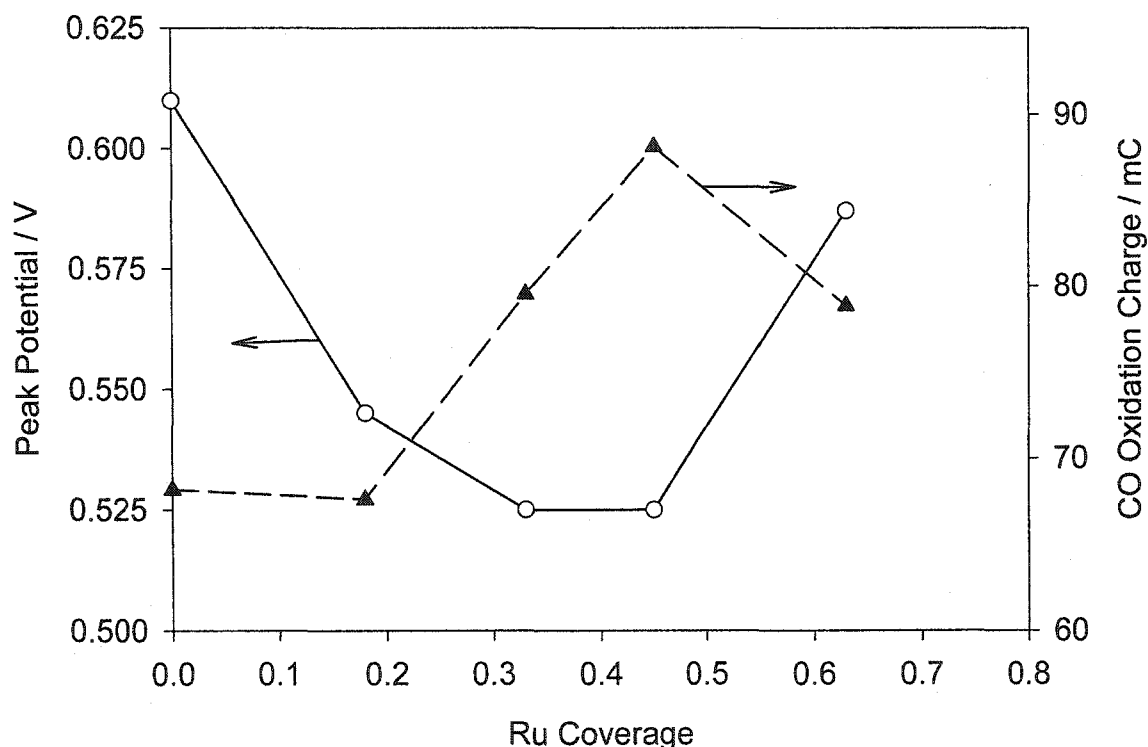


**Figure 3-10.** Dependence of CO stripping peak potential and charge on Ru coverage for Pt-Ru<sub>ad</sub>.

The adsorbed CO stripping voltammetry on commercial Johnson Matthey 50:50 Pt-Ru alloy and E-TEK (Pt-Ru)Ox (1:1 a/o Pt:Ru) (Figure 3-9g and f) display a single sharp peak at 0.510 V, which is 15 mV lower than that for Pt-Ru<sub>ad</sub>-0.33/0.45. Unlike methanol electrooxidation, these commercial nanoparticle alloy Pt-Ru catalysts demonstrate a slightly higher activity toward adsorbed CO electrooxidation than

nanoparticle Pt-Ru<sub>ad</sub> catalysts. This is because the 1:1 Pt-Ru alloys provide the maximum number of Pt/Ru pairs. Notably, the optimum surface composition for the electrooxidation of methanol and adsorbed CO over nanoparticle Pt-Ru<sub>ad</sub> catalysts is the same, between ca. 30~50% Ru coverage.

The CO stripping charges were estimated by subtracting the background charge from the charge measured from the CO stripping peaks between the relevant potential limits. Errors are unavoidable for such estimation due to the overlap of the Faradaic CO electrooxidation charge with charges associated with the formation of oxygen-containing species on bare metal surface sites exposed upon the oxidative removal of adsorbed CO. In addition, the upper limit potential (0.7 V) of the sweeps was not high enough to oxidize all the adsorbed CO for high Ru coverage Pt-Ru<sub>ad</sub> catalysts due to the shift of the CO oxidation peak to high potential. The charge was normalized to the real surface area and presented in Figure 3-10. It was found that the per unit surface area CO stripping charge depends on surface Ru coverage. The most active Pt-Ru<sub>ad</sub> catalyst (Pt-Ru<sub>ad</sub>-0.45) for CO electrooxidation displays the maximum charge per unit surface area (325  $\mu\text{C}/\text{cm}^2$ ). The increase of CO stripping charge with Ru coverage up to 45% Ru is likely due to an increase in the contribution of double-layer charge with Ru surface concentration. Recently, Behm and co-workers<sup>66</sup> reported that, for adsorbed monolayer CO stripping, the contribution of double-layer charge increases with Ru content, reaching up to 50% of the total stripping charge at approximately 40% Ru. The other explanation is that the ratio of CO to Ru is more than 1:1. Some researchers suggested that the ratio of CO to Ru can be as high as 2:1.<sup>136</sup> No matter what the reason, the non-linear relationship between CO stripping charge and real surface area certainly suggests that measurements of specific surface areas of the

Pt-Ru system using the CO stripping charge may not be accurate. One should be very careful when applying CO stripping charge to the measurement of Pt-Ru surface area.

#### 4. Conclusions

Nanoparticle Pt-Ru<sub>ad</sub> catalysts can be prepared by surface reductive deposition of Ru onto nanoparticle Pt using pre-adsorbed hydrogen on a Pt surface as reducer. The deposition is self-limited; it stops after around 18 % of the substrate surfaces was covered at each deposition, and it can be repeated over and over to obtain high Ru surface coverage. Such Ru deposition does not significantly modify the Pt substrate surface area, which can be measured accurately before the deposition. This enables us to investigate the real activity of the technical-scale Pt-Ru<sub>ad</sub> catalysts toward methanol electrooxidation.

Several nanoparticle Pt-Ru<sub>ad</sub> catalysts with an estimated Ru surface coverage ranging from 18% to 75% were prepared. Their activities toward methanol electrooxidation were evaluated in a standard three-electrode electrochemical cell. Electrochemical measurements demonstrated that methanol electrooxidation is dependent on Ru surface coverage. The best activity was obtained for Pt-Ru<sub>ad</sub> with around 33% Ru coverage at both 22 °C and 60 °C between 0.4 V and 0.45 V. The bifunctional mechanism well explained the catalytic behavior of Pt-Ru<sub>ad</sub> nanoparticles, suggesting no significant fundamental difference as to methanol electrooxidation over technical scale and model Pt-Ru catalysts. However, real activities measured on Pt-Ru<sub>ad</sub> nanoparticles are much smaller than those observed on model Pt-Ru catalysts. The real activity of Pt-Ru<sub>ad</sub> exceeded that of the start-of-the-art Johnson Matthey Pt-Ru catalyst. The activity observed on Pt-Ru<sub>ad</sub>-0.33 is around 1.5 times of that measured on the Johnson Matthey 50:50 Pt-Ru alloy catalyst. The higher activity of nanoparticle Pt-Ru<sub>ad</sub> catalysts than nanoparticle Pt-Ru

alloy catalysts may suggest the importance of low-coordinated Ru sites for methanol electrooxidation.

For the electrooxidation of adsorbed monolayer CO, the dependence of oxidation potential on Ru surface coverage was also observed. CO is oxidized at lower potential over Pt-Ru<sub>ad</sub> with Ru coverage of 30~50%. In contrast to methanol electrooxidation, Pt-Ru<sub>ad</sub> nanoparticles display lower activity than commercial nanoparticle Pt-Ru alloy catalysts for CO oxidation, which is the result of the smaller number of Pt/Ru pair sites on Pt-Ru<sub>ad</sub> surfaces than on Pt-Ru alloy surfaces.

The performance of Pt-Ru<sub>ad</sub> as an anode catalyst in liquid feed PEM-DMFCs has been investigated; the results will be discussed in chapter 4.

## References

- (1) Janssen, M. M. P.; Moolhuysen, J. *Electrochim. Acta* **1976**, *21*, 869-878.
- (2) Leger, J. M. *J. Appl. Electrochem.* **2001**, *31*, 767-771.
- (3) Krausa, M.; Vielstich, W. *J. Electroanal. Chem.* **1994**, *379*, 307-314.
- (4) Goodenough, J. B.; Hamnett, A.; Kennedy, B. J.; Manoharan, R.; Weeks, S. A. *J. Electroanal. Chem.* **1988**, *240*, 133-145.
- (5) Lu, C.; Masel, R. I. *J Phys. Chem. B* **2001**, *105*, 9793-9797.
- (6) Tong, Y. Y.; Kim, H. S.; Babu, P. K.; Waszczuk, P.; Wieckowski, A.; Oldfield, E. J. *Am. Chem. Soc.* **2002**, *124*, 468-473.
- (7) Gasteiger, H. A.; Markovic, N.; Ross, P. N., Jr.; Cairns, E. J. *J. Phys. Chem.* **1993**, *97*, 12020-12029.
- (8) Gasteiger, H. A.; Ross, P. N., Jr.; Cairns, E. J. *Surf. Sci.* **1993**, *293*, 67-80.
- (9) Gasteiger, H. A.; Markovic, N.; Ross, P. N.; Cairns, E. J. *J. Electrochem. Soc.* **1994**, *141*, 1795-1803.
- (10) Gasteiger, H. A.; Markovic, N.; Ross, P. N.; Cairns, E. J. *Electrochim. Acta* **1994**, *39*, 1825-1832.

- (11) Markovic, N. M.; Gasteiger, H. A.; Ross, P. N.; Jiang, X. *Electrochim. Acta* **1995**, *40*, 91-98.
- (12) Gasteiger, H. A.; Markovic, N.; Ross, P. N., Jr.; Cairns, E. J. *J Phys. Chem.* **1994**, *98*, 617-625.
- (13) Kabbabi, A.; Faure, R.; Durand, R.; Beden, B.; Hahn, F.; Leger, J.-M.; Lamy, C. *J. Electroanal. Chem.* **1998**, *444*, 41-53.
- (14) Hoster, H.; Iwasita, T.; Baumgartner, H.; Vielstich, W. *J. Electrochem. Soc.* **2001**, *148*, A496-A450.
- (15) Iwasita, T.; Nart, F. C.; Vielstich, W. *Ber. Bunsen-Ges. Phys. Chem.* **1990**, *94*, 1030-1034.
- (16) Lin, W. F.; Iwasita, T.; Vielstich, W. *J Phys. Chem. B* **1999**, *103*, 3250-3257.
- (17) Liu, R. X.; Iddir, H.; Fan, Q. B.; Hou, G. Y.; Bo, A. L.; Ley, K. L.; Smotkin, E. S.; Sung, Y. E.; Kim, H.; Thomas, S.; Wieckowski, A. *J Phys. Chem. B* **2000**, *104*, 3518-3531.
- (18) Ianniello, R.; Schmidt, V. M.; Stimming, U.; Stumper, J. *Electrochim. Acta* **1994**, *39*, 1863-1869.
- (19) Hoster, H.; Iwasita, T.; Baumgartner, H.; Vielstich, W. *Chem. Phys. Phys. Chem.* **2001**, *3*, 337-346.
- (20) Iwasita, T.; Hoster, H.; John-Anacker, A.; Lin, W. F.; Vielstich, W. *Langmuir* **2000**, *16*, 522-529.
- (21) Lin, W. F.; Zei, M. S.; Eiswirth, M.; Ertl, G.; Iwasita, T.; Vielstich, W. *J Phys. Chem. B* **1999**, *103*, 6968-6977.
- (22) Chrzanowski, W.; Wieckowski, A. *Langmuir* **1997**, *13*, 5974-5978.
- (23) Chrzanowski, W.; Kim, H.; Wieckowski, A. *Catal. Lett.* **1998**, *50*, 69-75.
- (24) Chrzanowski, W.; Wieckowski, A. *Langmuir* **1998**, *14*, 1967-1970.
- (25) Herrero, E.; Feliu, J. M.; Wieckowski, A. *Langmuir* **1999**, *15*, 4944-4948.
- (26) Tremiliosi-Filho, G.; Kim, H.; Chrzanowski, W.; Wieckowski, A.; Grzybowska, B.; Kulesza, P. *J. Electroanal. Chem.* **1999**, *467*, 143-156.
- (27) Herrero, E.; Feliu, J. M.; Wieckowski, A. *Langmuir* **1999**, *15*, 4944-4948.
- (28) Crown, A.; Kim, H.; Lu, G. Q.; de Moraes, I. R.; Rice, C.; Wieckowski, A. *J. New Mat. Electrochem. Syst.* **2000**, *3*, 275-284.
- (29) Crown, A.; Moraes, I. R.; Wieckowski, A. *J. Electroanal. Chem.* **2001**, *500*, 333-343.

- (30) Crown, A.; Wieckowski, A. *Phys. Chem. Chem. Phys.* **2001**, *3*, 3290-3296.
- (31) Kim, H.; de Moraes, I. R.; Tremiliosi, G.; Haasch, R.; Wieckowski, A. *Surf. Sci.* **2001**, *474*, L203-L212.
- (32) Crown, A.; Johnston, C.; Wieckowski, A. *Surf. Sci.* **2002**, *506*, L268-L274.
- (33) Friedrich, K. A.; Geyzers, K. P.; Dickinson, A. J.; Stimming, U. *J. Electroanal. Chem.* **2002**, *524*, 261-272.
- (34) Cramm, S.; Friedrich, K. A.; Geyzers, K. P.; Stimming, U.; Vogel, R. *Fresenius J. Anal. Chem.* **1997**, *358*, 189-192.
- (35) Friedrich, K. A.; Geyzers, K. P.; Linke, U.; Stimming, U.; Stumper, J. *J. Electroanal. Chem.* **1996**, *402*, 123-128.
- (36) Davies, J. C.; Hayden, B. E.; Pegg, D. J.; Rendall, M. E. *Surf. Sci.* **2002**, *496*, 110-120.
- (37) Davies, J. C.; Hayden, B. E.; Pegg, D. J. *Surf. Sci.* **2000**, *467*, 118-130.
- (38) Davies, J. C.; Hayden, B. E.; Pegg, D. J. *Electrochim. Acta* **1998**, *44*, 1181-1190.
- (39) Lu, C.; Masel, R. I. *J Phys. Chem. B* **2001**, *105*, 9793-9797.
- (40) Massong, H.; Wang, H. S.; Samjeske, G.; Baltruschat, H. *Electrochim. Acta* **2000**, *46*, 701-707.
- (41) Samjeske, G.; Xiao, X. Y.; Baltruschat, H. *Langmuir* **2002**, *18*, 4659-4666.
- (42) Frelink, T.; Visscher, W.; van Veen, J. A. R. *Langmuir* **1996**, *12*, 3702-3708.
- (43) Frelink, T.; Visscher, W.; Cox, A. P.; Veen, J. A. R. v. *Ber. Bunsen-Ges. Phys. Chem.* **1996**, *100*, 599-606.
- (44) de Souza, J.; Iwasita, T.; Nart, F. C.; Vielstich, W. *J. Appl. Electrochem.* **2000**, *30*, 43-48.
- (45) Hamnett, A.; Kennedy, B. J.; Wagner, F. E. *J. Catal.* **1990**, *124*, 30-40.
- (46) Franaszczuk, K.; Sobkowski, J. *J. Electroanal. Chem.* **1992**, *327*, 235-246.
- (47) Lee, C. E.; Tiege, P. B.; Xing, Y.; Nagendran, J.; Bergens, S. H. *J. Am. Chem. Soc.* **1997**, *119*, 3543.
- (48) Lee, C. E.; Bergens, S. H. *J. Phys. Chem. B* **1998**, *102*, 193-199.
- (49) Lee, C. E.; Bergens, S. H., 145(2), 4182 *J. Electrochem. Soc.* **1998**, *145*, 4182.
- (50) Watanabe, M.; Genjima, Y.; Turumi, K. *J. Electrochem. Soc.* **1997**, *144*, 423-427.
- (51) Watanabe, M.; Motoo, S. *J. Electroanal. Chem.* **1975**, *60*, 267-273.

- (52) Watanabe, M.; Motoo, S. *J. Electroanal. Chem.* **1975**, *60*, 275-283.
- (53) Vigier, F.; Gloaguen, F.; Leger, J. M.; Lamy, C. *Electrochim. Acta* **2001**, *46*, 4331-4337.
- (54) Swathirajan, S.; Mikhail, Y. M. *J. Electrochem. Soc.* **1991**, *138*, 1321-1326.
- (55) Chu, D.; Gilman, S. *J. Electrochem. Soc.* **1996**, *143*, 1685-1690.
- (56) Watanabe, M.; Uchida, M.; Motoo, S. *J. Electroanal. Chem.* **1987**, *229*, 395-406.
- (57) Radmilovic, V.; Gasteiger, H. A.; Ross Jr, P. N. *J. Catal.* **1995**, *154*, 98-106.
- (58) Schmidt, T. J.; Gasteiger, H. A.; Behm, R. J. *Electrochem. Comm.* **1999**, *1*, 1-4.
- (59) Bonnemann, H.; Brinkmann, R.; Britz, P.; Endruschat, U.; Mortel, R.; Paulus, U. A.; Feldmeyer, G. J.; Schmidt, T. J.; Gasteiger, H. A.; Behm, R. J. *J. New Mat. Electrochem. Sys.* **2000**, *3*, 199-206.
- (60) Takasu, Y.; Fujiwara, T.; Murakami, Y.; Sasaki, K.; Oguri, M.; Asaki, T.; Sugimoto, W. *J. Electrochem. Soc.* **2000**, *147*, 4421-4427.
- (61) Takasu, Y.; Itaya, H.; Iwazaki, T.; Miyoshi, R.; Ohnuma, T.; Sugimoto, W.; Murakami, Y. *Chem. Comm.* **2001**, *4*, 341-342.
- (62) Waszczuk, P.; Solla-Gullon, J.; Kim, H. S.; Tong, Y. Y.; Montiel, V.; Aldaz, A.; Wieckowski, A. *J. Catal.* **2001**, *203*, 1-6.
- (63) Tong, Y. Y.; Kim, H. S.; Babu, P. K.; Waszczuk, P.; Wieckowski, A.; Oldfield, E. J. *Am. Chem. Soc.* **2002**, *124*, 468-473.
- (64) Dickinson, A. J.; Carrette, L. P. L.; Collins, J. A.; Friedrich, K. A.; Stimming, U. *Electrochim. Acta* **2002**, *47*, 3733-3739.
- (65) Lizcano-Valbuena, W. H.; Paganin, V. A.; Ernesto R. Gonzalez *Electrochim. Acta* **2002**, *47*, 3715-3722.
- (66) Jusys, Z.; Kaiser, J.; Behm, R. J. *Electrochim. Acta* **2002**, *47*, 3693-3706.
- (67) Friedrich, K. A.; Geyzers, K. P.; Dickinson, A. J.; Stimming, U. *J. Electroanal. Chem.* **2002**, *524*, 261-272.
- (68) Dinh, H. N.; Ren, X.; Garzon, F. H.; Zelenay, P.; Gottesfeld, S. *J. Electroanal. Chem.* **2000**, *491*, 222 - 233.
- (69) Arico, A. S.; Antonucci, P. L.; Modica, E.; Baglio, V.; Kim, H.; Antonucci, V. *Electrochim. Acta* **2002**, *47*, 3723-3732.

- (70) O'Grady, W. E.; Hagans, P. L.; Pandya, K. I.; Maricle, D. L. *Langmuir* **2001**, *17*, 3047-3050.
- (71) Weaver, M. J.; Chang, S.-C.; Leung, L.-W. H.; Jiang, X.; Rubel, M.; Szklarczyk, M.; Zurawski, D.; Wieckowski, A. *J. Electroanal. Chem.* **1992**, *327*, 247-260.
- (72) Gómez, R.; Feliu, J. M.; Aldaz, A.; Weaver, M. J. *Surf. Sci.* **1998**, *410*, 48-61.
- (73) Schmidt, T. J.; Noeske, M.; Gasteiger, H. A.; Behm, R. J.; Britz, P.; Brijous, W.; Bonnemann, H. *Langmuir* **1997**, *13*, 2591-2595.
- (74) Green, C. L.; Kucernak, A. *J. Phys. Chem. B* **2002**, *106*, 1036-1047.
- (75) Cattaneo, C.; Pinto, M. I. S. d.; Mishima, H.; Mishima, B. A. L. d.; Cornaglia, D. L. L. *J. Electroanal. Chem.* **1999**, *461*, 32-39.
- (76) Ross, P. N. *Electrochim. Acta* **1991**, *36*, 2053-2062.
- (77) Nashner, M. S.; Frenkel, A. I.; Somerville, D.; Hills, C. W.; Shapley, J. R.; Nuzzo, R. G. *J. Am. Chem. Soc.* **1998**, *120*, 8093-8101.
- (78) Hamnett, A. *Catal. Today* **1997**, *38*, 445-158.
- (79) Napporn, W. T.; Laborde, L.; Leger, J. M.; Lamy, C. *J. Electroanal. Chem.* **1996**, *404*, 153-159.
- (80) Beden, B.; Lamy, C.; Leger, J. M. in: Bockris, J. O'. M.; Conway, B. E.; White, R. E. (Eds), *Modern Aspects of Electrochemistry*, vol 22, Plenum, New York, **1992**, p. 97.
- (81) Wasmus, S.; Kuver, A. *J. Electroanal. Chem.* **1999**, *461*, 14-31.
- (82) Christensen, P. A.; Hamnett, A.; Troughton, G. L. *J. Electroanal. Chem.* **1993**, *362*, 207-218.
- (83) Christensen, P. A.; Hamnett, A.; Munk, J.; Troughton, G. L. *J. Electroanal. Chem.* **1994**, *370*, 251-258.
- (84) Frelink, T.; Visscher, W.; Van Veen, J. A. R. *J. Electroanal. Chem.* **1995**, *382*, 65-72.
- (85) Takasu, Y.; Iwazaki, T.; Sugimoto, W.; Murakami, Y. *Electrochem. Comm.* **2000**, *2*, 671-674.
- (86) Van Der Wiel, A. *Chem. Weekblad.* **1952**, *48*, 597.
- (87) Pott, G. T. *British Patent Application 7429/74* (see also British Patent 1,106,708).
- (88) Kinoshita, K.; Stonehart, P. Preparation and Characterization of Highly Dispersed electrocatalytical Materials, in: Bockris, J. O'M.; Conway, B. E. (Eds) *Modern aspects of electrochemistry*, Plenum Press, New York, **1977**, *12*, 183-266.



- (89) Janssen, M. M. P.; Moolhuysen, J. *Electrochim. Acta* **1976**, *21*, 861-868.
- (90) Szabo, S.; Bakos, I. *J. Electroanal. Chem.* **1987**, *230*, 233-240.
- (91) Szabo, S.; Bakos, I.; Nagy, F. *J. Electroanal. Chem.* **1989**, *271*, 269-277.
- (92) Bakos, I.; Szabo, S. *J. Electroanal. Chem.* **1994**, *369*, 223-226.
- (93) Bakos, I.; Szabo, S. *J. Electroanal. Chem.* **1993**, *344*, 303-311.
- (94) Del Angel, P.; Dominguez, J. M.; Del Angel, G.; Montoya, J. A.; Capilla, J.; Lamy-Pitara, E.; Barbier, J. *Topics in Catalysis* **2002**, *18*, 183-191.
- (95) Del Angel, P.; Dominguez, J. M.; Del Angel, G.; Montoya, J. A.; Lamy-Pitara, E.; Labruquere, S.; Barbier, J. *Langmuir* **2000**, *16*, 7210-7217.
- (96) Espinosa, G.; Del Angel, G.; Barbier, J.; Bosch, P.; Lara, V.; Acosta, D. *J. Mol. Catal. A-Chem.* **2000**, *164*, 253-262.
- (97) Barbier, J.; Marecot, P.; Delangel, G.; Bosch, P.; Boitiaux, J. P.; Didillon, B.; Dominguez, J. M.; Schifter, I.; Espinosa, G. *Appl. Catal. A-Gen.* **1994**, *116*, 179-186.
- (98) Bertin, V.; Bosch, P.; Delangel, G.; Gomez, R.; Barbier, J.; Marecot, P. *J. Chim. Phys.-Chim. Biol.* **1995**, *92*, 120-133.
- (99) Dumas, J. M.; Rmili, S.; Barbier, J. *J. Chim. Phys.-Chim. Biol.* **1998**, *95*, 1650-1665.
- (100) Micheaud-Especel, C.; Bazin, D.; Guerin, M.; Marecot, P.; Barbier, J. *React. Kinet. Catal. Lett.* **2000**, *69*, 209-216.
- (101) Micheaud, C.; Marecot, P.; Guerin, M.; Barbier, J. *Appl. Catal. A-Gen.* **1998**, *171*, 229-239.
- (102) Micheaud, C.; Marecot, P.; Guerin, M.; Barbier, J. *J. Chim. Phys.-Chim. Biol.* **1997**, *94*, 1897-1905.
- (103) Micheaud, C.; Guerin, M.; Marecot, P.; Geron, C.; Barbier, J. *J. Chim. Phys.-Chim. Biol.* **1996**, *93*, 1394-1411.
- (104) Szabo, S.; Bakos, I. *React. Kinet. Catal. Lett.* **1997**, *62*, 267-271.
- (105) Szabo, S.; Bakos, I. *Preparation of Catalysts Vii* **1998**, *118*, 269-276.
- (106) Szabo, S.; Bakos, I. *React. Kinet. Catal. Lett.* **1998**, *65*, 259-263.
- (107) Pieck, C. L.; Marecot, P.; Barbier, J. *Appl. Catal. A-Gen.* **1996**, *134*, 319-329.
- (108) Pieck, C. L.; Marecot, P.; Barbier, J. *Appl. Catal. A-Gen.* **1996**, *141*, 229-244.
- (109) Pieck, C. L.; Marecot, P.; Barbier, J. *Appl. Catal. A-Gen.* **1996**, *143*, 283-298.

- (110) Dumas, J. M.; Geron, C.; Hadrane, H.; Marecot, P.; Barbier, J. *J. Mol. Catal. A-Chem.* **1992**, *77*, 87-98.
- (111) Bakos, I.; Szabo, S. *J. Electroanal. Chem.* **2003**, *547*, 103-107.
- (112) Bakos, I.; Szabo, S. *Electrochim. Acta* **2001**, *46*, 2507-2513.
- (113) Szabo, S.; Bakos, I. *React. Kinet. Catal. Lett.* **2000**, *71*, 245-251.
- (114) Brankovic, S. R.; Wang, J. X.; Zhu, Y.; Sabatini, R.; Mcbreen, J.; Adzic, R. R. *J. Electroanal. Chem.* **2002**, *524*, 231-241.
- (115) Brankovic, S. R.; Mcbreen, J.; Adzic, R. R. *Surf. Sci.* **2001**, *479*, L363-L368.
- (116) Brankovic, S. R.; Wang, J. X.; Adzic, R. R. *Electrochem. Solid-State Lett.* **2001**, *4*, A217-A220.
- (117) Brankovic, S. R.; Mcbreen, J.; Adzic, R. R. *J. Electroanal. Chem.* **2001**, *503*, 99-104.
- (118) Brankovic, S. R.; Wang, J. X.; Adzic, R. R. *J. Serb. Chem. Soc.* **2001**, *66*, 887-898.
- (119) Rard, J. A. *Chem. Rev.* **1985**, *85*, 1-39.
- (120) Hadzijordanov, S.; Angersteinkozlowska, H.; Vukovic, M.; Conway, B. E. *J Phys. Chem.* **1977**, *81*, 2271-2279.
- (121) Lin, W. F.; Christensen, P. A.; Hamnett, A. *Phys. Chem. Chem. Phys.* **2001**, *3*, 3312-3319.
- (122) Wang, W. B.; Zei, M. S.; Ertl, G. *Phys. Chem. Chem. Phys.* **2001**, *3*, 3307-3311.
- (123) Lin, W. F.; Zei, M. S.; Kim, Y. D.; Over, H.; Ertl, G. *J Phys. Chem. B* **2000**, *104*, 6040-6048.
- (124) Lin, W. F.; Christensen, P. A.; Hamnett, A.; Zei, M. S.; Ertl, G. *J Phys. Chem. B* **2000**, *104*, 6642-6652.
- (125) Lin, W. F.; Christensen, P. A.; Hamnett, A. *J Phys. Chem. B* **2000**, *104*, 12002-12011.
- (126) Brankovic, S. R.; Wang, J. X.; Zhu, Y.; Sabatini, R.; McBreen, J.; Adzic, R. R. *J. Electroanal. Chem.* **2002**, *524*, 231-241.
- (127) Lee, C. E. doctorate thesis, Spring **2003**.
- (128) Hadzi-Jordanov, S.; Angerstein-Kozlowska, H.; Vukovic, M.; Conway, J. J. *Electrochem. Soc.* **1978**, *125*, 1471-1480.
- (129) Kotz, R.; Stucki, S. *J. Electrochem. Soc.* **1984**, *172*, 211-219.

- (130) Vukovic, M. *J. Chem. Soc. Faraday Trans.* **1990**, 86, 3743-3746.
- (131) Winterlin, J. *Adv. Catal.* **2000**, 45, 131-206.
- (132) Massong, H.; Wang, H. S.; Samjeske, G.; Baltruschat, H. *Electrochim. Acta* **2000**, 46, 701-707.
- (133) Lu, G.-Q.; Waszczuk, P.; Wieckowski, A. *J. Electroanal. Chem.* **2002**, 532, 49 - 55.
- (134) Sanicharane, S.; Bo, A.; Sompalli, B.; Gurau, B.; Smotkin, E. S. *J. Electrochem. Soc.* **2002**, 149, A554-A557.
- (135) Koper, M. T. M.; Lukkien, J. J.; Jansen, A. P. J.; van Santen, R. A. *J Phys. Chem. B* **1999**, 103, 5522-5529.
- (136) Kinoshita, K.; Ross, P. N. *J. Electroanal. Chem.* **1977**, 78, 313-318.

## Chapter 4

### Nanoparticle Pt-Ru<sub>ad</sub> Catalysts for Direct Methanol Fuel Cells

#### Part II : Performance as Anode Catalysts for Direct Methanol Fuel Cells

##### 1. Introduction

Direct methanol fuel cells (DMFCs) based on polymer electrolyte membrane (PEM) technology consist of a proton exchange membrane (e.g. Nafion<sup>®</sup>-117) sandwiched between two porous electrodes containing electrocatalysts. Methanol is delivered to the anode where it is oxidized directly to carbon dioxide over the anode electrocatalyst (Eq. 4-1). Oxygen (from air) is supplied to the cathode where it is reduced by electrons and combined with protons to form water (Eq. 4-2). Carbon dioxide and water are the products of the overall cell reaction (Eq. 4-3).<sup>1-4</sup>



DMFCs are best suited for road transportation applications as an alternative to the internal combustion engine (ICE), and for portable power applications (cell phones, laptops, military communication equipment etc.) as an alternative to batteries.<sup>3, 4</sup> The closest alternatives to DMFCs for such applications are H<sub>2</sub>/air PEMFC systems operating on either reformat (H<sub>2</sub> + CO<sub>2</sub>, generated on-board using reformers), or on compressed H<sub>2</sub> gas stored on-board. As pointed out in Chapter 1, compared with H<sub>2</sub>/air PEMFC systems operating on reformat, DMFC systems have advantages including simple

system design, ease of operation, reduced weight and volume, and lower cost. Compared with H<sub>2</sub>/air PEMFC systems operating on high pressure H<sub>2</sub> gas stored on-board, DMFC systems use liquid methanol as fuel. Liquid methanol is easier to handle, to store, and to distribute than high pressure (5000-10000 psi) H<sub>2</sub>. In addition, methanol has a higher energy density than hydrogen and it is available in large quantities. It is worthwhile to point out that the reforming process and compression of H<sub>2</sub> gas require energy that must be subtracted from the net energy value of the fuel before it is combusted in the fuel cell.

On the other hand, there are distinct disadvantages to use of DMFCs. The major disadvantage is that the performance is poor and the power density is low compared to H<sub>2</sub>/O<sub>2</sub>-PEMFCs. The poor performance and the low power density are the result of the sluggish kinetics of methanol electrooxidation at the anode, and of cathode polarization resulting from methanol crossover.<sup>1,3</sup> Methanol crossover also results in loss of fuel by evaporation from the cathode. These key issues have hindered the development of practical DMFCs since they were devised, and they remain largely unresolved despite much effort by researchers over the last 40 years. Some of the limitations can be overcome by using large amounts of electrocatalyst (Pt based). But the cost of Pt makes this solution impractical. The development of highly effective, and economical methanol electrooxidation catalysts has, therefore, been a topic of intense research efforts.<sup>5</sup> Pt-based binary,<sup>6</sup> ternary,<sup>7</sup> and quaternary<sup>8</sup> catalysts are active toward methanol electrooxidation, and they are stable in acid media. Of the catalysts developed, Pt-Ru remains the state-of-the-art methanol electrooxidation catalyst in the anodes of prototype DMFCs.<sup>4</sup> In recent studies, it has been found that nanoparticle Pt-Ru<sub>ad</sub> catalysts, prepared either using the self-limiting surface reductive deposition method by us (Chapter 3), or

using the spontaneous deposition technique by Wieckowski and co-workers,<sup>9, 10</sup> are almost twice as active (in terms of real activity) as the state-of-the-art commercial Pt-Ru alloy catalysts (e.g. Johnson Matthey HiSPEC-6000™) as measured in H<sub>2</sub>SO<sub>4</sub>. The superior activity of Pt-Ru<sub>ad</sub> nanoparticle catalysts may be due to the large number of low-coordinated surface Ru sites, one of the main characteristics of adatom systems. Also Wieckowski and co-workers showed recently by NMR spectroscopy that the presence of Ru<sub>ad</sub> on Pt surfaces decreases the back-donation of Pt to CO (electronic effects), weakening the Pt-CO bond, and thereby increasing the CO electrooxidation rate. They also revealed that the presence of Ru<sub>ad</sub> substantially enhances the rate of CO surface diffusion. They suggested that, in addition to the conventional bi-functional mechanism, surface dynamic effects (CO mobility) may play a much more important role in enhancing CO tolerance than previously thought.<sup>10, 11</sup> The performance of nanoparticle Pt-Ru<sub>ad</sub> catalysts in actual prototype DMFCs has not been well studied.<sup>12</sup> Whether such adatom catalysts can survive incorporation and operation in a fuel cell has been questioned.<sup>5, 13, 14</sup> Wasmus and co-workers state that neither chemisorbed nor electrosorbed foreign metals on Pt are a practical way to make fuel cell catalysts because variations in cell voltages during fuel cell operation may lead to desorption of the foreign metal into the electrolyte.<sup>5</sup> Further, surface segregation of Pt-Ru systems has been observed under certain conditions. For example, Ross and co-workers<sup>13</sup> observed a strong surface enrichment in Pt for Pt-Ru alloys annealed at 800 °C in UHV. The bulk composition of a sample was 70.2 % Pt, but the annealed surface had a composition of 92.1 % Pt. Arico and co-workers<sup>15</sup> recently reported that Pt enrichment occurs in practical nanoparticle Pt-Ru alloy catalysts, particularly those with low bulk Ru content

alloys. For example, a sample with a bulk composition of  $\text{Pt}_{72}\text{Ru}_{28}$  (XRD-derived) had a surface composition of  $\text{Pt}_{90}\text{Ru}_{10}$  (XPS-derived). This composition was measured prior to the implantation of Pt-Ru nanoparticles into MEA. These studies suggest that surface segregation of Pt-Ru<sub>ad</sub> systems during the preparation (hot-pressing) and operation of DMFCs may occur and it may limit times and activities of Pt-Ru<sub>ad</sub> nanoparticle catalysts. In order to evaluate the performance of Pt-Ru<sub>ad</sub> nanoparticles as anode catalysts in DMFCs, and in order to address if Pt-Ru<sub>ad</sub> systems can survive the fabrication and operation of DMFCs, an “*in situ*” investigation of the electrocatalytic activity and stability of nanoparticle Pt-Ru<sub>ad</sub> catalysts in prototype PEM-DMFCs under variable operation conditions was carried out.

## 2. Experimental

### 2.1 Materials

See Chapter 3.

### 2.2 Preparation of Pt-Ru<sub>ad</sub> Catalysts

The nanoparticle unsupported and carbon supported Pt-Ru<sub>ad</sub> catalysts were prepared by the self-limiting surface reductive deposition method described in Chapter 3. The samples used in this study are shown in Table 4-1, and designated Pt-Ru<sub>ad</sub>- $\theta$  (unsupported),  $\theta$  is the estimated Ru surface coverage\*, or PtRu<sub>ad</sub>/C- $\phi$  (carbon supported),  $\phi$  is the surface Ru concentration\*\*. The measurements of Ru surface concentration and the estimation of Ru surface coverages were described in Chapter 3.

### 2.3 Fabrication of Membrane Electrode Assemblies

The membrane electrode assemblies (MEAs) of geometrical area 5 cm<sup>2</sup> were

**Table 4-1.** Pt-Ru<sub>ad</sub> catalysts prepared by surface reductive deposition of Ru onto nanoparticle Pt and Pt/C.

Pt Substrates	Unsupported Pt-Ru <sub>ad</sub>					Carbon supported Pt-Ru <sub>ad</sub>			
	Pt black					Pt/C			
						20wt % Pt	20wt % Pt	20wt % Pt	40wt % Pt
Deposition	1	2	3	5	7	1	2	3	2
Ru Surface Concentration	0.18	0.38	0.57	0.85	1.31	0.58	0.74	0.85	N/A
Estimated Ru Surface Coverage	0.18	0.33	0.45	0.63	0.75	N/A	N/A	N/A	N/A

\* Ru coverage ( $\theta_{Ru}$ ): the ratio of the number of *exposed surface* Ru atoms to the number of surface atoms originally on the Pt substrate.

\*\* Surface Ru concentration ( $\phi$ ): the ratio of the number of total Ru atoms deposited to the number of surface atoms originally on the Pt substrate.

fabricated using the decal transfer method developed at the Los Alamos National Laboratory.<sup>16, 17</sup> Fuel cell grade Johnson Matthey Pt black (27 m<sup>2</sup>/g) was used as the cathode catalyst and the loading at the cathode was maintained at ca. 2 mg/cm<sup>2</sup> in all the cells. For the unsupported nanoparticle catalysts, a catalyst/ionomer ink was prepared by suspending the catalyst in water (e.g., 13 mg catalyst in 150 mg H<sub>2</sub>O), and ultrasounding (Branson, Model 1210 ultrasonic bath) for 30 min to thoroughly wet and disperse the catalyst. Enough 5% Nafion<sup>®</sup> solution (ElectroChem. Inc.) was then added to the mixture to give a dry ink composition of 80 wt.% catalyst with 20 wt.% Nafion<sup>®</sup> ionomer. The mixtures were ultrasounded for another 2 h at room temperature to obtain uniformly



dispersed inks. For carbon supported catalysts, the catalyst/ionomer ink was prepared by suspending the catalyst in 5% Nafion<sup>®</sup> solution diluted with 2-propanol (e.g. 200 mg Nafion<sup>®</sup> solution in 65 mg 2-propanol) to give a dry ink composition of 70 wt.% catalyst with 30 wt.% Nafion<sup>®</sup> ionomer. The mixtures were stirred and ultrasounded alternately (1 h stirring, 1 h ultrasounding) for a total of 6 h. The catalyst inks were painted onto 5 cm<sup>2</sup> Teflon<sup>®</sup> decals at around 70 °C, and then baked in an oven at 135 °C for 5 min to cure the catalyst/Nafion<sup>®</sup> composite. Nafion<sup>®</sup>-117 membranes were cleaned and converted into the acid form by boiling in 3% H<sub>2</sub>O<sub>2</sub> for 1 h, in 0.5 M H<sub>2</sub>SO<sub>4</sub> for 2 h, and in ultra-pure water for 2 h with the water being changed every 30 min. The cleaned membranes were stored in ultra-pure water, and dried on a vacuum table at 60 °C for 45 min right before use. The catalyst layers were transferred from the Teflon decals to the Nafion<sup>®</sup> membranes by hot-pressing (125 to 127 °C, 1450 to 1550 psig for ca. 2.5 min).

#### *2.4 Operation of Direct Methanol Fuel Cells*

The membrane electrode assemblies were mounted into commercial fuel cell hardware (ElectroChem. Inc. FC05-01SP). The current collectors of the hardware were made of low porosity, high purity graphite blocks with serpentine flow fields. The cell was held between two gold-plated copper contact plates using a set of retaining bolts positioned around the periphery of the cell. Electrical heaters were placed behind each of the copper plates. Separate voltage connectors and thermocouple wells were in each cell block to provide accurate measurement and temperature control. Teflon<sup>®</sup>-treated carbon paper (ElectroChem. Inc. 30 wt.% polytetrafluoroethylene (PTFE)) was used as backing layers to allow for even distribution of reactants. PTFE gaskets were inserted to prevent the cell from leaking. The fuel cells were operated by pumping 1.0 M aqueous methanol

(Sigma-Aldrich, ACS HPLC grade, 99.93%) through the anode compartment at 4.0 mL/min, with zero back pressure, from a reservoir at ambient temperature, and by flowing dry oxygen (Praxair) through the cathode compartment at 400 standard cubic centimetres per minute (sccm) at 20 psig back pressure. Pure oxygen was used to maximize the activity of the cathode so that the differences in cell performance would reflect as much as possible the differences in anode catalyst activity. Prior to taking polarization data, the fuel cells were conditioned for 3 days using the following procedure: the DMFC was heated to 60 °C at open circuit with methanol solution circulating through the anode, and with oxygen flowing through the cathode. The cell was then run at 20 mA/cm<sup>2</sup> for 4 h. The cell temperature was raised to 90 °C, and the cell was operated at 100 mA/cm<sup>2</sup> for another 4 h. The cell was then shut down by turning off the load, heat, methanol and oxygen supply, and left overnight at room temperature. Fresh methanol solution was used at the following day. The performance of the DMFCs stabilized after such conditioning. The cell potential-current curves were obtained using an 890 Series computer-controlled fuel cell test load (Scribner Associate Inc.). The reported cell voltages are not IR compensated.

### *2.5 Cyclic Voltammetry*

Cyclic voltammetry on the anode and cathode catalyst layers in the assembled, stabilized fuel cells was performed using a Pine Bipotentiostat Model AFCBP1 controlled with Pinechem 2.00 software.<sup>18-20</sup> The cyclic voltammograms were recorded in the fuel cell blocks at ambient temperature, with the working electrode under purified water flowing at 8 mL/min, and the other electrode was used as the counter and reference electrode by supplying it with humidified H<sub>2</sub> at 100 mL/min at zero back pressure. The

temperature of the hydrogen humidifier was 35 °C. The potential was scanned from 0 to 700 mV versus the counter/reference electrode at 10 mV/s.

### 3. Results and Discussion

#### 3.1 Unsupported Pt-Ru<sub>ad</sub> Anode Catalysts

The study on the optimum surface composition of Pt-Ru<sub>ad</sub> nanoparticle catalysts for methanol electrooxidation carried out in a typical 3-electrode electrochemical cell showed that Pt-Ru<sub>ad</sub> nanoparticles with 0.33 Ru surface coverage were the most active at both 22 °C and 60 °C (Chapter 3). In order to investigate the optimum surface composition of Pt-Ru<sub>ad</sub> as anode catalyst in actual DMFCs, membrane electrode assemblies were fabricated using Pt-Ru<sub>ad</sub> nanoparticles with various Ru surface coverages as the anode catalyst. Pt black was used as the cathode catalyst, and Nafion®-117 was used as the solid electrolyte membrane. The catalyst loadings were 2 mg/cm<sup>2</sup> in both anode and cathode, and the DMFCs were operated at 60 °C and 90 °C. The cell polarization curves are shown in Figure 4-1. It can be seen that at 60°C, the best performance was obtained using Pt-Ru<sub>ad</sub>-0.33, followed in decreasing order by Pt-Ru<sub>ad</sub>-0.45, 0.63, 0.75, 0.18, and 0. This activity sequence is consistent with that obtained in the 3-electrode experiments carried out in 1.0 M H<sub>2</sub>SO<sub>4</sub> +1.0 M CH<sub>3</sub>OH at 60°C (Chapter 3, Figure 3-5). As expected, the DMFC performance improved as the temperature was increased. More interestingly, the order of DMFC performance as a function of surface composition of Pt-Ru<sub>ad</sub> anode catalyst also changed upon increasing the temperature. At 90 °C, Pt-Ru<sub>ad</sub>-0.33, 0.45, and 0.63 had nearly the same cell performance. This result supports those observations on the dependence of the optimum surface composition of Pt-Ru catalysts on temperature (see Chapter 3).<sup>21,22</sup> Specifically, the optimum surface

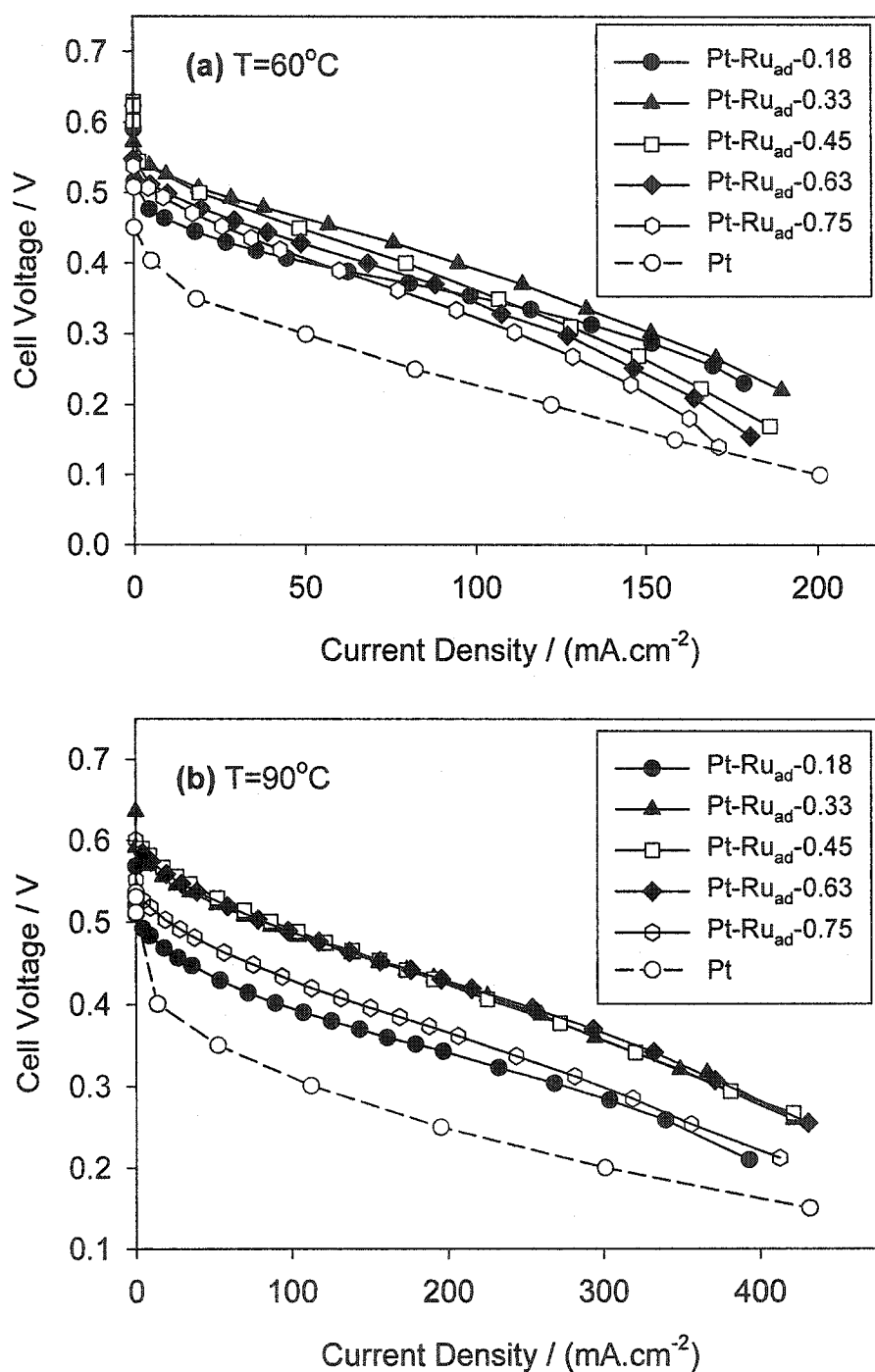
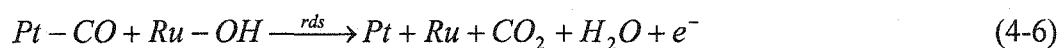


**Figure 4-1.** Polarization curves for a series of DMFCs operating with Pt-Ru<sub>ad</sub> anode catalysts of differing surface composition. Anode: 2 mg/cm<sup>2</sup> Pt-Ru<sub>ad</sub> catalyst, 1.0 M methanol at 4.0 ml/min, and zero back pressure. Cathode: 2 mg/cm<sup>2</sup> Pt-black catalyst, 20 psig dry oxygen at 400 sccm.

composition of Pt-Ru catalysts shifts from low to high Ru coverages with increases in temperature. Therefore, it can be predicted that for a PEM-DMFC operating over a wide temperature range, use of an anode catalyst composed of a mixture of Pt-Ru catalysts with variable surface compositions (e.g., from 10% to 50% Ru) may benefit the overall cell performance. The optimum Ru surface coverage for the DMFCs operating at 90 °C was ca. 50%. This result can be interpreted by the well-known bifunctional mechanism.<sup>21</sup> According to this mechanism, at high temperature, methanol dehydrogenation to adsorbed CO (Eq. 4-4), as well as water dissociation to adsorbed OH (Eq. 4-5) are rapid relative to the rate of reaction between surface adsorbed CO and OH, which is rate-determining (Eq. 4-6). A Pt-Ru surface ratio of 1:1 will maximize the product of the surface coverage of adsorbed CO and OH, thereby maximizing the rate-determining step for methanol electrooxidation (Chapter 1).



To the best of our knowledge, there is only one other report regarding the investigation of the optimum surface composition of practical Pt-Ru nanoparticles as anode catalysts in prototype PEM-DMFCs. In this study, Arico and co-workers<sup>15</sup> prepared unsupported nanoparticle Pt-Ru alloy catalysts of various compositions. They used these alloy nanoparticles as anode catalyst in DMFCs, and the cells were evaluated at 130 °C. The optimum surface composition, as determined by XPS, was found to be ca. 40 %.

As discussed in Chapter 3, Pt-Ru<sub>nd</sub> nanoparticles exhibited higher inherent activity toward methanol electrooxidation in H<sub>2</sub>SO<sub>4</sub> than commercial Johnson Matthey Pt-Ru

nanoparticles (HiSPEC-6000™, 1:1 a/o Pt:Ru). For example, Pt-Ru<sub>ad</sub>-0.33 is 1.6 times more active than Johnson Matthey Pt-Ru at 60 °C and 0.4 V in terms of the per surface site activity (see insert in Figure 4-2a). In order to compare the performance of Pt-Ru<sub>ad</sub> nanoparticles with commercial Pt-Ru alloy nanoparticles as anode catalyst in prototype PEM-DMFCs, a membrane electrode assembly was fabricated using Johnson Matthey Pt-Ru black (HiSPEC-6000™, 1:1 a/o Pt:Ru, ca. 70 m<sup>2</sup>/g) as the anode catalyst. This MEA was manufactured, conditioned, and operated using the identical procedure as for Pt-Ru<sub>ad</sub> anode catalysts. Under such conditions, the cathodes should have approximately equal activities, and the differences in cell performance should be due to anode effects. To check for experimental errors that may have occurred during fabrication of the MEAs, two MEAs were fabricated and evaluated for each type of anode catalyst. The results showed that polarization data are reproducible. Figure 4-2 shows the polarization curves measured at 60 °C and 90 °C. The currents are normalized to the total surface area of the anode catalyst, which was obtained using the specific surface area of the catalyst and the anode catalyst loadings. It can be seen that in the kinetically controlled (low current) region, the Johnson Matthey Pt-Ru catalyst is more active than Pt-Ru<sub>ad</sub>-0.33. This is contrary to the results obtained using the 3-electrode cell (1.0 M H<sub>2</sub>SO<sub>4</sub>+1.0 M MeOH), which shows that the Johnson Matthey Pt-Ru nanoparticles are less active than Pt-Ru<sub>ad</sub>-0.33 nanoparticles (insert, Figure 4-2a). This inversion of the real activity of Johnson Matthey Pt-Ru versus Pt-Ru<sub>ad</sub> observed between PEM-DMFCs and 3-electrode cells suggests that the Johnson Matthey Pt-Ru anode structure is different from the Pt-Ru<sub>ad</sub>

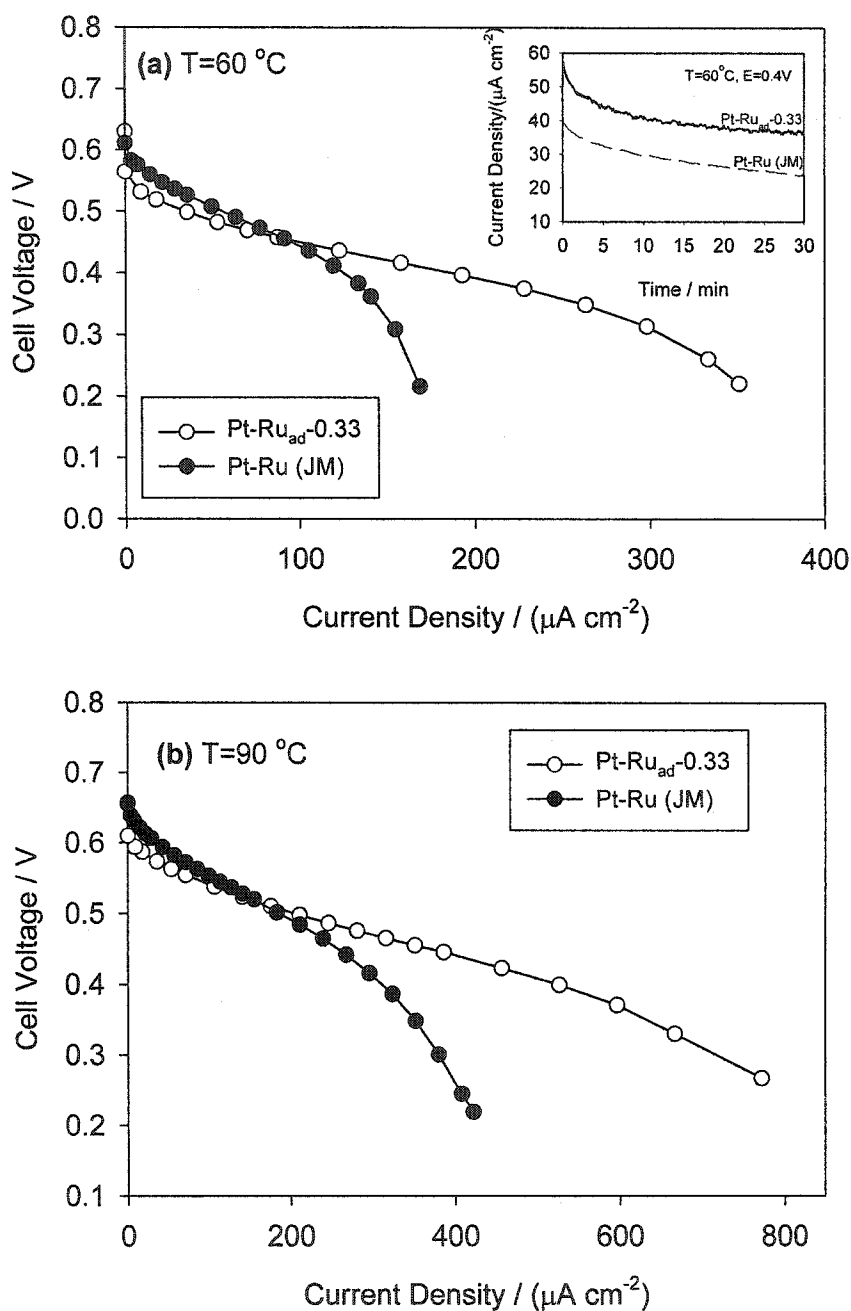


**Figure 4-2.** DMFC polarization curves with currents normalized by the total surface area of the anode catalysts. Anode:  $2\text{ mg/cm}^2$  catalyst,  $1.0\text{ M}$  methanol at  $4.0\text{ ml/min}$ . Cathode:  $2\text{ mg/cm}^2$  Pt-black catalyst,  $20\text{ psig}$  dry oxygen at  $400\text{ sccm}$ . The insert is the potentiostatic methanol oxidation current densities normalized by the real surface area of the catalysts. The currents were measured in a 3-electrode cell containing  $1.0\text{ M MeOH} + 1.0\text{ M H}_2\text{SO}_4$ .

anode structure. Catalyst layer structures determine the catalyst utilization and methanol, CO<sub>2</sub> mass transport.<sup>23,24</sup> Some catalyst particles, which are isolated from other particles (no electronic conductivity) and/or from Nafion<sup>®</sup> (no ionic conductivity), will not contribute to the cell performance. Others, which have good electronic and ionic conductivity but are less accessible to methanol, will only have a limited catalytic efficiency.<sup>25, 26</sup> For example, if particles locate at a hydrophobic microenvironment formed by the backbone chain of Nafion<sup>®</sup>, they will not be readily accessible to hydrophilic methanol; or if CO<sub>2</sub> formed on the catalyst surfaces is trapped around the catalyst particles in some micropores, it will prevent the catalysts from contacting with methanol.<sup>27-29</sup> The perfect anode layer structure should be that all catalyst particles are exposed to three-phase reaction zones (catalyst/electrolyte/methanol)(Chapter 1), and with no limitations to transport of methanol and CO<sub>2</sub> anywhere inside the electrode layer. In this study, the Johnson Matthey Pt-Ru anode may have a better structure, thus higher catalyst utilization, than the Pt-Ru<sub>ad</sub> anode. In addition, the Johnson Matthey catalyst may be activated during the fabrication of the MEA and/or the conditioning of the DMFC because this catalyst contains certain amounts of metal oxides in the as-received form, these oxides could be reduced during the conditioning of the DMFC, resulting in surface reconstruction.<sup>30</sup> Pt-Ru<sub>ad</sub> does not appear to change much. As a result, the higher activity of Pt-Ru<sub>ad</sub> over Johnson Matthey Pt-Ru alloy measured in the 3-electrode cell was overcome in the PEM-DMFC by the difference in electrode structure and, probably, in surface reconstruction of the catalysts. This study demonstrates that a good catalyst must be highly active after incorporation, conditioning, and it must generate a suitable electrode structure.



It should be pointed out that the better performance observed on Pt-Ru<sub>ad</sub>-0.33 than that measured on the Johnson Matthey Pt-Ru in the high cell current density (low cell voltage) region does not suggest that Pt-Ru<sub>ad</sub>-0.33 is more active than Johnson Matthey Pt-Ru. This is simply because that in the high current region, methanol and/or CO<sub>2</sub> mass transport dominates the cell performance.

It was found (Chapter 3) that the mass activities (currents per mg catalyst) of Johnson Matthey Pt-Ru alloy and E-TEK (PtRu)Ox (at 60 °C, 0.4 V, 1.0 M H<sub>2</sub>SO<sub>4</sub>, and 1.0 M CH<sub>3</sub>OH) were nearly the same (ca.18 mA/mg). They were higher than that of Pt-Ru<sub>ad</sub>-0.33 (ca.10 mA/mg) because the specific surface areas of these commercial catalysts are quite high (see insert of Figure 4-3a). Figure 4-3 shows the cell polarization curves with currents normalized to per mg anode catalysts. In contrast with the 3-electrode experiments, the mass activity of the E-TEK (PtRu)Ox catalyst, measured in the PEM-DMFC is lower than that of the Johnson Matthey Pt-Ru, and even lower than that of the Pt-Ru<sub>ad</sub>-0.33. The poor performance of the E-TEK (PtRu)Ox catalyst in the DMFC can be explained from two aspects. First, the structure of the anode made of the E-TEK (PtRu)Ox is poor, which results in a significant loss in catalyst utilization. Second, surface restructuring of (PtRu)Ox catalyst may have occurred during the fabrication and operation of the DMFC. This surface restructuring may have resulted in a loss in activity of (PtRu)Ox. This needs to be investigated further. Nevertheless, the importance of electrode structures and catalyst reconstruction during the fabrication and operation of DMFCs should not be underestimated.

Figure 4-4 shows plots of power density versus current density for these DMFCs. Also included in this graph are the cell polarization curves. The peak power output for

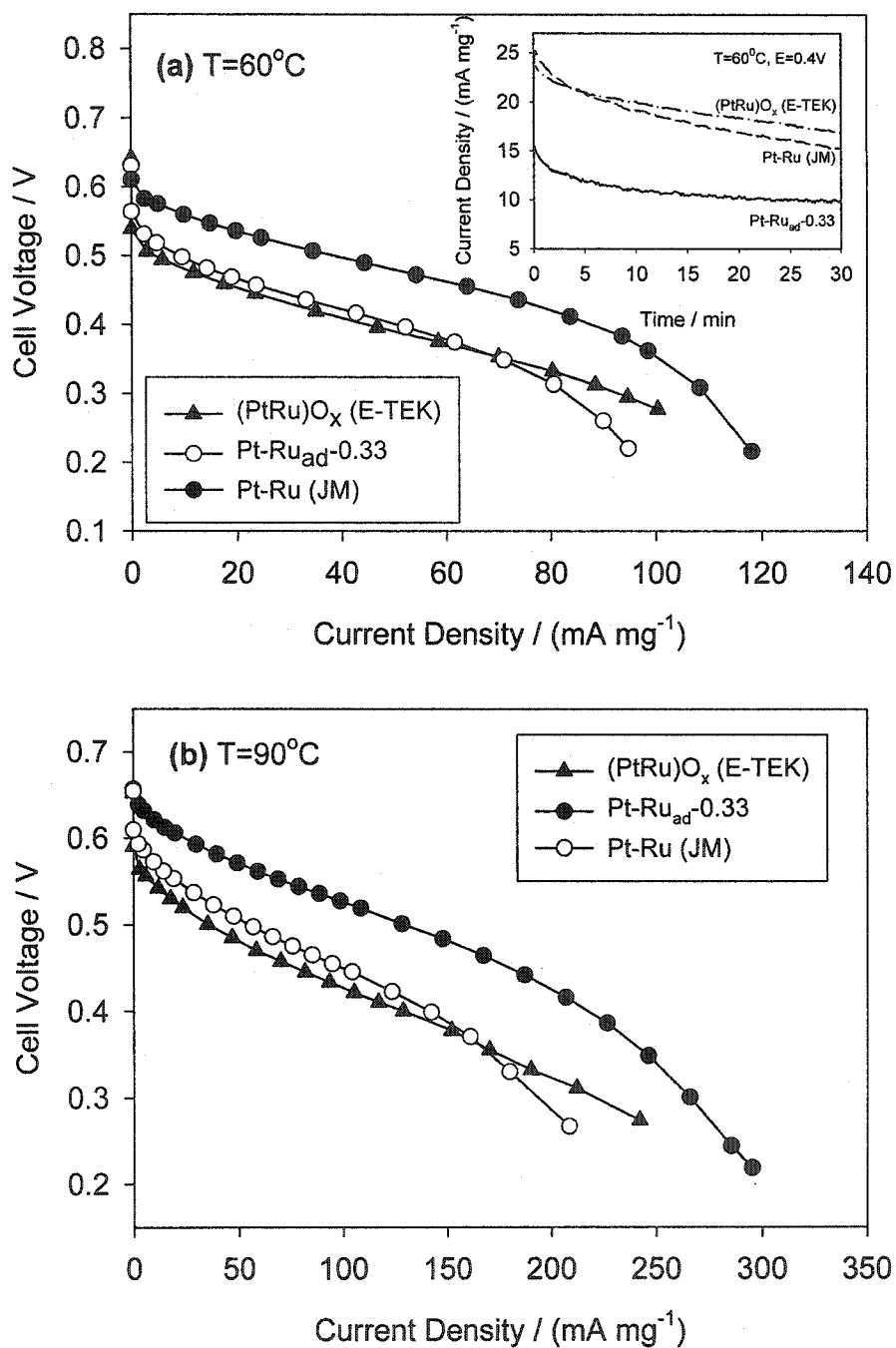


**Figure 4-3.** DMFC polarization curves with currents normalized by the mass of the anode catalyst. Anode: 2 mg/cm<sup>2</sup> catalyst, 1.0 M methanol at 4.0 ml/min. Cathode: 2 mg/cm<sup>2</sup> Pt-black catalyst, 20 psig dry oxygen at 400 sccm. The insert is the potentiostatic methanol oxidation current densities normalized by the mass of the catalysts. The currents were measured in a 3-electrode cell containing 1.0 M MeOH + 1.0 M H<sub>2</sub>SO<sub>4</sub>.

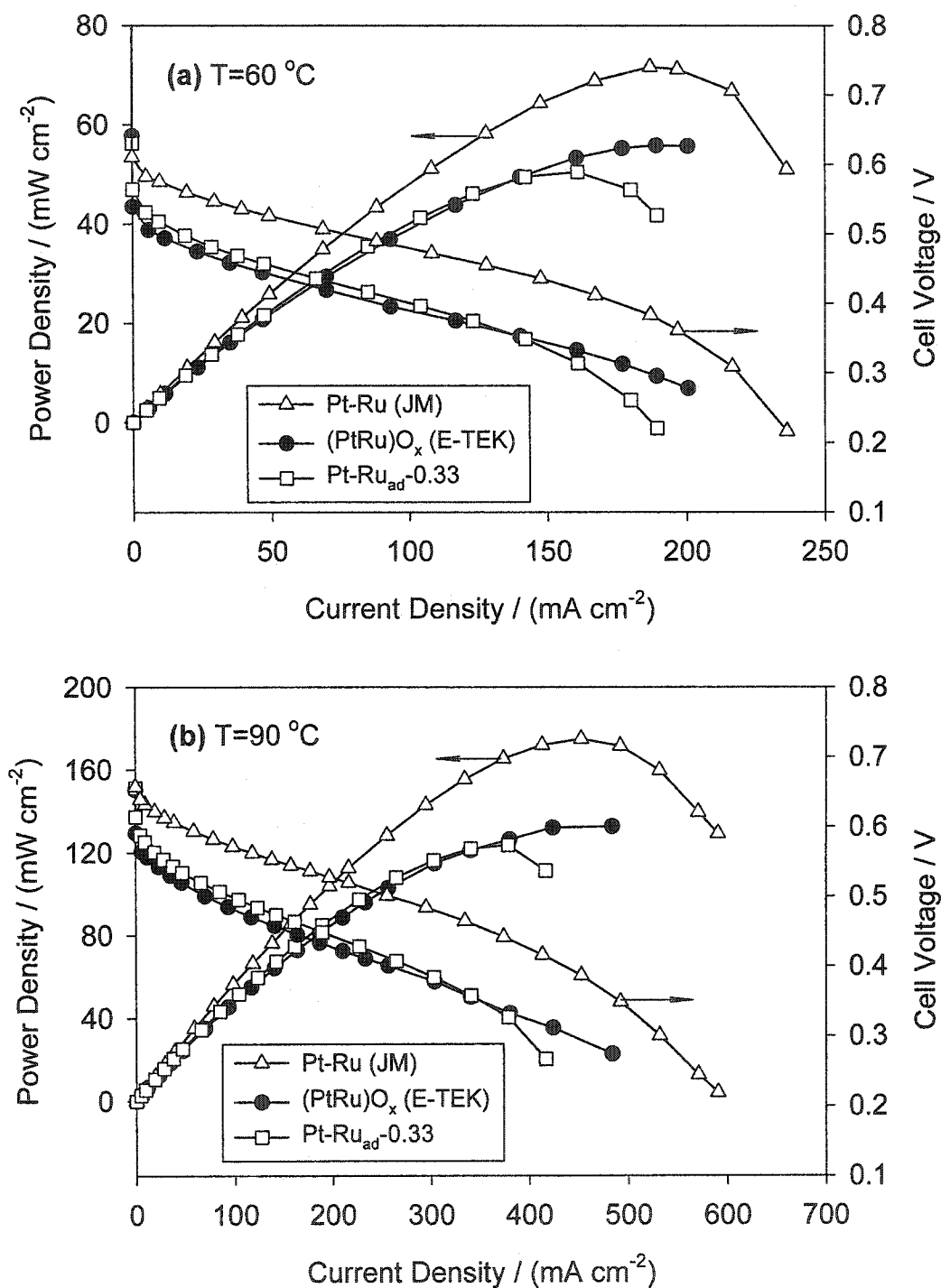


**Figure 4-4.** Power-current and voltage-current curves for DMFCs employing Pt-Ru<sub>ad</sub>, Pt-Ru from Johnson Matthey and (Pt-Ru)O<sub>x</sub> from E-TEK anode catalysts. Anode: 2 mg/cm<sup>2</sup> catalyst, 1.0 M methanol at 4.0 ml/min. Cathode: 2 mg/cm<sup>2</sup> Pt-black catalyst, 20 psig dry oxygen at 400 sccm. Currents are normalized to the geometrical area of the electrodes.

the Pt-Ru<sub>ad</sub> cell approaches 125 mW/cm<sup>2</sup> at ca. 400 mA/cm<sup>2</sup> and at 90 °C. This maximum power is about 70% that of the Johnson Matthey Pt-Ru cell (175 mW/cm<sup>2</sup> at ca. 450 mA/cm<sup>2</sup>), and is comparable to that of the E-TEK (PtRu)Ox cell (130 mW/cm<sup>2</sup> at ca. 450 mA/cm<sup>2</sup>). The operating temperature has a significant effect on the power output. For example, increasing the operating temperature from 60 °C to 90 °C increased the power density of the Pt-Ru<sub>ad</sub> cell from 50 mW/cm<sup>2</sup> to 125 mW/cm<sup>2</sup>. In another literature example, 400 mW/cm<sup>2</sup> peak power density has been reported for a Nafion<sup>®</sup>-112 DMFC (2.2 mg/cm<sup>2</sup> Pt-Ru on anode, 2.2 mg/cm<sup>2</sup> Pt black on cathode) operating at 130°C on 5 atm oxygen.<sup>17</sup> However, the anode fuel must be pressurized to keep the fuel in a liquid state if a cell is operated over 100 °C. The design of such a high temperature liquid feed PEM-DMFC is complex, and was not pursued for this investigation. Vapour operation without anode compartment pressurization seems less attractive than liquid feed due to the requirement for a sophisticated heat exchanger to remove CO<sub>2</sub> from the gaseous cell exhaust stream (gaseous methanol, water, and CO<sub>2</sub>).<sup>4</sup> It should be pointed out that cell designs (e.g., flow fields, cell shape and sizes, current collectors) affect the performance of DMFCs.<sup>27,31-33</sup> Our DMFCs are not optimized for that.

### *3.2 Supported Pt-Ru<sub>ad</sub> Anode Catalysts*

In order to reduce the loading of precious metals, noble metal catalysts are often dispersed on high specific surface area supports. The use of supports substantially increases the specific surface area of the catalysts, providing more active sites per gram of precious metal. Vulcan<sup>™</sup> XC-72 (BET area ca. 250 m<sup>2</sup>/g) is the most common support used for the preparation of DMFC catalysts because it has a relatively small amount of micropores (allowing more homogeneous distribution of catalyst particles), and it has a

reasonably high specific surface area (sufficient to accommodate high loadings of metal nanoparticles).<sup>4</sup> We prepared a series of carbon-supported PtRu<sub>ad</sub> using Vulcan<sup>TM</sup> XC-72R supported Pt nanoparticles (20 wt.% Pt, 112 m<sup>2</sup>/g, E-TEK) as substrate by the surface reductive deposition technique (see Table 4-1 in experimental section). It should be pointed out that, during the deposition of Ru<sub>ad</sub> onto Pt/C, Ru<sup>3+</sup> was not only reduced by Pt-H leading to the formation of Ru<sub>ad</sub> on Pt surfaces, but it was also adsorbed on the carbon support surfaces. This is suggested by the high Ru surface concentration obtained after a single deposition (58% Ru). As pointed out in Chapter 3 (Eq. 3-12), the maximum Ru surface concentration obtained after a single deposition is 33% Ru if the Ru only deposited on Pt. It is likely that the Ru<sup>3+</sup> adsorbed by the carbon support was reduced by methanol during operation of the DMFC, resulting in a (Pt-Ru<sub>ad</sub> + Ru)/C catalyst. The Ru deposited on carbon surfaces may contribute to the activity toward methanol electrooxidation at elevated temperatures. Unfortunately, it is not possible to discriminate between the Ru on Pt surfaces and on carbon surfaces with the data obtained during this study. A TEM analysis will be carried out in the future to address this issue. The surface concentration of the PtRu<sub>ad</sub>/C (defined as the ratio of the number of total Ru<sub>ad</sub> deposited to the number of surface atoms of Pt substrate) does not reflect the actual surface concentration of the Pt-Ru<sub>ad</sub> phase, but it serves as an indication of the total amount of Ru deposited. MEAs were fabricated using PtRu<sub>ad</sub>/C as anode catalyst, unsupported Pt black as cathode. The cathode catalyst loading was maintained at 2 mg/cm<sup>2</sup> to remain consistent with MEAs using unsupported Pt-Ru<sub>ad</sub> anode. The anode catalyst loading was ca. 0.65 mg/cm<sup>2</sup> for PtRu<sub>ad</sub>/C with 20 wt. % Pt. Smotkin and co-workers<sup>34</sup> reported that MEAs prepared using PtRu/C (20 wt.% metal loading, 1:1 a/o Pt:Ru) as anode catalyst

showed no improvement in cell performance with anode loadings above ca. 0.5 mg/cm<sup>2</sup>. We found that it is difficult to transfer (PtRu<sub>ad</sub>/C)/Nafion<sup>®</sup> composite layers containing high metal loading to Nafion<sup>®</sup>-117 membranes from Teflon<sup>®</sup> decal by hot-pressing without increasing the content of Nafion<sup>®</sup> ionomer in the catalyst layer. It appears that the decal transfer technique used in this study does not work well for the fabrication of high catalyst loading MEAs using carbon supported Pt-Ru catalysts, particularly for those Pt-Ru/C with low metal content (e.g., 20 wt.% Pt-Ru).

Figure 4-5 shows the cell polarization curves measured at 60 °C and 90 °C. It can be seen that PtRu<sub>ad</sub>/C-0.74 (after two depositions) performs the same as PtRu<sub>ad</sub>/C-0.85 (after three deposition cycles), and slightly better than PtRu<sub>ad</sub>/C-0.58 (after a single deposition). This trend is similar to that observed for unsupported Pt-Ru<sub>ad</sub>. The performance of the commercial carbon supported Pt-Ru alloy nanoparticles (E-TEK, 20 wt.% Pt-Ru on Vulcan<sup>™</sup> XC-72R) was also tested as anode catalyst in a PEM-DMFC, and the result is included in Figure 4-5. The PtRu<sub>ad</sub>/C was as active as the commercial Pt-Ru/C (E-TEK) at all temperatures studied (note that the specific surface area of PtRu<sub>ad</sub>/C and E-TEK Pt-Ru/C are similar, ca. 112 m<sup>2</sup>/g). These results show that the supported Pt-Ru<sub>ad</sub> systems have performances similar to supported Pt-Ru alloy systems in PEM-DMFCs. This result may suggest that Ru-Pt<sub>ad</sub>/C, prepared by the deposition of Pt on Ru/C, may work as well as the state-of-the-art commercial alloy form Pt-Ru/C as anode catalyst in PEM-DMFCs. The use of adatom form Ru-Pt<sub>ad</sub>/C to replace alloy form Pt-Ru/C would significantly reduce the cost of anode catalysts, because the more expensive Pt (\$512/g) is only deposited on the surface of the less expensive Ru (\$72/g) nanoparticles in submonolayer amounts. Adzic and coworkers<sup>35-39</sup> investigated the

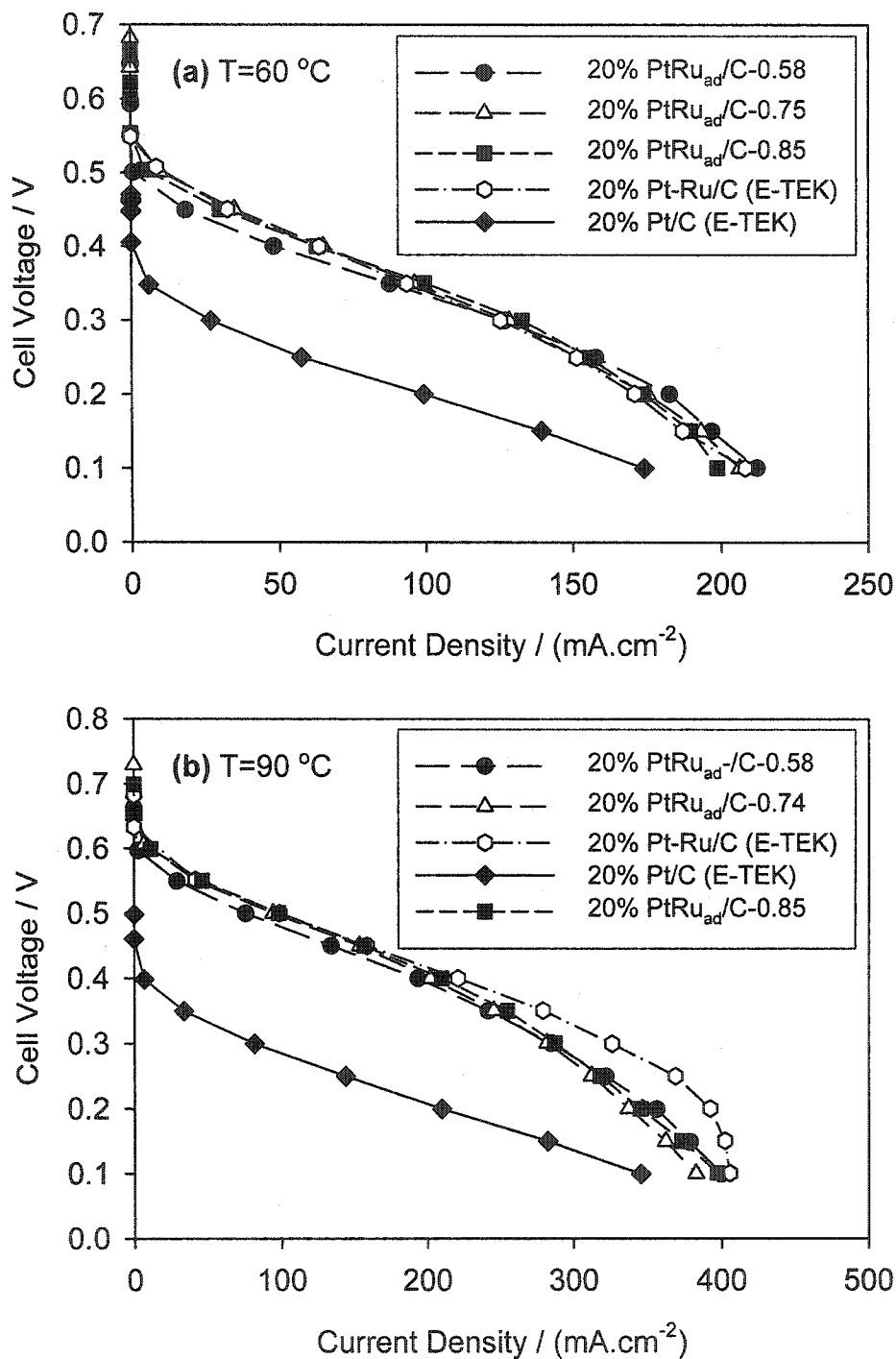


**Figure 4-5.** Polarization curves for DMFCs with carbon supported Pt-Ru<sub>ad</sub> anode catalysts. Anode:  $0.65 \pm 0.2\text{ mg/cm}^2$  PtRu<sub>ad</sub>/C (20 wt.% Pt) catalyst, 1.0 M methanol at 4.0 ml/min. Cathode:  $2\text{ mg/cm}^2$  Pt-black catalyst, 20 psig dry oxygen at 400 sccm. Currents are normalized to the geometrical area of the electrodes.

activity of Ru-Pt<sub>ad</sub>/C prepared by spontaneous deposition of Pt<sub>ad</sub> onto Ru/C for electrooxidation of H<sub>2</sub> and CO. They reported that, despite the several times lower Pt loading, Ru-Pt<sub>ad</sub>/C catalysts have activities and CO tolerance surpassing those of commercial Pt-Ru/C alloy catalysts (50-50 Pt-Ru). No attempts have been reported so far to explore the activity of Ru-Pt<sub>ad</sub>/C toward methanol electrooxidation or as anode catalyst in PEM-DMFCs.

A 40 wt.% metal loading PtRu<sub>ad</sub>/C catalyst was prepared by the surface reductive deposition method using 40 wt.% Pt/C (E-TEK) as the substrate. The relatively high metal content in this 40 wt.% PtRu<sub>ad</sub>/C catalyst allows the fabrication of a MEA with relatively high anode catalyst loading without a significant increase in the thickness of the catalyst layer. A MEA with anode metal loading of 1 mg/cm<sup>2</sup> was fabricated using this catalyst. The cell polarization curves are presented in Figure 4-6. Also included in this figure is the performance of a MEA containing the unsupported Pt-Ru<sub>ad</sub> anode. Figure 4-6 shows that the performance of the 1 mg/cm<sup>2</sup> PtRu<sub>ad</sub>/C (after two depositions) anode is equal to the performance of the 2 mg/cm<sup>2</sup> unsupported Pt-Ru<sub>ad</sub> catalyst (after two depositions). This result shows that the use of high specific surface area supported Pt-Ru<sub>ad</sub> improves the per gram performance of the catalyst. Therefore, high specific surface area catalysts can be used to reduce the amount of precious metal catalysts and still maintain performance.

### *3.3 Stability of Pt-Ru<sub>ad</sub> and Catalyst Utilization*

The Pt-Ru<sub>ad</sub> nanoparticle catalysts prepared in this study may be subject to surface reconstruction (Ru segregation, redistribution, and/or dissolution) during the fabrication of MEAs and the operation of DMFCs. This reconstruction may occur because Ru atoms



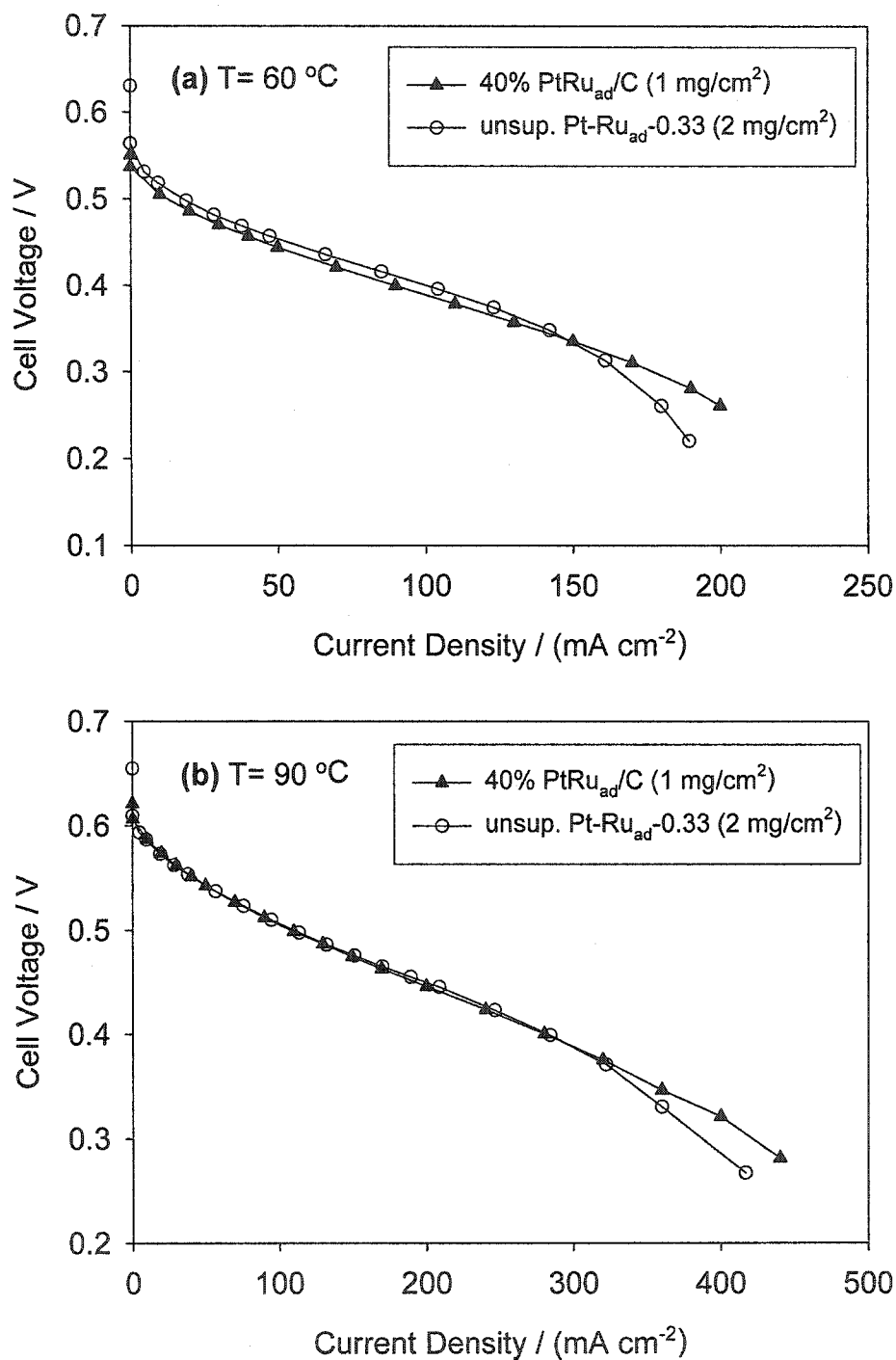


**Figure 4-6.** Comparison of carbon supported and unsupported Pt-Ru<sub>ad</sub> as anode catalyst in a PEM-DMFC. Anode: 1.0 M methanol at 4.0 ml/min. Cathode: 2 mg/cm<sup>2</sup> Pt-black catalyst, 20 psig dry oxygen at 400 sccm. Currents are normalized to the geometrical area of the electrodes.

are only *adsorbed* onto the Pt surface under our preparation conditions. These Ru adatoms may be low-coordinated, have high surface energy, and thereby have a tendency to undergo surface redistribution in order to minimize surface energy. The stability of the surface structures is therefore a general issue for Pt-Ru<sub>ad</sub> systems and deserves to be addressed here.<sup>5</sup> Due to the lack of direct techniques to characterize the distribution of Ru<sub>ad</sub> on highly dispersed nanoparticle Pt-Ru<sub>ad</sub> surfaces, cyclic voltammetry and fuel cell performance were used to obtain rough information about possible surface changes. It is well known that cyclic voltammograms of Pt-Ru surfaces are dependant on Ru surface coverage and distribution. For example, the peak resolution in the “hydrogen region” decreases, and currents in the ‘double layer region’ increase with increase in Ru surface coverage (Chapter 3).<sup>40-43</sup> Further, it appears that if Ru<sub>ad</sub> forms 3-D islands on Pt surfaces, a peak at ca. 100 mV will appear in the cyclic voltammogram, which is related to the formation and stripping of surface adsorbed hydrogen from Ru islands (Chapter 3),<sup>44-50</sup> or to the oxidation of Ru.<sup>35</sup> In Chapter 3, we reported the cyclic voltammograms of various freshly prepared Pt-Ru<sub>ad</sub> catalysts (Figure 3-4). These cyclic voltammograms were measured in 1.0 M H<sub>2</sub>SO<sub>4</sub> at ambient temperature. In this study, we measured the cyclic voltammograms of these Pt-Ru<sub>ad</sub> nanoparticles after they have been incorporated in the anode layer of MEAs and the MEA-DMFCs have been conditioned and operated for several days. The measurements were carried out in the fuel cell test block at room temperature. The anode served as the working electrode by circulating Ar-purged, purified water. The Pt black cathode was used as counter and reference electrodes by supplying it with humidified H<sub>2</sub> (1 atm). The potentials were reported versus this reference electrode. Typical CVs are shown in Figure 4-7. Currents are normalized to per

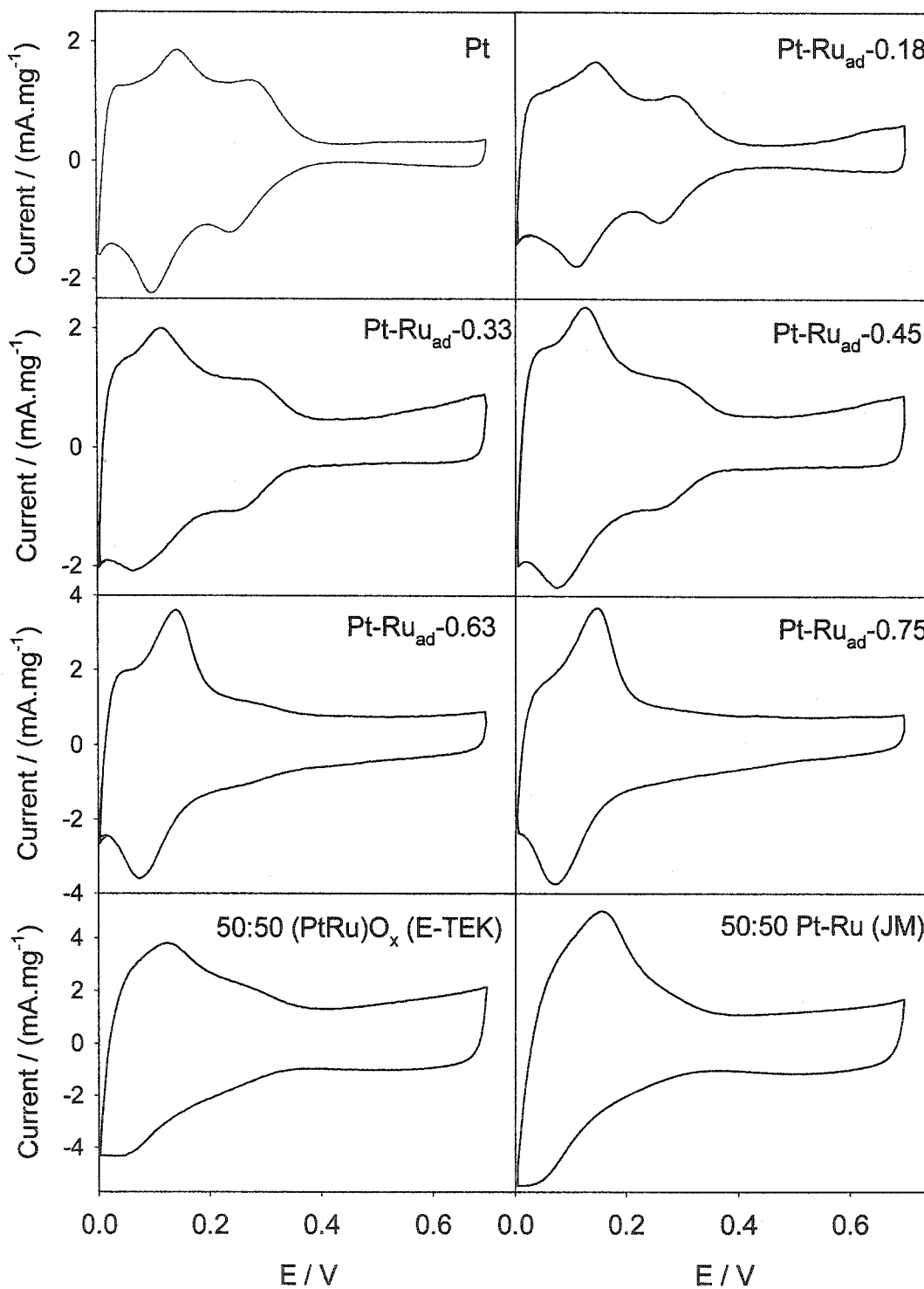


**Figure 4-7.** Cyclic voltammograms of anode catalysts recorded in PEM-DMFCs at 25 °C, 10 mV/s sweep rate. The anode catalyst loading is 2 mg/cm<sup>2</sup>.

gram catalysts. It can be seen that, with increasing Ru coverage, the peak resolution in the “hydrogen region” decreases, and currents in the “double layer region” increase. A sharp peak at ca. 120 mV appears when the Ru coverages are higher than 0.33, and its intensity increases with Ru coverage. All these features closely resemble those previously observed on freshly prepared Pt-Ru<sub>ad</sub> in H<sub>2</sub>SO<sub>4</sub> (Chapter 3 Figure 3-4). By comparing the individual CV recorded in MEA to that recorded in H<sub>2</sub>SO<sub>4</sub> for the same Pt-Ru<sub>ad</sub>, it was found that no significant changes occur before and after hot-pressing and running. Cyclic voltammetry, therefore, indicates that no significant surface reconstructions (Ru redistribution and dissolution) were observed for Pt-Ru<sub>ad</sub> during the fabrication of the MEAs.

The stability of a PEM-DMFC with PtRu<sub>ad</sub>/C-0.58 (20 wt.% Pt) anode catalyst was tested at 60 °C and 90°C. The data are shown in Figure 4-8. The cell was run for 20 total days at 8 hour per day. A typical day operation procedure is as follows. First, the cell was heated to 60 °C at open circuit (ca. 10 min) with 1.0 M aqueous methanol circulating through the anode compartment at 4.0 mL/min, and oxygen flowing through the cathode at 400 sccm and 20 psig back pressure. The cell was then operated at 20 mA/cm<sup>2</sup> (ca. 0.45 V) for 1.5 h, at 50 mA/cm<sup>2</sup> (ca. 0.4 V) for 1 h, and at 100 mA/cm<sup>2</sup> (ca. 0.35 V) for another hour. The cell was then polarized by sweeping the cell potential back and forth from open circuit to 0.1 V several times until a reproducible polarization curve was obtained (ca. 10 cycles). After the sweeps, the cell current was held at 100 mA/cm<sup>2</sup>, and the cell was heated to 90°C (ca. 10min). The cell was then operated at 100 mA/cm<sup>2</sup> (ca. 0.45 V) for 1.5 h, and 200 mA/cm<sup>2</sup> (ca. 0.35 V) for another 1.5 h. Potential sweeps were performed again. Finally, the electronic load and heating were turned off, and the

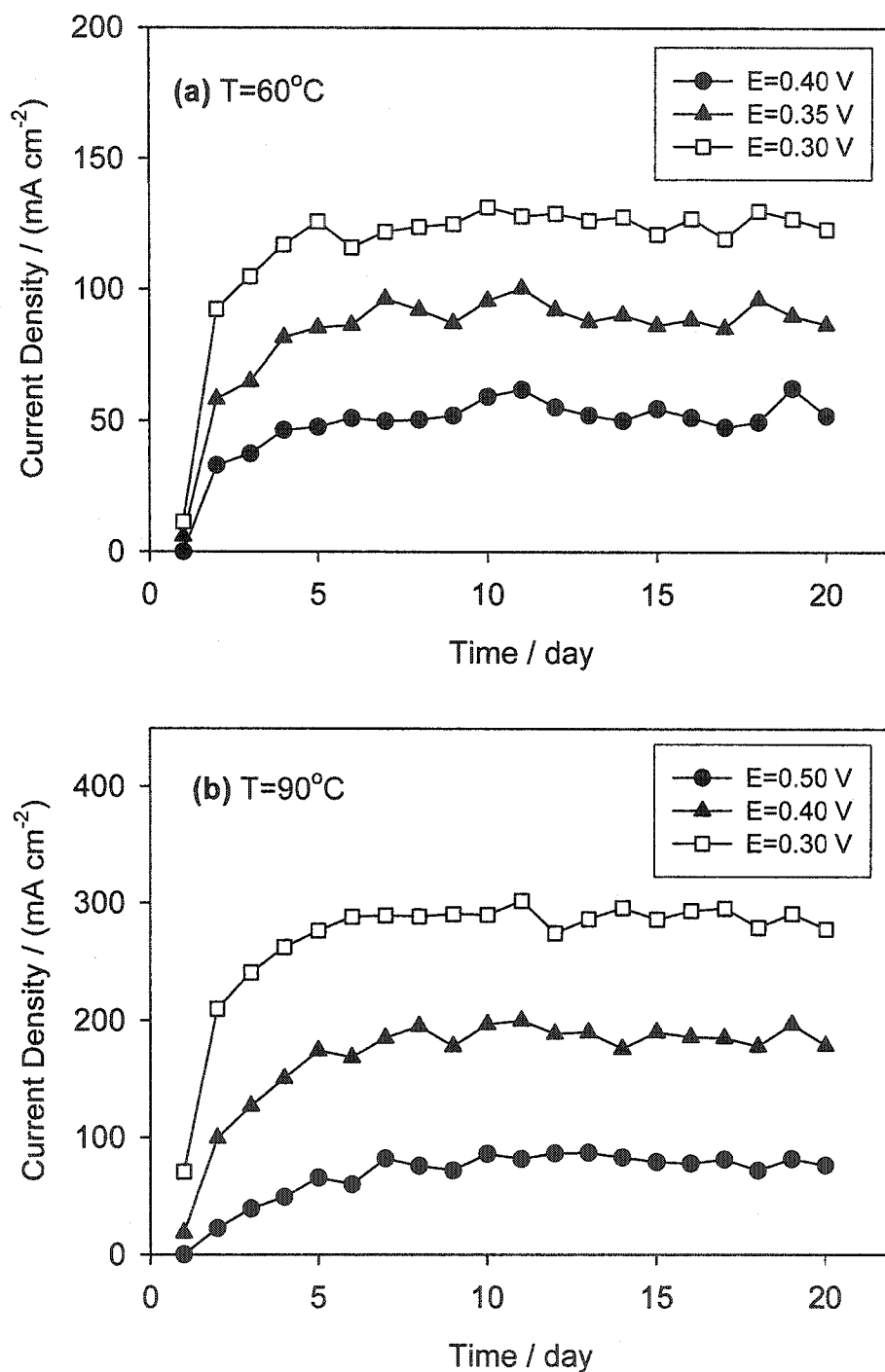


**Figure 4-8.** Durability test for the PEM-DMFC with PtRu<sub>ad</sub>/C anode catalyst. Anode: 0.68 mg/cm<sup>2</sup> PtRu<sub>ad</sub>/C-0.58 (20 wt.% Pt) catalyst, 1.0 M methanol at 4.0 ml/min. Cathode: 2 mg/cm<sup>2</sup> Pt-black catalyst, 20 psig dry oxygen at 400 sccm. Currents are normalized to the geometrical area of the electrode.

methanol and oxygen supply were shut down. The cell was left off overnight with the anode under aqueous methanol solution and the cathode under air. Fresh methanol was used the following day. As Figure 4-8 shows, no loss in performance was observed over 20 days operation. This result indicates that no Ru dissolution and/or redistribution occur that is large enough to affect the catalytic activity. This encouraging result implies that Pt-Ru<sub>ad</sub> catalysts can survive normal cell operation and load changes. Surface reconstruction doesn't seem to be a serious issue for these Pt-Ru<sub>ad</sub> nanoparticle catalysts.

The catalyst utilization in the cathodes of DMFCs, as expressed by Equation 4-7,<sup>18-20</sup> was estimated in this study. The electrochemically active surface areas of Pt nanoparticles in the cathodes were measured using the cyclic voltammograms of Pt nanoparticles recorded in the fuel cells. The electrochemically active surface areas reflect the total surface areas of Pt nanoparticles that are effectively accessed by protons and electrons in the cathode layers. The total surface area was calculated using the Pt loading (2 mg/cm<sup>2</sup>) and specific surface area of Pt nanoparticles (27 m<sup>2</sup>/g). It was found that ca. 80-85% utilization was attained for the nanoparticle Pt cathode catalysts. The utilization of nanoparticle Pt-Ru<sub>ad</sub> anode catalysts should presumably be the same as that of Pt cathode catalysts due to their similar properties, such as identical particle size. Noticeably, not all electrochemically active surface areas can be utilized for electrode reactions because of the inaccessibility of reactants to some of these surface sites. Therefore, the actual catalyst utilization is always smaller than the estimated.

$$\text{catalyst utilization} = \frac{\text{electrochemically active surface area}}{\text{total surface area}} \quad (4-7)$$

#### 4. Conclusions

Unsupported and carbon supported nanoparticle Pt-Ru<sub>ad</sub> catalysts have been prepared using the surface reductive deposition technique. The performance of these nanocomposites as anode catalysts in liquid feed PEM-DMFCs has been evaluated. It was found that the surface composition of unsupported Pt-Ru<sub>ad</sub> nanoparticles has a significant influence on their activities as anode catalysts in DMFCs. The optimum Ru surface coverage was ca. 35% for DMFCs operating at 60 °C, and ca.30-60% for DMFCs operating at 90 °C. Carbon supported Pt-Ru<sub>ad</sub> catalysts display higher mass activities than unsupported Pt-Ru<sub>ad</sub>. Comparable cell performance can be obtained using carbon supported Pt-Ru<sub>ad</sub> with much lower metal loading than unsupported. The maximum power density measured on Pt-Ru<sub>ad</sub> approaches 70 % of that obtained on the state-of-the-art commercial Pt-Ru alloy catalyst from Johnson Matthey, despite the specific surface area of Pt-Ru<sub>ad</sub> being only 40 % that of the Johnson Matthey Pt-Ru catalyst.

Cyclic voltammetry showed that no obvious surface restructuring of Pt-Ru<sub>ad</sub> occurred during the fabrication and operation of the DMFCs. A PEM-DMFC using PtRu<sub>ad</sub>/C anode catalyst was operated for 20 days on an intermittent basis with no obvious deterioration in the cell performance. This result suggests that Pt-Ru<sub>ad</sub> nanoparticle catalysts can be used in practical DMFCs.

#### References

- (1) Hogarth, M. P.; Hards, G. A. *Plat. Met. Rev.* **1996**, *40*, 150-159.

- (2) Cameron, D. S.; Hards, G. A.; Harrison, B.; Potter, R. J. *Plat. Met. Rev.* **1987**, *31*, 173-181.
- (3) Ren, X.; Zelenay, P.; Thomas, S.; Davey, J.; Gottesfeld, S. *J. Power Sources* **2000**, *86*, 111-116.
- (4) Aricò, A. S.; Srinivasan, S.; Antonucci, V. *Fuel Cells* **2001**, *1*, 133-161.
- (5) Wasmus, S.; Kuver, A. *J. Electroanal. Chem.* **1999**, *461*, 14-31.
- (6) Watanabe, M.; Motoo, S. *J. Electroanal. Chem.* **1975**, *60*, 267-273.
- (7) Ley, K. L.; Liu, R.; Pu, C.; Fan, Q.; Leyarovska, N.; Segre, C.; Smotkin, E. S. *J. Electrochem. Soc.* **1997**, *144*, 1543-1548.
- (8) Reddington, E.; Sapienza, A.; Gurau, B.; Viswanathan, R.; Sarangapini, S.; Smotkin, E. S.; Mallouk, T. E. *Science* **1998**, *280*, 1735-1737.
- (9) Waszczuk, P.; Solla-Gullon, J.; Kim, H. S.; Tong, Y. Y.; Montiel, V.; Aldaz, A.; Wieckowski, A. *J. Catal.* **2001**, *203*, 1-6.
- (10) Tong, Y. Y.; Kim, H. S.; Babu, P. K.; Waszczuk, P.; Wieckowski, A.; Oldfield, E. *J. Am. Chem. Soc.* **2002**, *124*, 468-473.
- (11) Tong, Y. Y.; Oldfield, E.; Wieckowski, A. *Faraday Discuss.* **2002**, *121*, 323-330.
- (12) Cao, D.; Bergens, S. H. *J. Electroanal. Chem.* **2002**, *533*, 91-100.
- (13) Gasteiger, H. A.; Ross, P. N., Jr.; Cairns, E. J. *Surf. Sci.* **1993**, *293*, 67-80.
- (14) Markovic, N. M.; Ross, P. N. *Surf. Sci. Rep.* **2002**, *45*, 121-229.
- (15) Arico, A. S.; Antonucci, P. L.; Modica, E.; Baglio, V.; Kim, H.; Antonucci, V. *Electrochim. Acta* **2002**, *47*, 3723-3732.
- (16) Wilson, M. S.; Gottesfeld, S. *J. Appl. Electrochem.* **1992**, *22*, 1-7.
- (17) Ren, X.; Wilson, M. S.; Gottesfeld, S. *J. Electrochem. Soc.* **1996**, *143*, L12-L15.
- (18) Thomas, S. C.; Ren, X.; Gottesfeld, S. *J. Electrochem. Soc.* **1999**, *146*, 4354-4359.
- (19) Dinh, H. N.; Ren, X.; Garzon, F. H.; Zelenay, P.; Gottesfeld, S. *J. Electroanal. Chem.* **2000**, *491*, 222 - 233.
- (20) He, C. Z.; Qi, Z. Q.; Hollett, M.; Kaufman, A. *Electrochem. Solid-State Lett.* **2002**, *5*, A181-A183.
- (21) Gasteiger, H. A.; Markovic, N.; Ross, P. N.; Cairns, E. J. *J. Electrochem. Soc.* **1994**, *141*, 1795-1803.



- (22) Neergat, M.; Leveratto, D.; Stimming, U. *Fuel Cells* **2002**, *2*, 25-30.
- (23) Gottesfeld, S. (with Zawodzinski, T.), Polymer electrolyte fuel cells, in: Tobias, C.; Gerischer, H.; Kolb, D.; Alkire, R. (Eds.), *Advances in Electrochemistry and Electrochemical Engineering*, Wiley/VCH, New York, **1997**, *5*, 195.
- (24) Metha, V.; Cooper, J. S. *J. Power Source* **2003**, *114*, 32-53
- (25) Arico, A. S.; Creti, P.; Poltarzewski, Z.; Mantegna, R.; Kim, H.; Giordano, N.; Antonucci, V. *Mater. Chem. Phys.* **1997**, *47*, 257-262.
- (26) Arico, A. S.; Creti, P.; Giordano, N.; Antonucci, V.; Antonucci, P. L.; Chuvilin, A. *J. Appl. Electrochem.* **1996**, *26*, 959-967.
- (27) Argyropoulos, P.; Scott, K.; Taama, W. M. *Electrochim. Acta* **1999**, *44*, 3575-3584.
- (28) Argyropoulos, P.; Scott, K.; Taama, W. M. *J. Appl. Electrochem.* **1999**, *29*, 661-669.
- (29) Scott, K.; Taama, W. M.; Argyropoulos, P.; Sundmacher, K. *J. Power Sources* **1999**, *83*, 204-216.
- (30) Dinh, H. N.; Ren, X.; Garzon, F. H.; Zelenay, P.; Gottesfeld, S. *J. Electroanal. Chem.* **2000**, *491*, 222 - 233.
- (31) Scott, K.; Argyropoulos, P.; Yiannopoulos, P.; Taama, W. M. *J. Appl. Electrochem.* **2001**, *31*, 823-832.
- (32) Scott, K.; Taama, W. M.; Argyropoulos, P. *J. Power Sources* **1999**, *79*, 43-59.
- (33) Amphlett, J. C.; Peppley, B. A.; Halliop, E.; Sadiq, A. *J. Power Sources* **2001**, *96*, 204-213.
- (34) Liu, L.; Pu, C.; Viswanathan, R.; Fan, Q.; Liu, R.; Smotkin, E. S. *Electrochim. Acta* **1998**, *43*, 3657-3663
- (35) Brankovic, S. R.; Wang, J. X.; Zhu, Y.; Sabatini, R.; McBreen, J.; Adzic, R. R. *J. Electroanal. Chem.* **2002**, *524*, 231-241.
- (36) Brankovic, S. R.; McBreen, J.; Adzic, R. R. *J. Electroanal. Chem.* **2001**, *503*, 99-104.
- (37) Brankovic, S. R.; McBreen, J.; Adzic, R. R. *Surf. Sci.* **2001**, *479*, L363-L368.
- (38) Brankovic, S. R.; Wang, J. X.; Adzic, R. R. *Electrochem. Solid-State Lett.* **2001**, *4*, A217-A220.

- (39) Brankovic, S. R.; Wang, J. X.; Adzic, R. R. *J. Serb. Chem. Soc.* **2001**, *66*, 887-898.
- (40) Lee, C. E.; Bergens, S. H. *J. Phys. Chem. B* **1998**, *102*, 193-199.
- (41) Gasteiger, H. A.; Markovic, N.; Ross, P. N., Jr.; Cairns, E. J. *J. Phys. Chem.* **1993**, *97*, 12020-12029.
- (42) Iwasita, T.; Hoster, H.; John-Anacker, A.; Lin, W. F.; Vielstich, W. *Langmuir* **2000**, *16*, 522-529.
- (43) Ticanelli, E.; Beery, J. G.; Paffett, M. T.; Gottesfeld, S. *J. Electroanal. Chem.* **1989**, *258*, 61-77.
- (44) Krausa, M.; Vielstich, W. *J. Electroanal. Chem.* **1994**, *379*, 307-314.
- (45) Iwasita, T.; Hoster, H.; John-Anacker, A.; Lin, W. F.; Vielstich, W. *Langmuir* **2000**, *16*, 522-529.
- (46) Lin, W. F.; Christensen, P. A.; Hamnett, A. *Phys. Chem. Chem. Phys.* **2001**, *3*, 3312-3319.
- (47) Wang, W. B.; Zei, M. S.; Ertl, G. *Phys. Chem. Chem. Phys.* **2001**, *3*, 3307-3311.
- (48) Lin, W. F.; Zei, M. S.; Kim, Y. D.; Over, H.; Ertl, G. *J Phys. Chem. B* **2000**, *104*, 6040-6048.
- (49) Lin, W. F.; Christensen, P. A.; Hamnett, A.; Zei, M. S.; Ertl, G. *J Phys. Chem. B* **2000**, *104*, 6642-6652.
- (50) Lin, W. F.; Christensen, P. A.; Hamnett, A. *J Phys. Chem. B* **2000**, *104*, 12002-12011.

## Chapter 5

### A Direct 2-Propanol Polymer Electrolyte Fuel Cell<sup>†</sup>

#### 1. Introduction

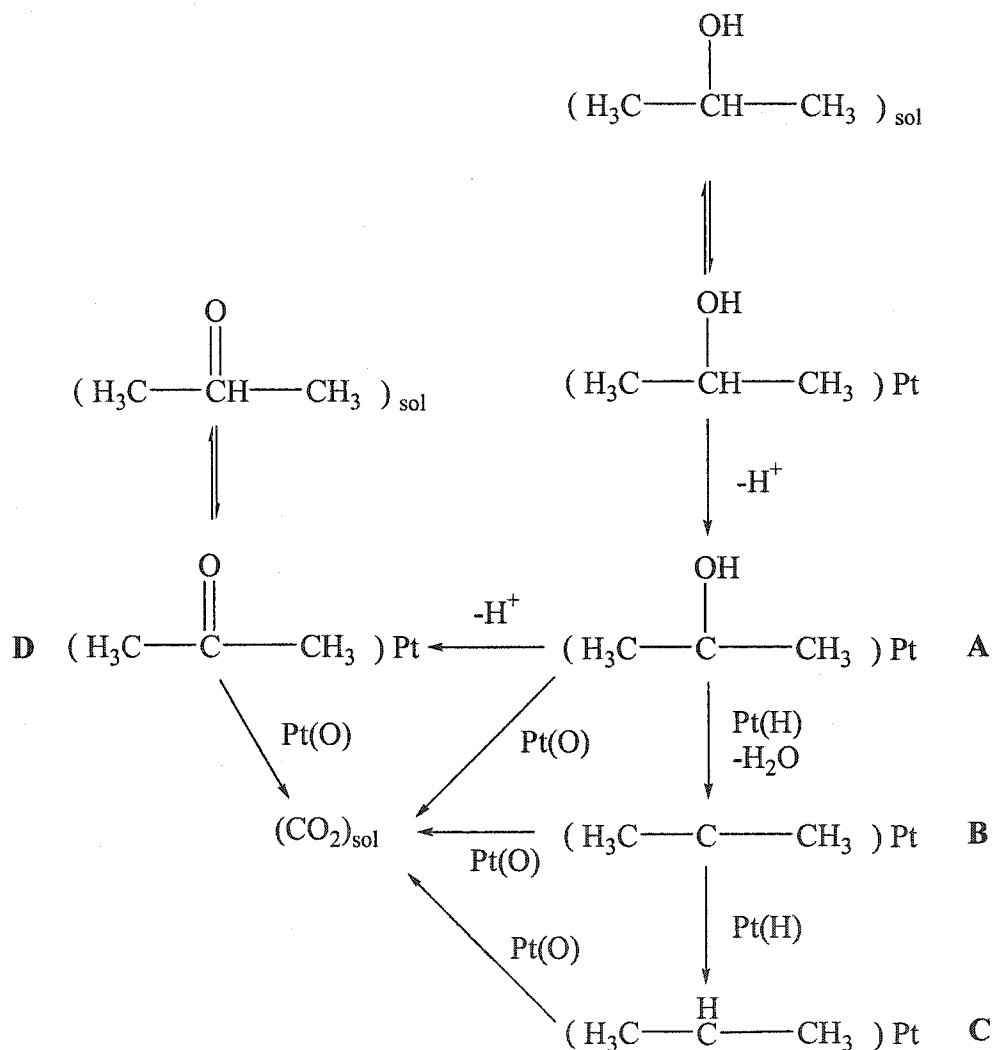
Direct methanol fuel cells (DMFCs) using Pt-Ru anode electrocatalysts are the most studied type of direct alcohol fuel cell.<sup>1-3</sup> The most imminent commercial application for such cells is likely as power sources for portable electronic devices.<sup>4,5</sup> The challenges associated with developing practical DMFCs include poisoning of anode electrocatalysts by CO or related species obtained from methanol, crossover of methanol from the anode to the cathode, and cathode poisoning by methanol.<sup>2,6</sup> One approach to address these issues is to use alcohols that are less prone to crossover and electrocatalyst poisoning than methanol, and preferably are more feasible toward electrooxidation than methanol.

The electrooxidation of 2-propanol over platinum-based electrodes was studied by several groups during the 1990's.<sup>7-10</sup> The major oxidation product is acetone at low potentials ( $< 0.4$  V vs. RHE),  $\text{CO}_2$  is negligible. A proposed mechanism for the electrooxidation of 2-propanol over Pt surfaces is given in Scheme 5-1.<sup>8,9</sup> The interaction of 2-propanol with Pt surfaces leads to the formation of physisorbed 2-propanol species. These species undergo a dehydrogenation at the  $\alpha$ -C atom, yielding the adsorbate A, which is bound to Pt surface through the  $\alpha$ -C atom. Adsorbate A undergoes a further dehydrogenation forming adsorbate D, which can be attached to the surface through a  $\pi$ -

---

<sup>†</sup> A version of this chapter has been published. Cao, D. X.; Bergens, S. H. *J. Power Sources* **2003**, *124*, 12-17.

bonding interaction with Pt ( $\pi$ -bonded  $\eta^2$  acetone species). This bond would be weak; therefore, the displacement of adsorbate **D** by 2-propanol is likely to occur, generating free acetone. Meanwhile, hydrogenolysis of adsorbate **A** can occur to produce adsorbates **B** and **C**. Adsorbates **A**, **B**, **C**, and **D** may be oxidized at high potentials to  $\text{CO}_2$ . The dehydrogenation of 2-propanol to acetone is the dominant and fastest path.<sup>10</sup>



**Scheme 5-1.** Reaction scheme of 2-propanol oxidation on a platinum electrode in acidic solution.

Wang et al.<sup>11</sup> reported the first fuel cell to operate directly on 2-propanol as fuel (DPFC). Their cell consisted of a Pt-Ru nanoparticle anode ( $4 \text{ mg/cm}^2$ ), a Pt black

cathode ( $4 \text{ mg/cm}^2$ ), and an  $\text{H}_3\text{PO}_4$ -doped polybenzimidazole (PBI) membrane electrolyte. The cell was operated at  $170 \text{ }^\circ\text{C}$  using methanol, ethanol, 1-propanol, and 2-propanol as fuel. 2-Propanol provided the worst cell performance as fuel of the alcohols tested. The cell voltage operating on 2-propanol at  $200 \text{ mA/cm}^2$  was low, less than  $0.2 \text{ V}$ . During the course of our investigations, Qi and co-workers<sup>12, 13</sup> reported operation of a direct 2-propanol fuel cell using Pt-Ru and Pt blacks as anode and cathode catalysts, respectively, Nafion<sup>®</sup>-112 as membrane electrolyte, and air at the cathode. They found that the direct 2-propanol fuel cell shows much higher performance than a direct methanol fuel cell, especially, at current densities lower than ca.  $200 \text{ mA/cm}^2$ . The better performance of 2-propanol than methanol is attributed to the faster electrooxidation kinetics and lower crossover of 2-propanol than methanol.

In this study, we report and compare our results using 2-propanol and methanol as fuel in the same polymer electrolyte membrane direct alcohol fuel cell. The cell contained one of the most active commercially available methanol anode catalysts (Johnson Matthey HiSPEC<sup>™</sup>-6000, 50-50 Pt-Ru, specific surface area ca.  $70 \text{ m}^2/\text{g}$ ), a relatively thick Nafion<sup>®</sup>-117 membrane, and high surface area unsupported Pt black cathode catalyst (specific surface area ca.  $27 \text{ m}^2/\text{g}$ ). The cell was operated at relatively high temperatures ( $90 \text{ }^\circ\text{C}$ ) using pure oxygen as oxidant to maximize the activity of the cathode in order to study the limitations of the anode.

## 2. Experimental

The membrane electrode assemblies were fabricated using the decal transfer method developed at the Los Alamos National Laboratory.<sup>14</sup> Unsupported Pt-Ru black of

nominal 1:1 atomic ratio (Johnson Matthey, HiSPEC™-6000, specific surface area ca. 70 m<sup>2</sup>/g) and unsupported Pt black (Johnson Matthey, fuel cell grade, specific surface area ca. 27 m<sup>2</sup>/g) were used as the anode and cathode catalysts, respectively. Catalyst/ionomer inks were prepared as follows. A suspension of catalyst in water was ultrasonicated for 30 min (to wet and disperse the catalyst), enough 5% Nafion® solution (ElectroChem. Inc) was then added to give a dry ink composition of 80 wt.% catalyst and 20 wt.% Nafion® ionomer, and the mixture was ultrasonicated for 2 h further to obtain a uniformly dispersed ink. A Nafion®-117 membrane was cleaned and converted into the acid form by boiling in 3% H<sub>2</sub>O<sub>2</sub> for 1 h, followed by boiling in 0.5 M H<sub>2</sub>SO<sub>4</sub> for 2 h, and finally boiling in ultra-pure water for 2 h with the water being changed every 30 min. The cleaned membrane was stored in ultra-pure water and dried on a heated vacuum table before use. The catalyst inks were painted onto 5 cm<sup>2</sup> Teflon® decals to give a metal loading of approximately 2 mg/cm<sup>2</sup> unless stated otherwise in the text. The catalyst inks were transferred from the Teflon® decals to the Nafion® membrane by hot-pressing (125 to 127 °C, 1450 to 1550 psig for ca. 2.5 min). The membrane electrode assemblies were then mounted into commercial fuel cell hardware (ElectroChem. Inc.) using Teflon®-treated carbon papers (ElectroChem. Inc.) as backings/current collectors. Aqueous solutions of 2-propanol (Fisher Scientific, certified ACS grade) or methanol (Sigma-Aldrich, ACS HPLC grade, 99.93%) were pumped through the anode flow field at 4 mL/min, zero back pressure, and circulated back to the fuel reservoir. The temperature of the reservoir was maintained below 40 °C to condense the vapor and release gaseous products. Dry oxygen (Praxair, UHP) was supplied from a cylinder to the cathode at 600 standard cubic centimeter per minute (sccm) at 20 psig back pressure unless specified

otherwise in the text. Pure oxygen was used to maximize the activity of the cathode. All experiments were carried out at 90 °C cell temperature. The polarization curves were obtained using the 890 Series computer-controlled fuel cell test load (Scribner Associate Inc.). All reported cell potentials are not IR compensated. Each fuel cell was conditioned for 3 days before recording any polarization data as follows. The fuel cell was heated from ambient temperature to 60 °C at open circuit with 1.0 M methanol solution circulating through the anode compartment and oxygen flowing through the cathode compartment. The cell was then operated under a constant, low load (20 mA/cm<sup>2</sup>) for 4 h, the temperature was raised to 90 °C, and the cell was operated at 100 mA/cm<sup>2</sup> for another 4 h. The cell was then shut down by switching off the load, heating, methanol, and oxygen, and was left overnight at room temperature. This procedure was repeated two more times each using fresh methanol solutions. It was found that the performances of DMFCs conditioned this way were both maximized and stable.

The cell was switched from operation on methanol to operation on 2-propanol as follows. After the methanol polarization data were recorded, pure water was pumped through the anode and cathode compartments of the cell for 4 h each to wash the methanol out of the cell and the Nafion<sup>®</sup> membrane. Oxygen was then passed through the cathode compartment, and the cell was short-circuited for 10 s to burn off any traces of adsorbed methanol on the cathode and anode catalyst surfaces. A 2.0 M solution of 2-propanol was then fed to the anode compartment, the cell was heated to 90 °C within 30 min at open circuit, and the electronic load was applied. The voltage-current polarization data were recorded from zero current (open circuit) to high currents in 0.05 A current

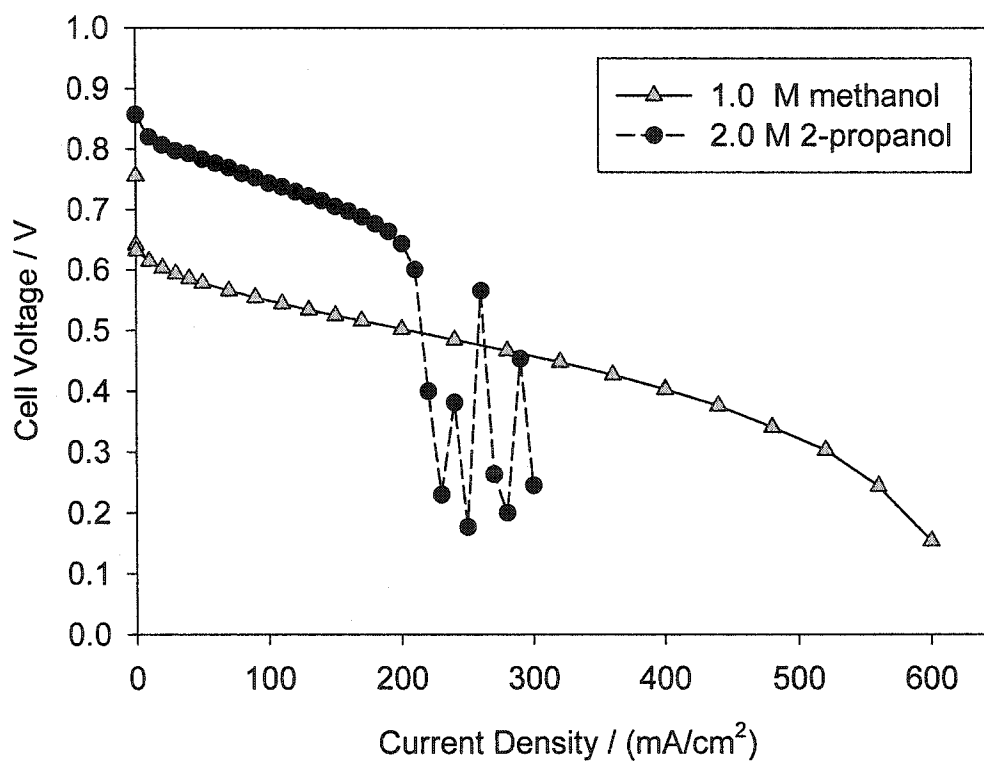
increments. The current was held for 30 s after each increment before the cell voltage was recorded.

### 3. Results

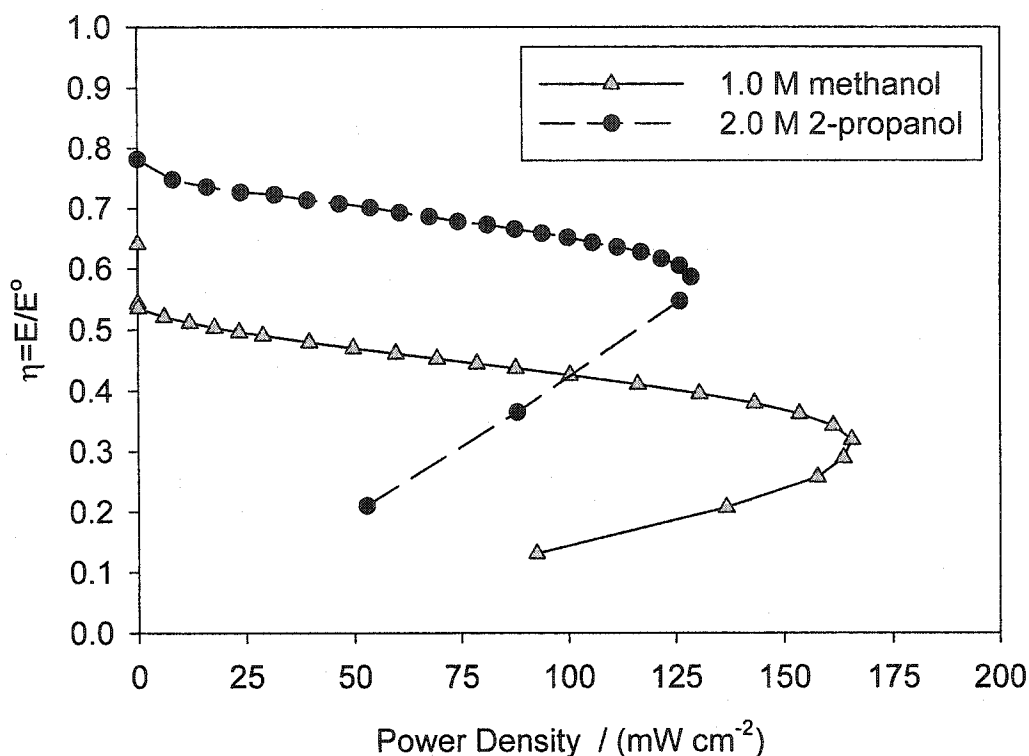
Figure 5-1 shows typical voltage-current polarization curves of the same fuel cell operating on 2.0 M 2-propanol and 1.0 M methanol as fuel. The performance of the cell operating on 2-propanol is substantially higher than the cell operating on methanol at current densities lower than ca. 200 mA/cm<sup>2</sup>. For example, the cell voltage at 120 mA/cm<sup>2</sup> is ca. 200 mV higher operating on 2-propanol than on methanol. Similar observations were made by Qi and co-workers.<sup>12, 13</sup> These performances are the highest we are aware of for a direct alcohol fuel cell. Unfortunately, the high performance of the cell operating on 2-propanol rapidly drops when the current density exceeds ca. 200 mA/cm<sup>2</sup>. The cell voltage oscillates around 0.2 V at current densities higher than 200 mA/cm<sup>2</sup>.

Figure 5-2 compares the electrical efficiency (approximated here as  $\eta = E_{\text{cell}}/E^\circ$ , where  $E^\circ = 1.097$  V for 2-propanol,<sup>15</sup> and 1.18 V for methanol<sup>1, 3</sup>) and power density of the cell operating on 1.0 M methanol and 2.0 M 2-propanol. It can be seen that the 2-propanol cell displays an electrical efficiency nearly 1.5 times that of the cell operating on methanol at power densities below 125 mW/cm<sup>2</sup>. The maximum power density of the cell operating on 2-propanol approaches 75 % of that operating on methanol. Further, the maximum power density of the cell operating on 2-propanol was achieved at 59% electrical efficiency, whereas the maximum power density with methanol was achieved at only 32% electrical efficiency.





**Figure 5-1.** Performance of a direct 2-propanol fuel cell versus a direct methanol fuel. Anode: 2 mg/cm<sup>2</sup> Pt-Ru black catalyst (Johnson Matthey), 2.0 M iPrOH or 1.0 M MeOH at 4.0 mL/min. Cathode: 2 mg/cm<sup>2</sup> Pt-black catalyst, 20 psig dry oxygen at 600 sccm.



**Figure 5-2.** Plots of electrical efficiency versus power density for a direct 2-propanol fuel cell and a direct methanol fuel cell. Anode: 2 mg/cm<sup>2</sup> Pt-Ru black catalyst (Johnson Matthey), 2.0 M iPrOH or 1.0 M MeOH at 4.0 mL/min. Cathode: 2 mg/cm<sup>2</sup> Pt-black catalyst, 20 psig dry oxygen at 600 sccm.

The effects of electrocatalyst loading, of 2-propanol concentration, and of oxygen pressure on cell performance were investigated to gain insight into the origins of the performance drop at high current densities. Figure 5-3 and Figure 5-4 show the effects of cathode and anode electrocatalyst loading on cell performance, respectively. At constant anode loading, increasing the cathode loading from 2 to 3.2 mg/cm<sup>2</sup> Pt black did not significantly improve either the cell voltage at low current densities, nor did it decrease the voltage drop at high current densities (Figure 5-3). This result shows that the cathode

loading is not a major limiting factor in the performance of these cells operating on oxygen, and it suggests that cells operating on 2-propanol require lower cathode loadings than cells operating on methanol. At constant cathode loading, increasing the anode electrocatalyst loading from 2 to 4 mg/cm<sup>2</sup> results in an increase in the limiting current density, but it has no significant effect on the cell voltages at current densities lower than ca. 200 mA/cm<sup>2</sup> (Figure 5-4). This result strongly implies the voltage drop at high current densities is an anode phenomenon.

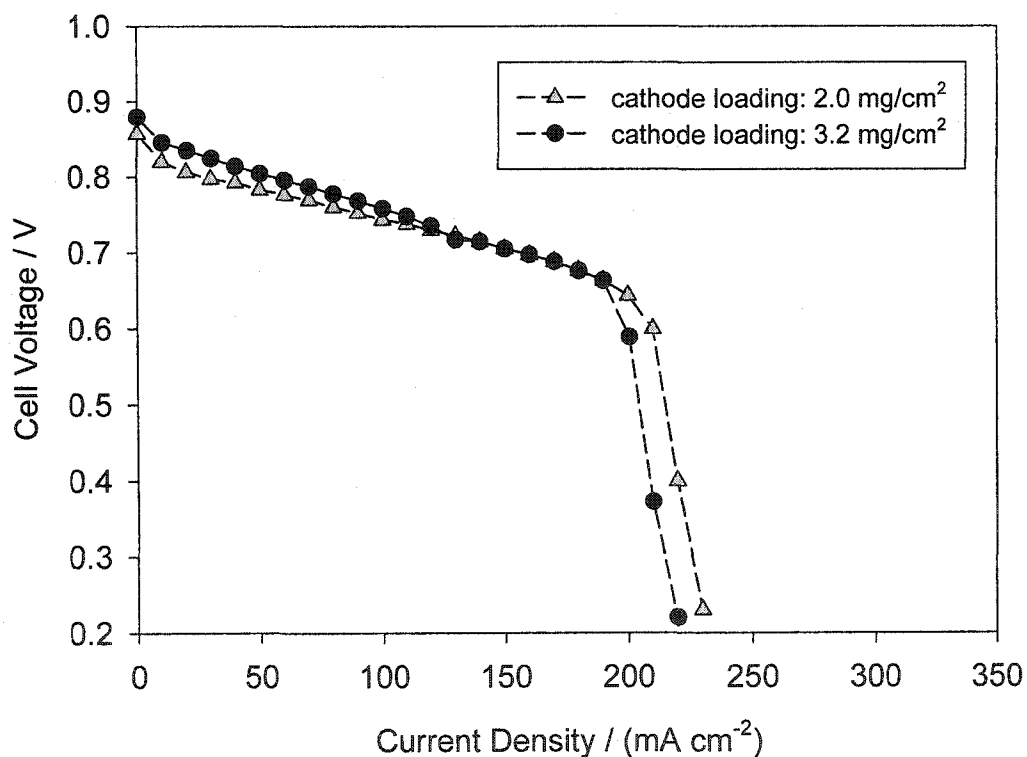


**Figure 5-3.** Effect of cathode catalyst loading on performance of a direct 2-propanol fuel cell. Anode: 2 mg/cm<sup>2</sup> Pt-Ru black catalyst (Johnson Matthey), 2.0 M iPrOH at 4.0 mL/min. Cathode: Pt-black catalyst, 20 psig dry oxygen at 600 sccm.

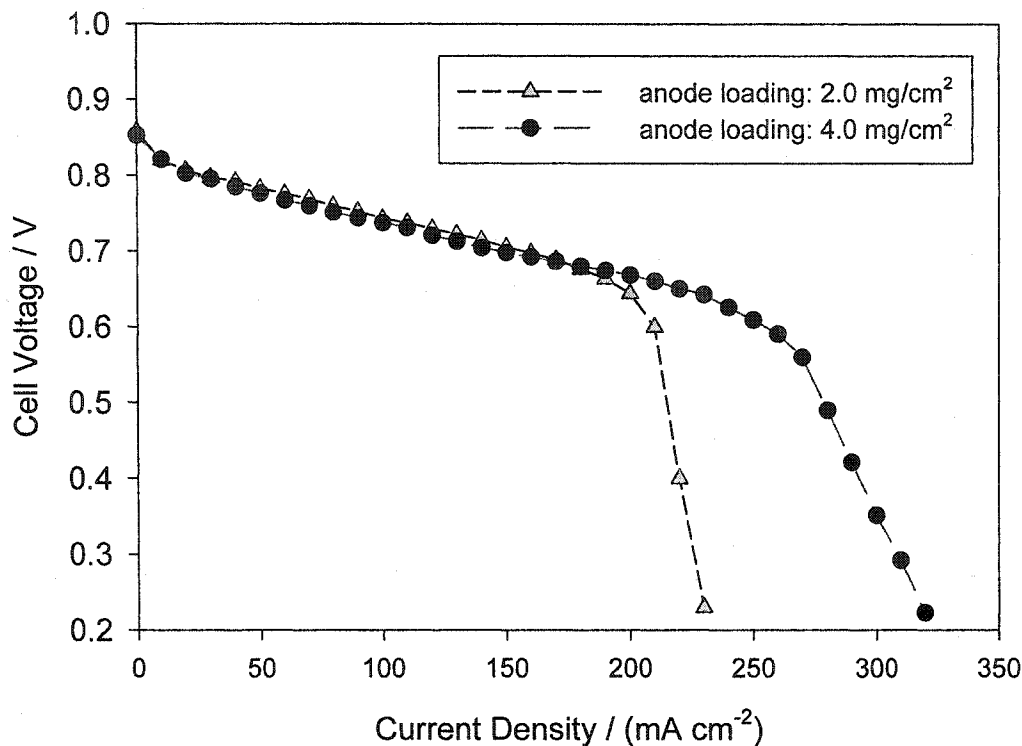


**Figure 5-4.** Effect of anode catalyst loading on performance of a direct 2-propanol fuel cell. Anode: Pt-Ru black catalyst (Johnson Matthey), 2.0 M iPrOH at 4.0 mL/min. Cathode: 2 mg/cm<sup>2</sup> Pt-black catalyst, 20 psig dry oxygen at 600 sccm.

Figure 5-5 shows how the performance of two cells with different anode loadings changes upon increasing the concentration of 2-propanol in the fuel feed from 1.0 to 2.0 M. The cell voltage was found to be largely independent of this change in concentration of 2-propanol when operating at current densities less than 200 mA/cm<sup>2</sup>. For both cells, however, the limiting current increased by ca. 80 mA/cm<sup>2</sup> upon the increase in 2-propanol concentration. This result is in contrast with those of Qi and co-workers, who found the performance using 1.0 M was higher than when using 2.0 M 2-propanol. They proposed the performance drop at higher concentrations of 2-propanol resulted from crossover and cathode poisoning. We believe the increase in performance of our cell with 2-propanol concentration results from use of a thicker Nafion<sup>®</sup> membrane (117 vs 112),

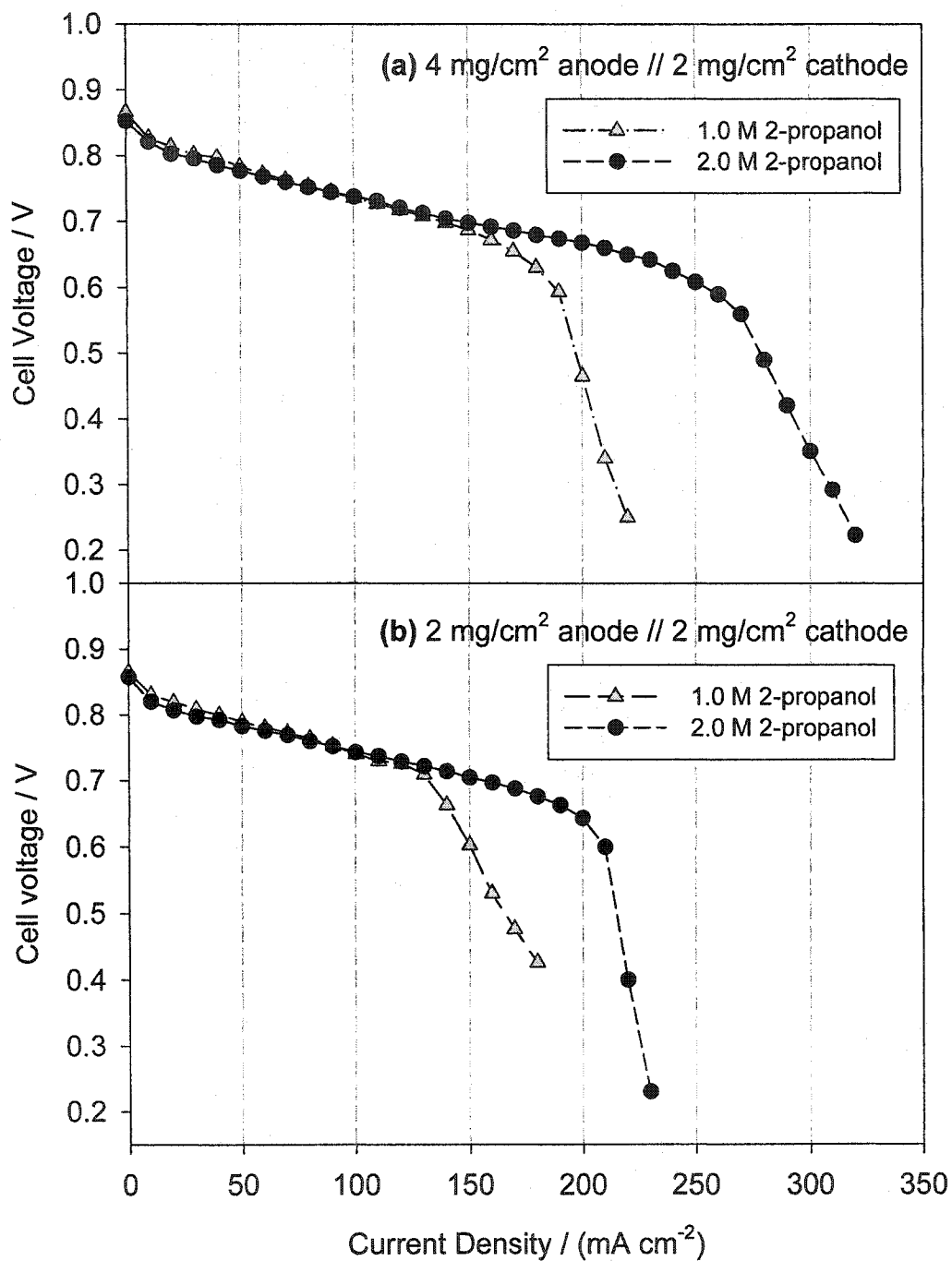


**Figure 5-5.** Effect of 2-propanol concentration on performance of a direct 2-propanol fuel cell. Anode: (a) 4 mg/cm<sup>2</sup>, (b) 2 mg/cm<sup>2</sup> Pt-Ru black catalyst (Johnson Matthey), iPrOH aqueous solution at 4.0 mL/min. Cathode: 2 mg/cm<sup>2</sup> Pt-black catalyst, 20 psig dry oxygen at 600 sccm.

from use of an oxygen cathode, and perhaps from use of a more active anode catalyst (Johnson Matthey HiSPEC™-6000, 50-50 Pt-Ru). Use of higher concentrations (e.g. 3.0 ~ 4.0 M) of 2-propanol further increased the limiting current of the cells, but at the expense of weakening the membrane electrode assembly. Specifically, exposure to higher concentrations of 2-propanol under these operating conditions apparently dissolved the recast Nafion® ionomer in the catalyst layer, resulting in delamination of the catalyst from the membrane. Further, we observed excessive swelling of the Nafion® membrane after disassembling cells that had operated on high concentrations of 2-propanol over a period of several hours. These results do imply, however, that direct 2-propanol fuel cells can, in principle, operate at high concentrations of 2-propanol provided dissolution and swelling of the membrane can be avoided.

Figure 5-6 shows the effect of reducing the oxygen pressure on cell performance. Reducing the oxygen pressure from 20 to 0 psig decreased the performance of the cell. For example, the open circuit voltage decreased by ca. 80 mV, and the voltage at 200 mA/cm<sup>2</sup> decreased by ca. 120 mV. This decrease in cell voltage is substantially larger than the decrease in Nernst cathode potential calculated for this pressure change

$$\left( \Delta E_{cathode} = \frac{RT}{nF} \ln\left(\frac{\Delta p_{O_2}}{p^0}\right) \right) \approx 5 \text{ mV}.$$

This result implies that 2-propanol crossover occurs to some extent, that the presence of 2-propanol decreases the cathode potential, and that cathode poisoning by 2-propanol is less severe than by methanol. The cathode appears less susceptible to poisoning by 2-propanol at higher oxygen pressures.

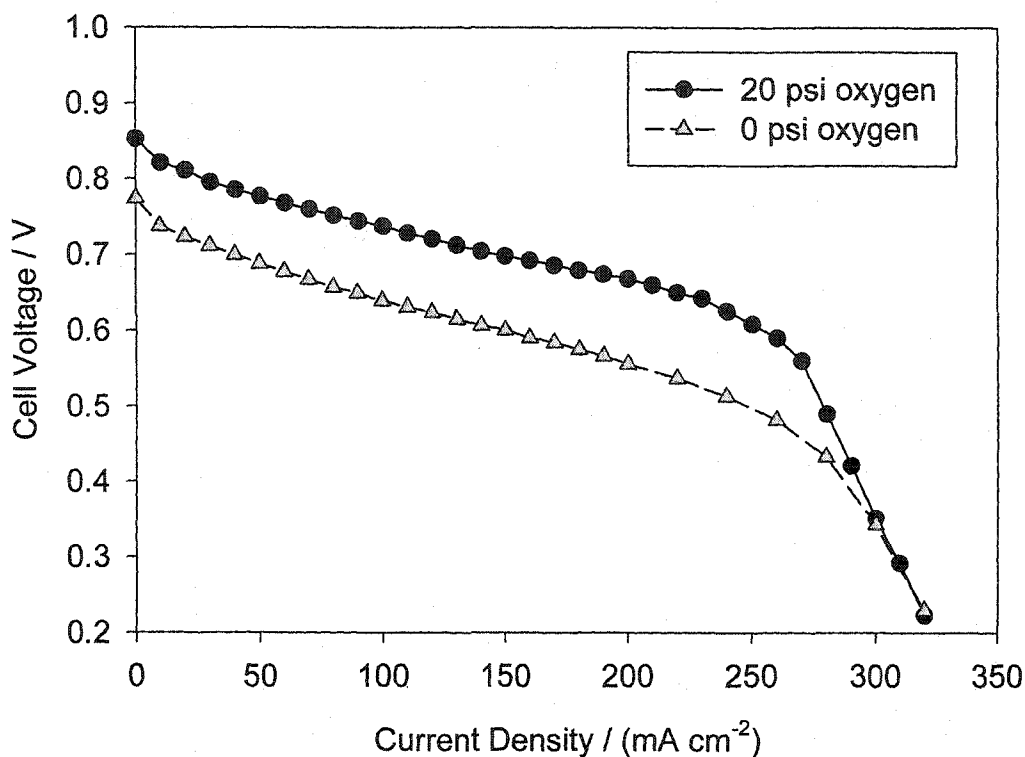


**Figure 5-6.** Effect of oxygen pressure on performance of a direct 2-propanol fuel cell. Anode: 4 mg/cm<sup>2</sup> Pt-Ru black catalyst (Johnson Matthey), 2.0 M i-PrOH at 4.0 mL/min. Cathode: 2 mg/cm<sup>2</sup> Pt-black catalyst, dry oxygen at 600 sccm.

In accordance with the results of Qi and co-workers, we also found that operation of the cell under constant load at current densities less than 200 mA/cm<sup>2</sup> results in rapid drops in cell voltage to nearly 0 V that abruptly occur after ca. 30 minutes of run time. However, the performance is restored by either short-circuiting the cell for brief periods of time, or by leaving the cell at open-circuit until the cell voltage is restored (ca. 15 s). That short-circuiting the cell restores performance may explain the oscillation observed at current densities higher than ca. 200 mA/cm<sup>2</sup> (Figure 5-1).

2-Propanol dehydrogenates over Pt and other catalysts at moderately elevated temperatures to generate acetone and hydrogen. The reaction can be driven by removing hydrogen or acetone from the system, and it has been investigated as a method to upgrade heat.<sup>16-23</sup> This process apparently also occurs during operation of the 2-propanol fuel cell at 90 °C. Hydrogen gas evolution at the anode is observed at low current densities. This evolution slows to a stop as the current density is increased, and it resumes as the current density is then reduced. Thus it appears that some 2-propanol is internally reformed to acetone and hydrogen. The amount of hydrogen consumed by electrooxidation in the fuel cell increases with increasing current density. This hydrogen evolution was not reported by Qi and co-workers.

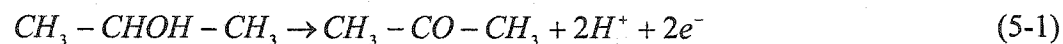
#### 4. Discussion

The performance of the cell at different oxygen pressures indicates that 2-propanol crossover occurs, and that the presence of 2-propanol reduces the cathode potential, but to a lesser extent than does methanol. It appears that cells can operate on 2-propanol with lower cathode loadings than cells can operate on methanol. Qi and co-workers reached a similar conclusion by reversing the connections of their cell and driving the current with an external power source.

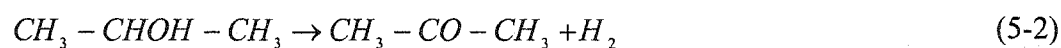
The observation that increasing the cathode loading had little effect on the cell performance, combined with the observations that increasing either the anode loading or the 2-propanol concentration increased the maximum current density before the rapid voltage drop, indicates that the voltage drop is an anode phenomenon. We propose the



following four reactions occur at the anode operating on 2-propanol fuel at 90 °C. First is the direct electrochemical oxidation of 2-propanol to acetone (Eq. 5-1). As per the kinetic



and mechanistic studies of Pastor, Sun and their co-workers,<sup>8,10</sup> this reaction is rapid, and it is the predominant electrooxidation reaction of 2-propanol at low anode potentials. Second is the non-electrochemical catalytic dehydrogenation of 2-propanol to acetone (Eq. 5-2).



Hydrogen evolution at the anode operating at current densities less than ca. 100 mA/cm<sup>2</sup> indicates the rate of this reaction is greater than the rate of electrooxidation in this current range. Third is electrooxidation of hydrogen. Fourth is deep oxidation of 2-propanol or perhaps acetone. This deep oxidation appears to be the slowest of the four reactions at current densities less than ca. 200 mA/cm<sup>2</sup>, and it may lead to poisoning of the anode, as proposed by Qi and co-workers. Another possibility is that a build up of acetone at the membrane/anode interface blocks mass transport to the anode. More investigation is required to determine the extent that these processes poison the anode. Increasing either the anode loading or the 2-propanol concentration had little effect on cell performance at current densities less than ca. 200 mA/cm<sup>2</sup>. This unusual result requires further investigation, but it does indicate that cells can operate on 2-propanol fuel with lower anode and cathode loadings than cells operating on methanol. Increasing either the anode loading or the 2-propanol concentration did increase the maximum current that could be obtained before the rapid voltage drop. These results suggest that the rapid voltage drop occurs after a certain ratio of acetone to anode active sites of acetone to 2-propanol is

reached in the anode-Nafion<sup>®</sup> assembly, and that acetone causes a rapid increase in the anode voltage, either by deep oxidation leading to poisoning, or by some sort of mass transport process. Again, further investigations are required to determine the origins of these observations.

## 5. Conclusions

The performance of a polymer electrolyte membrane direct 2-propanol fuel cell was investigated at 90 °C operating temperature. The cell consisted of a Pt-Ru (atomic ratio of 1:1) black anode, a Pt black cathode, and a Nafion<sup>®</sup>-117 membrane electrolyte. The cell was operated with aqueous 2-propanol as fuel and with oxygen as oxidant. The performance of the cell operating on 2-propanol is substantially higher than when it was operating on methanol at current densities lower than ca. 200 mA/cm<sup>2</sup>. The electrical efficiency of the direct 2-propanol fuel cell is nearly 1.5 times that of direct methanol fuel cells at power densities below 125 mW/cm<sup>2</sup>. Studies on the effects of electrocatalyst loading, of 2-propanol concentration, and of oxygen pressure on cell performance indicate that the cells operating on 2-propanol require lower anode and cathode loadings than cells operating on methanol. Cathode poisoning by 2-propanol is less severe than by methanol. Hydrogen gas evolution observed at the anode at low current densities indicated that catalytic dehydrogenation of 2-propanol occurred over the anode catalyst. A rapid voltage drop occurred at high current densities and after operating the cell for extended periods of time at constant current. The rapid voltage drop is an anode phenomenon.

These results, along with those of Qi and co-workers indicate that 2-propanol is a promising fuel candidate for a direct alcohol fuel cell. One of the more attractive features of such a system is the high operating efficiency at moderate current densities. The major challenges of this approach are anode poisoning by deep oxidation and by acetone buildup, and 2-propanol crossover. The development of anode catalysts and anode structures that are immune to these deficiencies is the more consequential to these challenges. The results presented here also suggest that internal reforming of 2-propanol to acetone and hydrogen in Nafion<sup>®</sup>-based fuel cells at temperatures greater than 80 °C is a promising approach. These issues and further investigation of the proposals presented in this study are under further investigation in this laboratory.

## References

- (1) Lamy, C.; Lima, A.; LeRhun, V.; Delime, F.; Coutanceau, C.; Leger, J. M. *J. Power Sources* **2002**, *105*, 283-296, and see references there.
- (2) Aricò, A. S.; Srinivasan, S.; Antonucci, V. *Fuel Cells* **2001**, *1*, 133-161.
- (3) Larminie, J.; Dicks, A. *Fuel cell systems explained*; Wiley: New York, 2000.
- (4) Kordesch, K.; Simader, G. *Fuel cells and their applications*; VCH: New York, 1996.
- (5) Ren, X.; Zelenay, P.; Thomas, S.; Davey, J.; Gottesfeld, S. *J. Power Sources* **2000**, *86*, 111-116..
- (6) Wasmus, S.; Kuver, A. *J. Electroanal. Chem.* **1999**, *461*, 14-31, and see references there.
- (7) Gao, P.; Chang, S. C.; Zhou, Z. H.; Weaver, M. J. *J. Electroanal. Chem.* **1989**, *272*, 161-178.
- (8) Pastor, E.; Gonzalez, S.; Arvia, A. J. *J. Electroanal. Chem.* **1995**, *395*, 233-242.
- (9) Beltowska-Brzezinska, M.; Luczak, T. Holze, R. *J Appl. Electrochem.* **1997**, *27*, 999-1011.

- (10) Sun, S-G.; Lin, Y. *J. Electroanal. Chem.* **1994**, *375*, 401-404.
- (11) Wang, J. T.; Wasmus, S.; Savinell, R. F. *J. Electrochem. Soc.* **1995**, *142*, 4218-4224.
- (12) Qi, Z. G.; Hollett, M.; Attia, A.; Kaufman, A. *Electrochem. Solid-State Lett.* **2002**, *5*, A129-A130.
- (13) Qi, Z. G.; Kaufman, A. *J. Power Sources* **2002**, *112*, 121-129.
- (14) Ren, X.; Wilson, M. S.; Gottesfeld, S. *J. Electrochem. Soc.* **1996**, *143*, L12-L15.
- (15) Calculated based the cell reaction:  $\text{CH}_3\text{-CHOH-CH}_3(\text{l}) + 1/2\text{O}_2(\text{g}) \rightarrow \text{CH}_3\text{-CO-CH}_3(\text{l}) + \text{H}_2\text{O}(\text{l})$  and the free energy of formation of these species obtained from the CRC Handbook of Chemistry and Physics, CRC Press, Boca Raton, 2000.
- (16) Mooksuwan, W.; Kumar, S. *Int. J. Energy Res.* **2000**, *24*, 1109-1122.
- (17) Meng, N.; Ando, Y.; Shinoda, S.; Saito, Y. *Bull. Chem. Soc. Jpn.* **1999**, *72*, 669-672.
- (18) Saito, Y.; Yamashita, M.; Ito, E.; Meng, N. *Int. J. Hydrog. Energy.* **1994**, *19*, 223-226.
- (19) Yamashita, M.; Kawamura, T.; Suzuki, M.; Saito, Y. *Bull. Chem. Soc. Jpn.* **1991**, *64*, 272-278.
- (20) Saito, Y.; Kaneyama, H.; Yoshida, K. *Int. J. Energy Res.* **1987**, *11*, 549-558.
- (21) Kim, T. G.; Yeo, Y. K.; Song, H. K. *Int. J. Energy Res.* **1992**, *16*, 879-916.
- (22) Dio, T.; Tanaka, T. *Proceedings of ASME/JSES International Solar Energy Conference*, Stine W, Kreider J, Watanabe K. (eds), **1992**, 285-290.
- (23) Dio, T.; Takashima, T.; Tanaka, T. *Proceedings of ASME/JSES International Solar Energy Conference* **1995**, 93-98.

## Chapter 6

### Conclusions

Pt-Ru nanoparticles are the state-of-the-art anode catalysts for direct methanol fuel cells. The evaluation of these nanoparticle Pt-Ru catalysts is difficult because there are no proven methods to measure their specific surface areas (number of active sites) and their surface ratios of Pt to Ru. In this study, we developed two methods to prepare known surface area of Pt-Ru<sub>ad</sub> (adatoms) nanoparticles by depositing a submonolayer of Ru<sub>ad</sub> onto known surface area Pt nanoparticles. The surface ratios of Pt to Ru<sub>ad</sub> of these nanoparticle Pt-Ru<sub>ad</sub> catalysts were estimated by measuring the amounts of Ru<sub>ad</sub> deposited. These nanoparticle Pt-Ru<sub>ad</sub> catalysts with known surface area and known surface composition were studied for methanol electrooxidation in typical 3-electrode electrochemical cells and in prototype direct methanol fuel cells.

The first method developed is the organometallic deposition of Ru<sub>ad</sub> onto Pt.<sup>1</sup> This deposition uses a fairly air-stable, easily prepared Ru<sub>4</sub>(μ-H)<sub>4</sub>(CO)<sub>12</sub> as Ru precursor. The deposition was carried out under 60 atm H<sub>2</sub> and at room temperature in a hexanes solution. During the deposition, CO from Ru<sub>4</sub>(μ-H)<sub>4</sub>(CO)<sub>12</sub> adsorbed and remained adsorbed on the evolving Pt-Ru<sub>ad</sub> surface. The adsorbed CO blocked one or more sites of the evolving Pt-Ru<sub>ad</sub> surface from further reaction with the remaining Ru precursor in the solution; therefore, the deposition self-poisons by adsorbed CO at a specific surface Ru concentration. The adsorbed CO is easily removed from the Pt-Ru<sub>ad</sub> surface by exposure to air or by electrooxidation after deposition. The deposition self-poisons when ca. 0.05

surface equivalents  $Ru_{ad}$  are deposited on blacked Pt gauze, and when ca. 0.10 surface equivalents  $Ru_{ad}$  are deposited on nanoparticle Pt black.

This self-poisoning deposition overcomes the drawbacks suffered by the deposition using  $Ru(COD)(\eta^3-C_3H_5)_2$  (COD is 1,5-cyclooctadiene) as Ru precursor, a method previously developed in this group by Lee and co-workers.<sup>2,3</sup> Ru deposition by hydrogenation of  $Ru(COD)(\eta^3-C_3H_5)_2$  over Pt imposed the following requirements. First, the specific surface area of the Pt substrate must be known in order to determine the stoichiometry of the hydrogenation. Second, it is necessary to monitor the stoichiometry of the hydrogenation (by monitoring the amount of cyclooctane produced in solution using gas chromatography) at low temperatures and to physically remove the Pt- $Ru_{ad}$  surface from the hydrogenation mixture when the desired surface stoichiometry is reached. Third, it is necessary to maintain reaction-rate limiting kinetics (not mass-transport limiting) during the hydrogenation to ensure uniform coverage of Pt by  $Ru_{ad}$ . The self-poisoning deposition developed in this study eliminated all these requirements. In addition, although  $Ru(COD)(\eta^3-C_3H_5)_2$  is relatively easy to prepare in slightly impure form, it is difficult to prepare and maintain in rigorously pure form as needed, whereas  $Ru_4(\mu-H)_4(CO)_{12}$  is easy to make and to handle.

The second method investigated is the surface reductive deposition of  $Ru_{ad}$  onto Pt.<sup>4-8</sup> Nanoparticle Pt surfaces were first saturated by adsorbed hydrogen by reacting with hydrogen gas. The Pt surfaces saturated with adsorbed hydrogen were then exposed to aqueous  $RuCl_3$  at room temperature. Ru was reduced by pre-adsorbed hydrogen to form Pt- $Ru_{ad}$  nanoparticles with ca. 0.18 surface equivalents  $Ru_{ad}$ . The deposition was repeated several times, with each reaction depositing ca. 0.18 surface equivalents more

$\text{Ru}_{\text{ad}}$  onto the  $\text{Pt-Ru}_{\text{ad}}$  nanoparticles. This deposition is a self-limiting, one-step, non-electrochemical deposition. It was carried out at room temperature in aqueous medium using the most common  $\text{RuCl}_3$  as Ru precursor. We believe that this surface reductive deposition is one of the most convenient methods to prepare nanoparticle  $\text{Pt-Ru}_{\text{ad}}$ .

A series of nanoparticle  $\text{Pt-Ru}_{\text{ad}}$  catalysts with estimated Ru coverage between 0.18 and 0.75 were prepared using this surface reductive deposition. The activities of these nanoparticle  $\text{Pt-Ru}_{\text{ad}}$  catalysts for methanol electrooxidation were studied in typical 3-electrode cells (1.0 M  $\text{H}_2\text{SO}_4$  + 1.0 M  $\text{CH}_3\text{OH}$ ) and in DMFCs. It was found that the  $\text{Pt-Ru}_{\text{ad}}$  with Ru surface coverage of ca. 0.33 ( $\text{Pt-Ru}_{\text{ad}}\text{-0.33}$ ) is the most active for methanol electrooxidation in  $\text{H}_2\text{SO}_4$  at both 22 °C (0.45 V) and 60 °C (0.4 V), and it also shows the best performance in prototype DMFCs operating at 60 °C.  $\text{Pt-Ru}_{\text{ad}}$  nanoparticles with Ru coverages between 0.33 and 0.63 show similar activities in DMFCs operating at 90 °C.

$\text{Pt-Ru}_{\text{ad}}\text{-0.33}$  is found to be ca. 1.5 times more active than the state-of-the-art commercial Pt-Ru catalyst (Johnson Matthey HiSPEC™-6000, 50-50 Pt-Ru) in terms of the real activity measured in 3-electrode cells in  $\text{H}_2\text{SO}_4$ . But Johnson Matthey Pt-Ru performs better than  $\text{Pt-Ru}_{\text{ad}}\text{-0.33}$  in prototype DMFCs. This is an interesting observation that needs to be further investigated. One possible reason is that the structure of the electrode fabricated using these commercial Pt-Ru nanoparticles is different from that fabricated using  $\text{Pt-Ru}_{\text{ad}}$  nanoparticles.

The stability of  $\text{Pt-Ru}_{\text{ad}}$  as fuel cell catalysts has been questioned because  $\text{Pt-Ru}_{\text{ad}}$  may be subject to surface reconstruction (Ru segregation, redistribution, and/or dissolution) during the fabrication and operation of DMFCs.<sup>9</sup> However, no obvious

surface restructuring of the Pt-Ru<sub>ad</sub> nanoparticles occurred during the fabrication and operation of the DMFCs in this study. A DMFC using PtRu<sub>ad</sub>/C anode catalyst was operated for 20 days. No deterioration in cell performance was observed, suggesting that Pt-Ru<sub>ad</sub> nanoparticle catalysts are stable enough to be used in practical DMFCs.

A liquid feed, polymer electrolyte membrane based direct 2-propanol fuel cell was investigated.<sup>10</sup> The cell consisted of a Pt-Ru (atomic ratio of 1:1) black anode catalyst (Johnson Matthey, HiSPEC™-6000), a Pt black cathode (Johnson Matthey), and a Nafion®-117 membrane electrolyte. The cell was operated at 90 °C with aqueous 2-propanol as fuel and with oxygen as oxidant. The performance of the cell operating on 2-propanol is substantially higher than operating on methanol at current densities lower than ca. 200 mA/cm<sup>2</sup>. The electrical efficiency of the direct 2-propanol fuel cell is nearly 1.5 times that of direct methanol fuel cell at power densities below 125 mW/cm<sup>2</sup>. Studies on the effects of electrocatalyst loading, of 2-propanol concentration, and of oxygen pressure on cell performance indicate that cells operating on 2-propanol require lower anode and cathode catalyst loadings than cells operating on methanol. Cathode poisoning by 2-propanol is less severe than by methanol. Hydrogen gas evolution was observed at the anode at low current densities, indicating that catalytic dehydrogenation of 2-propanol occurred over the anode catalyst along with the electrooxidation of 2-propanol to acetone. The much higher performance of the direct 2-propanol fuel cell than the direct methanol fuel cell is mainly attributed to the faster kinetics of electrooxidation of 2-propanol to acetone than electrooxidation of methanol to CO<sub>2</sub>. A rapid voltage drop occurred at high current densities and after operating the cell for extended periods of time at constant currents. The rapid voltage drop is likely due to deactivation of the anode catalyst



resulting from the poisoning by deep oxidation of 2-propanol and by acetone buildup. Therefore, anode catalysts with high selectivity for electrooxidation of 2-propanol to acetone are needed. The promising results obtained by this exploratory study on direct 2-propanol fuel cells imply that direct 2-propanol fuel cells could become a very attractive member in the fuel cell family. Much more work is needed because this is a very new research area.

Production of CO-free hydrogen for fuel cells by selective catalytic dehydrogenation of 2-propanol to acetone (internally or externally) should be investigated. This H<sub>2</sub> production route would provide an alternative to the conventional hydrogen generation processes (steam reforming, partial oxidation, and autothermal reforming), in which CO-containing H<sub>2</sub> is produced. CO must be removed because it poisons the anode catalyst in the low temperature PEMFC.

## References

- (1) Cao, D. X.; Bergens, S. H. *J. Electroanal. Chem.* **2002**, *533*, 91-100.
- (2) Lee, C. E.; Tiege, P. B.; Xing, Y.; Nagendran, J.; Bergens, S. H. *J. Am. Chem. Soc.* **1997**, *119*, 3543-3549.
- (3) Lee, C. E.; Bergens, S. H. *J. Phys. Chem. B* **1998**, *102*, 193-199.
- (4) Cao, D. X.; Bergens, S. H. *Electrochim. Acta* **2003**, *48*, 4021-4031.
- (5) Janssen, M. M. P.; Moolhuysen, J. *Electrochim. Acta* **1976**, *21*, 869-878.
- (6) Janssen, M. M. P.; Moolhuysen, J. *Electrochim. Acta* **1976**, *21*, 861-868.
- (7) Szabo, S.; Bakos, I. *J. Electroanal. Chem.* **1987**, *230*, 233-240.
- (8) Szabo, S.; Bakos, I.; Nagy, F. *J. Electroanal. Chem.* **1989**, *271*, 269-277.
- (9) Wasmus, S.; Kuver, A. *J. Electroanal. Chem.* **1999**, *461*, 14-31.
- (10) Cao, D. X.; Bergens, S. H. *J. Power Sources* **2003**, *124*, 12-17.